Report No. CG-D-39-82

(12) ~~AD-E 271 446~~

LORAN-C SIGNAL STABILITY STUDY: ST. LAWRENCE SEAWAY

JULY 1982

FINAL REPORT

Superseded AD-A132476 nc.

Prepared by

U.S. DEPARTMENT OF TRANSPORTATION
United States Coast Guard
Office of Research and Development
Washington, D.C. 20593

NOTICE

This document is disseminated under the sponsorship of the Department of Transportation in the interest of information exchange. The United States Government assumes no liability for its contents or use thereof.

The contents of this report do not necessarily reflect the official view or policy of the Coast Guard; and they do not constitute a standard, specification, or regulation.

This report, or portions thereof may not be used for advertising or sales promotion purposes. Citation of trade names and manufacturers does not constitute endorsement or approval of such products.

The United States Goverment does not endorse products or manufacturers. Trade or manufacturer's names appear herein solely because they are considered essential to the object of this report.

AD-A126093

Technical Report Documentation Page

1. Report No.	2. Government Accession No.	3. Recipient's Catalog No.
CG-D-39-82	[redacted]	

4. Title and Subtitle

LORAN-C SIGNAL STABILITY STUDY: ST. LAWRENCE SEAWAY

5. Report Date
July 1982

6. Performing Organization Code
G-DST-1

7. Author(s)
D. C. Slagle, R. J. Wenzel

8. Performing Organization Report No.
CG-D-39-82

9. Performing Organization Name and Address
Department of Transportation
U.S. Coast Guard
Office of Research and Development
Washington, DC 20593

10. Work Unit No. (TRAIS)
2110

11. Contract or Grant No.

12. Sponsoring Agency Name and Address
Department of Transportation
U.S. Coast Guard
Office of Research and Development
Washington, DC 20593

13. Type of Report and Period Covered
INTERIM REPORT
August 1981 to June 1982

14. Sponsoring Agency Code
G-DST-1

15. Supplementary Notes

16. Abstract

Since 1977, the U.S. Coast Guard has been conducting studies of the suitability of Loran-C as a precision aid to navigation in the harbor-harbor entrance (HHE) areas of the continental U.S. The final phase of this effort involves an assessment of the stability of the signals of the existing Loran-C system along with an examination of stability improvement methods. The final efforts were begun early in 1981 with the deployment of loran data collection sets (the so-called "harbor monitors") in select harbor areas. In cooperation with the St. Lawrence Seaway Development Corporation, the St. Lawrence Seaway Authority and the Canadian Coast Guard, these efforts were extended to the St. Lawrence Seaway area in late 1981. Resulting data is analyzed in the report and indicates the performance of the existing Loran-C system is inadequate to support precision applications in the St. Lawrence. The performance of Differential Loran-C is hypothesized and found to be, at best, marginal due to suboptimal system geometry. The performance which would result with the addition of another transmitting station is also hypothesized. With this improved geometry, "raw" Loran-C performance is still found inadequate but Differential Loran-C, yielding maximum cross-track errors of 27 meters (99.9% probability), leaves 23 meters error margin for the largest vessels.

17. Key Words	18. Distribution Statement
Loran-C, Differential Loran-C, Harbor-Harbor Entrance, Harbor Monitor, Temporal Variations, Error Ellipse, Double Range Difference	Document is available to the U.S. Public through the National Technical Information Service, Springfield, Va 22161

19. Security Classif. (of this report)	20. Security Classif. (of this page)	21. No. of Pages	22. Price
Unclassified	Unclassified		

Form DOT F 1700.7 (8-72) Reproduction of completed page authorized

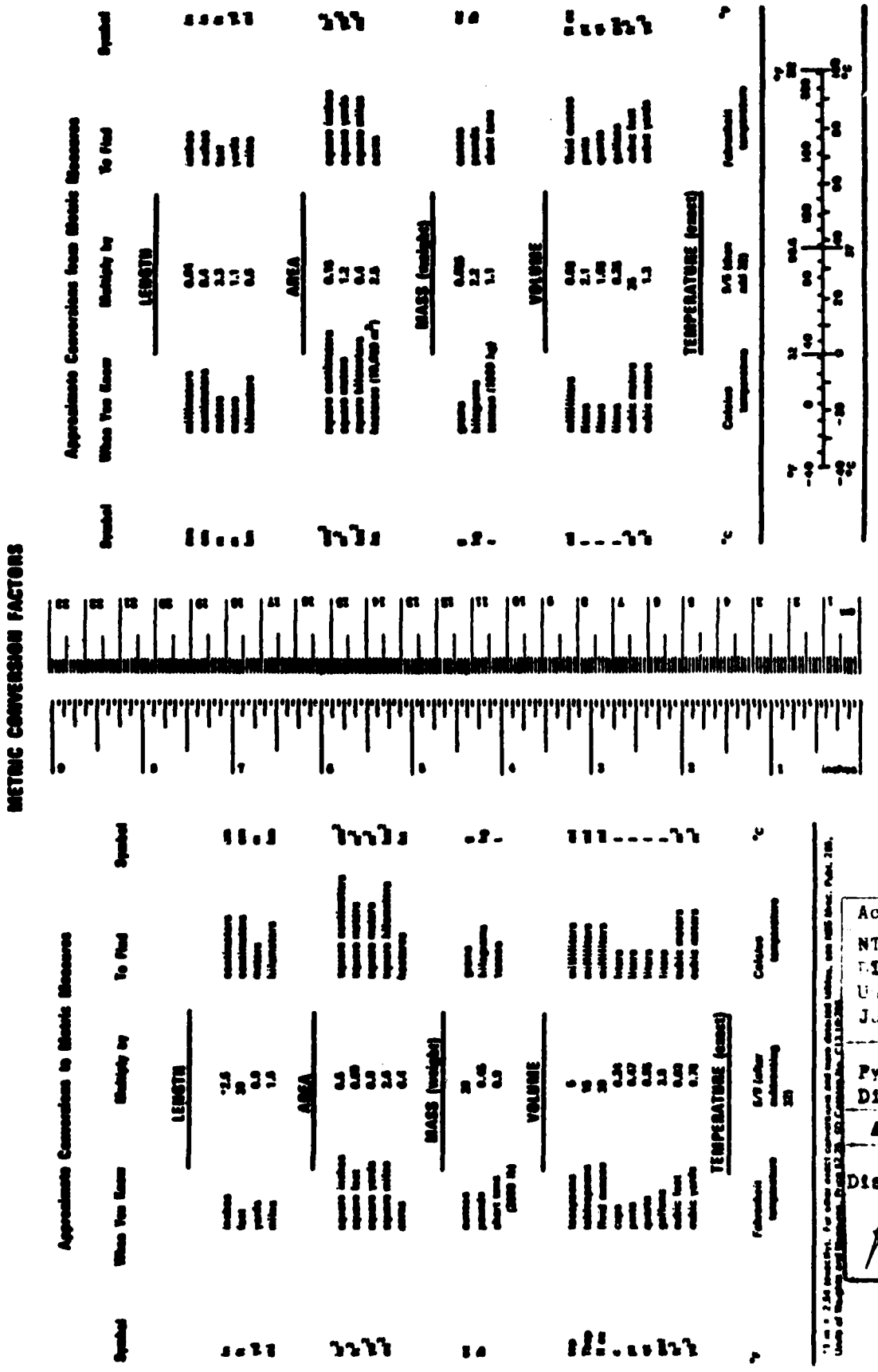

Accession For
NTIS GRA&I
DTIC TAB
Unannounced
Justification
By
Distribution/
Availability Codes
Dist | Avail and/or Special

DTIC COPY INSPECTED 3

TABLE OF CONTENTS

TABLE OF CONTENTS (CON'T)

LIST OF ILLUSTRATIONS

LIST OF ILLUSTRATIONS (CONTINUED)

LIST OF ILLUSTRATIONS (CONTINUED)

LIST OF TABLES

EXECUTIVE SUMMARY

In mid-1981, the St. Lawrence Seaway Development Corporation, St. Lawrence Seaway Authority, and Canadian and U.S. Coast Guards began a joint effort to explore the capability of Loran-C to meet precision, all-weather navigation requirements in the Seaway. Loran-C surveys of major portions of the Seaway have been made and guidance equipment demonstrations are planned for late summer 1982 and beyond.

Critical questions of concern relate to the stability of the existing Loran-C grid in the Seaway and the feasibility of methods to improve the stability. To begin to address these questions, Loran-C data collection equipment sets were deployed at several sites along the Seaway in late 1981. The U.S. Coast Guard, as part of an ongoing R&D project, had developed equipment, the so-called Harbor Monitor Set, which was ideally suited to a study of this nature. Unfortunately, most sets were already deployed at sites throughout the U.S. Originally, therefore, only one Harbor Monitor Set was deployed in the Seaway - at the Eisenhower Lock, Massena, N.Y., October 1981.

The Loran-C receivers to be used with future Harbor Monitor Sets were available for use so, along with some teleprinters/cassette data recorders, these were made into so-called "Ad Hoc" equipment sets and deployed at three additional sites along the Seaway in December 1981. Additionally, the Canadian Coast Guard was in the process of developing Loran-C data collection equipment for use in a buoy-auditing project. Development was accelerated and these sets were deployed at two sites along the Seaway late in the period of this report. In early February 1982, USCG R&D Center personnel installed another Harbor Monitor Set at Tibbetts Point N.Y. A preliminary analysis of the data collected with these equipment sets is provided in this report.

Data obtained by the Harbor Monitor Sets has been of excellent quality - far exceeding the quality obtained in the St. Marys River Stability Study for which earlier versions of the equipment were developed. Conversely, except for a critically important month long period during which the Canadian Coast Guard was able to obtain data at Iroquois Lock, continual problems have been encountered trying to get reliable data from the other sites. The key feature of the Harbor Monitor Set that leads to the higher reliability is the remote control capability. Via phone line access, project personnel at the R&D Center are able to closely monitor the status of the equipment on a daily basis. Problems which threaten to cause loss of data, primarily a result of electrical power interruption, can be detected and corrected in a timely fashion. Unfortunately, similar problems are not detected at the other sites until considerable data has been lost. Thus, a major conclusion of the study to date is that Harbor Monitor Sets should be deployed at all sites.

A major stumbling block in the execution of a study such as this is identified at the beginning of the report: there are no standard guidelines for determing navigation system requirements for restricted waterways. Thus, the recommendations of a report describing navigation system accuracy, or ways to improve it, lack a foundation. The report acknowledges this problem and offers an <u>assumed</u> set of requirements. The assumptions are based on similar

experiences to date and the results of ongoing "requirements" studies. Wherever possible, care has been taken to tabulate the results of the stability study in a method amenable to update when more concrete requirements can be stated.

Prior to considering any of the data obtained along the Seaway, the report presents an extensive series of predictions. The predictions are based on a model of the nature of Loran-C time difference variations which has been developed over the years along with an extrapolation of data obtained at Harbor Monitor sites located along the northeast U.S. coast. The methodology involved in the prediction process provides a framework in which the data can be viewed and allows an extensive set of conclusions to be drawn from the limited data base.

The predictions indicate the stability of "raw" (unaugmented) Loran-C is inadequate for precision use throughout the shipping season in the Seaway. Data from Massena and Tibbetts Point confirm this. Extending the use of the prediction model, Differential Loran-C performance, using shore stations at Massena and Wellesley Island, is hypothesized. Adequate performance is expected except for several reaches in the region from the Brockville Narrows to the Thousand Island Bridge. Here, adequate performance is defined to mean the 99.9% probability cross-track error estimate leaves at least 10 meters for guidance error for a vessel with a beam of 34 meters. Further investigation shows the major problem is the suboptimal geometry associated with the loran grid in the Seaway. Fixes obtained by Loran-C over the course of a year, or just the shipping season, will form an elliptical pattern at any point of measurement. In the Seaway, the <u>longer</u> axis of the ellipse is nearly perpendicular to the predominant course. The geometry is bad enough to mean that if the prediction regarding the magnitude of the short term variations were either true or optimistic, Differential Loran-C could not produce satisfactory performance in these reaches.

In spite of the sub-par data base, an elaborate series of analysis techniques allows us to determine that the predictions regarding the short term variations were pessimistic. In the process, we discover that the predictions regarding the magnitude of the long term variations were optimistic. The resulting conclusion, although more data is needed to "harden" the estimates, is that Differential Loran-C appears capable of the desired performance - barely.

This having been said, we caution that Differential Loran-C is merely a concept - never having been implemented. Results of this study to date indicate a <u>flawlessly</u> operated Differential Loran-C system would produce satisfactory performance with a moderate amount of room left for imperfect surveying and other practical limitations. Again, the magnifying effect of poor loran geometry is the source of the problem. Differential Loran-C tests are encouraged so that an appreciation for the "other practical limitations" can be gained. Resulting insights will allow the statement of the "final word" on the subject. The concept to bear in mind is that we are contemplating the first operational use of Differential Loran-C in an area where there is scant room for error.

As a final note, and as a result of the conclusions regarding poor existing geometry, we introduce a consideration of what would result were another Loran-C transmitting station added to the existing chain. With a station at North Bay, Ontario, predictions show "raw" Loran-C still will not produce satisfactory performance throughout the shipping season. The use of a single differential monitor station, in conjunction with this new transmitting station, however, allows performance which easily exceeds all requirements. This suggests the addition of the new transmitting station would allow enough room for error that a "milder" alternative (e.g., daily corrections) to full Differential Loran-C could be considered. The alternatives which require a new transmitting station involve considerable expense and, therefore, risk. At present, they are offered as subjects for careful scrutiny in future studies.

1. INTRODUCTION

1.1 USCG Harbor/Harbor Entrance Loran-C R&D Studies.

Since 1977 the U.S. Coast Guard has been sponsoring Research and Development studies to assess the capability of the Loran-C radionavigation system to support precision navigation requirements typically encountered in piloting situations. The studies have centered on four areas of investigation:

a. Measuring the year-round stability of the loran signals in selected harbor/harbor entrance (HHE) areas.

b. Investigating methods of enhancing system performance for areas in which system stability/geometry is not adequate for high precision use.

c. Developing survey techniques to precisely determine the loran coordinates at critical "waypoints" in channels.

d. Developing modern guidance equipment which displays loran information in a manner most useful to a mariner in piloting situations.

Two guidance equipment systems, developed for the USCG by the Johns Hopkins Applied Physics Lab (APL) under this program, have proven to be effective in exploiting the high precision of Loran-C in stable signal areas. One such system, called PILOT (Precision Intracoastal LOran Translocator), features a graphical display of the HHE area being transitted and is intended for permanent installation on a vessel. The other system, called PLAD (Portable Loran Assist Device) features an alpha-numeric display of ship's position relative to channel waypoints, and is designed to be carried aboard a vessel by pilots. Both devices are described in more detail in reference 1.

1.2 St Lawrence Seaway Development Corporation Interests.

In February 1981, the Office of Comprehensive Planning of the Saint Lawrence Seaway Development Corporation (SLSDC) asked for an APL/USCG simulator demonstration of PILOT. As a result of the simulator demonstration, the SLSDC concluded Loran-C, perhaps only as a part of an integrated navigation package, had the potential to satisfy navigation requirements on the St. Lawrence Seaway. Thus, SLSDC asked for USCG assistance in sponsoring a PILOT/PLAD demonstration on the St. Lawrence Seaway.

In August 1981, SLSDC and USCG personnel conducted a trackline survey of the St. Lawrence Seaway from the vicinity of Ogdenburg, N.Y. to Cornwall, Ontario. PILOT chartlets were prepared for the surveyed area and a verification run was made in late October 1981.

Meanwhile, with a reasonable assurance that the survey and PILOT chartlet preparation efforts would be a success, agency heads from the SLSDC, the Saint Lawrence Seaway Authority and the Canadian Coast Guard (CCG) met with the Commandant of the USCG to discuss further plans. It was determined that a stability study would be initiated and that representatives from all four agencies would form a "Precision All-Weather Navigation System" (PAWNS) Steering Committee. The committee would initially be concerned with insuring the loran studies were underway and then proceed to study matters such as precision requirements and requirements for an integrated systems package.

By late October 1981, USCG and CCG personnel began deploying several types of loran data collection units along the St Lawrence Seaway. It should be noted that these diverse units were deployed on a hurried basis so that conditions during the end of the shipping season could be monitored. At a subsequent meeting of the Steering Committee it was determined that an early, initial review of the data should be made so that any equipment or data compatability problems could be identified and rectified before the next critical period of the season (i.e., the Fall of 1982) was entered. This report summarizes data collection results to date and addresses the problem areas of concern to the Steering Committee.

1.3 Applicability of Harbor Monitor Program to Seaway

It should be emphasized at the start that there is considerable concern as to the suitability of the USCG Harbor Monitor Program for answering all of the questions of concern in the St. Lawrence Seaway. The USCG Stability Studies are directed at providing a general characterization of Loran-C accuracy throughout all coastal and harbor areas of the continental U.S. With such a broad objective in mind, the experiment strategy recognizes it is impossible to obtain year-round data in every area of interest. This is not just a result of inability to procure enough equipment - the availability of skilled technicians to support the equipment is considerably more of a limitation. Thus the program attempts to follow a strategy which features spatial sampling adequate to allow interpolation of the results to all areas of interest.

Additionally, the program features time sampling, i.e., data is not collected on a continuous basis throughout the year. A key consideration here is that whereas recent advances in computer technology have made it possible to amass and maintain huge data bases at reasonable costs, the analysis will only be as "believable" as the data. To maintain data base integrity, unfortunately, requires skilled technical review of the data being accepted as valid (e.g., not produced by faulty instrumentation). Thus, in spite of the computer revolution, the cost of the data base remains, essentially, directly proportional to size and a reasonable quantity/quality tradeoff must be sought.

Drawing on the results of numerous experiments conducted over the years plus the benefits of many years of Loran-C system operational observations, the USCG adopted the two hour per day sampling strategy as the tradeoff commensurate with the harbor monitor effort. Whereas there is agreement on

the Steering Committee that the strategy is a correct one for the general Loran-C characterization, there is concern it may not be adequate for special, in-depth applications such as the Seaway. Thus, considerable care will be given in this report, and in further work, to discuss and test the strategy.

1.4 Treatment of System Requirements in This Report

Ideally, the goal of a study such as this should extend beyond simply stating what the stability of the Loran-C system is or could be made to be. It should assess the existing or potential stability with respect to navigation system accuracy requirements. At present, however, there are no standard methodologies for quantifying accuracy requirements in restricted waterways. The consequence is that although system stability/accuracy can be described in highly quantified terms, the ultimate question "is it good enough?" must typically be avoided.

Reference 11 documents results of ongoing U.S. Coast Guard sponsored studies to address this "requirements" problem. Although results to-date are encouraging, it must be conceded that the questions are non-trivial and prospects for definitive answers in the near future are not good. It should also be emphasized that this is not a "Loran-C per se" problem: the same unanswered questions apply to all precision navigation systems be they conventional visual or radionavigation systems. A major task of the Steering Committee will be to provide some answers to the "requirements" question.

Having recognized that system requirements cannot yet be conclusively stated, the report also recognizes a statement of existing stability, or ways to improve stability, without reference to any requirement, is of marginal utility. Conversely, the report recognizes a tutorial on the nature of Loran-C instabilities and "enhancement" techniques can be of significant value. A meaningful statement of requirements probably cannot be made without an understanding of such issues. Thus, the report proceeds with an assumed set of requirements. Since these assumed requirements may someday prove to be in need of revision, considerable effort is made to present the results in a form amenable to future update.

In developing the assumed requirements, past experiences are drawn upon. As indicated in reference 4, the originally stated requirement for the St. Marys River navigation system was 10 feet. When it became apparent that no practical system could provide such accuracy (but that it probably was not required), Loran-C was offered as a "100 foot system." This report demonstrates why requirements statements of this nature are to be avoided. In deference to the people involved in drawing up the St. Marys River requirements statements, they actually meant to say that 10 feet (later 100 feet) was the requirement in the "tightest reaches." A key concept for anyone who would state requirements to recall is that, at least for fixed location earth-bound systems, both measurement accuracy and the "geometry factors" which transform the measurement errors to position errors vary from point to point in the service area. (For satellite or celestial systems,

the geometry also varies from time to time.) A system is best designed when this varying accuracy is made to be the best in the tightest channels. In the case of the St. Marys River, the 100 foot accuracy is only required in a region comprising about 10 % of the river length. Over-specification by an order of magnitude, as was done several times in the St. Marys River, will typically render a system "non-cost-beneficial."

Another important consideration demonstrated in this report is that accuracy is a two-dimensional quantity for marine applications. As an example, we can imagine a situation in which the true requirement is only that cross-track error be less than 100 feet. If this is not explicitly stated, we could incorrectly declare inadequate a system which features a 50 foot cross-track accuracy in the area of concern because the total (root-sum-squared of cross-track and along-track) error exceeds 100 feet.

With this background as to motives, the report makes the following assumptions about St. Lawrence Seaway requirements:

(1) Because of the orientation of the Loran-C error ellipses and the predominant courses of the Seaway (to be described), cross-track error is the key parameter. Along-track errors (indeed, actual error ellipses) for all reaches are furnished in the Appendices in case future work indicates the need for examination of these quantities.

(2) Cross-track error requirements are assumed to be direct functions of channel width and vessel width. Specifically, the total allowable cross-track error is assumed to be defined as one-half the channel width minus one-half the beam of the largest vessel using the Seaway. This relationship causes the requirements to be more stringent in the narrower reaches - as desired.

(3) Of the total allowable error, some portion must be allocated to the navigation system and some to guidance error (i.e., trackkeeping ability). The Loran-C errors are specified at the 99.9% probability level. The 95% probability levels are also provided as an example of how to use the mathematics of Appendix A to extend the analysis to any probability.

(4) Maximum guidance errors of 10 meters are assumed as the basis for requiring Loran-C chain enhancements. As with the loran, there is no reason to expect the guidance error should be independent of the reach characteristics but an assumption of some sort is required. The 10 meters represents a stringent demand on trackkeeping skills but is consistent with the stringent 99.9% demands being placed on the Loran-C and is assumed consistent with normal demands imposed by the narrowness of the channels for which it is an issue. Extensive use of tables is made so that the results can be extended to whatever guidance errors future studies may indicate to be appropriate.

1.5 Report Overview.

Section 2 begins with a description of the various equipment sets used

to collect data thus far. Next, a synopsis of data collection efforts to date is presented. Section 2 concludes with the presentation of a newly developed data collection set and a discussion of compatability for all of the sets.

Section 3 begins the discussion of the adequacy of the data collection strategy by introducing a model for Loran-C variations. The need for the model, and how it relates to both the system requirements and the scope of the experiment is developed. Due to late starts and/or site and equipment problems, we do not yet have a sufficient data base to say the final word on the adequacy of Loran-C in the Seaway. We can, however, use the model to make some preliminary predictions. We draw upon data obtained from Northeast U.S. chain operational and harbor monitor sites to make the predictions which conclude Section 3. The adequacy of these predictions can be tested somewhat with data collected thus far in the Seaway and with data collected from future efforts. The model will probably need future refinement, but can serve to steer future efforts in the right direction.

In Section 4 we present the results of the data collection efforts. The results are encouraging, both in regards to the stability they indicate and the agreement with the predictions. What is not encouraging, however, is the problem we have experienced in obtaining usable data. Of particular concern is the inadequacy of the so-called "Ad Hoc" data sites which, it is shown, threatens to compromise future efforts. We confirm the preliminary conclusion of Section 3 that an additional monitor site may be needed.

Section 5 provides some brief comments regarding the implementation of differential Loran-C - a non-trivial undertaking. An alternative is introduced for initial consideration.

Section 6 summarizes the conclusions - the prime one being that data collection efforts/equipment must be upgraded before this fall. Conclusions about the sampling strategy are also presented. Finally, the significant effect that existing chain geometry has on the error budget and the viability of Loran-C as a precise navaid for the Seaway is discussed. The report ends with a tabulation of the the recommendations that seem indicated from the results to date. In short, further efforts with upgraded equipment are recommended for the stability study and a test implementation of Differential Loran-C is urged.

2. STABILITY STUDY EQUIPMENT/SITES

2.1 USCG Harbor Monitor Sets

As discussed in paragraph 1.1, the USCG has developed a so-called "Harbor Monitor Set" for use in the HHE Loran-C Stability Study project element. The set consists of a survey grade Loran-C receiver, the Internav 404, a small micro-computer, and miscellaneous support equipment allowing battery back-up and remote (via telephone) access to the collected data. The equipment is designed to accomodate a "low density data analysis" of loran signals as described in reference 2. Simply stated, this means data is collected during only two hours of the day - generally from 11 to 12, AM and PM. Figure 2-1 shows the prime components of the system in block diagram form.

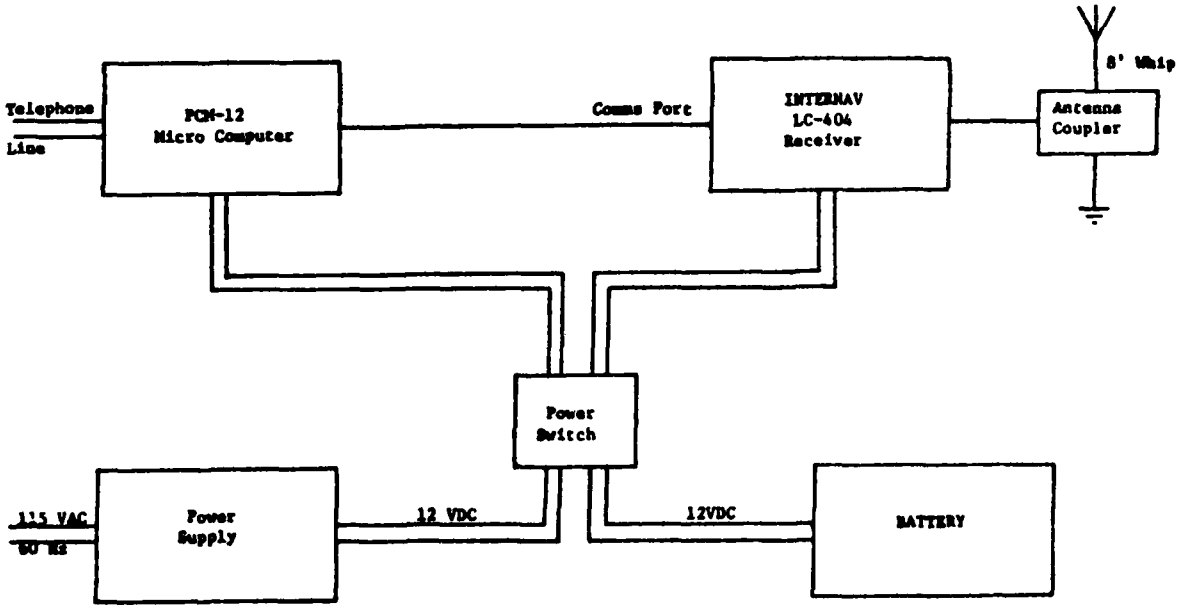

Figure 2-1 Harbor Monitor Set Block Diagram

Simulator tests have shown the Loran-C receiver has a "servo loop time constant" of about 6-8 seconds under conditions typically encountered at harbor monitor sites. Thus the receiver output is sampled every 40 seconds so that the samples can be treated as statistically independent. The micro-computer uses a real-time clock to begin the sampling period at the prescribed time. At the end of the sampling period, the mean, standard deviation, and minimum and maximum values of each time difference are

recorded. Depending upon the number of signals being observed, available memory will hold from 10 to 20 days of data. Phone line access to the micro-computer allows retrieval of the stored data. It also allows a remotely located operator to prompt the computer to exercise any receiver command which a local operator could enter via the front panel controls. Finally, the entire micro-computer program can be changed via the phone line. The concern about the adequacy of this type of data for the study at hand was introduced in Section 1.3. Reference 2 addresses the "adequacy" question to a certain extent and more comments will be provided in the body of this report.

Regardless of the question of "inadequacy," a Harbor Monitor Set was installed at Eisenhower Lock, Massena, N.Y. on 21 October 1981 because it met one vital criterion: it was immediately available for deployment. Data suitable for low density analysis has been obtained from the Massena Harbor Monitor set from October 1981 to date and is presented in subsequent sections of this report.

On 1 February 1982, an additional Harbor Monitor Set was installed on USCG property at Tibbetts Point (Cape Vincent) N.Y. Subsequently, the Harbor Monitor Set was relocated to a nearby facility in the area. Data from the site(s) from 2 February 1982 to date is available and is discussed in this report. Figure 2-2 shows the harbor monitor set installed at Massena.

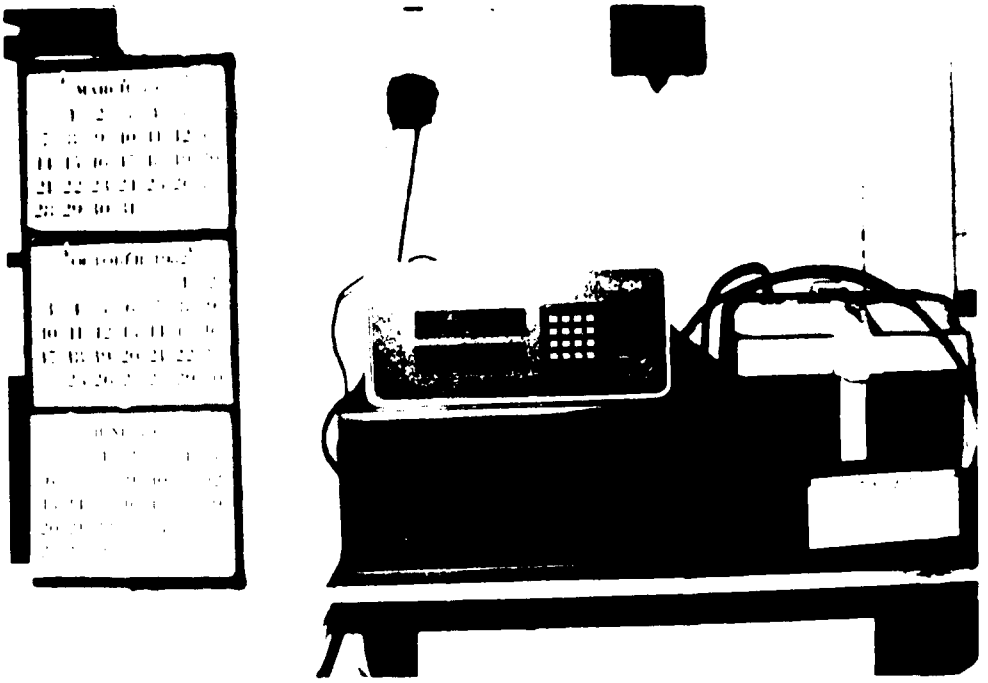

Figure 2-2 Harbor Monitor Set at Massena, N.Y.

2.2 CCG Loran-C Buoy Auditing Equipment.

The Canadian Coast Guard had been in the process of developing protoype equipment sets to support a program of auditing the position of buoys via Loran-C. The equipment is comprised of an Internav 404 Loran-C receiver (the same receiver used with the Harbor Monitor Sets), a Motorola microprocesser and a Texas Instruments teleprinter/data recorder. By using data recording cartridges, the sets are capable of storing significantly more data than the Harbor Monitors - thereby allowing a true "high density" analysis of the loran data. Figure 2-3 shows the prime components of the system in block diagram form.

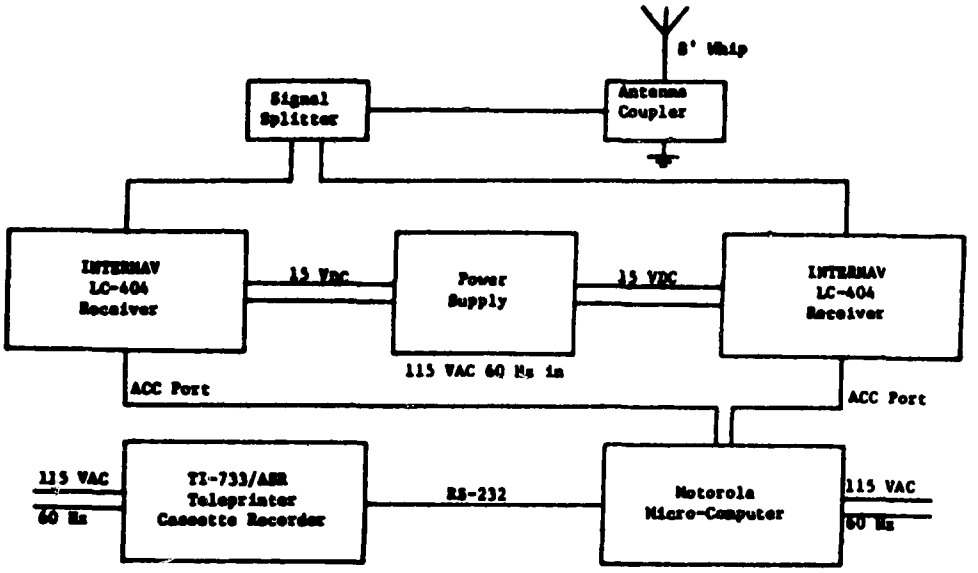

Figure 2-3 Buoy Auditing Set Block Diagram

Two receivers are used because of a buoy auditing project requirement. The micro-computer obtains samples of the data from the receivers approximately once every 2 seconds. After 100 samples are obtained, the micro-computer sends the computed mean and standard deviation of the time differences to the cassette recorder. Such data is recorded throughout the day and the cassettes must be changed about every fourth day.

The only major drawback of this equipment set is that it cannot be remotely accessed. Consequently, monitoring of the equipment status by experienced project personnel is not possible on a day-to-day basis (nor is it necessary - for the buoy auditing project). An additional drawback is that the units were still in the development stage when they had to be

pressed into service for the purposes of this study. Thus, this is actually the first true field test and evaluation of the units. The first set was deployed at Fort Wellington on 9 February 1982. Due to electrical grounding problems at the sites, no useful data was obtained. The site was moved several hundred yards to where a good equipment ground could be established on 11 March 1982 and good results were achieved. Soon, however, power and equipment problems, causing loss of data from 2 to 19 April 1982, were encountered. On 20 April 1982, the equipment was relocated to the nearby Prescott CCG Base. A second set was installed at Iroquois Lock, Ont. on 21 April 1982. Although data suitable for "high density" analysis has been obtained, only that subset of the total data base which is compatible with the Massena and Tibbets Point data base is analyzed in this report. Figure 2-4 shows the Buoy Auditing Equipment at Iroquois Lock.

Figure 2-4 Buoy Auditing Set at Iroquois Lock

2.3 "AD HOC" Loran-C Data Collection Units.

Because of the limited availability of either Harbor Monitor Sets or Buoy Auditing Sets, along with the need to get data from several sites as soon as possible, extraordinary means were taken. USCG had additional Internav 404 Loran-C receivers available. Texas Instrument teleprinters were also available for recording data directly from the receivers (without an intervening micro-computer). Figure 2-5 shows the prime components of the system in block diagram form.

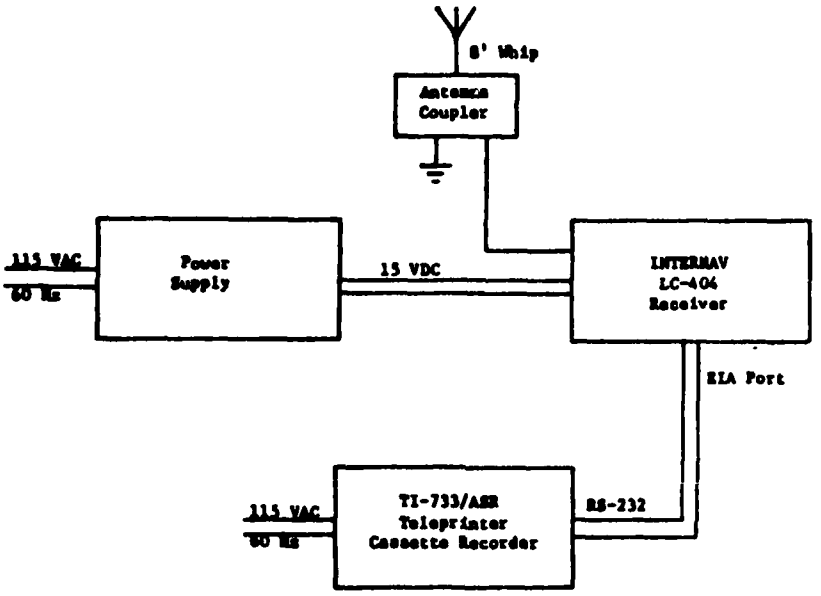

Figure 2-5 Ad Hoc Equipment Set Block Diagram

Via front panel entry, the receiver can be made to automatically send a message to the teleprinter at a rate of some integer multiple of 10 GRI. Originally, the setting was every 6020 GRI which, for rate 9960, resulted in a message about every 10 minutes. At that rate, cassette tapes had to be changed about every 10 days. In late April 1982, the sampling rate was changed to one sample about every 3 minutes.

The output message consists of an instantaneous sample of the output of each servo loop (including the master servo loop) along with the receiver's current estimate of the signal-to-noise ratio for each station being tracked. The entire message is recorded on the cassette. As a general comment on the receiver, special notice should be made of the master servo loop output as shown in the column labeled "GRI" in the figures of Appendix F (e.g., figures F-1, F-2). For the 9960 chain, the reading would ideally

be 99600.00. A deviation from this reading provides the operator with an indication of the internal oscillator stability (adjustment recommended if the reading differs by more than 0.20 from the ideal). More importantly, the receiver software applies a portion of this offset (computed as the ratio of the TD to 99600) to correct the measured time difference for oscillator error.

Off-line averaging of these samples can be accomplished to make the data more nearly compatible with the HMS data. As with the data obtained from the buoy auditing sets, only the subsets of the total data base which correspond to HMS data are obtained and analyzed in this report. Figure 2-6 shows the "Ad Hoc" Equipment at Beauharnois Lock.

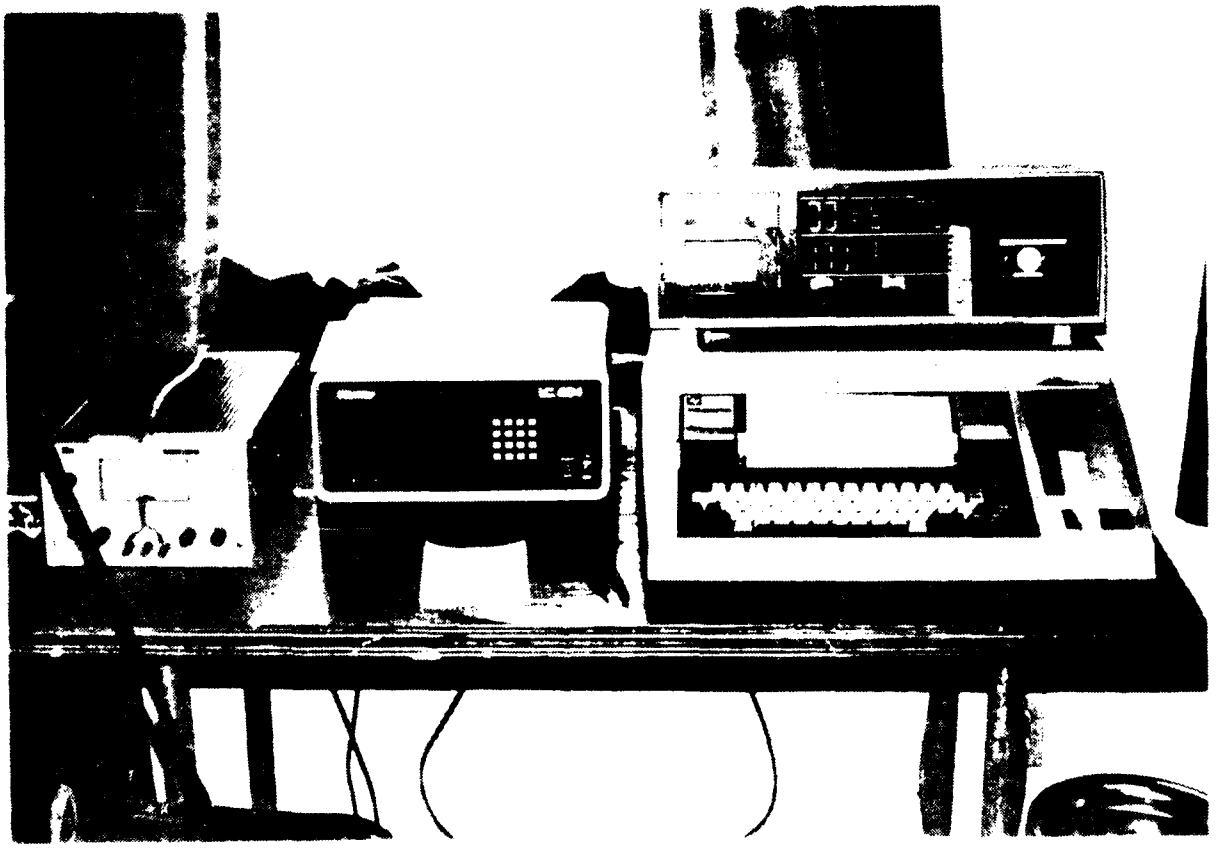

Figure 2-6 Ad Hoc Equipment Set at Beauharnois Lock

The Ad Hoc equipment approach to data collection is suboptimal for numerous reasons which will be discussed in later sections. Primarily, it requires periodic operator assistance and, without the ability to remotely

access the data, the day-to-day operation of the system cannot be properly monitored. Nevertheless, the sets were deployed at CCG sites at Beauharnois, and Cote Ste. Catherine, and at the USCG station at Tibbetts Point in late December 1981. Similar CCG equipment was installed at Iroquois Lock on 17 March 1982. Failure of the teleprinter at Tibbetts Point resulted in the loss of data at that site. For this reason, the equipment was replaced, as discussed in Section 2.1, as soon as a harbor monitor set became available. The equipment at Iroquois Lock was replaced on 21 April 1982 as discussed in paragraph 2.2 above. A series of problems was encountered at Cote Ste. Catherine so this site was shut down on 5 May 1982 and a nearby site was established at the St. Lawrence Seaway Authority facility at Brossard.

The locations of these and all other monitor sites are indicated in figure 2-7. On a smaller scale, figure 2-8 shows the relation of the Seaway to the stations of the Loran-C triad which provides the signals examined in this report.

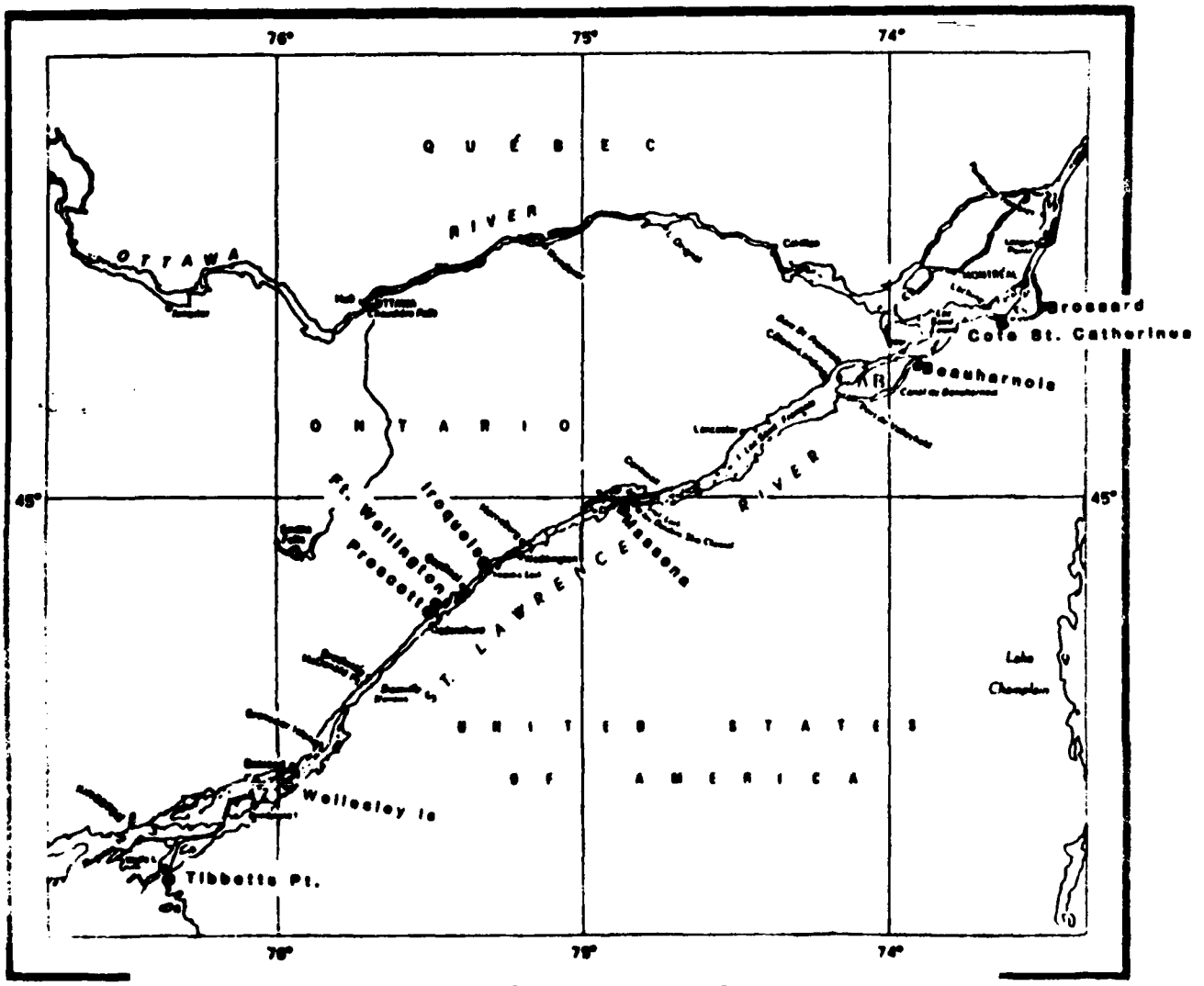

Figure 2-7 Location of St. Lawrence Seaway Loran-C Data Collection Sites

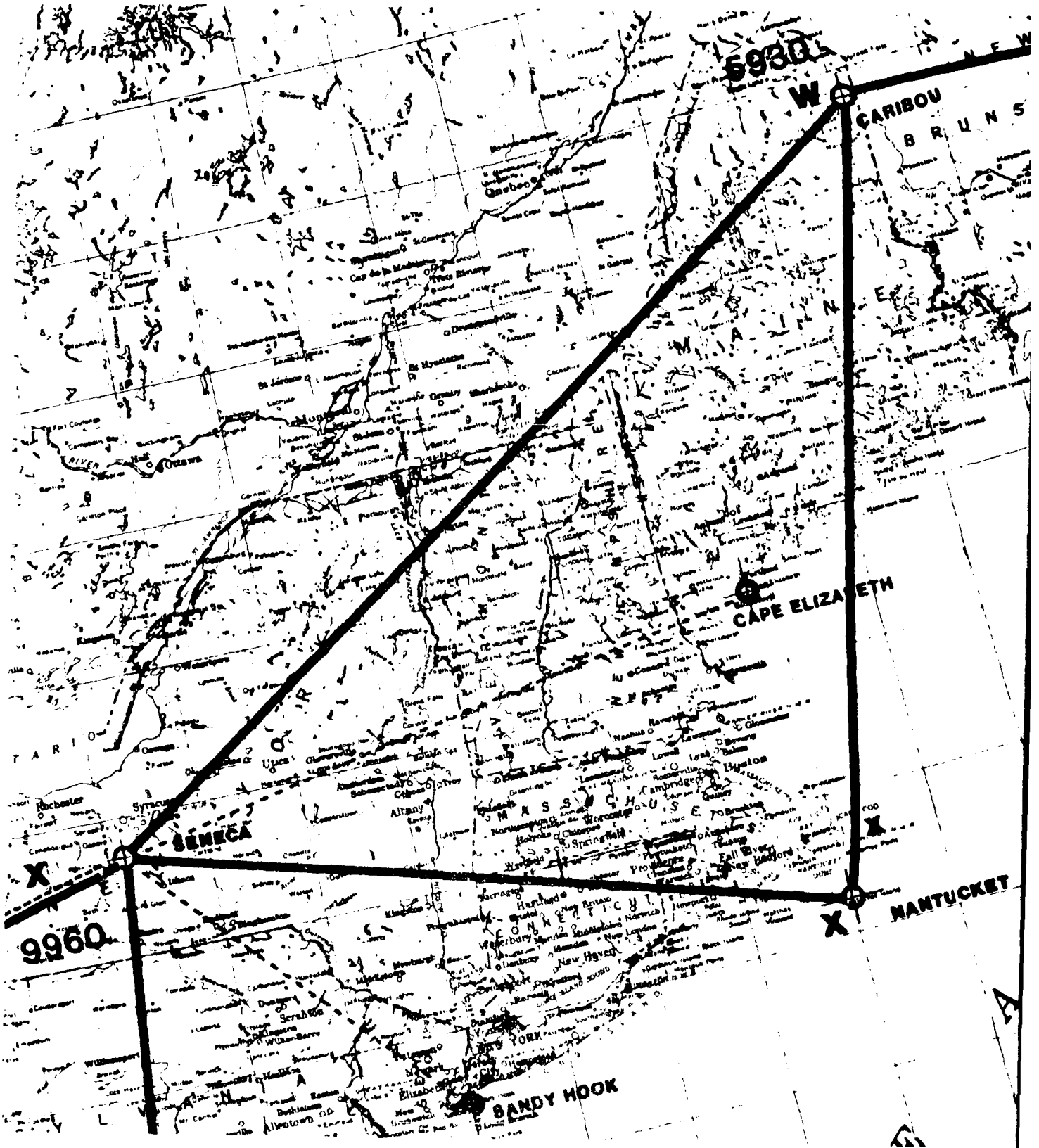

Figure 2-8 9960-W/X Loran-C Triad Stations

2.4 Improved USCG Harbor Monitor Sets.

As mentioned in Section 1.3, the Harbor Monitor Set described in paragraph 2.1 is deemed adequate for original USCG Harbor Monitor project needs. During the past year, however, several additional applications, for which the equipment is not ideally suited, have become apparent. For reasons such as this, USCG has taken steps to develop a more general purpose set. The set features an off-the-shelf micro-computer (both of the sets described in paragraphs 2.1 and 2.2 above require user hardware development), will allow for high density data storage and can be accessed/controlled from a remote location via telephone. Perhaps more importantly, the sets have been developed to incorporate receiver automatic control features which over a year of harbor monitor experience has shown desirable.

Engineering development of these units was completed by USCG Research and Development Center personnel in early May 1982 and a test "field deployment" was started in mid-May. These units, called "Type D Harbor Monitors," will be available for other deployments in the August 1982 timeframe and are mentioned later in this report for consideration.

2.5 Data Collection Set Compatability.

As this report will show, it is possible to make "low density analysis" comparisons among the data collected by the myriad equipment deployed thus far. The basic approach, however, is extremely time-consuming and yields statistically sub-optimal results. A secondary purpose of this report will be to address the suitability of each type of set and make recommendations for future data collection efforts.

3. PERFORMANCE PREDICTIONS.

3.1 Need For A Prediction Model.

In conducting a Loran-C stability study, one is initially faced with several experimental design problems. For the portion of the St. Lawrence Seaway of interest - nearly two hundred miles in length - the first important question involves spacing of monitor sites. Although no formal deterministic proof can be offered, it is reasonable to assume that if a monitor site were located at every mile along the river, adequate knowledge of the spatial nature of the variations could be obtained. As a practical matter, and besides involving prohibitively expensive site installation costs, it would not be possible to obtain suitable sites in all cases at such a spacing. Additionally, site operation and maintenance would become an unmanageable effort. Thus, it becomes necessary to settle for a much smaller number of monitor sites. Even with only six sites, the establishment of suitable sites - particularly in a rushed timeframe - and operating and maintaining the site equipment - become non-trivial tasks. (The brief history of the sites provided in section 2 gives an indication of the scope of the problems. More examples will be shown throughout the report). The availability of data from six sites is therefore the best we can hope for and it is no longer reasonable to blindly assume we have an adequate number. Clearly, the need for a site spacing methodology, such as could be obtained if an adequate model were available, exists.

Another experimental design problem involves the time between samples. Again, although no formal proof is demanded, all involved will feel comfortable with samples obtained every second of the year (including leap seconds where appropriate) from each site. Even with only six sites, sampling at the rate mentioned above involves the accumulation of well over 1 billion bytes of "data" over the period of a year. In these days, such a data base can be constructed at a small cost. This having been said, a disclaimer is in order. Whereas all involved feel comfortable if such a data base, consisting of "known-to-be-valid-data" is presented to them, nobody cares to assume the responsibility to assure, or pay someone to assure, all of the data is valid. This "data base integrity" problem (as opposed to data base storage or data base manipulation) is an elementary concept introduced early in management information system courses/seminars (in the 60's the buzzwords were different, the concept was known as "garbage-in-garbage-out." Only the size of the problem has changed - by orders of magnitude). Numerous examples of invalid data will be presented later in this report along with suggested corrective action for future data collection efforts. It will suffice at this point to simply note that the "once per second" sampling strategy, given available resources, exceeds our analysis (including editing) capabilities by several orders of magnitude. A less intense sampling strategy is needed. Again, this translates to a need for a model of the variations.

3.2 System Requirements.

Although numerous models of loran system variations have been developed over the years, none are perfect. Additionally, most are not directly applicable to the types of questions that must be addressed in the St. Lawrence Seaway study. For this reason, this report will involve significant discussions of modeling techniques which the authors feel are most useful for our purposes.

It is noted that early discussions of the Steering Committee concentrated heavily on questions of sampling strategy. A key source of disagreement centered on the fact that the navigation system requirements were not properly stated (or understood). For example, as late as February 1982, the SLSDC received a report from a contractor identifying "Loran-C Requirements" in various reaches of the river. For many of the reaches, (i.e., those with "half-channel widths" of 100 feet or less) it was indicated that Loran-C should produce a cross-track error, 99.9% of the time less than about 7 meters. At about the same time (specifically, at the 17 February 1982 meeting of the Steering Committee) USCG presented the plot shown in figure 3-1. It is noted here that figure 3-1 shows no half-channel width of less than 200 feet (61 meters).

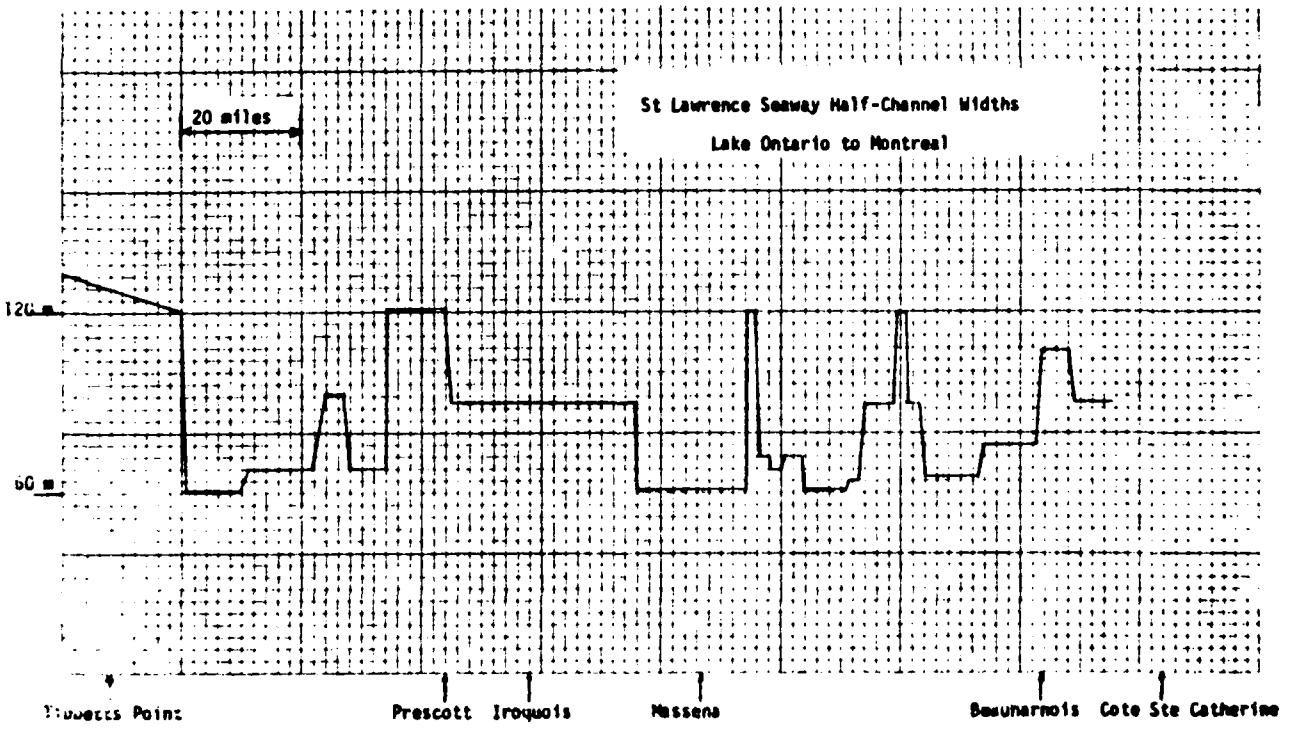

Figure 3-1 Preliminary Description of St. Lawrence Seaway Half-Channel Widths

It should also be noted that USCG was neither trying to "sell Loran-C" nor "kill Loran-C." It was simply assumed in February (and will be shown herein) that Loran-C cannot give 7 meter accuracy 99.9% of the time in the St. Lawrence Seaway. If 7 meters (99.9%) is indeed a valid Loran-C requirement, then this report will serve the purpose of proving Loran-C will not work. If however, other means can be employed in certain reaches (street lights can be used in several of the reaches for which Loran-C was stated as being required), then the job becomes more difficult and we are forced to continue.

The report will proceed under the assumption that it is worthwhile to consider the question: "what will it take for Loran-C to provide accuracy on the order of 25-30 meters?" Under this assumption, vice the 7 meter accuracy criterion, it becomes possible to construct a reasonably useful error model and both the sampling strategy and the number of monitor sites becomes appropriate for answering the questions being asked.

3.3 The Nature of Loran-C Positional Errors.

We have concluded the previous section without explicitly stating the Loran-C performance requirement. The need to take this approach can be seen by examining early Steering Committee attempts at accuracy requirement statements. Specifically, very early in the study, considerable time was spent trying to find a suitable performance metric. Such figures of merit as "CEP" or "d-rms" were scrutinized for applicability. As part of the presentation made at the 17 February Steering Committee meeting, USCG emphasized the concept of the error ellipse - the pattern of positional errors in the fixes provided by Loran-C and most other positioning systems. The concept is well illustrated in figure 3-2 which was obtained by processing harbor monitor set TD data using the math of Appendix A. The data was obtained at Groton, Ct. during the period 1 January to 31 March 1982.

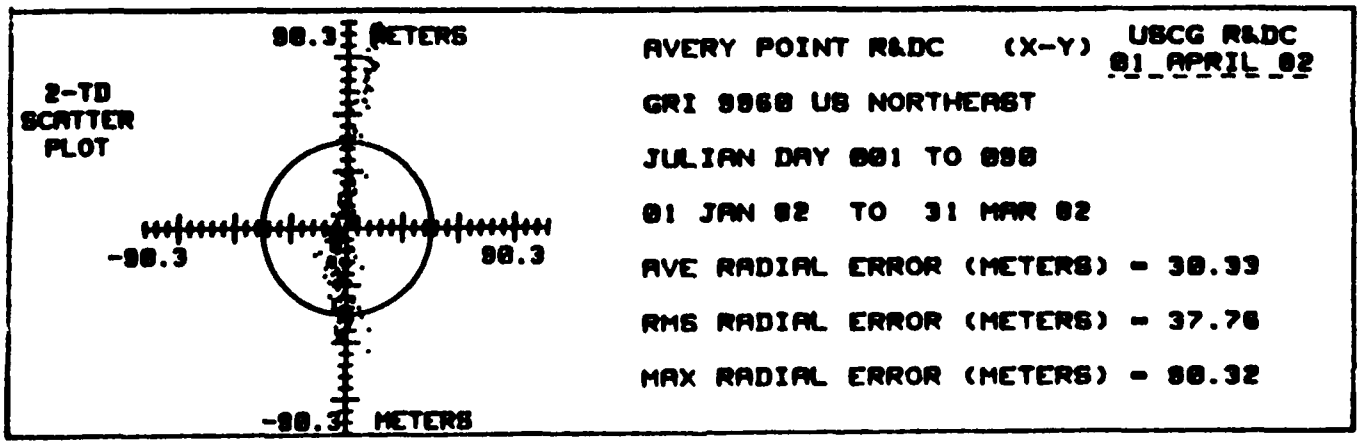

Figure 3-2 Fix Scatter Plot of Loran-C Fixes at Avery Point (Groton)

Figures of merit such as CEP or d-rms are very useful in considering large scale, general accuracy questions such as those involved in general loran chain planning. For questions relating to use of existing loran coverage in the St Lawrence Seaway, however, the requirements are too demanding for general metrics. We must concentrate on specific requirements and, for the Seaway, this means cross-track error. As can be seen from a quick glance at figure 3-2, the error pattern at Groton is predominantly oriented at a bearing of about 000° T. If the course of a particular channel in the Groton area were 000° T (it is!), cross-track errors less than about 10 meters could be expected almost all the time. Alternatively, for a course of 090° T, cross-track errors as large as 90 meters can be reasonably expected. This order of magnitude swing in error as a function of course is an extreme example but illustrates the significant contrast with the "one-dimensional" metrics such as CEP or drms which do not change as a function of course.

In considering existing loran coverage errors, along with alternative configurations (e.g., as obtained by the use of differential corrections), we cannot afford to be so imprecise as to consider only d-rms or CEP. Detailed application of this concept will be explored in later sections. For now we simply note that error ellipses and associated cross-track error performance should be estimated for each reach requiring Loran-C. This having been said, we can return to a discussion of system requirements.

In 1978, the SLSDC received a contractor report (reference 3) outlining the characteristics (including course and minimum channel width) of the 103 reaches of the Seaway from Montreal harbor to Tibbetts Point. In March 1982, SLSDC received a report from another contractor which integrated the reach characteristic table with a preliminary statement by the Steering Committee regarding navigation system performance. The statement was that the cross-track error of the navigation system should be 5 meters less than 20% of the channel width - 99.9% of the time. The resulting tabular presentation of requirements is included in Appendix E. At the May 1982 Steering Committee meeting, the Seaway Authority presented a further refinement of this table. This version approaches that of figure 3-1, with more detail, and is also provided in Appendix E. The table is converted to a "half-channel-width" plot and shown in figure 3-3.

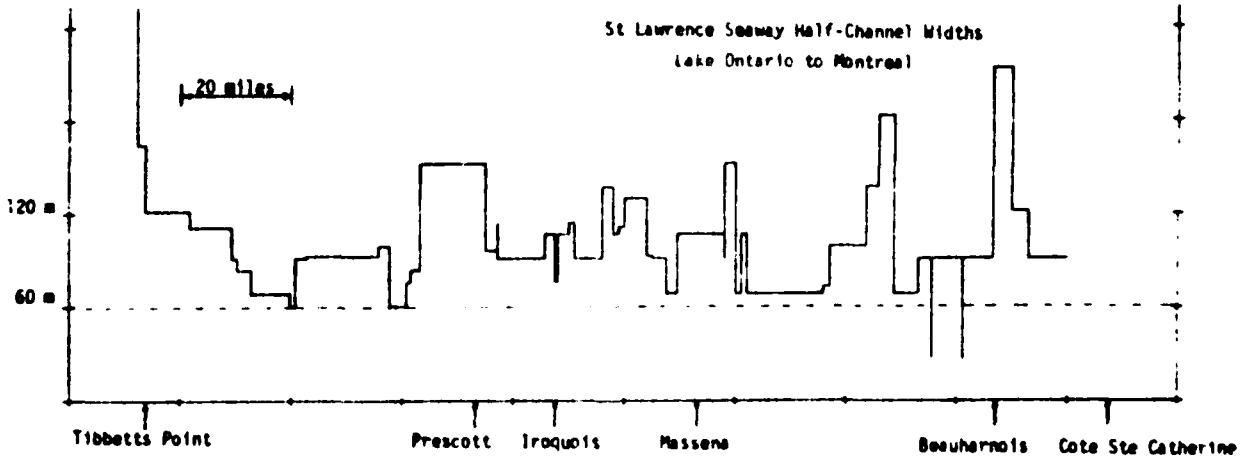

Figure 3-3 Updated Description of St. Lawrence Seaway Half-Channel Widths

The two "spikes" shown just south of Beauharnois represent bridges. In this report we will assume Loran-C is not required to navigate under these structures.

At this point in the discussion of system requirements, i.e., having identified cross-track error and channel width as key ingredients, we move to a consideration of the Loran-C system to complete the discussion.

3.4 Basic Model - The Double Range Difference.

As developed in Appendix A, we can generate error ellipses for any point along the river as soon as we can obtain a measure of the standard deviations of the TD's produced by the two major Loran-C baselines in the area (9960-W and 9960-X) along with a measure of the correlation coefficient between the two baselines. In spite of the fact that the literature is replete with references to these three quantities, it is unfortunately true that they are, strictly speaking, totally fictitious. In obtaining data from the monitor sites, we are obtaining samples of random processes. Over the period of a year, these processes cannot be considered stationary - even in the widest sense. Specifically, this means we are collecting observations of random variables whose means, standard deviations and correlation coefficient change from time to time. Thus the math of Appendix A, or any number of similar developments, cannot be directly applied.

Moreover, the development of Appendix A and related treatments assume the variations are Gaussian in nature. Again, strictly speaking, this is not true. Thus, again, direct application cannot be made.

All of this simply means that we must be clever in our modeling and analysis techniques. The Gaussian assumption is popular because it very nearly approximates the nature of variations encountered in many applications. As will be developed, we need to break the total data variation model down into its constituent parts and on a case-by-case basis, determine ways to approximate the Gaussian model. Although numerous statistical methods exist to check for the validity of the Gaussian assumption, we will shy away from these more rigid treatments in this report and simply use examples extracted from the data base to illustrate applicability of the model.

With proper attention to details of the model, along with use of the concepts provided in Appendix B, considerable headway can be made in examining the suitability of Loran-C to satisfy some St. Lawrence Seaway navigation requirements.

The major constituents of the Loran-C time difference variations are as follows:

a. Seasonal Component. This component, in most cases, is the largest contributor to the net error budget. It has a period of 1 year. Examples of this type of variation are discussed in Appendix B and shown in figure 3-4. If the time series of figure 3-4.a is "low pass filtered" by use of a 4-week sliding average, a "smoothed TD" data plot, as in figure

(a) Actual Data From 9960-W Baseline

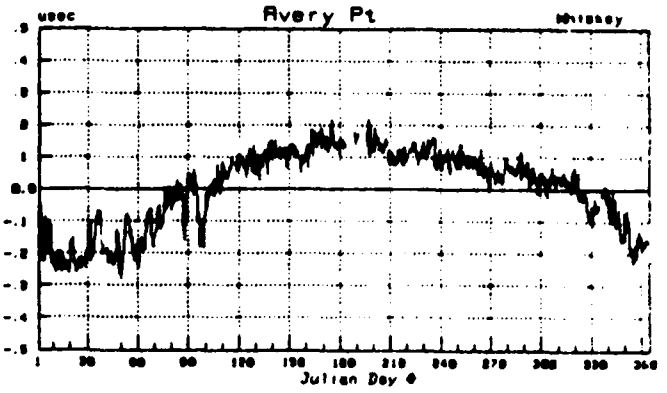

(b) Sliding 21-Day Average

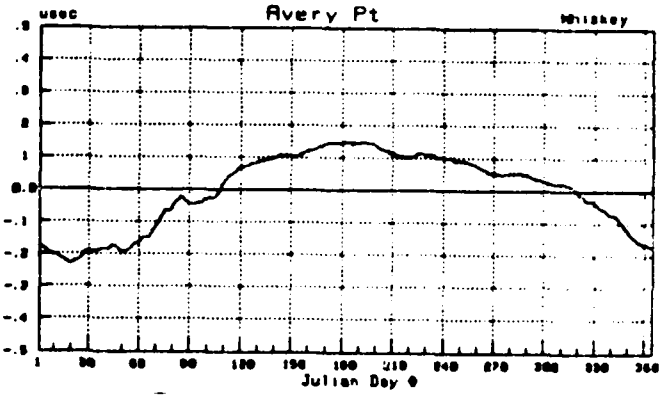

(c) "Residuals"

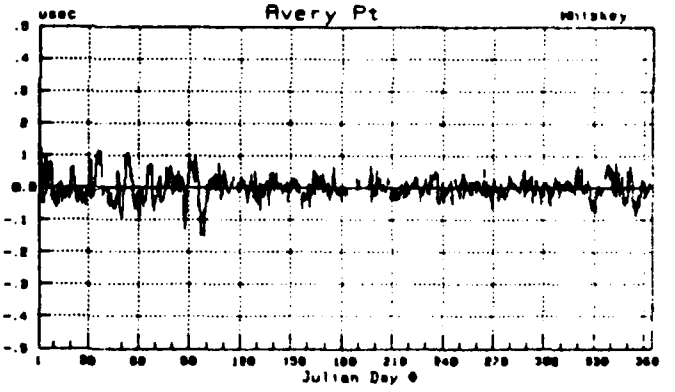

Figure 3-4 9960-W Loran-C Data at Avery Point, Ct.

3-4.b results. The peak-to-peak value (or any related measure such as zero-to-peak or rms value) is found to closely follow the "modified" double-range difference (DRD) model which is described in detail in Appendix B. Basically, DRD (measured in kilometers) is a direct measure of what hyperbolic LOP the user is "on" with respect to the hyperbolic LOP of the System Area Monitor (SAM). If the observer is on the same LOP as the SAM, the DRD is zero. If the observer is on an LOP which is closer to the master station than the SAM's LOP is, the DRD is positive. As developed in Appendix B, we have found it necessary to not count saltwater paths in the calculation of DRD. The regression analysis plotted in figure 3-5 illustrates this "goodness of fit" of the seasonal variations as a function of DRD for the 9960-W and -X baselines. Given the slowly varying nature of

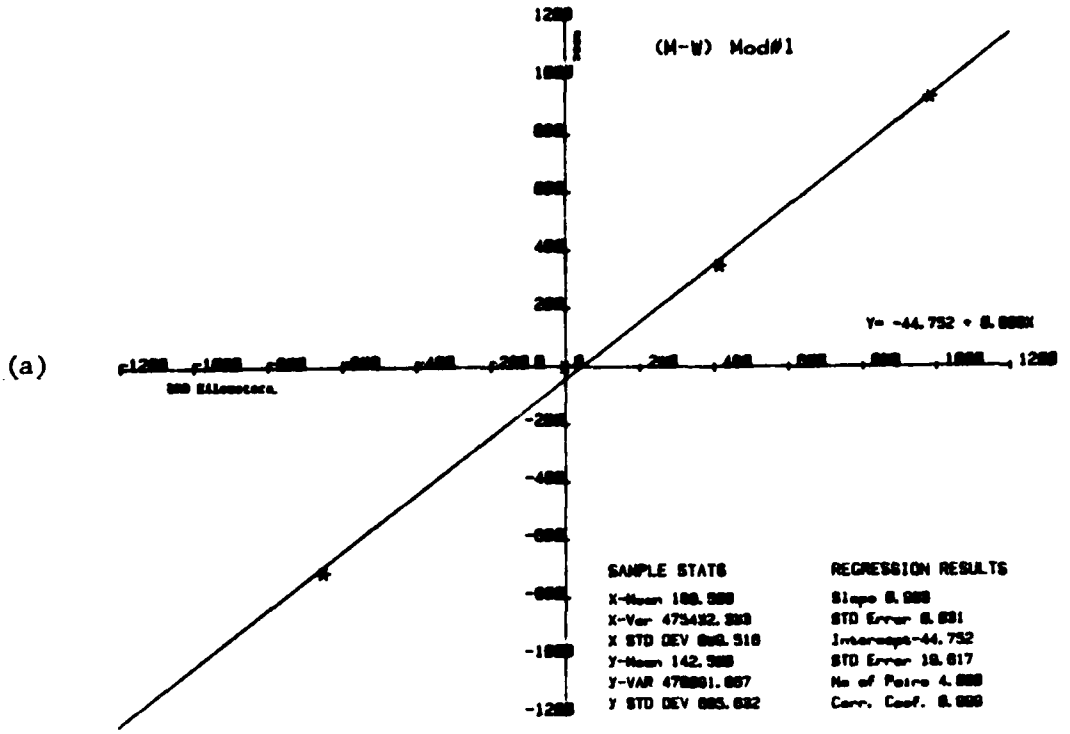

(a)

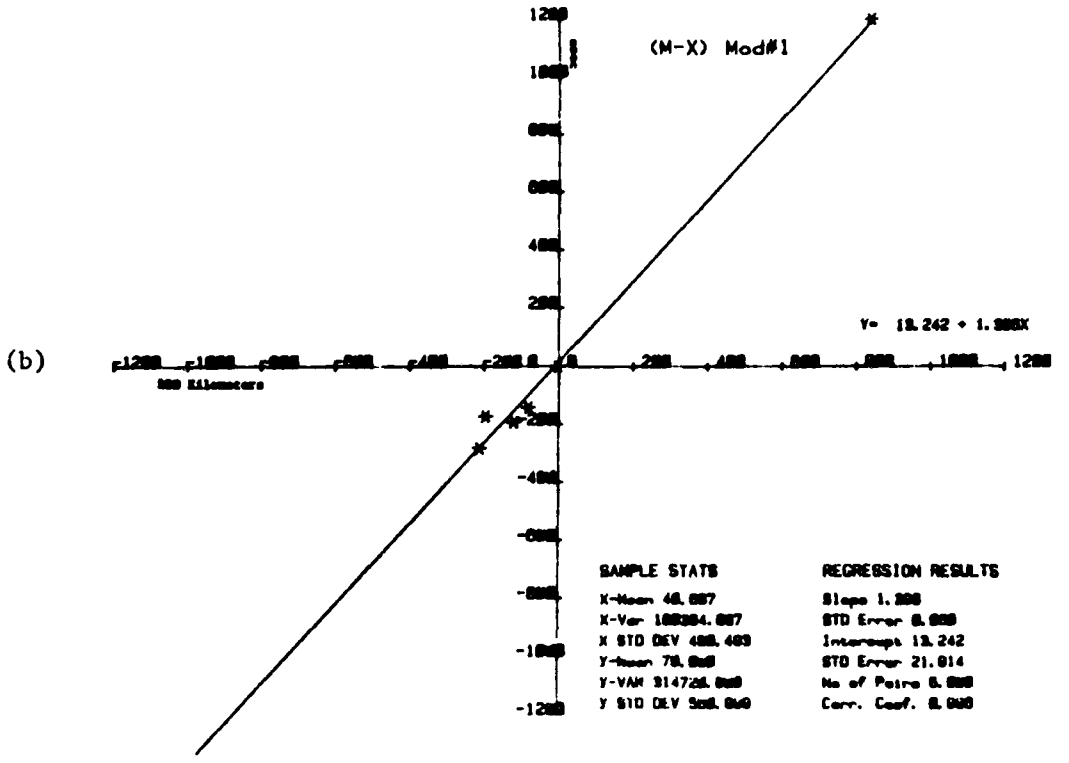

(b)

Figure 3-5 9960-W/X Regression Lines: Seasonal Loran-C TD Variations vs Modified Double Range Difference

this error component, the twice a day sampling strategy used in the low density analysis is entirely adequate for measuring, and hypothesizing correction schemes for, this type of error.

b. Medium-Term Component. Here we are talking about variation occurring over periods ranging from several days to several weeks. Examples can be seen in figure 3-4.c in which the seasonal component has been removed from the total data record (accomplished by subtracting the data in figure 3-4.b from the data in figure 3-4.a). It can be seen that these variations are typically smaller than the seasonal variations and that the "magnitude" of the variations differs from season to season. The variations are most significant in the winter months -extending from late October to late April in northern regions. They are minimal in the summer. In a statistical sense, these variations are found to follow the modified double range difference model very well. Twice a day sampling is adequate to measure the variations and form the basis for a correction strategy.

c. Short-Term Component. These variations occur over periods ranging from several hours to a few days. The fact that these variations can occur as rapidly as within a few hours is the prime reason for the concern which has been expressed by the Steering Committee. It is agreed that the low density sampling strategy is not adequate for a deterministic statement of the size of these variations. It is noted, however, that significant variations over a period of several hours are rare occurrences. Moreover, the variations are smaller than the seasonal or medium term components. Finally, since most of the examples of variations assigned to this category occur over the period of a day or so, the low density analysis provides an adequate statistical measure of the size to be expected. Concentration on the larger components, augmented with this statistical measure of the short-term component, is argued to be the correct strategy for proper use of the resources presently available.

d. Near-Instantaneous Variation Component. These are considered to be any variations which occur over the period of up to an hour or so. These variations, for practical purposes, are considered to be equipment related and not associated with changes in signal propagation characteristics. Examples can be seen when equipment is changed at transmitting stations, when corrections are made to chain timing by the control station, or when there are receiving equipment problems. These variations are small but cannot be considered negligible when considering the capability of Loran-C for precise applications. In general, no attempt need be made to measure these types of variations by use of remote monitors. Observations of the effects can be obtained by examining chain operating records and by laboratory measurements or simulations. The lab measurements should be merged with the field measurements to obtain the total error description. For the purposes of this study, we will be concerned with these type variations only to guard against their effects creeping into our instrumentation (i.e., make sure our receivers are installed/operated properly).

3.5 Application of Model Using A Priori Estimates.

Reference 4 featured a direct application of the double range difference model described in Appendix B. An ultimate goal of the St. Lawrence Seaway studies will be to duplicate the analyses as well as adding refinements such as the modified range calculation presented in Appendix B. Unfortunately, for reasons already alluded to and to be illustrated in section 4, we simply do not yet have the data base to allow direct application of the model. Thus we will present a crude, "first cut" analysis based on USCG harbor monitor program data obtained at sites outside the St. Lawrence Seaway region. Since these performance predictions are made without considering any St. Lawrence Seaway data, we call them "a priori" estimates.

The presentation will be primarily heuristic and serves the purpose of illustrating the role of key parameters that must be estimated before the data collection effort can be called a success. An auxiliary purpose is to show how much can be done with no St. Lawrence data. How very little we can presently go beyond this level illustrates how subpar the data collection results to date have been.

We begin by noting Appendix A allows us to state the performance at any Seaway reach if we can obtain estimates of σ_w, σ_x and ρ_{wx} - the standard deviations of the two prime TD's in the area and the correlation coefficient between the TD's - at any point of interest. We have previously noted that these quantities vary. For our first cut at estimating performance, however, we will ignore this technicality.

Appendix C contains the details of the estimation procedure. In it we first look at the seasonal component of the time difference variations. We argue that this component is so predominant in the St Lawrence Seaway region that we can closely approximate the year-round standard deviations by considering only this component. We compute estimated peak-to-peak variations for each TD at the center of each reach. We argue the seasonal variation pattern is approximatedly sinusoidal and equate the rms value of a sinusoid with the indicated peak-to-peak value to the appropriate standard deviation. Thus we obtain estimates of σ_w and σ_x for each reach.

To estimate the correlation coefficients, we argue the seasonal components have a correlation coefficient approaching unity. Using arguments suggested by Ligon in reference 5, we argue the "shorter-term" components have a correlation coefficient of about 0.5. We show how a total correlation coefficient is formed from a weighted combination of these constituents. A total correlation coefficient value of at least 0.95 is most likely but we choose a more conservative estimate (results in larger predicted errors) of 0.90 and use this value for all reaches. Resulting "95% probability contour" ellipses are generated for each reach - and listed in Appendix D. The projections of these contours on corresponding cross-track/along-track axes are computed as explained in Appendix A. The resulting cross-track errors are listed in Table 3-1.

Reach #	Course	Reach Center	Half-Width	"Raw" CTE Prod #1	Reach #	Course	Reach Center	Half-Width	"Raw" CTE Prod #1
1		- - - - - - - - - -	N/A	- - - - - -	43	237	44-02.4/75-14.0	91	203
2	256°T	45-56.1/73-46.3	91 m	113 m	44	227	44-01.0/75-15.0	114	216
3	226	45-52.9/73-48.6	91	152	45	248	44-01.6/75-16.0	107	186
4	241.5	45-50.0/73-52.1	122	146	46	241.5	44-01.0/75-17.2	107	198
5	218	45-19.0/73-54.4	213	184	47	284	44-00.0/75-19.3	76	222
6		- - - - - - - - - -	N/A	- - - - - -	48		- - - - - - - - - -	N/A	- - - - - -
7	208.5	45-16.6/73-55.0	91	149	49	286	44-00.2/75-19.4	107	222
8	226	45-15.0/73-58.6	91	156	50	227	44-00.1/75-20.0	91	218
9	237	Included with 11	91	152	51	236.5	44-00.4/75-23.4	91	207
10		- - - - - - - - - -	N/A	- - - - - -	52	221.5	44-00.4/75-25.2	91	225
11	248.5	45-13.0/74-00.7	91	141	53	236	44-00.5/75-25.7	91	207
12	270	45-13.2/74-04.4	91	108	54	238	Included with 53	114	207
13		- - - - - - - - - -	N/A	- - - - - -	55	220	44-43.6/75-28.2	96	228
14	287.5	45-13.0/74-00.7	91	70	56	238	44-02.6/75-29.0	182	208
15	263.5	45-13.2/74-12.2	68	126	57	223	44-39.9/75-33.6	152	229
16	262.5	45-12.9/74-16.4	182	162	58	231	44-35.7/75-38.2	182	223
17	269	45-11.6/74-18.4	137	172	59	223	44-35.2/75-40.8	83	235
18	234.5	45-09.3/74-22.3	99	171	60	233	44-34.4/75-41.8	76	222
19	268.5	45-07.6/74-25.2	73	126	61	236	44-33.8/75-42.4	61	217
20	229	45-07.0/74-27.9	68	179	62	222	44-33.2/75-43.2	61	237
21	267.5	45-05.9/74-29.2	89	178	63	217	44-31.8/75-46.1	99	241
22	226	45-04.6/74-31.0	68	181	64	194	44-29.5/75-46.5	93	233
23	230.5	45-03.1/74-33.3	68	172	65	218	44-28.4/75-48.4	93	237
24	253	45-02.6/74-35.0	89	133	66	216	Included with 65	93	- - -
25	241	45-01.8/74-37.6	68	172	67	259	44-28.0/75-50.4	93	243
26	299	45-00.7/74-39.7	68	186	68	207	Included with 67	93	243
27	236	45-00.1/74-40.4	107	178	69	226	44-22.8/75-52.6	93	232
28	278	45-00.2/74-41.6	68	97	70	228	Included with 69	93	232
29	234	44-59.7/74-43.2	152	183	71	218	44-20.0/75-54.9	91	242
30	257	Included with 31	91	127	72	214	Included with 71	61	242
31	267	44-59.4/74-44.5	107	122	73	219	Included with 71	68	242
32		- - - - - - - - - -	N/A	- - - - - -	74	235	44-18.1/75-58.9	68	220
33	257	44-57.9/74-56.2	68	157	75	236	Included with 74	68	242
34	257	44-57.4/74-58.6	91	157	76	231	Included with 74	68	242
35	233	44-57.0/75-00.3	93	200	77	239	44-16.2/76-02.6	83	216
36	248.5	44-56.4/75-02.4	130	177	78	228	44-16.4/76-04.5	91	238
37	282	44-55.8/75-04.8	130	148	79	246	44-13.6/76-09.4	111	199
38	233	44-55.6/75-05.8	111	204	80	263	44-12.8/76-16.1	122+	148
39	295	44-55.1/75-07.3	107	166	81	183.5	44-10.8/76-19.4	122+	275
40	220	44-54.6/75-08.6	137	215	82	213	44-07.2/76-22.1	168	275
41	237.5	44-53.4/75-10.4	91	199	83	234	44-03.6/76-25.9	381	242
42	256	44-52.8/75-12.2	91	166					

Table 3-1 "Raw" Loran-C (9960-W/X) Cross Track Error (Preliminary) 95% Probability Predictions for St. Lawrence Seaway Reaches

A comparison of the predicted cross-track errors and corresponding half-channel widths shows that "un-augmented Loran-C" simply cannot yield satisfactory year-round performance: the error ellipse extends well outside the channel in 95% of the reaches. Thus the need for differential corrections of some sort is indicated.

Before proceeding to a consideration of differential corrections, we should make a statement about the probability contour used. If the random variables were truly Gaussian (normal), we would not be satisfied with the 95% contour - exceeding the channel boundaries 5% of the time is clearly an unacceptable performance goal. However, we have already noted we have a distribution which follows a nearly sinusoidal pattern - i.e., one distinctly different from the Gaussian distribution, particularly regarding extremes of variation. We can illustrate the difference by comparing a one-dimensional sinusoid to a Gaussian random variable. A gaussian random variable remains within two standard deviations of the mean about 95% of the time. It remains within three standard deviations of the mean about 99.75% of the time. Thus, if a time difference were truly Gaussian distributed, we would expect year-round experimentation to show that if the deviation from the mean exceeded some value, say X, 5% of the time, it would exceed the value 1.5 X 0.25% of the time.

For the sinusoid-type variation we expect to see in the St. Lawrence Seaway, this will not be the case. For a pure sinewave, for example, simple trigonometry shows the deviation from the mean which is not exceeded 95% of the time is about 99.7% of the zero-to-peak value. Thus, if X again represents the deviation from the mean which is only exceeded 5% of the time, 1.003 X represents the value never exceeded. We simply mention all this in passing - along with an observation from the harbor monitor program that, in situations wherein the seasonal component is predominant, the "95%" error ellipse closely approximates the maximum error (i.e., 100% probability) contour. Thus the cross track errors listed in Table 3-1 are good estimates of the maximum expected error. The sinusoidal vice Gaussian nature of the variations is the reason why.

We should now move the discussion to predictions of differential Loran-C performance. As outlined in Appendix C, we hypothesize a differential monitor station at the Eisenhower Locks near Massena, N.Y. We show how it is necessary to re-compute the double range differences and corresponding standard deviations for the seasonal component of the variations. The "differential action," in most reaches, removes a considerable portion of the seasonal component of the variation so that it is no longer appropriate to ignore the shorter term components in estimating the total variation. Additionally, it becomes necessary to compute a separate estimate of the total correlation coefficient for each reach. We hypothesize a representative short term noise standard deviation (20 nanoseconds) and, using the formulation of Appendix C, devise appropriate total standard deviation and correlation coefficient estimates. Resulting error ellipses are presented in Appendix D and "95%" probability cross-track errors are listed in Table 3-2 in the column labelled "'Diff' CTE Pred # 1."

Epoch #	Course	Half-Width	"Bias" CTE Prod #1	"Drift" CTE Prod #1
1		- - - - - - N/A - - - - - -		
2	356°T	91 m	113 m	27 m
3	226	91	182	43
4	341.5	122	146	35
5	218	213	184	42
6		- - - - - - N/A - - - - - -		
7	288.5	91	140	41
8	225	91	186	38
9	237	91	182	33
10		- - - - - - N/A - - - - - -		
11	248.5	91	141	30
12	270	91	168	32
13		- - - - - - N/A - - - - - -		
14	287.5	91	70	17
15	263.5	69	135	23
16	262.5	102	102	27
17	289	137	172	38
18	234.5	99	171	27
19	288.5	73	185	31
20	229	69	170	35
21	287.5	69	178	36
22	226	69	181	37
23	239.5	69	172	27
24	263	69	133	23
25	241	69	172	25
26	259	69	186	24
27	236	107	178	25
28	278	69	97	19
29	234	102	163	19
30	257	91	- - -	
31	267	107	127	22
32		- - - - - - N/A - - - - - -		
33	267	69	157	24
34	257	91	157	24
35	239	93	200	27
36	248.5	130	177	26
37	282	130	148	24
38	233	111	204	27
39	255	107	185	26
40	220	137	216	28
41	237.5	91	199	28
42	256	91	166	25
43	232	91	203	28
44	227	114	216	29
45	248	107	185	27
46	241.5	107	198	27
47	265	76	222	29
48		- - - - - - N/A - - - - - -		
49	265	107	222	29
50	227	91	218	29
51	238.5	91	207	29
52	221.5	91	226	31
53	238	91	207	30
54	238	114		
55	260	86	226	31
56	238	182	208	29
57	223	102	229	31
58	231	102	223	32
59	223	83	236	34
60	233	76	222	32
61	226	61	217	31
62	222	61	237	35
63	217	99	241	34
64	194	93	233	36
65	218	83	237	34
66	216	93		
67	209	93	243	35
68	207	93		
69	226	93	232	33
70	238	93		
71	218	91	242	34
72	214	61		
73	219	69		
74	236	69	220	31
75	235	69		
76	231	69		
77	239	83	216	30
78	259	91	239	34
79	246	111	199	26
80	263	122+	148	28
81	193.5	122+	275	46
82	213	185	275	38
83	234	281	242	32

Table 3-2 Differential Loran-C Cross Track Error (Preliminary) 95% Probability Predictions for St. Lawrence Seaway (Differential Corrections From Massena)

(Note: Thus far in this section, as well as in Appendix C, we have used the terms "seasonal component" and "shorter term component" as the basis for the differential Loran-C predictions. This choice of words implies a similarity with the categorization of the "frequency" components defined at the end of Section 3.4. For the purposes of the discussions in this section, there is no reason to refute this similarity. In reality, there is a subtle but important distinction to be made. The importance of the distinction does not affect the discussions until Section 4. Thus, we will avoid pursuing this matter until Section 4.2 where the introduction of actual data into the discussions helps illustrate the concepts and ease the presentation.)

From a first glance at Table 3-2 it appears the Massena differential monitor solved all problems: the cross-track errors are smaller than the corresponding half-channel widths in all cases - with considerable error margin. However, with the large seasonal component of the variations removed, we expect the "residuals" to more closely fit the Gaussian model (although still not perfectly). Thus, we can no longer use the "95% is essentially 100%" sinusoidal case argument and should develop a more conservative Gaussian error estimate.

We choose the figure 99.9% - a somewhat arbitrary figure - for a number of reasons. First we should note we still have a non-Gaussian component so that we really expect the results from a "99.9% Gaussian analysis" to be conservative. Next we note the navigation season only extends from about 1 April to about 15 December - thus excluding most of the worst time of the "loran year." Whereas use of the 95% probability figure produces overly optimistic predictions, use of some figure such as 99.99+% would produce overly pessimistic predictions (besides being a number which exceeds the availability percentage of Loran-C signals). Neither extreme is called for at this point in the study and the 99.9% figure is offered as a reasonable compromise. Finally, we should note we are talking about a single AID to navigation - not an input to a robot navigator. The 99.9% figure leaves room (about 9 hours per year, 6 hours per shipping season) for the navigator.

Using the formulas of Appendix A, we find the "size" of the ellipse is increased by a factor of 1.52 in going from a probability of 95% to a probability of 99.9%. Cross-track errors for this predicted probability are listed in Table 3-3 in the column called "'Conservative' Differential CTE Pred # 1." The values in the column labelled "error margin" are computed by subtracting the conservative cross-track error predictions from the half-channel widths.

In examining the table, we see the "conservative" error prediction never exceeds the half-channel-width. Thus, the centerline of a vessel following the loran with no guidance error never goes outside the channel - at the 99.9% probability level. We must note, however, that the "half-width" of the largest vessels can be 17 meters in the Seaway. Thus, 17 meters is a number of concern. We place three asterisks in the table for any reach with an error margin less than this value. Three asterisks thus indicate

Reach #	Course	Half-Width	"Raw" CTE Prod #1	"Diff" CTE Prod #2	"Conservative" Differential CTE Prod #2	Error Margin
1				N/A		
2	350°T	91 *	113 *	27 *	61 *	50 *
3	224	91	102	42	66	25 *
4	041.5	122	146	35	86	67
5	218	213	194	42	64	149
6				N/A		
7	288.5	91	140	41	82	29
8	226	91	105	35	70	33
9	237	91	102	33	70	41
10				N/A		
11	248.5	91	141	30	66	46
12	270	91	108	22	53	88
13				N/A		
14	287.5	91	70	17	35	65
15	263.5	68	105	23	35	35
16	242.5	102	102	27	[illegible]	141
17	269	137	172	30	43	94
18	234.5	99	171	27	41	88
19	285.5	73	105	21	32	41
20	229	68	179	25	39	29
21	207.5	68	170	25	39	29
22	226	68	101	27	41	27
23	230.5	68	170	27	41	27
24	253	68	133	23	35	33
25	241	68	172	25	38	30
26	209	68	106	24	35	32
27	235	107	170	25	38	69
28	270	68	97	19	29	39
29	234	102	103	19	29	123
30	257	91	- - -			67
31	267	107	127	22	33	74
32				N/A		
33	297	68	157	24	36	32
34	257	91	107	24	35	55
35	233	93	200	27	41	52
36	048.5	130	177	25	39	91
37	262	130	148	24	35	94
38	253	111	204	27	41	70
39	255	107	168	25	38	69
40	220	137	215	28	43	94
41	237.5	91	199	28	43	48
42	255	91	164	26	39	44

Reach #	Course	Half-Width	"Raw" CTE Prod #1	"Diff" CTE Prod #1	"Conservative" Differential CTE Prod #1	Error Margin
43	237	91	205	28	43	48
44	227	114	216	28	43	-
45	248	107	185	27	41	66
46	241.5	107	198	27	41	66
47	286	76	222	29	44	35
48				N/A		
49	286	107	222	29	44	63
50	227	91	218	29	44	47
51	238.5	91	207	29	44	47
52	251.5	91	205	31	47	44
53	239	91	207	30	46	45
54	228	114				68
55	280	96	228	31	47	49
56	228	102	208	29	44	108
57	225	102	209	31	47	106
58	231	102	223	32	49	103
59	222	60	235	34	52	31
60	253	76	227	32	49	27
61	238	61	217	31	47	14 ***
62	222	61	227	32	49	8 ***
63	217	42	241	34	52	41
64	196	93	233	35	54	35
65	218	93	237	34	52	41
66	216	93				4
67	209	93	243	35	55	35
68	207	93				18
69	235	93	232	33	51	51
70	229	93				4
71	218	91	242	34	52	39
72	214	61				8 ***
73	219	68				16 ***
74	226	68	220	31	47	21 **
75	235	68				31 **
76	231	68				27 **
77	239	89	216	30	66	37
78	288	91	236	34	52	39
79	248	111	199	28	39	77
80	283	122*	148	28	43	79*
81	193.5	122*	275	46	70	52*
82	213	168	275	39	88	107
83	238	381	242	32	49	332

Table 3-3 Differential Loran-C Cross-Track Error Predictions - 95% and 99.9% Probability

situations wherein if the conservative error estimate is exceeded, part of a vessel with a half-width of 17 meters, following the loran with no guidance error, is outside the channel. We cannot, of course, expect zero ship guidance error. We assign two asterisks to a reach in which the error margin is less than 22 meters. Thus two asterisks indicate situations in which if the conservative error margin estimate is exceeded, part of a vessel with a "half-width" of 17 meters, following the loran with 5 meters or more guidance error, is outside the channel. One asterisk indicates a situation in which the conservative error estimate leaves less than 10 meters

for guidance error for a 17 meter "half-width" vessel. We do not offer these criteria as the ultimate design goal of the study - just as some figures of merit for the initial examination of predicted differential Loran-C performance.

In Table 3-3 we see two areas where asterisks are clustered - both being considerable distances from Massena. This suggests we consider adding another monitor station - in the vicinity of reach 74 at Wellesley Island. If we re-compute the predicted errors based on differential corrections from this station (for appropriate reaches only), we obtain the results indicated in Table 3-4.

Reach #	Course	Half-Width	"RAW" CTE Pred #1	"Diff" CTE Pred #2	"Conservative" Differential CTE Pred #2	Error Margin
56	238	152	208	28	43	109
57	223	152	229	27	41	111
58	231	152	223	27	41	111
59	223	83	235	27	41	42
60	233	76	222	28	43	33
61	236	61	217	27	41	20 **
62	222	61	237	29	44	17 **
63	217	99	241	28	43	56
64	194	93	233	25	38	55
65	218	93	237	29	44	49
66	216	93				49
67	209	93	243	28	43	50
68	207	93				50
69	225	93	232	29	44	49
70	228	93				49
71	218	91	242	29	44	47
72	214	61				17 **
73	219	68				24 *
74	235	68	220	28	43	25 *
75	235	68				25 *
76	231	68				25 *
77	239	83	216	28	43	40
78	228	91	238	29	44	47
79	246	111	199	29	44	67
80	263	122+	148	26	39	83+
81	193.5	122+	275	28	43	79+
82	213	165	275	32	49	116
83	234	381	242	32	49	332

Table 3-4 Revision to Table 3-3 Based on an Additional Differential Monitor at Wellesley Island

Comparing these results with those shown in Table 3-3 suggests it is appropriate to switch from Massena to Wellesley Island for corrections after reach 55. Table 3-5 is constructed using the two station differential control strategy thus obtained. We see we no longer have "three asterisk" situations so the attention must focus on how much room must be allowed for guidance error. Note that except for reaches 61, 62, and 72, at least 7 meters is allowed - a figure which could be argued to be very close to acceptable.

Reach #	Course	Half-Width	"Good" CTE Prod #1	"Bad" CTE Prod #2	"Conservative" Differential CTE Prod #2	Error Margin
1				N/A		
2	264**	91 m	113 m	27 m	41 m	80 m
3	226	91	102	43	66	26 *
4	241.5	122	146	35	56	67
5	218	213	156	48	64	140
6				N/A		
7	208.5	91	140	41	62	29
8	226	91	106	33	58	33
9	232	91	132	33	50	41
10				N/A		
11	248.5	91	141	33	46	46
12	270	91	108	22	33	58
13				N/A		
14	287.5	91	70	17	26	65
15	203.5	68	136	23	35	33
16	242.5	102	102	27	41	141
17	209	137	172	29	43	94
18	234.5	99	171	27	41	58
19	208.5	75	135	21	32	61
20	229	68	170	26	39	29
21	207.5	68	170	26	39	29
22	226	68	101	27	41	27
23	230.5	68	172	27	41	27
24	203	68	133	23	35	33
25	241	68	172	25	39	39
26	209	68	106	24	36	32
27	236	107	170	25	38	69
28	270	68	97	19	29	39
29	236	102	103	19	29	123
30	287	91	- - -			68
31	267	109	137	22	33	76
32				N/A		
33	257	68	157	24	36	32
34	257	91	157	24	36	56
35	233	93	200	27	41	52
36	248.5	130	177	26	39	91
37	262	130	140	24	36	94
38	233	111	206	27	41	70
39	256	107	165	25	38	69
40	270	137	216	29	43	94
41	217.5	91	199	26	43	66
42	256	91	166	26	39	66
43	237	91	200	26	43	66
44	227	114	216	26	43	71
45	248	107	186	27	41	66
46	241.5	107	199	27	41	66
47	266	76	222	29	44	32
48				N/A		
49	266	107	222	29	44	63
50	227	91	210	29	44	47
51	236.5	91	207	29	44	47
52	221.5	91	225	31	47	44
53	230	91	207	29	46	46
54	230	114				66
55	229	96	206	31	47	49
56	230	102	200	29	43	109
57	223	102	229	27	41	111
58	231	102	223	27	41	111
59	223	68	235	27	41	42
60	232	76	222	29	43	33
61	230	61	217	27	41	20 **
62	222	61	237	29	44	17 **
63	217	99	241	29	43	56
64	196	99	233	25	39	55
65	210	99	237	25	44	49
66	216	99				49
67	209	99	243	29	43	50
68	207	99				50
69	205	99	232	29	44	49
70	209	99				49
71	210	91	202	29	44	47
72	214	61				17 **
73	219	68				26 *
74	226	68	220	26	43	25 *
75	226	68				25 *
76	221	68				25 *
77	229	68	216	29	43	48
78	208	91	230	29	44	47
79	246	114	199	29	44	67
80	253	122+	166	26	39	83+
81	198.5	122+	276	29	43	79+
82	213	166	276	32	49	116
83	228	200	302	32	49	132

Table 3-5 Differential Loran-C Cross-Track Error Predictions - Monitors at Massena and Wellesley Island

Before we decide to try to locate another differential monitor station in the problematic reaches we should consider the source of the problem. As Table C-3 in Appendix C shows, with differential corrections being applied from Wellesley Island, there is a slight seasonal component which contributes to the total error budget in reaches 61, 62, and 72 through 76. Without trying to find a particular site which removes this, we should immediately move to consideration of an "optimal" monitor site - one which results in the removal of all seasonal variations. Error ellipses for reaches 61 and 62 under such conditions are shown on page D-32 which show the predicted 95% cross-track error is 28 meters. This translates to a 99.9% probability prediction of 43 meters - leaving an error margin of only 18 meters.

Thus, under our assumptions regarding the short-term standard deviations, we "bottom out" at the 99.9% level in these tight reaches. Our assumptions, of course, may be wrong so we cannot draw final conclusions at this point. It is important, however, to emphasize the source of the problem which becomes clear from examination of the error ellipses which are reproduced in figure 3-6 below. A general note about the error ellipse plots which appear throughout the remainder of the report is in order. The vertical axes of the plots have a true north-south orientation and the horizontal axes have a true east-west orientation. The straight line which extends from the origin, shown below at a heading of 236°T for Reach #61, indicates the channel course. Characteristics of the ellipse and the statistics from which it was generated are provided below each plot.

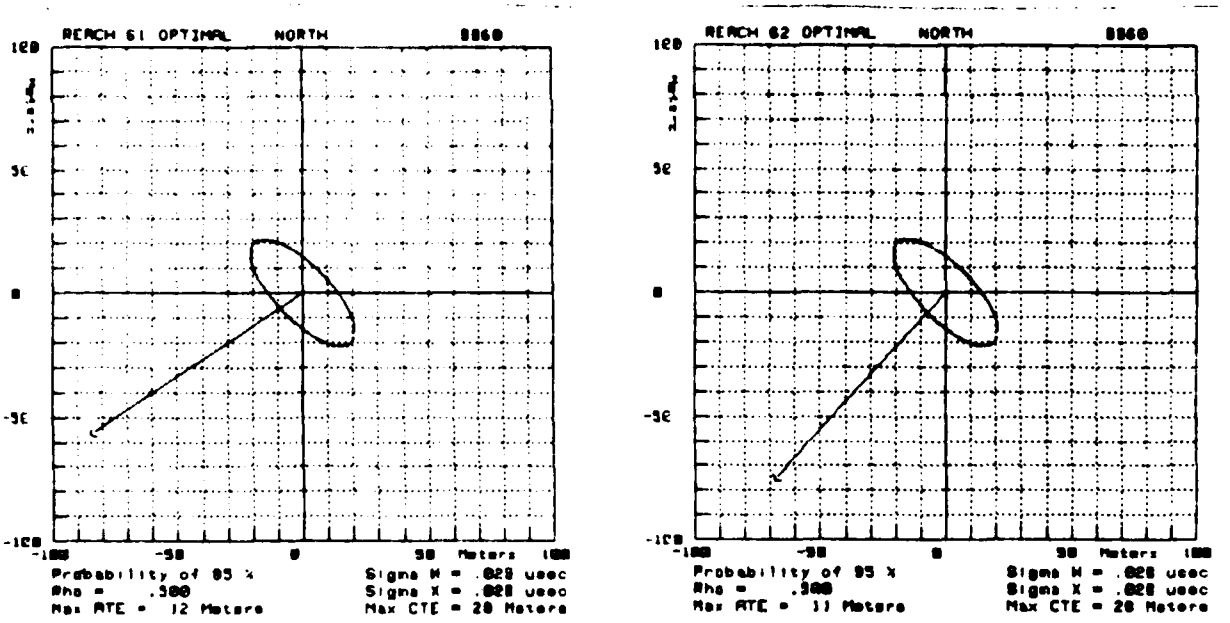

Figure 3-6 Differential Loran-C Error Ellipses at Reaches 61 and 62

The orientation of the ellipse with respect to the course, in these critically tight reaches, is essentially "worst case." If the orientation were rotated 90°, we would have cross-track errors of 11 or 12 meters and there would be no problem.

The ultimate conclusion may be that Loran-C will not work. Alternatively, we may decide to deploy some other system for these special reaches. We should note, however, the criticality of system geometry as well as the importance of obtaining good data in the vicinity of Wellesley Island.

3.6 Summary of Performance Predictions.

In Section 3 we have introduced a model for Loran-C time difference variations for use in the St. Lawrence Seaway study. We argued that the variations can be broken down into four "frequency" components. Two of these, it is claimed, can be adequately measured - deterministically - by the "low-density" sampling strategy used in the harbor monitor program. For the third component, it is argued, the low-density sampling strategy allows an adequate statistical measure. The remaining component is called "near-instantaneous" and it is claimed, since this is not "propagation phenomenon related," it is not necessary to deploy spatially separate monitors in the service area to monitor this. If the need is indicated, estimates of the "rapid" effects can be obtained from chain operational monitors. Whereas it has never been demonstrated that these "rapid" effects are perfectly monitored at some location other than the point of interest, that also is something which should be pursued only if the need is indicated - and in an extremely cautious and careful manner. For now, we must try to avoid "swallowing any camels while straining for gnats." As the next section will show, there appear to be many "camels" in the St. Lawrence Seaway.

To consider the spatial nature of the time difference variations we introduce the so-called "double-range-difference" model which has been used in similar studies of this nature. The model is described in Appendix B. We use data obtained from sites outside the St Lawrence area to apply the model. In other applications, a more empirical use of the model is made - and nothing presented here should be construed to imply we do not believe this is the desired approach. Unfortunately, we do not yet have the data base necessary to support this type of approach and had to turn to more "heuristic" methods. We did this to emphasize there is a theory for the types of variations we expect to see and that its presentation is too important to wait for an adequate data base. In applying the model, we did not have a convenient way to estimate all four frequency components so we considered only two types of components. In Section 4 we will further explore the subtle differences in the two different types of classification of variations. It is noted that in ignoring the distinction for the moment we do not compromise the validity of the predictions of this section. The presentation, crude as it may be, serves to focus our attention on the critical parameters and areas we must concentrate on for the rest of the study.

The predictions, which we call "a priori" since they are made without the benefit of observations in the region of interest, show that the performance to be obtained, year-round, with "raw" Loran-C is clearly inadequate for our requirements. Although we do not have a simple method of separating the shipping season from the entire year, the year-round errors are large enough for us to easily argue "raw" Loran-C will be inadequate throughout the shipping season. Similarly, the errors are large enough to argue a "simple" solution (e.g., the application of monthly or weekly corrections) does not appear promising. At this point it is not productive to speculate on the viability of such schemes as daily corrections so we move directly to consideration of "full Differential Loran-C," i.e., we assume corrections from the monitor are available to the user on, essentially, a real-time basis.

Hypothesizing a differential control site at Eisenhower Locks, we find adequate performance - at the 99.9% probability level, is predicted for most sites. A cluster of problematic reaches is seen in the vicinity of Wellesley Island. We hypothesize a differential monitor at Wellesley Island and find the errors are still "too large for comfort" in three of the reaches. Moreover, we find the errors are predicted to be too large no matter where we locate a differential correction station. This finding is based on an arbitrary assumption regarding the short term statistics of the variations so that we cannot rule out Loran-C at this time. We can, however, be aware of the "nearly worst case" effects of chain geometry which is identified as the prime culprit.

If data shows our assumptions about the time difference statistics were not overly pessimistic, the situation is not all that bad. Fortuitously, the areas of concern are located in reaches in which the proximity of small islands leads to consideration of a "hybrid system" solution. RACONS, for example could be located on the islands to "mark" the channel edges. The entire exercise shows, however, that consideration should be given to locating a monitor in the Wellesley Island vicinity.

Now that we have made all possible predictions, we should turn to a consideration of available data. In our considerations, we should first attempt to verify that the predicted "raw" Loran-C error ellipses are approximately representative of what actually happens. If this can be accomplished, we can verify our conclusion that with existing chain geometry, "true" Differential Loran-C must be employed. Next, we should try to verify the differential Loran-C predictions - particularly in the critical reaches near Wellesley Island. Although we do not expect available data to allow us to say the final word at this time, examining how much of the predictions of this Section can be tested provides an assessment of the effectiveness of the experiment to date.

4. DATA COLLECTION RESULTS

4.1 Data Availability

Data collection for the St Lawrence Seaway Loran-C stability study began at Eisenhower Locks (Massena, N.Y.) on 21 October 1981. As described in Section 2.1, data at Massena is collected every 12 hours. During each sampling period we measure and record the hourly average value and standard deviation of the 9960-W and 9960-X time differences. We also record the minimum and maximum value observed during the sampling period. All of this data is stored along with notations as to the date and time of the observations. In writing this report we have used data up to 11 June 1982 for Massena and thus have a total of over 450 sample periods. Although equipment problems have caused the loss of some data, we find we have obtained 98% of the desired data at Massena.

A 98% complete record, over a period of almost 8 months, should allow an adequate "low density" data analysis - particularly if the period includes all of the winter as the Massena record does. Unfortunately, Massena is the only site in the St Lawrence for which we have so much data. Thus, we can make fairly well substantiated statements about "raw Loran-C," but have problems in trying to verify differential Loran-C performance predictions. The problems are best seen by examining Table 4-1 which shows the "%-usable" (low density) data available to the authors at the time of this writing for the period from 21 October 1981 to 11 June 1982.

Site	Total %-usable
Massena	98%
Tibbetts Point	52%
Iroquois	20%
Prescott	7%
Beauharnois	4%
Cote Ste Catherine	0%
Brossard	0%

Table 4-1 Percent Usable Data from St. Lawrence Seaway Loran-C Sites

A reason for low data availability at some sites (e.g., Brossard) is the fact that the installations took place late in the October '81 - June '82 period. The fact, for example, that we expect a much higher performance record from the Brossard site over the next few months does nothing to alleviate the plight of the authors who are trying to report - now - on the results of the 8-month effort.

Another reason for the low data availability reflected in Table 4-1 for sites other than Tibbetts Point and Massena is the substantial "time delay" involved in obtaining the data. As an example, we should note that as of "close of business" on 21 June 1982, data from Massena and Tibbetts Point up to and including the first hourly sample taken on 21 June 1982 was obtained and examined by project personnel at the USCG Research and Development Center. This data was available to the authors that same day (it was not used due to a self-imposed deadline regarding the preparation of plots). This situation contrasts significantly with that associated with the data from other sites. As of 21 June 1982, no data beyond 18 May 1982 has been received and reviewed. The great question regarding the data from these other sites is: "suppose 'something broke' on 19 May 1982?" This is not merely a hypothetical question: situations such as this have already occurred several times during the course of this project. If this has happened, we have lost more than a month of data unless something has "fixed itself." Those with a mild technical background (e.g., those who own TV sets) can appreciate the unlikeliness of this happening.

A final major reason for low data availability is a feature found only at the "Ad Hoc" sites. Without a computer-based controller of some sort, the data is recorded without corresponding date/time information. The data is obtained at some integer multiple of 0.0996 seconds so that, ideally, one could reconstruct the times. If, however, power is temporarily interrupted, or if equipment malfunctions occur, we cannot reconstruct the date and time of the measurements unless an operator re-initializes the system and is meticulous about manually recording the date and time of re-initialization. Unfortunately, we do not have technically skilled operators at the Ad Hoc equipment sites and through this "improper initialization" mechanism, have lost a considerable amount of data. In many cases, the Loran-C data is available - "time of measurement unknown" - and this could be used to make some statements about "raw Loran-C" performance. Given the availability of data from Massena, however, we will be able to say all we need to about "raw Loran-C" so this is redundant information. The true value of data from sites other than Massena is that it could allow measurements of differential Loran-C performance. Accurate knowledge of the date and time of the observation, however, is critical for this analysis and, in many cases, this vital information has been lost.

Table 4-2 provides a breakdown of the "unusable data" causes for each site. From this we can see there are so many problems with the Ad Hoc data sites that we must seriously consider upgrading the sites with more reliable equipment. The major problem with the buoy auditing equipment sites are all related to untimely collection and review of the data. Serious consideration should be given to upgrading the equipment at these sites to allow remote (via phone) access.

Site	Comments
Prescott/Ft Wellington (2/10/82 - 6/8/82)	a. Buoy Auditing Equipment Set installed at Fort Wellington 2/10/82. b. 2/10/82 - 3/11/82: Data not valid due to gounding problems. c. 3/11/82 - 3/29/82: Data is valid but features several 1-1/2 to 2 day gaps whenever tapes ran out. d. 3/30/82 - 4/20/82: No valid data due to equipment and power failures. e. 4/20/82: equipment moved from Fort Wellington to CCG Base at Prescott. TD offsets recorded. f. 4/20/82 - 4/24/82: valid Data. g. 4/25/82 - 6/8/82: data not valid due to receiver problems. h. 6/8/82: receiver replaced, only 9960-W and 9960-X data being recorded. Summary: Insufficient data for a meaningful low density analysis. Of the data collected during the period 2/10/82 - 6/8/82, 14% is usable.
Iroquois Lock (3/17/82 - 5/14/82)	a. Installed 3/17/82 as an Ad Hoc type site. b. 3/17/82 - 4/20/82: good data with only one 7-hour period of lost data - due to a "cycle slip." c. 4/21/82: Buoy Auditing Set, with a signal splitter, installed. d. 4/21/82 - 5/3/82: Good data with the signal splitter. e. 5/3/82 - 5/14/82: Data lost due to lack of re-initialistion after a power loss. f. About 6/15/82: Splitter removed upon USCG recommendation. Offsets recorded. Summary: Iroquois Lock now features a single receiver using one antenna. 9960-W and 9960-X data being recorded. Of the data collected during the period 3/17/82 - 4/14/82, 78% is usable.
Beauharnois Lock (12/21/81 - 5/5/82)	a. Installed 12/21/81 as an Ad Hoc type site. b. 12/22/81 - 4/2/82: Data not valid due to poor grounding. 9960-X TD's and SNR readings unstable. c. 4/2/82: improved grounding. d. 4/2/82 - 5/5/82: About 75% of the data is invalid due to a "cycle slip" on the 9960-X baseline. Summary: Insufficient data for a meaningful low density analysis. Of the data collected during the period 12/21/82 - 5/5/82, 6% is usable.
[illegible] Ste. Catherine [illegible]/22/81 - 5/5/82)	a. Installed 12/22/81 as an Ad Hoc type site. b. 12/22/81 - 4/1/82: Data is not valid due to poor grounding. TD's and SNR's unstable. c. 4/1/82: Grounding improved. Subsequently discovered that the receiver "went bad" sometime between 4 and 11 Feb. 1982. Summary: None of the data is valid.
[illegible]ssard [illegible]4/82 - 5/5/82)	a. 5/4/82: Installed as an Ad Hoc type site. b. 5/5/82: No valid data due to grounding problems. 9960-X TD's and SNR's unstable. Summary: No further data available by "press time."

Table 4-2 Comments on Site Performance

Specific examples of the data obtained during the problem periods outlined above are provided in Appendix F.

4.2 Evaluation of Massena Data.

We begin the evaluation by considering the data collected at the Massena, N.Y. site. Plots of the time difference readings are provided in figures 4-1.a. and b. The data is plotted from Julian Day 1 to Julian Day 365 to be consistent with the plots introduced in Section 3 and the Appendices. Thus, the first (read from left to right) 155 days of data shown below comprise 1982 data whereas the data plotted to the right is from 1981.

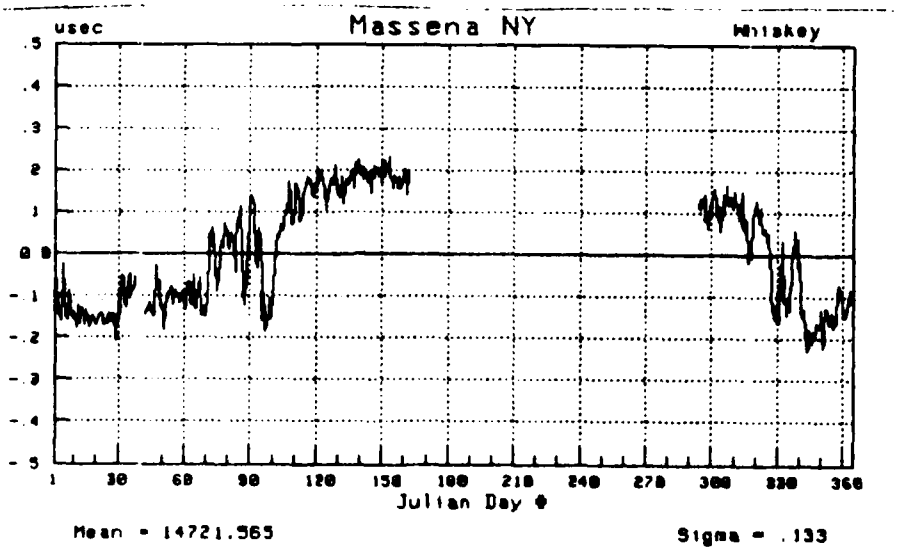

a.

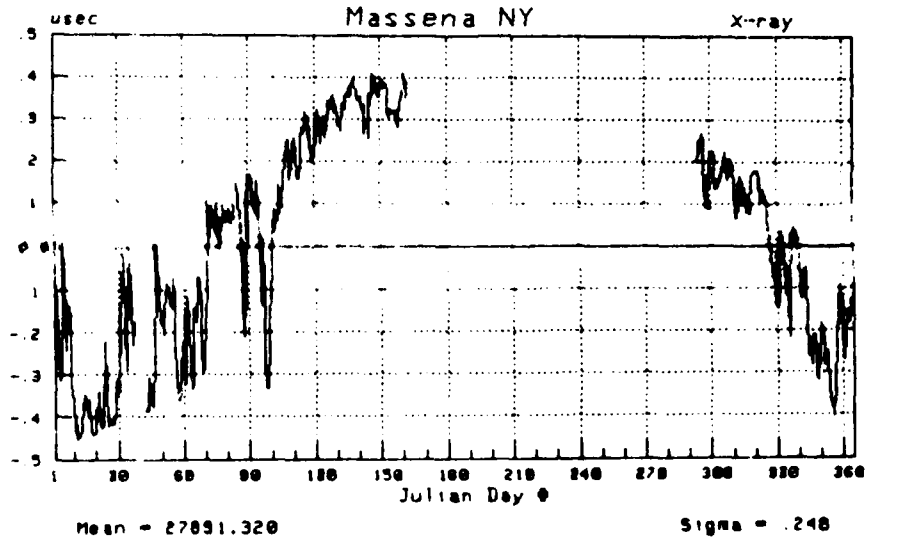

b.

Figure 4-1 9960-W/X Loran-C TD Plots - Massena

There are many things we can say about the data records but we should start by comparing the statistical results to the year-round predictions for "raw Loran-C" of Section 3. For the 9960-W baseline, we predicted a standard deviation of 0.144 usec. We see the results - for almost 8 months of data show a "sigma" of 0.133 usec. For 9960-X, we predicted a standard deviation of 0.255 usec and observe a "sigma" of 0.248 usec. We will have to wait several months for the final judgment on the predictions but note we expect both data records to remain fairly stable throughout the Summer and early Fall. Thus we can "dub in" a sequence of data points which follow the basic trend established by mid-June and compute the statistics of the results. They turn out to yield "sigmas" of 0.137 usec and 0.256 usec for 9960-W and 9960-X, respectively.

From this we can conclude the time differences at Massena agree with the pattern suggested by other N.E.U.S. data collection sites within 5%. In short, there are no surprises at Massena regarding the year-round standard deviations. The data points of figures 4-1.a. and b. are converted to position errors to produce the "scatter plot" shown in figure 4-2.

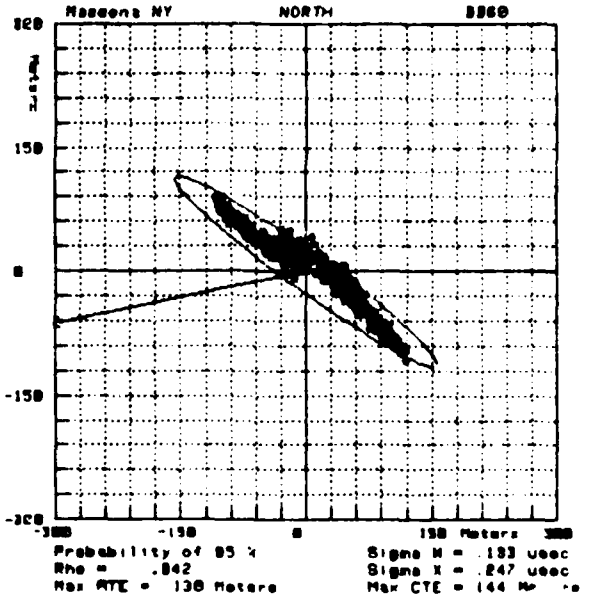

Figure 4-2 9960-W/X Loran-C Error Fix Scatter Plot - Massena

In the process of generating the ellipse that is included in figure 4-2, we have computed the correlation coefficient of the two time difference records. At 0.942, the observed value, as expected, is higher than the 0.90 value we used in Section 3 for the "raw Loran-C" predictions.

From the results presented thus far, we can draw several important conclusions:

a. The correlation coefficient prediction was low. As noted in Section 3, this was the result of a conscious attempt to generate conservative predictions. The standard deviations we have observed are not different from the predicted values in any statistically significant sense. This is a critical result. It suggests that with the simple "land/seawater modification" to the uniform propagation assumption described in Appendix B, the double-range difference model applies very well to observations in the vicinity of Massena, N.Y. Thus, we have no evidence of propagation anamolies thus far.

b. The error pattern of the actual fixes does not perfectly follow the "pure ellipse" pattern. This can be considered primarily a result of the non-gaussian nature of the processes involved. To a "very useful degree," however, the pattern is as predicted and the appropriateness of the "elliptical analysis" is verified.

c. In figure 4-3.a. and b., we compare observed results with predicted results. Table 4-3 summarizes the comparison.

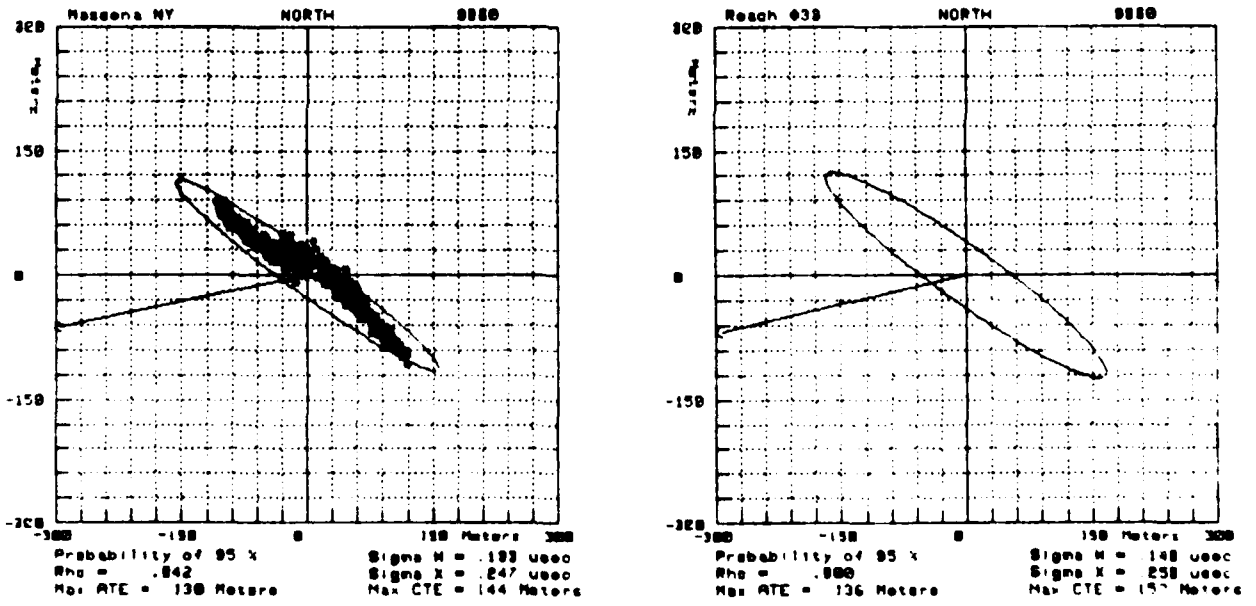

a. b.

Figure 4-3 Comparison of Predicted and Observed Error Ellipses - Massena

	Max CTE	Max ATE
Predicted 95% Ellipse	157 m	136 m
95% Ellipse Determined by Observed Statistics	144 m	130 m
Actual Observations	135 m	96 m

Table 4-3 Comparison of Predicted and Observed Errors - Massena

The observation here is that the 95% ellipses, for "raw Loran-C," year-round, provide predictions which exceed the largest errors actually observed. This verifies the contention of Section 3 that these predictions closely approximate 100% error contours.

The Massena data can be presented in several other ways. Indeed, the number of ways the data can be presented and analyzed is seemingly limitless.

This last statement leads to an aside comment regarding the importance of first obtaining the database. Stated differently, the authors can think of at least 57 different ways to present and analyze the observations made at Massena in January 1982 (in a similar study made about a decade ago for the old 9930-Z baseline, we seemed to "make a living" for several years by providing different presentations of the same data. We call this the "porno movie syndrome.") If, several years from now, we think of another analysis technique, we can immediately apply it. There will never again, however, be an opportunity to collect January 1982 data. Thus, the first priority is to obtain the data base - however modest it may at first appear.

Herein we will provide only some of the possible presentations (leaving room for "further study.") Figures 4.4.a. and 4.4.b. show the cross-track and along-track errors as a function of time. The seasonal nature of the variations is clearly illustrated.

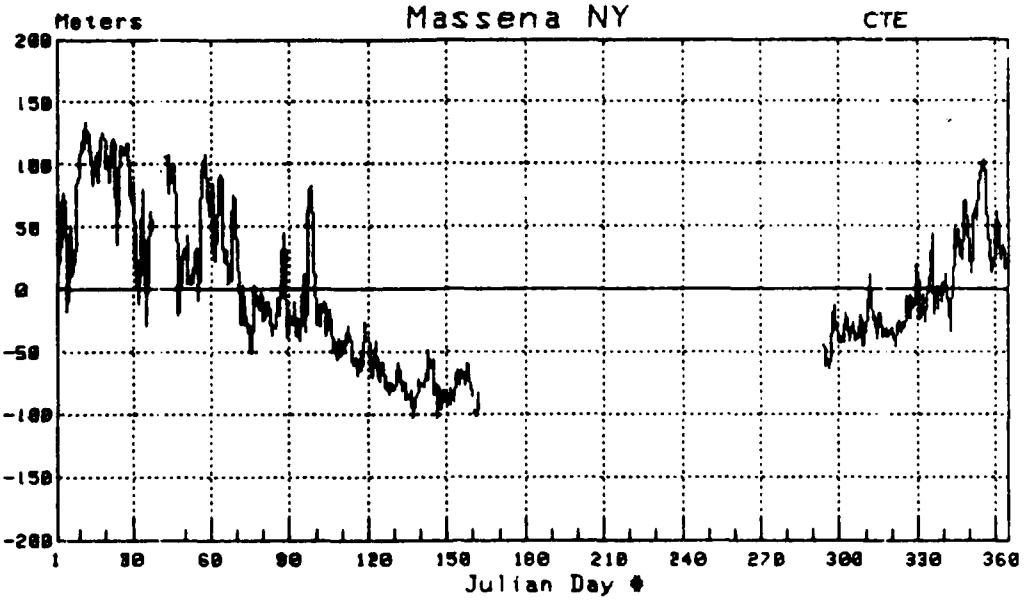

a.

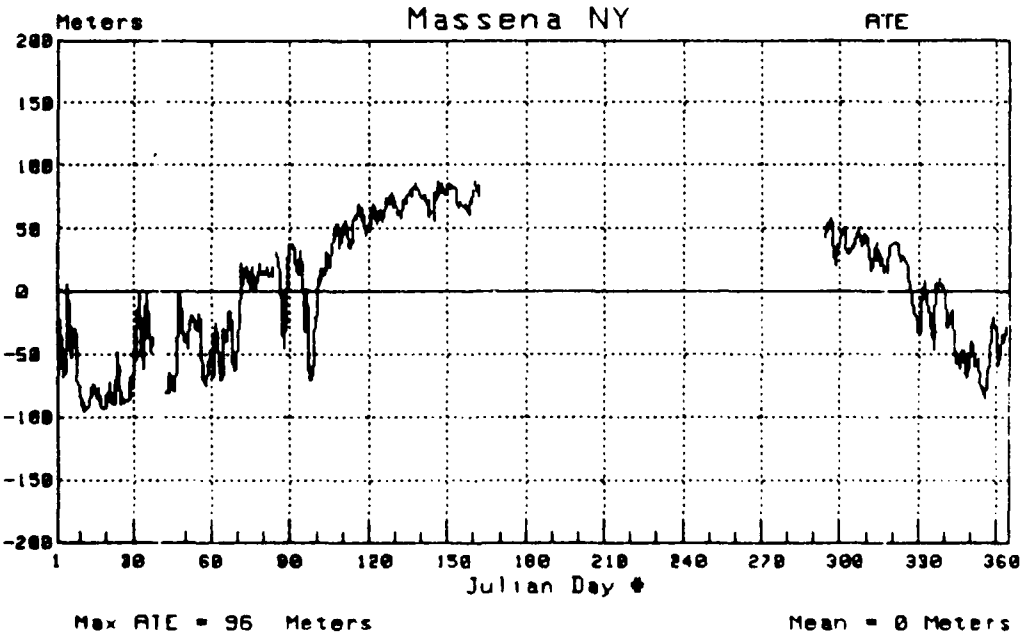

b.

Figure 4-4 Loran-C Fix CTE/ATE Plots - Massena

Figure 4-4 illustrates another important concept: how does one pick the reference value for the plots? Thus far we have chosen the reference point as the average value of all available data. If we were, for example, only interested in the month of May, we might examine figure 4-4 and erroneously conclude we are "stuck" with a seemingly consistent cross-track error of about 70 meters. The situation therefore is misleading for if we were truly interested only in May, we would have chosen the average position observed (or expected from previous studies) in May as the reference. A note of caution should be sounded that it is not yet clear at this point how this average value can be obtained for all waypoints. It is claimed, however, that this is a problem that can be addressed in a systematic fashion at a later date in the study. First we should attempt to determine if consideration of such details as this is warranted: perhaps there is some other fundamental limitation which will rule out the use of Loran-C in the Seaway. Only if no such limitations are found should we turn our attention to such details as this which is simply noted in passing.

Having said about all that need be said about "raw Loran-C" performance at Massena, we should proceed with an examination of how the data can be used to test other predictions of Section 3. Before attempting to construct differential Loran-C observations, we can examine the "frequency" components of the Massena data records. Figure 4-5 shows the total data record for the 9960-W baseline observations at Massena, the "low frequency" component (obtained by applying a 2-week sliding average filter to the raw data) and the residual "shorter-term" component. The plots are analogous to those of figure 3-4. The same components for the 9960-X baseline are shown in Figure 4-6.

If we try to compare the statistics of the residuals plotted in figures 4-5 and 4-6 with the 20-nanosecond "shorter-term" variation standard deviation used for the predictions of Section 3, we see substantial disagreement. The residuals for the 9960-W baseline have a standard deviation of 47 nanoseconds and the residuals for the 9960-X baseline have a standard deviation of 82 nanoseconds.

Actually, the problem is only that we are mixing models. This is an understandable thing to do given the small data base, and we will be tempted to do it throughout this section. We are now seeing the effects indicated in the note of section 3.5 regarding the classification of various components of the Loran-C time difference variations. The need for an in-depth discusion is now indicated.

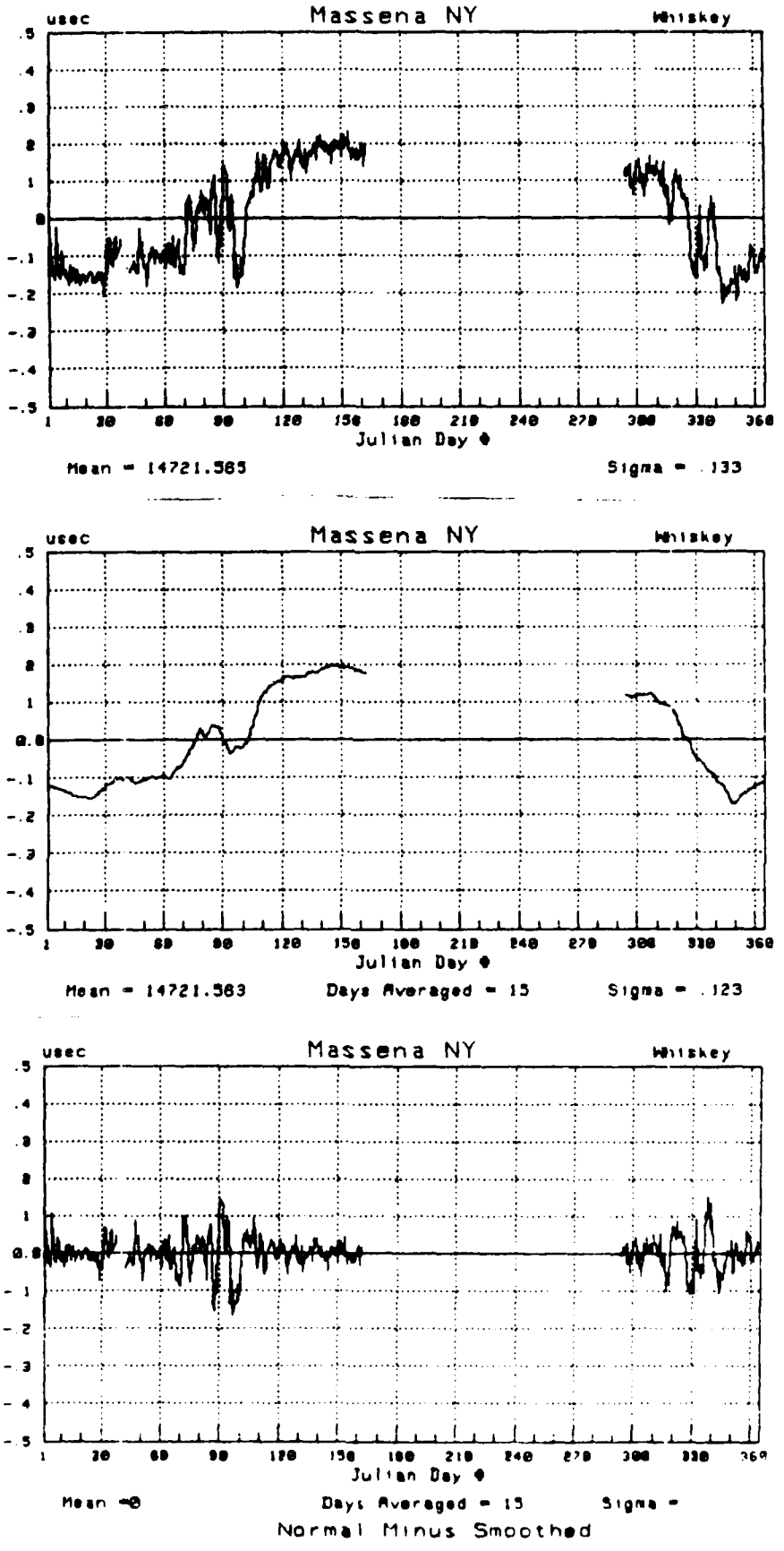

Figure 4-9 Breakdown of Frequency Components: 9960-W TD at Massena Using 15-Day Smoothing

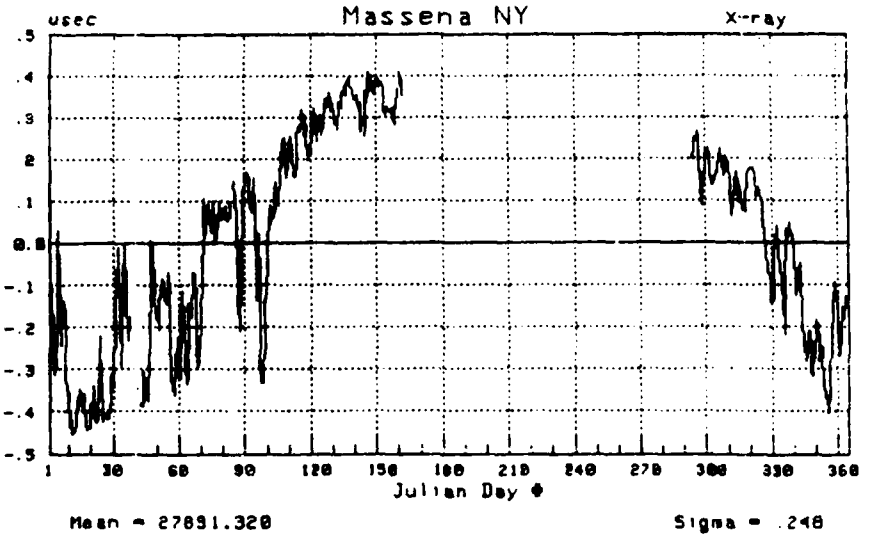

a.

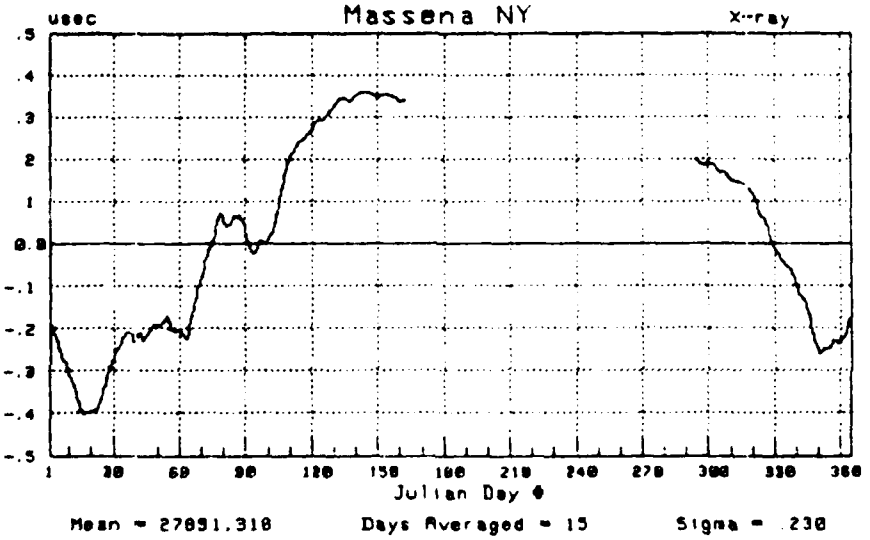

b.

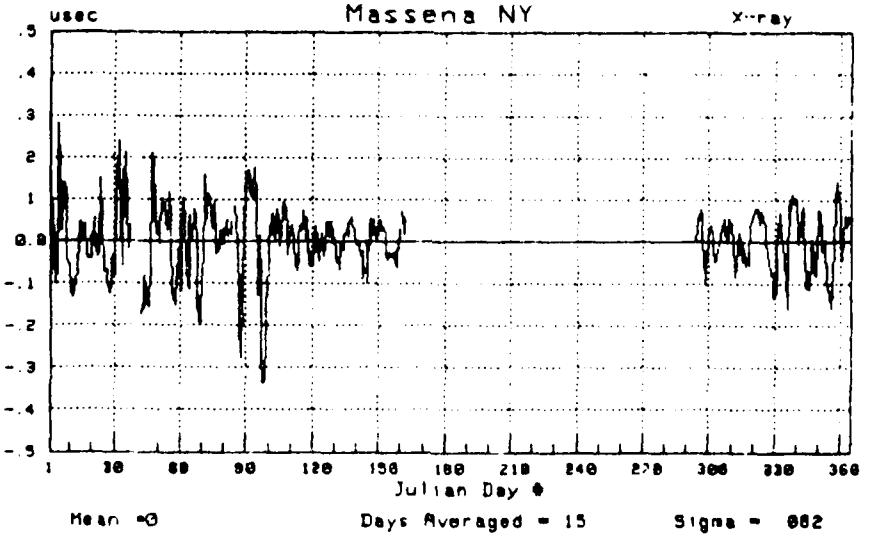

c.

Figure 4-6 Breakdown of Frequency Components: 9960-X TD at Massena Using 15-Day Smoothing

The 20 nanosecond figure used in Section 3.5 (and Appendix C) came from a differential Loran-C model and represented that component of the variations assumed independent from site to site. Thus we cannot obtain a direct measure of it by examining the Massena data alone. Ideally, we would obtain an estimate of it by subtracting the Massena data record from a data record obtained at a nearby site. Thus, we would simulate differential Loran-C performance at the other site and, by breaking the resulting data record down into a "seasonal" and "shorter-term" (more properly called "site-independent") component, could test the bases of the prediction model. We would hope to find the "seasonal" component properly represented by the double range difference and the "residual" component with a standard deviation of about $20\sqrt{2}$ nanoseconds. This then is the approach we would take if we had a reasonable database from another nearby site.

Since we do not have this other database, we will spend more time scrutinizing the Massena data. Although a suboptimal occupation, we can obtain valuable insight and the exercise is deemed worthwhile. Care must simply be taken, as we have already begun to emphasize, that we are not yet doing a direct differential Loran-C analysis.

In the preliminary discussion of the Loran-C time difference variation model in Section 3, we referred to Appendix B where, almost as an aside, we noted that the temporal and spatial nature of the TD variations were interrelated. We must now expand upon this concept and begin to introduce more detailed consideration of the variations. Use of the reasonably complete Massena data base will prove invaluable in illustrating the concepts. We begin by recalling Section 3.4 claimed there were 4 major frequency components we should consider. Having described the four components, we proceeded in Section 3.5 with predictions based on two components: one that is highly correlated from site to site and one that is independent from site to site. These two classifications of components (one having 4 constituents, the other having 2) are not directly related. Thus, we should call the four component classification the "temporal" one, and the two component classification the "spatial" one to emphasize the distinction.

At the low frequency end of the temporal classification, we find the so-called "seasonal" component is highly correlated from site to site and from baseline to baseline. Thus it fits in the highly correlated portion of the spatial classification. We see significant evidence of this correlation by comparing the plot of figure 4-5.b. to that of figure 4-6.b. and even to 3-4.b. At the other end of the temporal variation classification, we find the so-called "near instantaneous" frequency component. It is claimed that this component is also, to a large extent, highly correlated from site to site. Small data record discontinuities resulting from local timing corrections (corrections entered by the SAM that produce identical effects throughout the service area) comprise a large portion of this temporal component. Thus, when we chose the terminology "seasonal" and "shorter-term" components in Section 3.5, we were being somewhat misleading. Indeed, of all four temporal classification components, we expect only a small portion of the so-called "short-term" effects and the portion of the "near-instantaneous" effects produced by atmospheric noise to show substantial de-correlation from site to site. The prime contributors are the effects of weather fronts which pass between the

sites being compared along the signal path. These effects happen too slowly to be called "near-instantaneous" but too rapidly to be called "medium-term" or "seasonal" (as defined on pages 3-7 and 3-8). Thus, for the remainder of this report, we will be more detailed in our modeling and clear up the terminology by using the terms "spatially correlated" and "spatially independent" as the components of the spatial classification.

The application of the above discussion is that whereas we expect differential Loran-C corrections to remove much (depends on the Δ DRD) of the "low frequency" error shown in figures 4-5.b. and 4-6.b., we also expect a considerable portion of the "residual" errors shown in figures 4-5.c. and 4-6.c. to be removed. By using the 2-week filter in figures 4-5 and 4-6, we have merely separated the component bearing the temporal classification "seaonal" from the other components. We expect true differential Loran-C to do better so that figure 4-5.c. and 4-6.c. do not provide a good differential Loran-C "simulation."

Although we have just belabored the point that manipulation of "Massena only" data is a suboptimal approach to testing for expected differential Loran-C performance, there are some further steps we can take in trying to get a good "simulation." One reason for doing this is that Massena is our largest, highest quality data base. Another is that we can use it to lead into the next section where we can illustrate more detailed characteristics of the variation.

We proceed by noting our previous claim that we expect the "medium term" frequency component, as well as the "seasonal" frequency component to be highly correlated from site to site. Thus, we expect differential corrections to remove a certain portion (again, proportional to Δ DRD) of this component also. Importantly, just as with the seasonal component, we can remove this "spatially correlated" component through time domain filtering. Specifically, we can apply a sliding 3-day filter to the Massena data record and, by subtraction, remove both the seasonal and the medium term components (i.e., the components claimed to be almost entirely spatially correlated) from the other components. The process is illustrated for the 9960-W baseline in figure 4-7 and for the 9960-X baseline in figure 4-8.

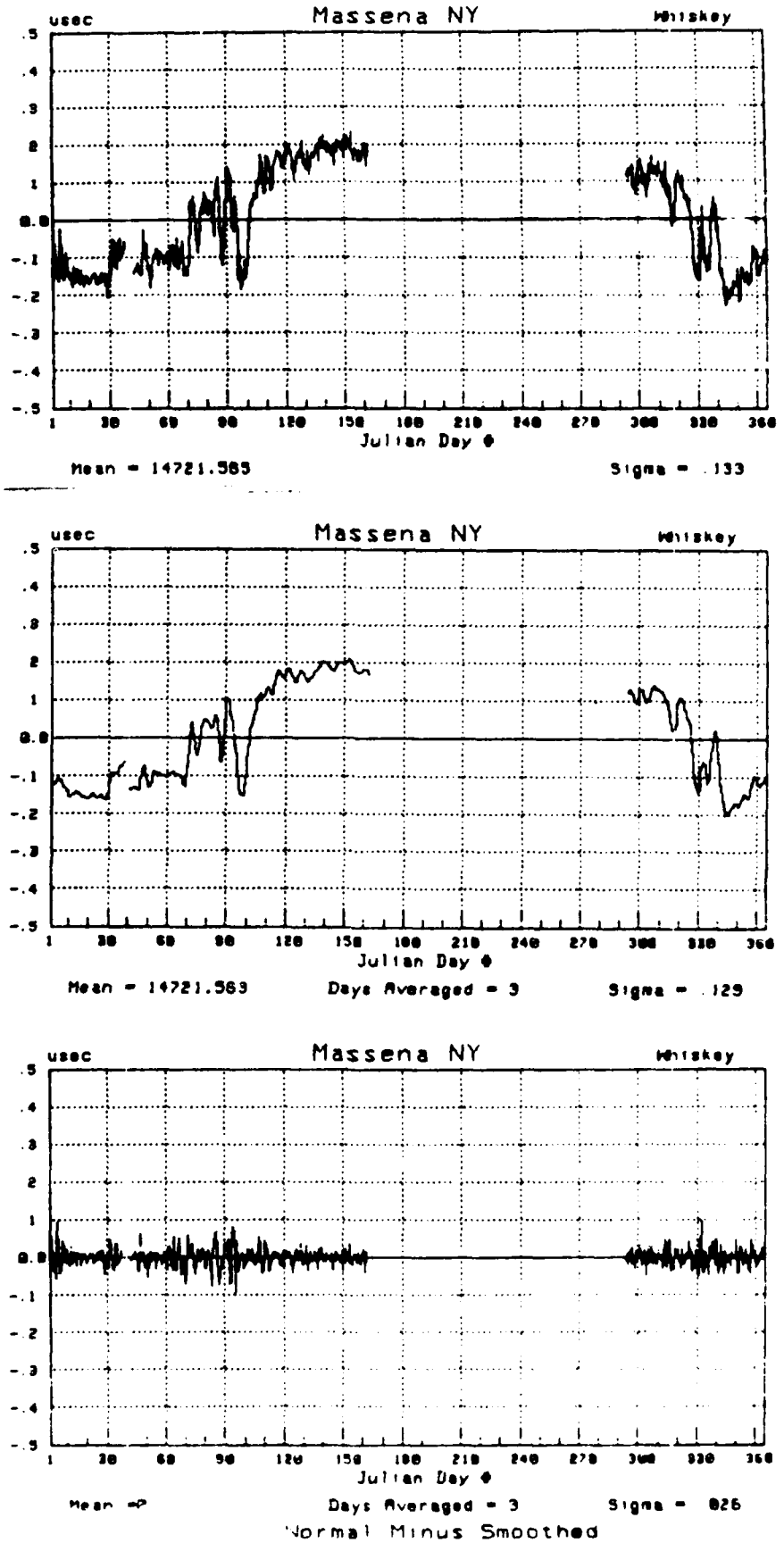

Figure 4-7 Breakdown of Frequency Components: 9960-W TD at Massena Using 3-Day Smoothing

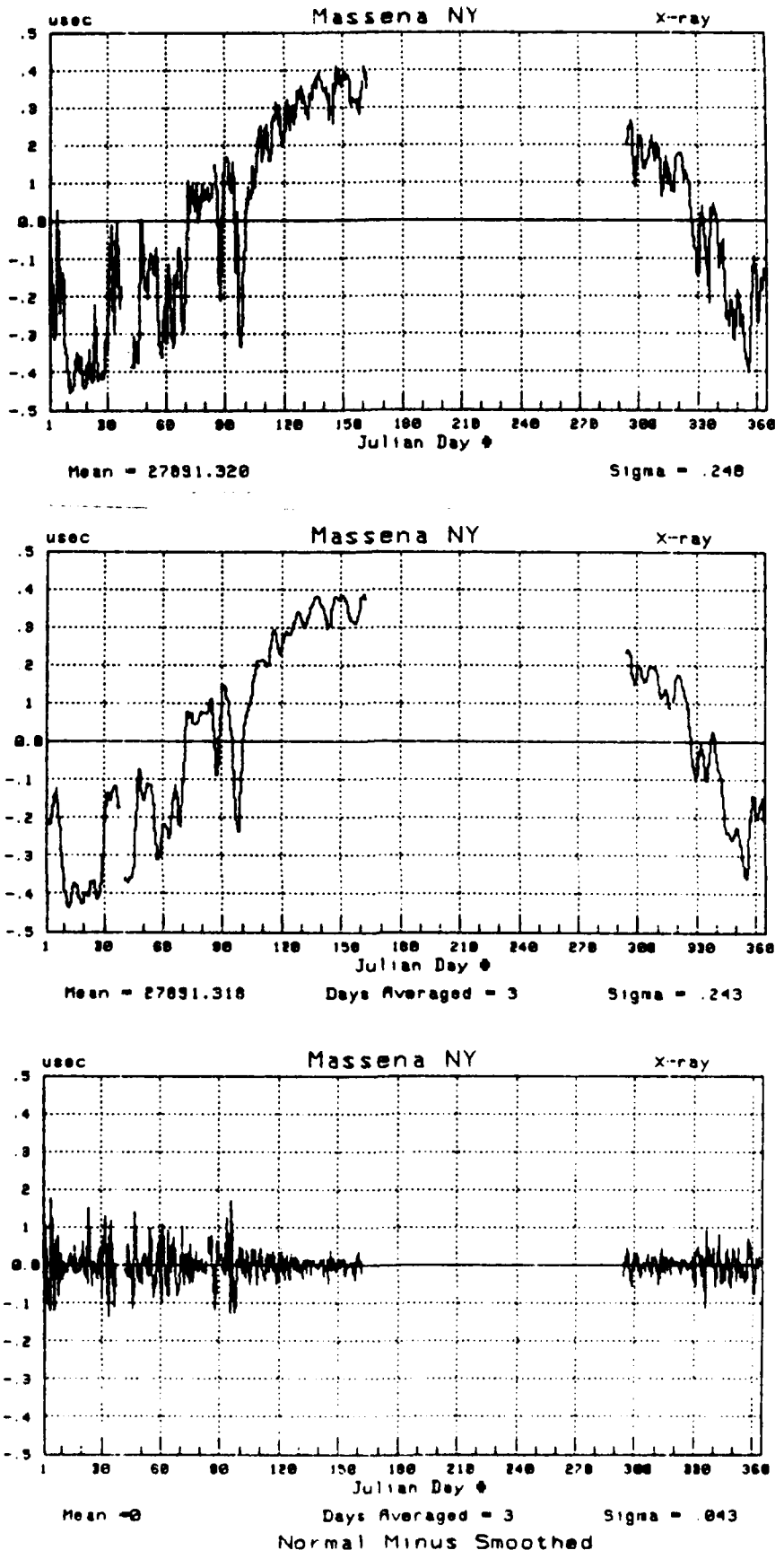

Figure 4-8 Breakdown of Frequency Components: 9960-X TD at Massena Using 3-Day Smoothing

We see that the standard deviations of the "residuals" have now been reduced to 26 and 43 nanoseconds for the 9960-W and 9960-X baselines respectively. This represents a substantial improvement over the 47 and 82 nanosecond residual standard deviations after the application of the 2 week filter and is approaching the figure we expect. The remaining disagreement is not an immediate cause of concern because we know that part of the remaining short term and near-instantaneous components are spatially correlated. Unfortunately, for these components, the spatial and temporal nature of the variations are significantly related so we cannot remove any more spatially correlated components by time domain filtering alone. Thus we have gone about as far as we can go with "Massena only" data

We should not conclude this section on such a negative note: the Massena data has proved extremely useful in verifying much of what was presented in Section 3. For "raw" Loran-C, the predicted statistics agree extremely well with those observed at Massena. Thus, we can verify the conclusion of Section 3 that raw Loran-C, year-round, is inadequate for the St Lawrence Seaway requirements. Although we could not obtain proper verification of the differential Loran-C statistics, this is a limitation to be encountered anytime data is available only from one site. From the Massena data, we saw no indications that our predictions are substantially out of line.

4.3 Evaluation of Data From Tibbetts Point

Our prime concern right now is to find some other site with reasonable data to further pursue the verification of our differential Loran-C performance predictions. Since we have a fairly complete data record from Tibbetts Point after early February 1982, we will start with that site. The extreme range from Massena makes this a fortunate site to have winter/spring data from.

The time difference records from Tibbetts Point are presented in figures 4-9 and 4-10 which include the "raw" data, the filtered (2-week) data and the "residuals."

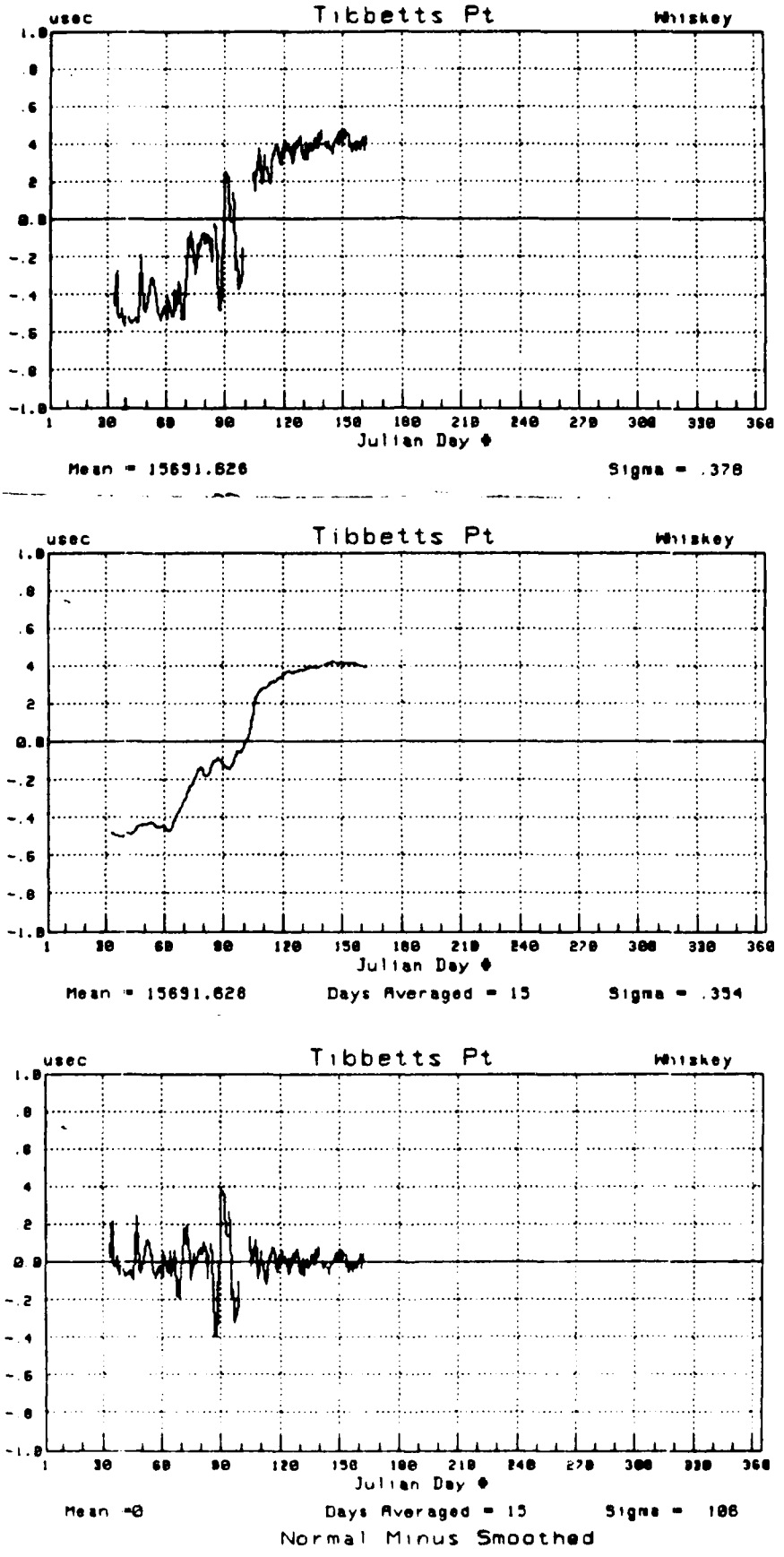

Figure 4-9 Breakdown of Frequency Components: 9960-W TD at Tibbetts Point Using 15-Day Smoothing

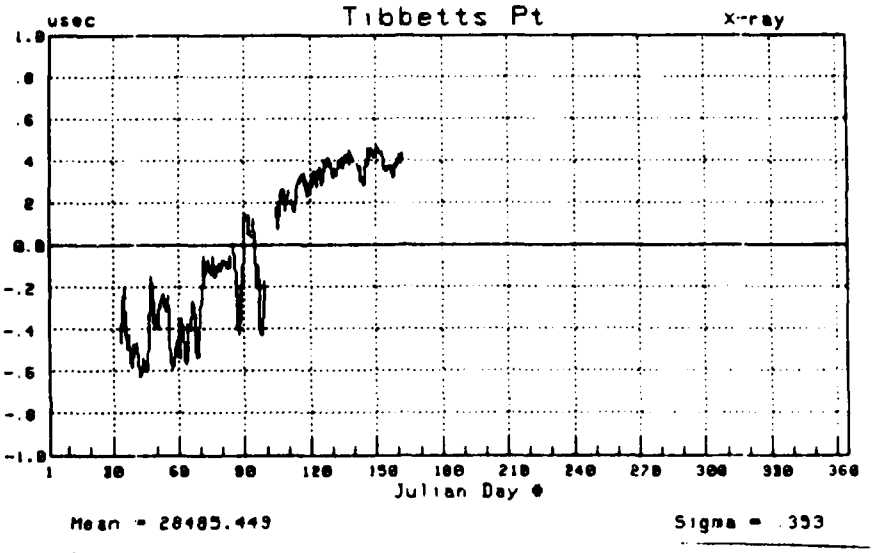

a.

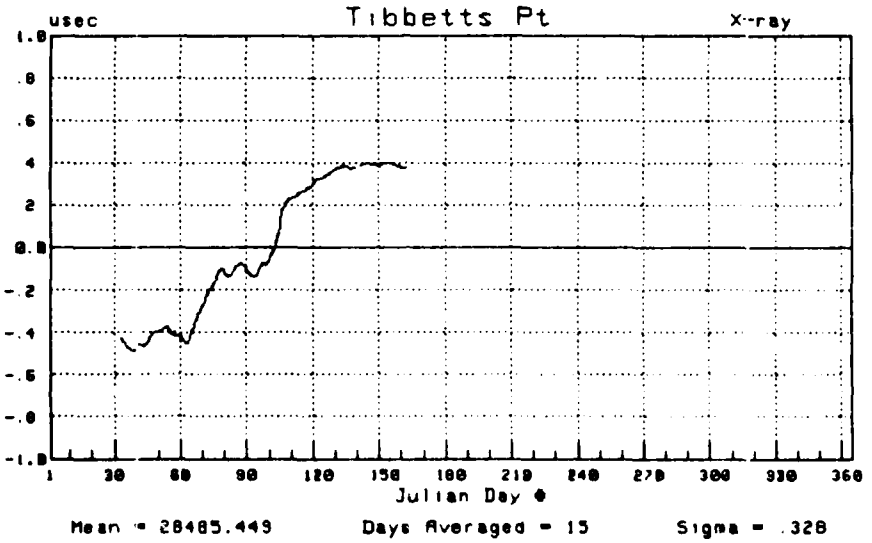

b.

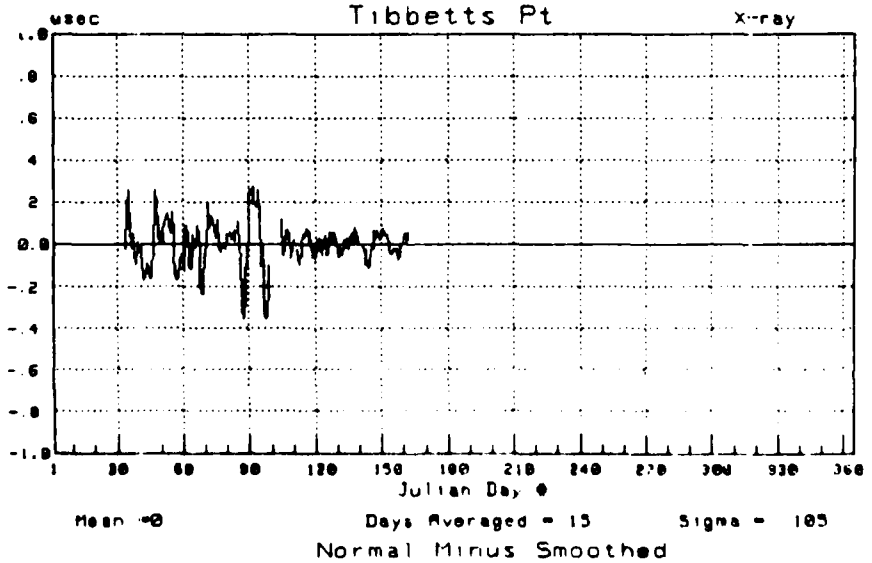

c.

Figure 4-10 Breakdown of Frequency Components: 9960-X TD at Tibbetts Point Using 15-Day Smoothing

The first comment we can make is that the peak-to-peak values of the seasonal component is about 900 nanoseconds for both baselines - 9960-W showing a slightly larger swing than 9960-X. Using the sinusoidal approximation, we would expect "sigmas" of about 320 nanoseconds. The computed "sigmas" turn out to be about 10% higher - a situation we might not encounter if we had data in January. For the most part, given we have only about 4-1/2 months of data, we conclude this is good agreement with the method used to predict "seasonal sigmas." (We are fortunate to have this particular 4-1/2 month period. Although not optimal, it allows a better estimate of the peak-to-peak variation than we would obtain from almost any other 4-1/2 month part of the year.)

We see a problem in that we predicted "sigmas" of 242 and 325 nanoseconds for 9960-W and 9960-X, respectively, at Tibbetts Point. Whereas the prediction error for 9960-X is less than 10%, it is over 50% for the 9960-W baseline. This observation, in conjunction with the observation that the Massena data agreed so well with the predictions based on other N.E.U.S. site data, suggests a significant violation of the uniform propagation (modified for "land/seawater") model. This is a significant finding (a "camel") and illustrates the utility of the low density analysis. Before considering implications of the problem for the differential Loran-C analysis, we should finish the discussion of "raw" Loran-C performance at Tibbetts Point.

Figure 4-11.a. is a scatter plot of the fixes obtained by using the Tibbetts Point data along with a superimposed error ellipse generated by using the observed statistics. The predicted error ellipse is provided as figure 4-11.b. to facilitate side-by-side comparison.

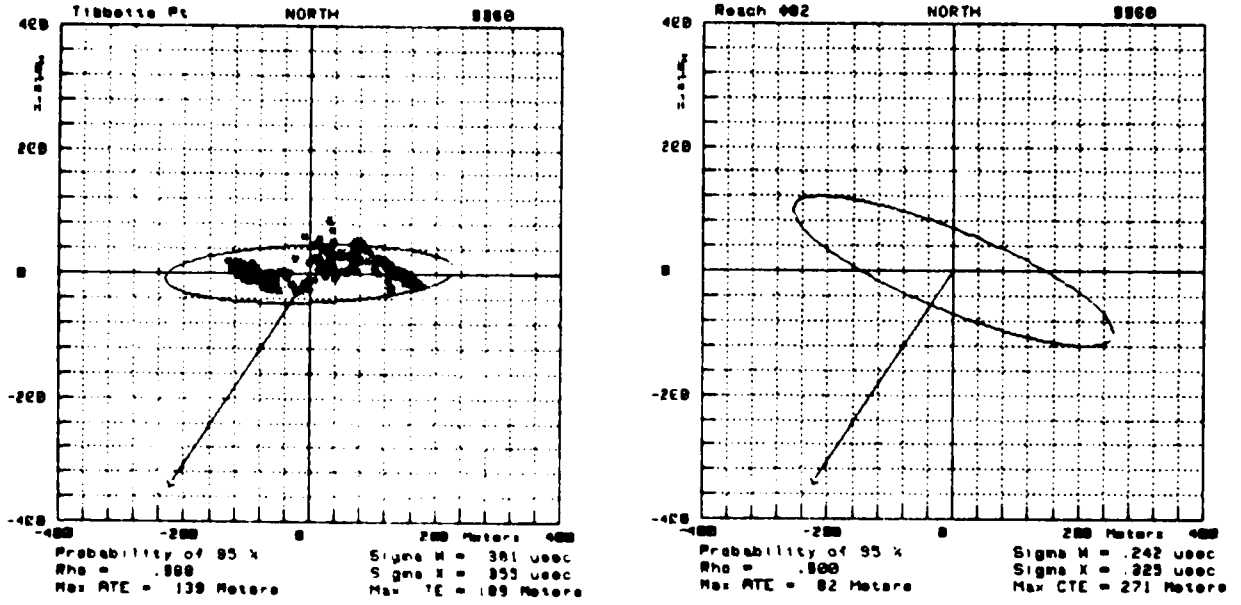

a. b.

Figure 4-11 Comparison of Predicted and Observed Error Ellipses - Tibbetts Point

Some comments are in order. First, we should note that the basic elliptical pattern is generally a correct representation of the actual distribution of errors. Next we note that the actual ellipse is rotated about 30° relative to the predicted ellipse. This rotation is a consequence of the incorrect estimate of the ratio of the variations for the two time differences (we predicted a "sigma-W/sigma-X ratio" of about 0.75 and observed one of about 1.07). Interestingly, the rotation (along with the effects of a much higher correlation coefficient than our conservative estimate) served the purpose of reducing the maximum cross-track error.

We should now move to a consideration of differential Loran-C performance at Tibbetts Point with corrections being applied from a monitor at Massena. We begin by subtracting the Massena data records from the corresponding records at Tibbetts Point. The results are shown in figures 4-12 and 4-13. Again, we provide the "raw" data, a filtered (2-week) version of the data, and the residuals of the filtering process.

We see that the peak-to-peak value of the seasonal component is about 600 nanoseconds for 9960-W and about 270 nanoseconds for 9960-X. By our sinusoidal approximation, we would thus estimate seasonal standard deviations of 212 and 95 nanoseconds, respectively. These are "close" to the computed values of 238 and 112. As with the comments on raw Loran-C at Tibbetts Point, we would expect better agreement if we had data from January.

The problem already noted in the discussion of the raw data at Tibbetts Point becomes even more pronounced when we compare these observations with our predictions of the differential variations. We predicted a "sigma-W" of 101 nanoseconds and a "sigma-X" of 76 nanoseconds. Thus we have a 136% error for 9960-W and a 47% error for 9960-X.

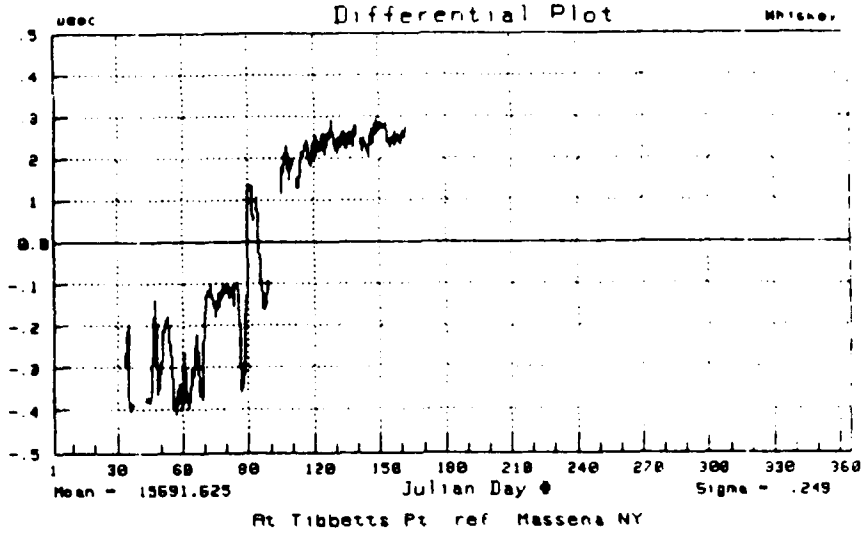

a.

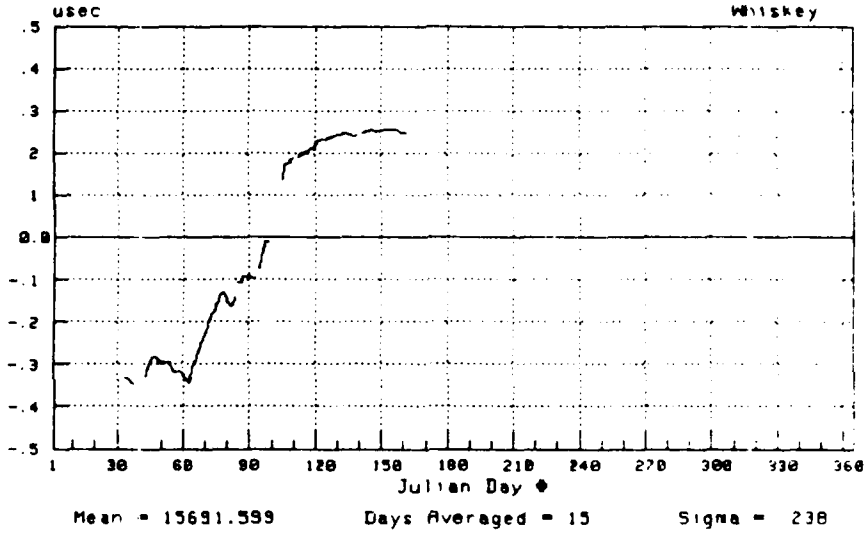

b.

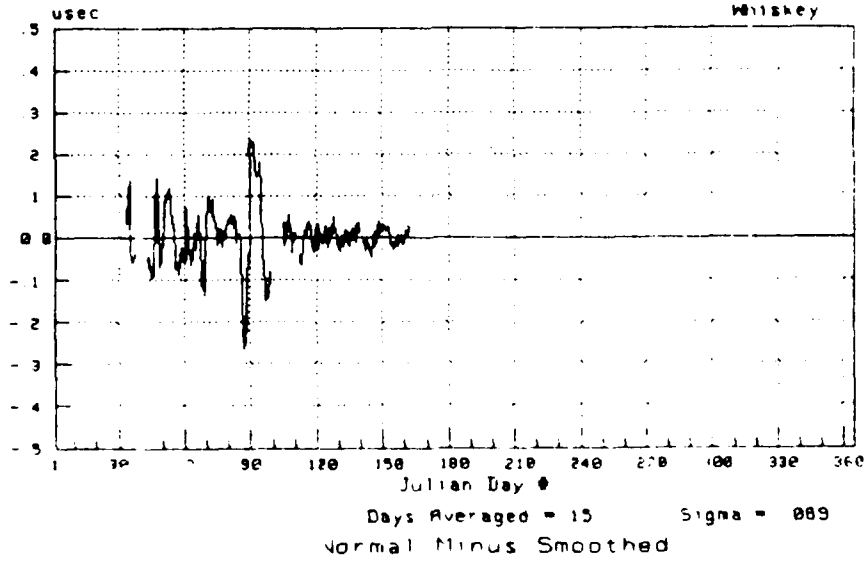

c.

Figure 4-12 Breakdown of 9960-W Differential Loran-C Frequency Components: Tibbetts Point Minus Massena Using 15-Day Smoothing

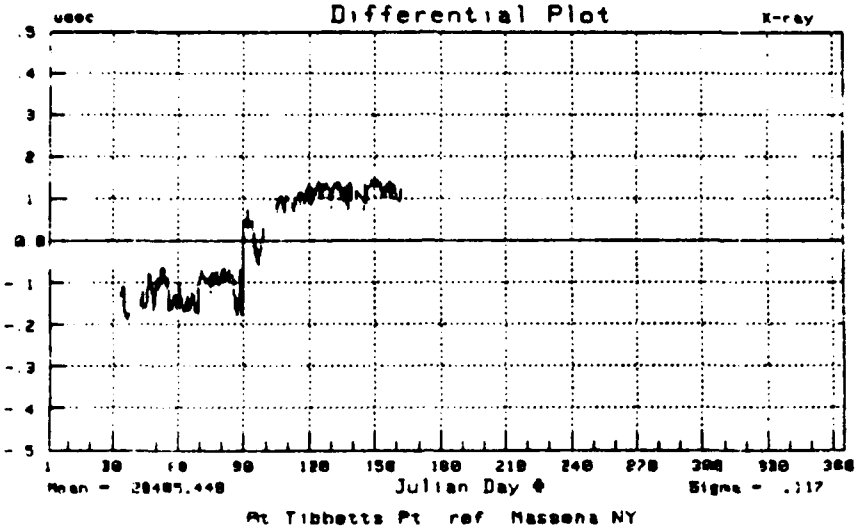

a.

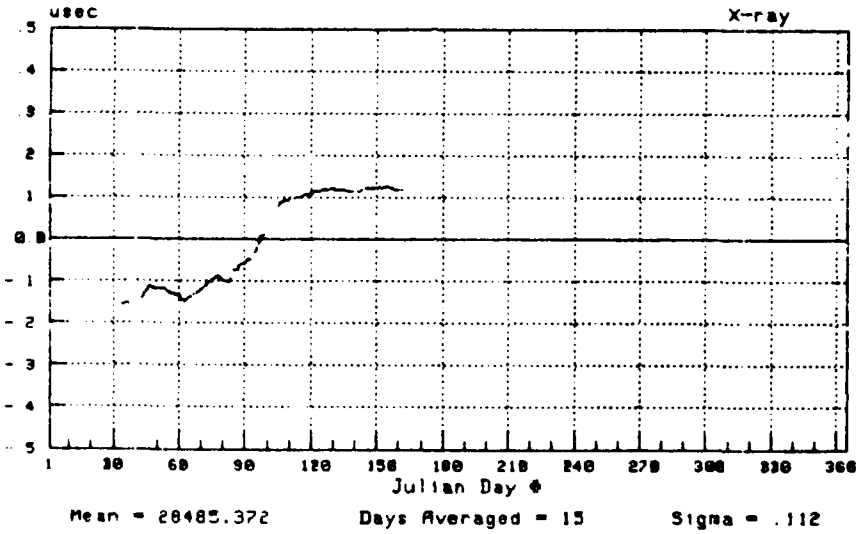

b.

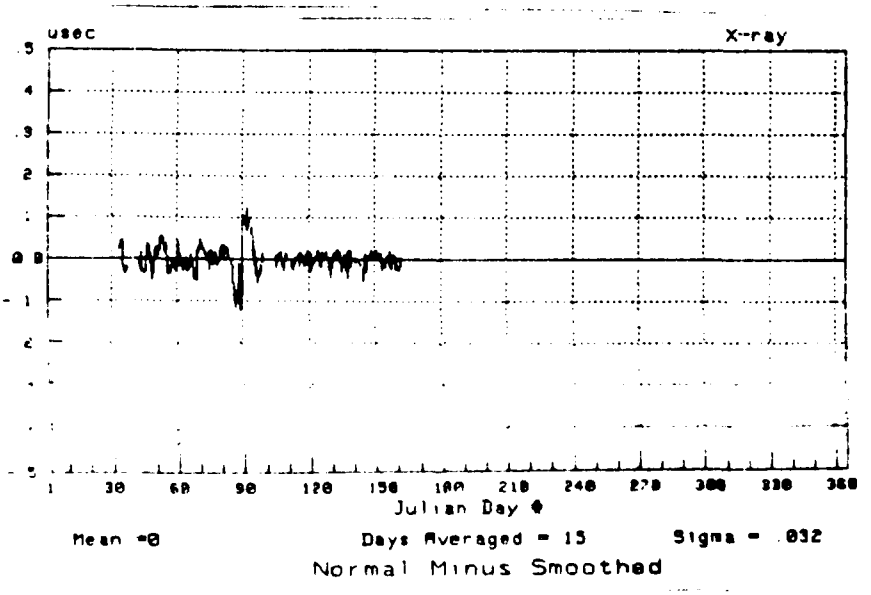

c.

Figure 4-13 Breakdown of 9960-X Differential Loran-C Frequency Components: Tibbetts Point Minus Massena Using 15-Day Smoothing

A scatter plot for the data contained in figures 4-12.a. and 4-13.a. is provided in figure 4-14 along with a plot of the predicted error ellipse. Primarily because of the incorrect prediction of the "sigma-W/sigma-X ratio," the actual ellipse is rotated about 50° from the predicted ellipse. Although the errors are much larger than we had predicted, it is interesting to note that the maximum cross-track error still leaves plenty of room in the vicinity of Tibbetts Point - Reach #82 has a half-channel width of 165 meters.

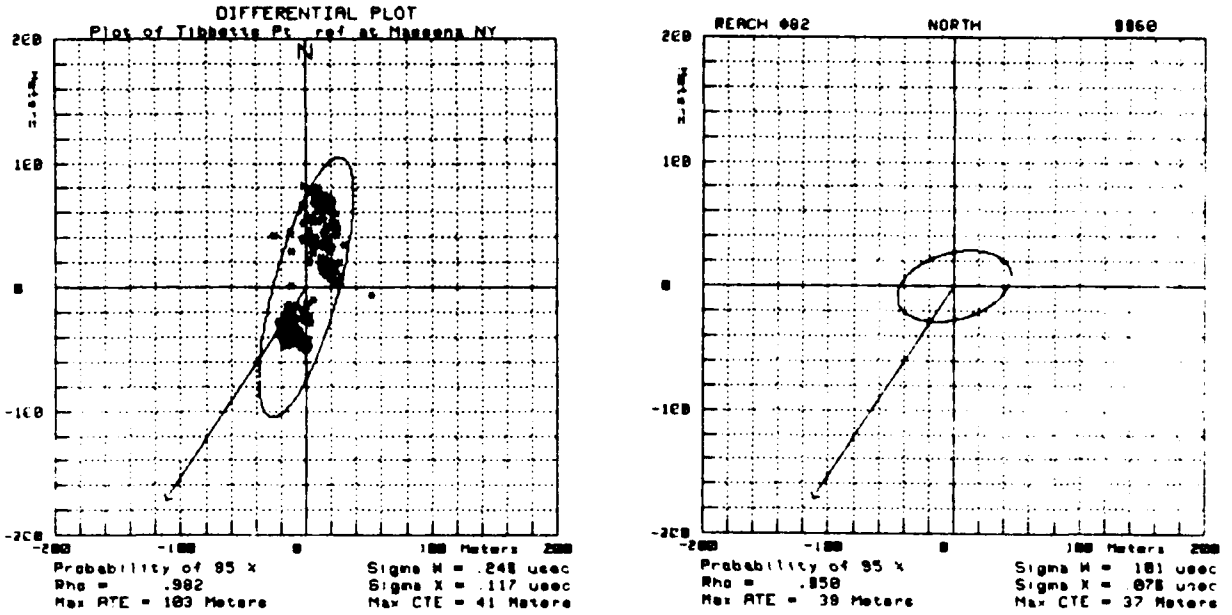

Figure 4-14 Comparison of Predicted and Observed Differential Loran-C Error Ellipses: Tibbetts Point Minus Massena

We must recall, however, that the prime use we need to make of the Tibbetts Point data is to determine how well we can predict what happens between Tibbetts Point and Massena. In this regard, we recall the Section 3 conclusion that it appears we need at least one more differential correction station - most likely one in the vicinity of Wellesley Island. We expect the establishment of such a site (or, perhaps, additional sites) will reduce a considerable portion of the seasonal variation shown in figures 4-12.b. and 4-13.b.

If we imagine, for the moment, that we can remove most of the seasonal component from the Tibbetts Point data by the application of differential corrections from some "yet-to-be-determined" site, we can focus our attention on the "residuals" shown in figures 4-12.c. and 4-13.c. We see standard deviations of 69 and 33 nanoseconds for 9960-W and 9960-X, respectively. Although roles have been reversed as to which TD varies more, we note we are left with standard deviations smaller than those for the "analogous" "Massena only" situation shown in figures 4-5.c. and 4-6.c. This is in spite of the fact that Tibbetts Point is as far southwest of Massena as one can go and still be in the Seaway. This illustrates the claims of the previous section that much of the variation remaining afte-

the seasonal frequency component has been removed is still spatially correlated. Unlike with the "Massena only" situation, we now have a means to "get at" this other dimension of the variations. A very important observation is that the 33 nanosecond standard deviation for 9960-X approaches the $20\sqrt{2}$ (i.e., 28) nanosecond standard deviation we used for the "spatially independent" component in our predictions.

At this point we should focus our attention on this 33 nanosecond statistic for the 9960-X baseline and review how it was obtained. First we subtracted the Massena data record from the Tibbetts Point data record to simulate differential Loran-C. In doing so, we fully expected the result to have all four frequency components remaining. The magnitude of the components was expected to be in accordance with the following breakdown:

a. Seasonal frequency component. We expected this component of the Tibbetts Point and Massena data records to have almost perfect spatial correlation. Note correlation does not imply a one-to-one relationship (i.e., when the Massena data slowly "rises," we expect to find the Tibbetts Point data slowly rising - but not necessarily by the same amount). Thus, we expect the differential corrections will remove only a certain percentage of this component of the variation - that dictated by ΔDRD considerations. Thus we expect to find a seasonal frequency component remnant in the "Tibbetts minus Massena" data.

b. Medium-Term frequency component. As with the seasonal frequency component, we expect almost perfect spatial correlation in this component of the Tibbetts Point and Massena variations. Also, we expect to be able to remove only the percentage of this component dictated by the ΔDRD. Thus this component is expected to be found in the "Tibbetts minus Massena" data.

c. Short-term frequency component. We expect this component to have <u>two</u> significant sub-components:

(1) A spatially correlated part which occurs for the same reasons the seasonal and medium term components occurred. Again, the percentage removed will be dictated by ΔDRD so the "Tibbetts minus Massena" data will contain some of this component.

(2) A spatially independent part due to the passage of fronts, etc. We do not expect to be able to remove any of this so it will be found, in toto, in the "Tibbetts minus Massena" data.

d. Near-instantaneous frequency component. We expect this component to have <u>three</u> significant sub-components:

(1) A spatially correlated part due to chain timing corrections, most of the effects of chain equipment changes, equipment problems at the SAM, and rapid weather effects that are localized to the vicinity of SAM. etc. We expect this sub-component to be <u>common</u> to all sites and thus not be present in the "Tibbetts minus Massena" data.

(2) A spatially correlated part that, like the seasonal and medium term components, is related to double range difference. This will be present in the "Tibbetts minus Massena" data because only the percentage

dictated by ΔDRD considerations is removed through differential corrections.

(3) A spatially independent sub-component due to local weather effects, local equipment reactions to chain equipment changes, and local noise, etc. This cannot be removed or reduced through differential corrections and will thus be present, in toto, in the "Tibbetts minus Massena" data.

By the time we had looked at only the "raw" Loran-C data at Tibbetts Point we knew we had encountered an anomaly in the double range difference which would impact on the worthiness of our predictions. The anomaly became even more noticeable when we actually accomplished the data record subtraction to simulate the effects of differential corrections from Massena being applied to a "site of interest" at Tibbetts Point. Since we had already concluded in Section 3 that we probably could not "make it" with only the monitor at Massena, this was not an immediate cause for alarm. Since the seasonal frequency component is hypothesized (based on considerable corroborating observations at other sites) to be almost perfectly spatially correlated, a comparison of this component in the "Tibbetts minus Massena" data to the predictions gave a measure of the error in the assumed ΔDRD. We assume we can remove this, and any other spatially correlated component or sub-component to any extent we find necessary (actually, at Tibbetts Point, because of the wide channel, no improvement is necessary) by appropriate selection of a closer differential correction station.

Putting this "assumed solvable" issue aside for the moment, we would like to attempt to "get at" an observed measure of the spatially independent component. The criticality of this quest is seen if we recall the final discussions in Section 3.5: because of geometry, it is the spatially independent component - the one that we cannot remove no matter where we locate the differential station - that appears to be the limiting factor in "tight reaches" such as #61 and #62. With our assumed statistics for the spatially independent component, we were already "too tight for comfort" in these reaches so that a critical goal of the data analysis should be to seek ways to confirm or refute these assumptions. If they are correct, or optimistic, we have severe problems. If they are pessimistic, we may be in good shape.

Thus, we removed the seasonal component in the "Tibbetts minus Massena" data in our first attempt to get at the "spatially independent only" portion of the variation. This, then, is how we arrived at the 33 nanosecond figure for 9960-X (and the 69 nanosecond figure for 9960-W).

This review complete, we can appreciate the question: are the 33/69 nanosecond figures representative of the spatially independent components - i.e., the best we can expect? From the discussion we can see we expect to find (if we somehow could) that the "real bottom line" is possibly better than the 33/69 nanosecond figures would indicate - but we cannot yet say how much better. We say this because sub-components decribed above to be "of type" b., c.(1), and d.(2) will be reduced as we move the differential control station closer to Tibbetts Point. By use of a time domain filter we cannot "get at" sub-component c.(1) without removing sub-component c.(2) (erroneously), nor can we get at sub-component d.(2). We can, however, remove sub-component b. by use of a 3-day filter. We do this in figures 4-15 and 4-16.

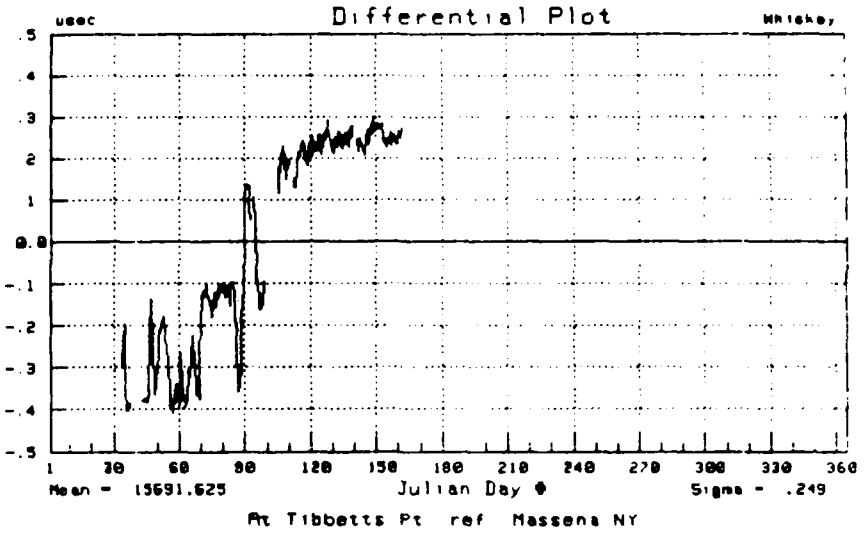

a.

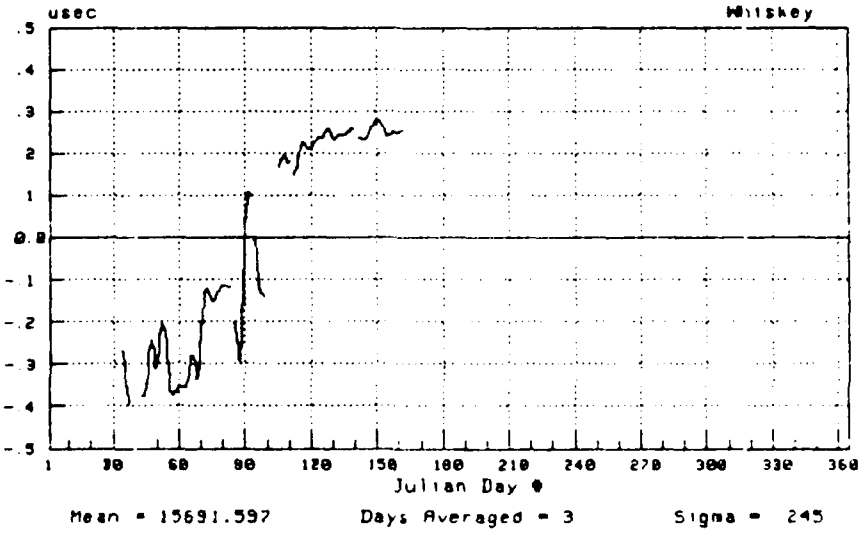

b.

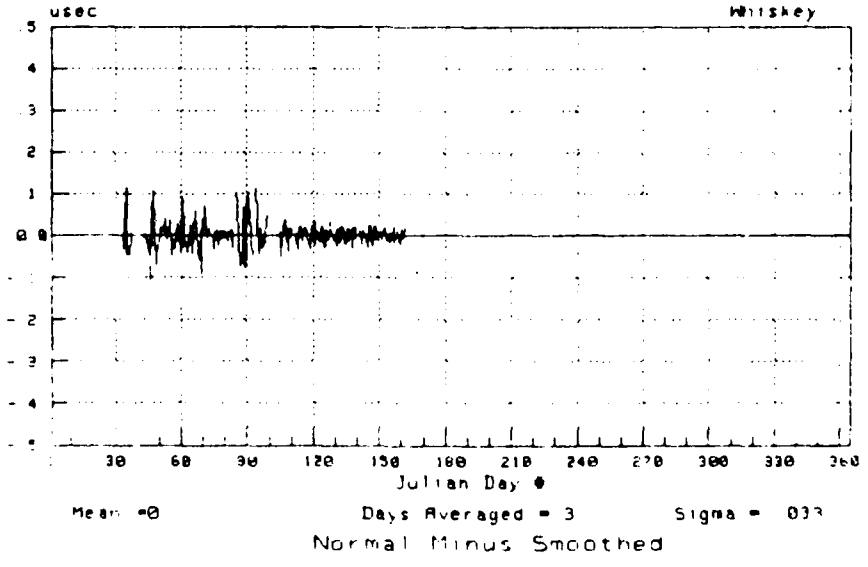

c.

Figure 4-15 Breakdown of 9960-W Differential Loran-C Frequency Components: Tibbetts Point Minus Massena Using 3-Day Smoothing

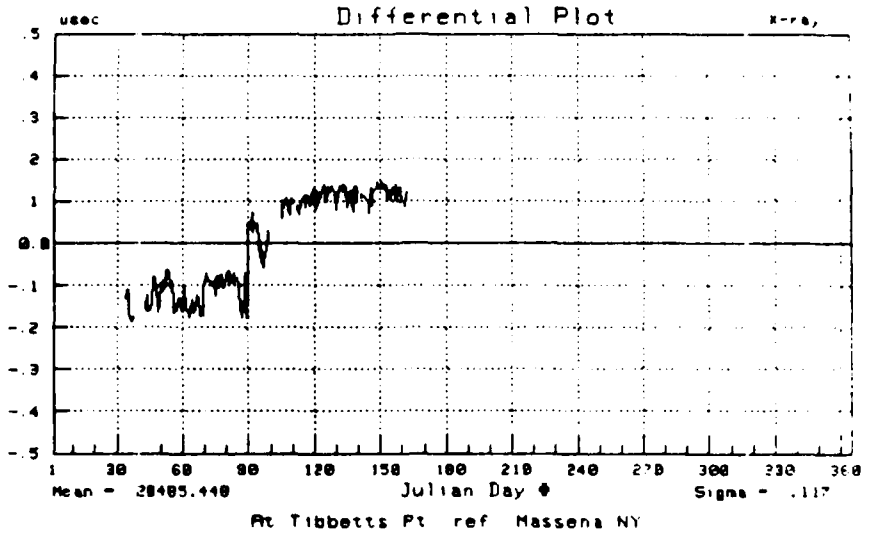

a.

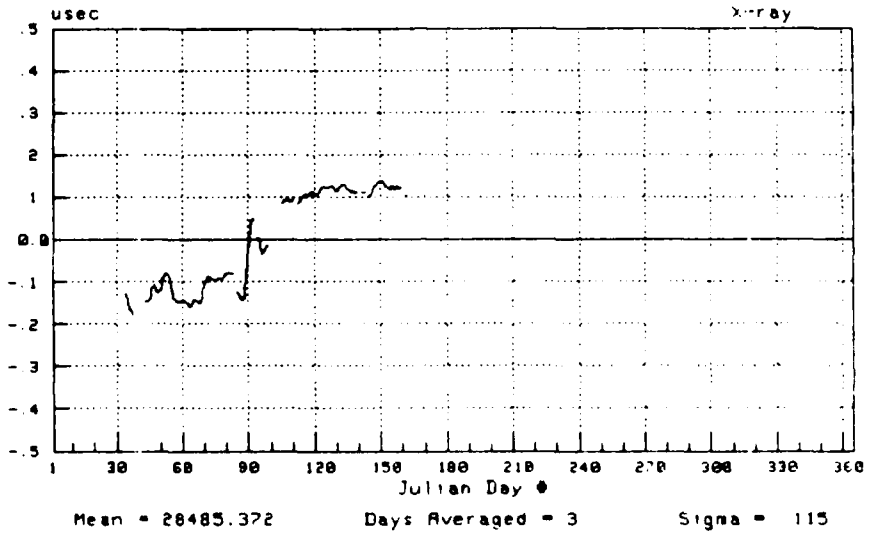

b.

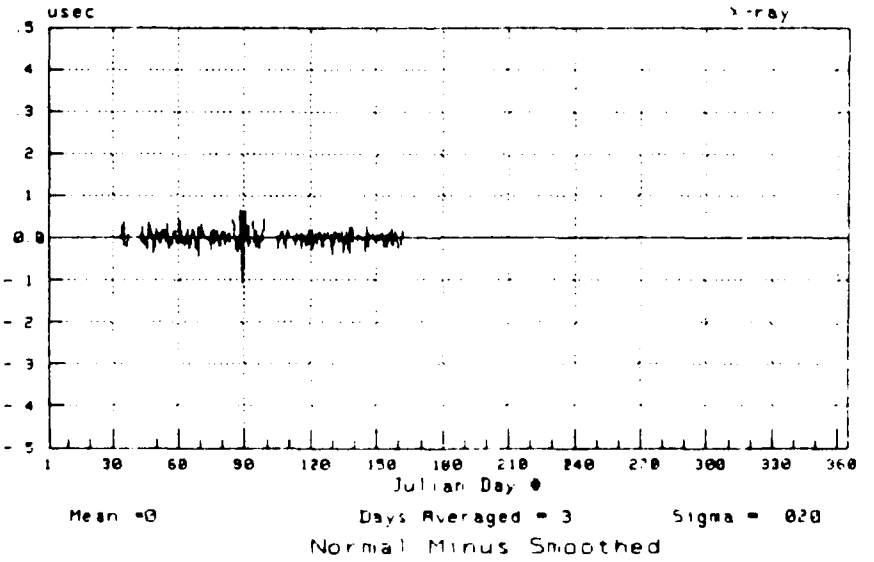

c.

Figure 4-16 Breakdown of 9960-X Differential Loran-C Frequency Components: Tibbetts Point Minus Massena Using 3-Day Smoothing

We see the significant effect this operation has had: the standard deviation for 9960-W has been reduced to 33 nanoseconds and the standard deviation for 9960-X has been reduced to 20 nanoseconds. Thus, we have reason for hope. Before considering the implications of these results we should pause to compare these results with the analogous situation for the "Massena only" analysis reflected in figures 4-7 and 4-8. Note that by subtracting the "3-day-filtered" component in both cases we removed the seasonal and medium term components. The difference in the plots (which resulted in a standard deviation reduction from 43 to 33 nanoseconds for 9960-W and from 26 to 20 nanoseconds for 9960-X) was obtained through "differential action." The difference represents how much of the "residual" variation was common to both sites (and thus removed in toto) and how much was related to ΔDRD (and thus removed in the percentage indicated by the ΔDRD).

(Note: A direct comparison of the 43 nanosecond figure to the 33 nanosecond figure does indeed confirm improvement. Likewise a comparison of the 26 and 20 nanosecond figures. There is more going on here, however, than the direct comparison indicates. Recall the formulation of Section 3 (and Appendix C) shows that when we implement differential Loran-C when there is no spatially correlated component, we actually expect the standard deviation to increase - by a factor of $\sqrt{2}$. Thus, our predictions had accounted for an increase in the standard deviation if there were no spatially correlated components. In view of this consideration, the reductions are even more significant in their implications.)

"Tantalizingly," we cannot distinguish between the two sources of improvement at present. At worst, all the improvement was due to the removal of common error terms. More likely, some of the improvement was due to the removal of the common error terms and some was removed because Massena is closer to Tibbetts Point than Sandy Hook, N.J. or Cape Elizabeth, Me, are. In this latter, more likely case, we can expect even further reduction in the residual variations if we locate a differential correction station closer to Tibbetts Point (which, it should be clear by now, we must do).

Bearing this "hoped for" further improvement in mind (besides recalling we are temporarily ignoring the question of how to get rid of the majority of the large spatially correlated components), we should turn to the all-important consideration of how the TD variations in figures 4-15.c. and 4-16.c. translate to positional errors. Those TD records are converted to position variations in the scatter plot of figure 4-17.

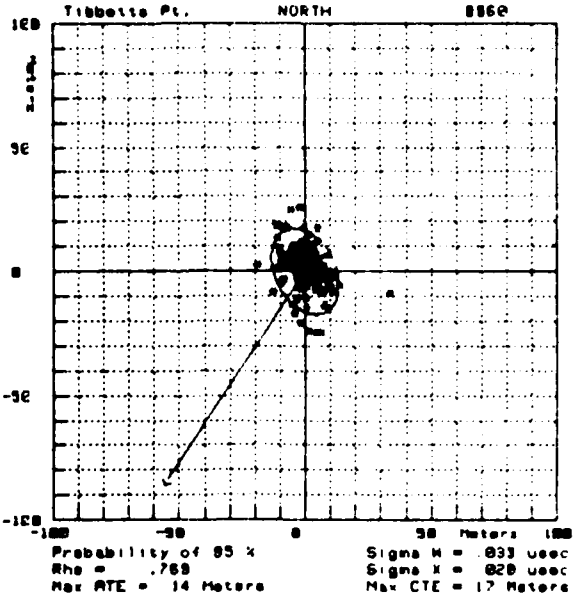

Figure 4-17 Error Ellipse for Differential Loran-C High Frequency Components: Tibbetts Point Minus Massena

From the plot we see further cause for optimism - a cause that has been evident in previous scatter plots. The increased "sigma-W/sigma-X ratio has again rotated the error ellipse. This is of absolutely no significance in the "wide open" channel near Tibbetts Point but is of immense concern in the tighter reaches such as #61 and #62 where, as indicated in Section 4, we were stymied by an almost "worst case" orientation of the major (larger) axis of the ellipse. Although the data was not obtained in the vicinity of these reaches, we can simulate what we now have reason to expect will occur in these reaches - with a nearby differential control station - by applying the geometry at these reaches to the Tibbetts Point data of figures 4-15.c. and 4-16.c. This is not a "reckless" thing to do since, because these reaches are closer to Massena than Tibbetts Point is, we expect even smaller variations would be observed at these sites. This simulation is accomplished in figure 4-18.

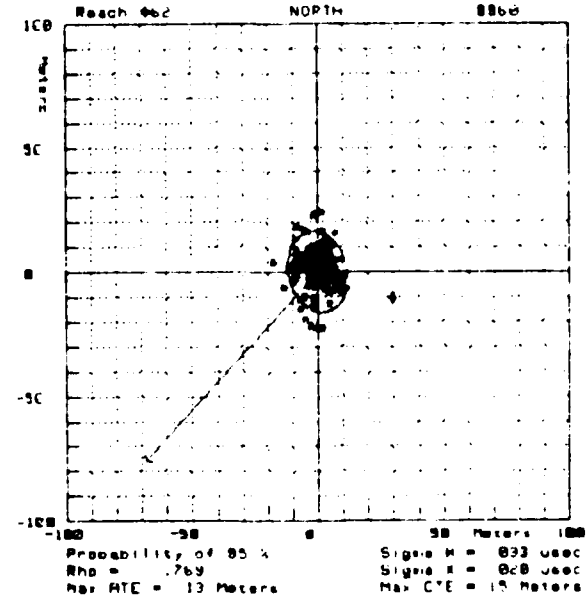

Figure 4-18 Application of the Loran-C Data of Figure 4-17 to the Geometry at Reach #62

Again, we see the "benign" change in the orientation of the ellipse. The significant reduction in the variation of the 9960-X TD is responsible for this. The phenomenon is illustrated, somewhat, in figure 4-19 where we show the actual LOP's at Reach #61. We see immediately, of course, that the crossing angles of the LOP's are far from optimal. More importantly, we see that the W LOP is nearly perpendicular to the course. Thus, variations in the 9960-W TD's produce substantial along-track errors but not much cross-track error. The 9960-X LOP is by no means parallel to the course but it does have a larger "cross-track-error-axis-projection" than the 9960-W LOP. Thus, a significant reduction in the 9960-X variations from what we predicted (i.e., a reduction from 28 nanoseconds to, at most, 20 nanoseconds) has a significant effect on the cross-track error near reaches #61 and 62.

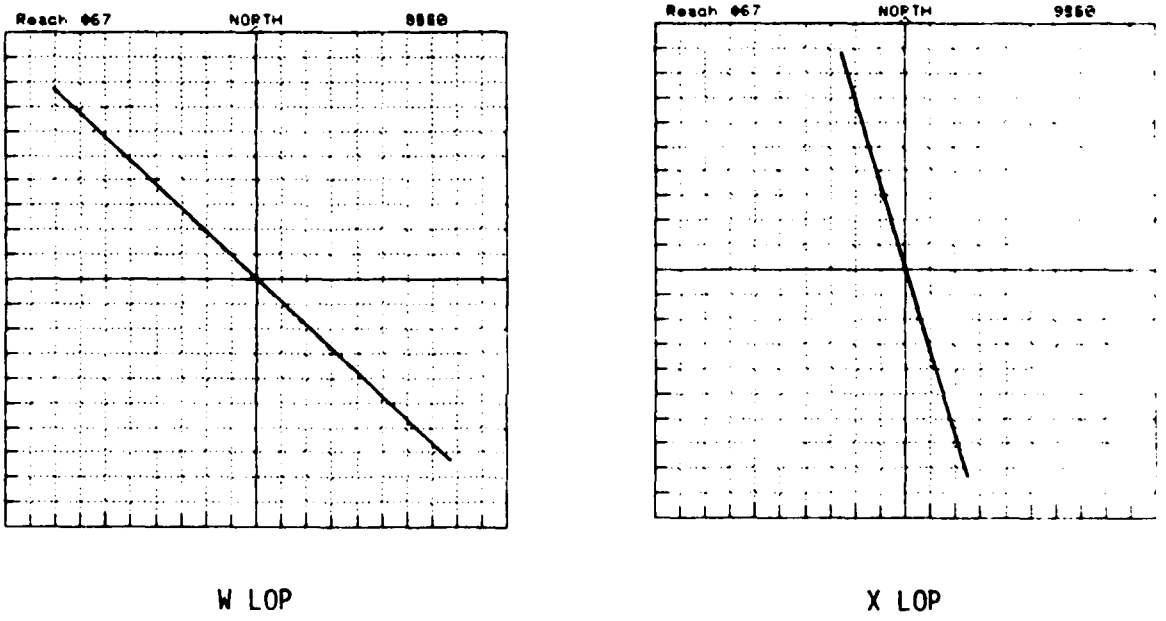

W LOP X LOP

Figure 4-19 9960-W/X Lines of Position at Reach #67

It is interesting at this point to note how the 95% percent contour is beginning to truly approach that gaussian characteristic - a small but noticeable percentage of the fixes of figure 4-18 are outside the contour (the data record shows 15 out of just over 200 points are outside the contour). In figure 4-20, we show the same scatter plot as in figure 4-18 but now superimpose the 99.9% probability contour.

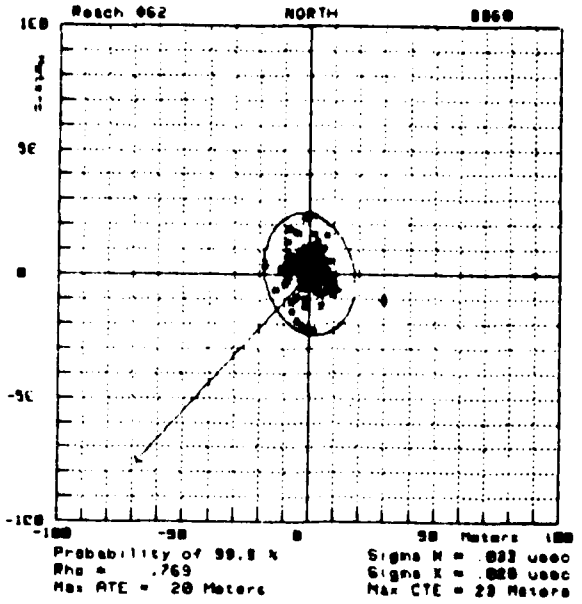

Figure 4-20 Same Data Points as in Figure 4-18 With 99.9% Probability Error Ellipse

Here we see direct evidence of applicability of the gaussian characteristics. We note that the one point which is outside the ellipse is "way out." This fix is a result of the data which shows up as a "spike" in figures 4-15.c. and 4-16.c. just before 1 April 1982 (Julian Day 91). The first thing we should say is that the large TD variations did not result in an abnormally large cross-track error so we are interested in the "anomaly" only in a statistical sense (i.e., "this time" the direction of the large positional error was benign but what about next year?). This anomalous point will be discussed in greater detail in the next section. For now, we will simply point out that the "wild behavior" at about 1 April 1982 is evident in all data records presented thus far - i.e., in both the 9960-W and 9960-X data records for both Massena and Tibbetts Point (check figures 4-5.c., 4-6.c., 4-9.c., and 4-10.c.). This indicates a portion of the anomaly is spatially related (specifically, of type c.(1)) and would have been further reduced by a closer differential correction station.

Before finishing up the discussion of the "Tibbetts minus Massena" data we should return to the question of the large seasonal and medium term frequency component that we temporarily put aside. Even though we do not yet know the "bottom line" on the spatially independent variations (though we know we must be approaching it) we see from figure 4-20 that we have some "breathing room" even after we allow for 17 meter vessel half-widths and as much as 10 meters for guidance error. Thus we can allow for "mild" spatially correlated components to be added to the spatially independent components - particularly for the 9960-W baseline in the vicinity of Reaches #61 and 62 - and still be safe. Thus, we could re-do the differential Loran-C predictions of Section 3 based on the new evidence about the size of the spatially independent components. We claim, however, that such an update is premature at present.

If we were to attempt an update, we would have to revise our estimation of the spatially correlated components as well as the spatially independent ones since available data also indicates the need. Given only two data sites however, our only recourse would be the application of another linear model - i.e., create straight lines of different slopes than those shown in figure 3-5: the basis for the predictions of Section 3. The updated slopes would have to be determined by forcing straight lines to pass through the Tibbetts Point and Massena data points.

Although at first glance this might seem like a very "artificial" thing to do it would be consistent with the most popular, classical approach to a non-linear problem. In the approach it is argued that, although a generally non-linear effect is conceded, a linear approximation to the variation is satisfactory for a small area about the operating region. The arguments are based on Taylor series considerations. If we were to use them, we would, in essence, be claiming that terms of higher order than the linear ones (there may be several independent variables) are negligibly small. For the case in point, we would be conceding that a simple linear relation does not hold all the way from the "origins" (Sandy Hook/Cape Elizabeth) to Tibbetts Point, but is very nearly what happens over the small area of the Seaway. Thus, we would be arguing the "bulk" of the non-linear effects have occurred before we get to the Seaway. Herein lies the reason we cannot use this approach: we already know, from section 4.2, that the Massena data agrees very well with what a simple linear extension of N.E.U.S. coast data suggests.

Thus, we know that if Tibbetts Point is "way off the curve," the bulk of the non-linear effects are occurring in the Seaway. Functionally, this means we have evidence that our relationships have significant higher order spatial derivatives - which translate to significant higher order Taylor series coefficients - in the Seaway. The practical implication is in regards to number of monitor stations we need and our estimates as to the safety margin the resulting system provides. To see this, suppose we use a linear approximation between Massena and Tibbetts Point. The assumed propagation velocity changes (the slopes determine by the regression analyses) would be greater than those used in Section 3. This would make our predictions about how far we can move away from the differential correction station without encountering unacceptably large errors <u>less</u> optimistic. This is a step in the right direction.

However, we would still be exhibiting too much optimism. Suppose that the propagation conditions that indicate the linear regreesion analysis slope that apparently holds true from the origins to Massena also hold true considerably further southwest along the Seaway. Worst case, it would hold true all the way to Reach #61. In this case we would need an even <u>steeper</u> slope to account for the variations from Reach #61 to Tibbetts Point. Thus our results, were we to revise the predictions of Section 3 based only on the data available to us now, would be much too optimistic. In summary, therefore, we desperately need information from other sites - ideally in the region between Wellesley Island and Reach #61.

In the following section, we will attempt to examine data from other sites. Before doing so, we should review the conclusions of this section. With data from Tibbetts Point as well as Massena, along with a substantial amount of data processing, we have reason to challenge the underlying assumptions of the predictions of Section 3 - for the southwest portion of the Seaway. We have concluded we were too optimistic about the spatially correlated component of the variations but too pessimistic about the spatially independent component. Given the discussion at the end of Section 3.5 regarding the implications of the assumed magnitude of the spatially independent component at Reaches #61 and 62, this type of finding is the "next best thing" to finding we were pessimistic in all regards. There is no (Loran-C) solution if the spatially independent component is too large. The spatially correlated component can be reduced by proper selection of the differential control station(s).

The concern now is whether or not we have adequate data from other sites to proceed with the selection process.

4.4 Evaluation of Data from Other Sites.

Examination of Table 4-1 does not give us much reason for hope in our further investigations. As it turns out, however, we are partially in luck. We have a very nearly complete data record from the Ad Hoc site at Iroquois Lock for the period from Julian Day 80 to Julian Day 108 (21 March to 18 April). Coincidentially, this is one of the two periods we are most concerned about - spanning a period which includes the opening of the shipping season. This, however, is not the real reason for the luck. The real reason can be seen by examining plots of the data records for this period from Massena and Tibbetts Point. The records are provided in figures 4-21 and 4-22.

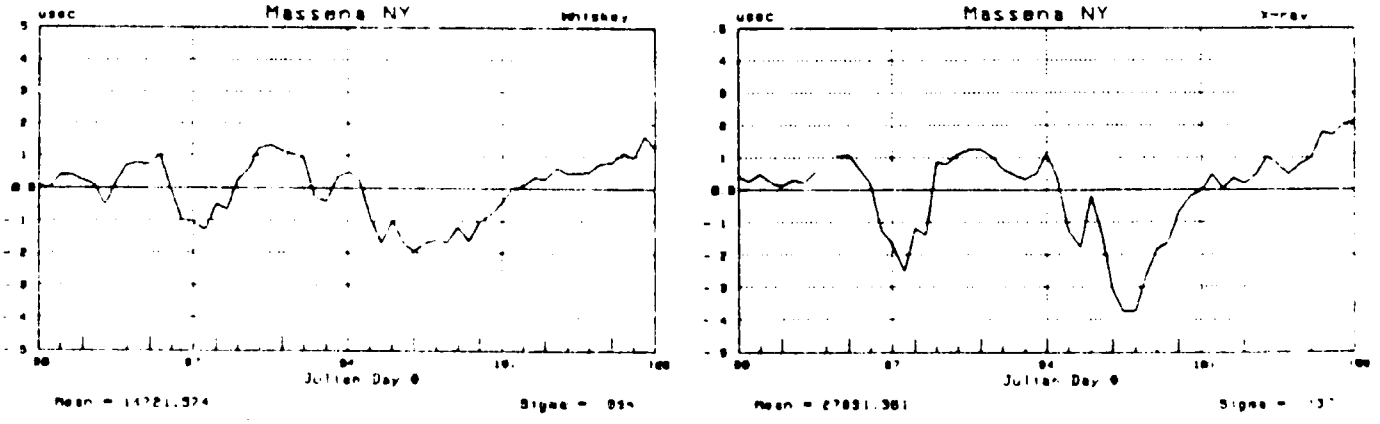

a. b.

Figure 4-21 Massena 9960-W/X Data for Julian Days 80 Through 108

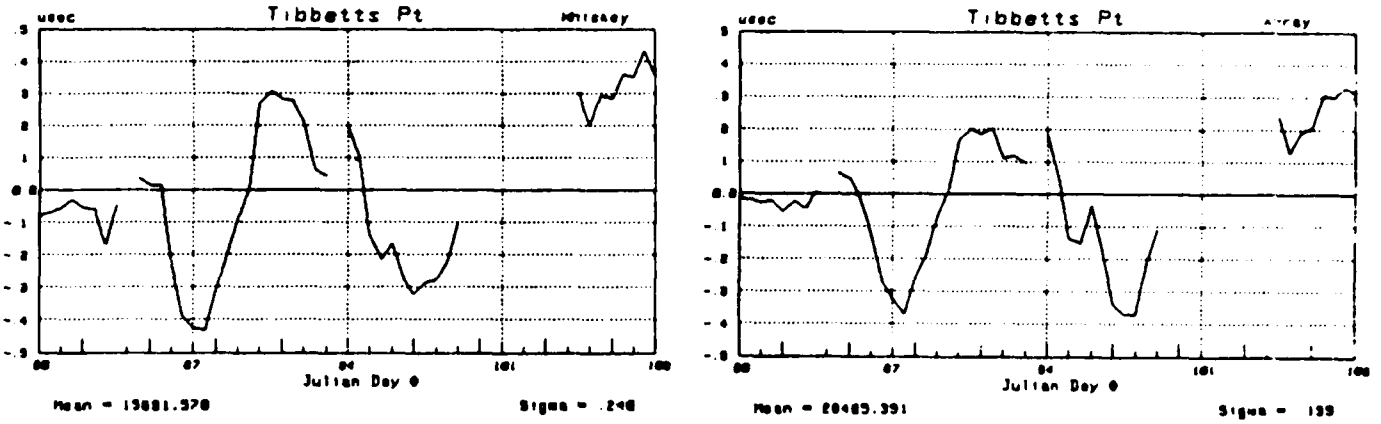

a. b.

Figure 4-22 Tibbetts Point 9960-W/X Data for Julian Days 80 Through 108

We see variations that are almost as large as the total variation seen throughout the year. This is not too surprising since we are concentrating on the "h·'h slope" portion of the seasonal component waveform, i.e., we are viewing the dramatic change from winter to summer. The comparison is illustrated in table 4-4.

Site/Baseline	"Seasonal Pk-Pk"	"30-Day Pk-Pk"
Massena - W	350 nsec	350 nsec
Massena - X	750	590
Tibbetts Point - W	900	850
Tibbetts Point - X	850	700

Table 4-4 Tabulation of 30-Day and Seasonal Peak-to-Peak Variations

Before proceeding, a few comments are in order. The "seasonal pk-pk" readings were obtained by examining the "filtered out" seasonal component. Thus, they were somewhat smaller than the total variation in the data record. The "30-day pk-pk" reading represents true "max minus min" readings. With such a short period, we do not have the luxury of examining all frequency components (e.g., a 2-week average is meaningless for the first or last week of the period. This makes a large impact on a 30-day data record). This illustrates the thought that we would prefer to have more data from other sites. Lacking this, we have the "next best thing." Given a choice of any 30-day period, March/April is preferable to other less eventful periods. An auxiliary benefit is that the shipping season begins on about 1 April so that our data record straddles the period of most critical concern.

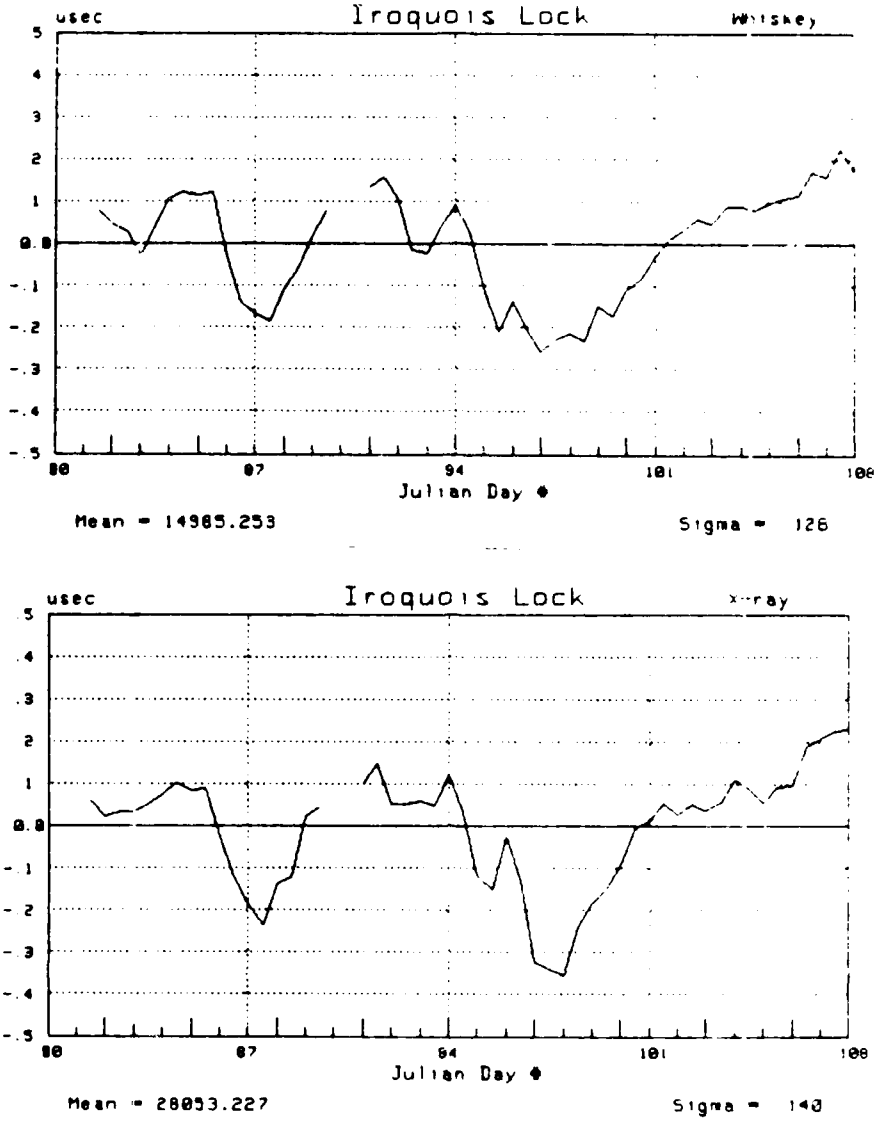

Figure 4-23 Iroquois Lock 9960-W/X Data for Julian Days 80 Through 108

Figure 4-23 shows the data of the period at Iroquois Lock.

We see strong correlation with corresponding plots of figures 4-21 and 4-22. Considering the "size" of the variations, we see much stronger agreement with the Massena data record than with the Tibbetts Point record, suggesting Iroquois Lock is closer to Massena in a "double-range-difference sense." Comparing the "sigmas," it appears the "closeness" of Iroquois Lock to Massena is more pronounced for the 9960-X baseline.

From Table C-2 we see Iroquois Lock (Reach #48), relative to Massena, has a Δ DRD of about 75 km for 9960-W and about 50 km for 9960-X. Tibbetts Point, relative to Massena, has a Δ DRD of about 320 km for 9960-W and about 170 km for 9960-X. Thus, we see why Iroquois Lock "looks more like" Massena than Tibbetts Point, and why Iroquois appears closer to Massena for the 9960-X baseline than for the 9960-W baseline. If we note the peak-to-peak variations at Iroquois Lock we obtain the values of Table 4-5

Site	DRD-W	30-Day Pk-Pk-W	DRD-X	30-Day Pk-Pk-X
Massena	460 km	350 nsec	540 km	590 nsec
Iroquois Lock	535	460	596	590
Tibbetts Point	780	860	720	700

Table 4-5 Tabulation of 30-Day Peak-to-Peak Variations With Modified Double Range Difference

This same data is plotted in figure 4-24.

a. 9960 - W

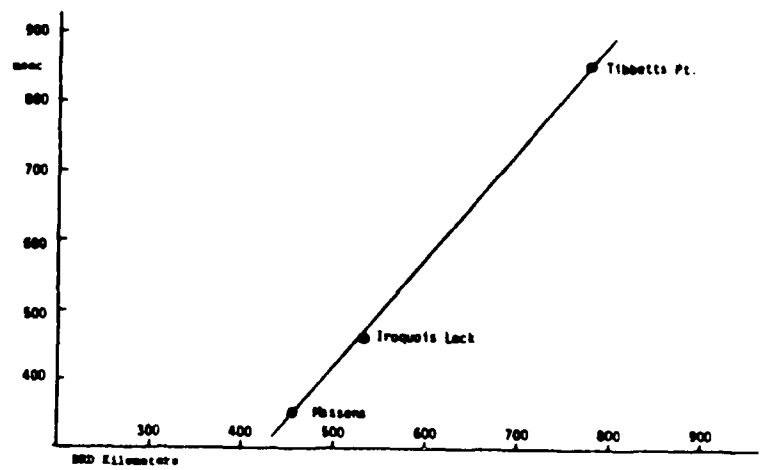

b. 9960 - X

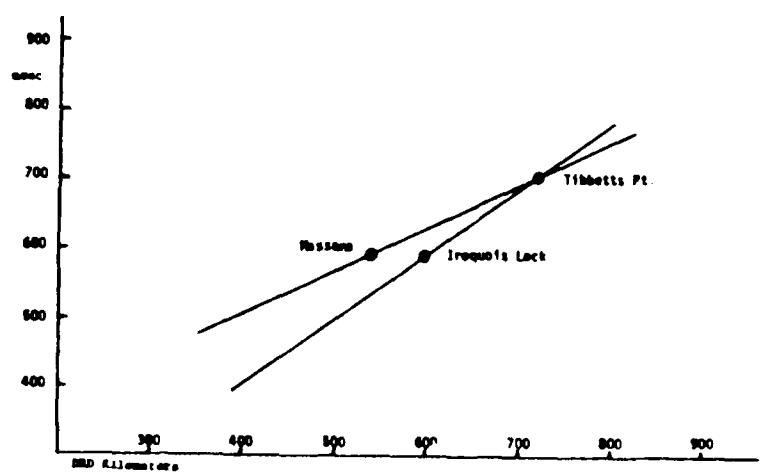

Figure 4-24 30-Day Peak-to-Peak TD Variations vs Double Range Difference

Recall we finished the last section with two unanswered questions: "how small is the spatially independent component of the variation?" and "where does the non-linearity in the spatially correlated component occur?" We are not yet able to address the first question but we can examine the second. The question affected the selection of two choices. The first choice was that a "local linear" approximation describes what happens between Massena and Tibbetts Point. The second is that there is some other site, closer to Tibbetts Point, which we should "pair with" Tibbetts Point in defining the slope of the straight line assumed to describe conditions in the "tight" reaches from #61 to #74. Adding these new observations, we can address the "choice" question of Section 4.3 and boldly state: "it depends."

Actually, the plots of figure 4-24 perfectly illustrate the concepts involved in the choices. In figure 4-24.a., we see a straight line approximation between Massena and Tibbetts Point looks valid: for the 9960-W baseline, the Iroquois Lock data plots almost right on the line. Conversely, the Iroquois data for 9960-X suggests, given we are concerned most about what happens between Iroquois and Tibbetts Point, we should draw a line of "steeper slope" through the Iroquois and Tibbetts Point data. But, suppose data from a site closer to Tibbetts Point, say Prescott, showed essentially the same variation as at Iroquois? In such a case, the line through the Tibbetts Point and Prescott data points would have a still steeper slope. Unfortunately, we find we have no other substantial data base to draw upon. Thus, we must make our final statements about the spatially correlated portion of the data at this point.

The question of the source of the non-linearity persists. It is interesting to note that in Section 4.3, we were worried about the 9960-W baseline in this regard. Given observations at only two sites in the area of interest, it was impossible to test for linear behavior. The only other source of information came from observations outside the area of interest. Since those observations tended to agree with observations at Massena, we feared a non-linear effect starting at some unknown location between Massena and Tibbetts Point. The criticality of some of the reaches between these sites was the reason for the fear.

With some data from Iroquois Lock, we at last can concentrate on the "operating region." It appears we can feel somewhat confident about a linear description of the variations between Massena and Tibbetts Point for 9960-W. We are tentative about these statements first because of the limited amount of data from Iroquois Lock (although the fact that it encompasses the most questionable part of the shipping season is a benefit). Another reason is that Iroquois Lock is a bit too far away from the area of critical concern for our purposes.

Regarding the 9960-X baseline, the Iroquois data seems (tentativeness works both ways) to confirm our fears. In view of the discussions at the end of Section 4.3, this is particularly disturbing - the 9960-X baseline is the larger contributor to cross-track error. Thus, we have still further reason to obtain measurements near Wellesley Island.

Before turning to an examination of what the Iroquois Lock data tells us about the spatially independent component, a final word is in order. Recall in Section 4.3 we concluded we were finding the "next best thing." Our predictions regarding the spatially independent component were proving

pessimistic. This is a joyful finding: there is nothing we can do to improve upon this component. The spatially correlated component was larger than we felt would be the case. This situation, fortunately, is "fixable." Thus, we know a solution exists, we are simply seeking a path to the optimal one. We have not yet found sufficient evidence to state what the answer is but are getting closer. Note we should avoid the temptation to simply "plan on two or three differential control stations between reaches 61 and 74." If one site (in addition to Massena) can be strategically located to solve the problem, this is the solution we should seek. The simplest solution typically proves to be the most reliable and the most successful.

We begin consideration of what the Iroquois data can tell us about the spatially independent component by generating the "Iroquois minus Massena" data plots shown in figures 4-25 and 4-26.

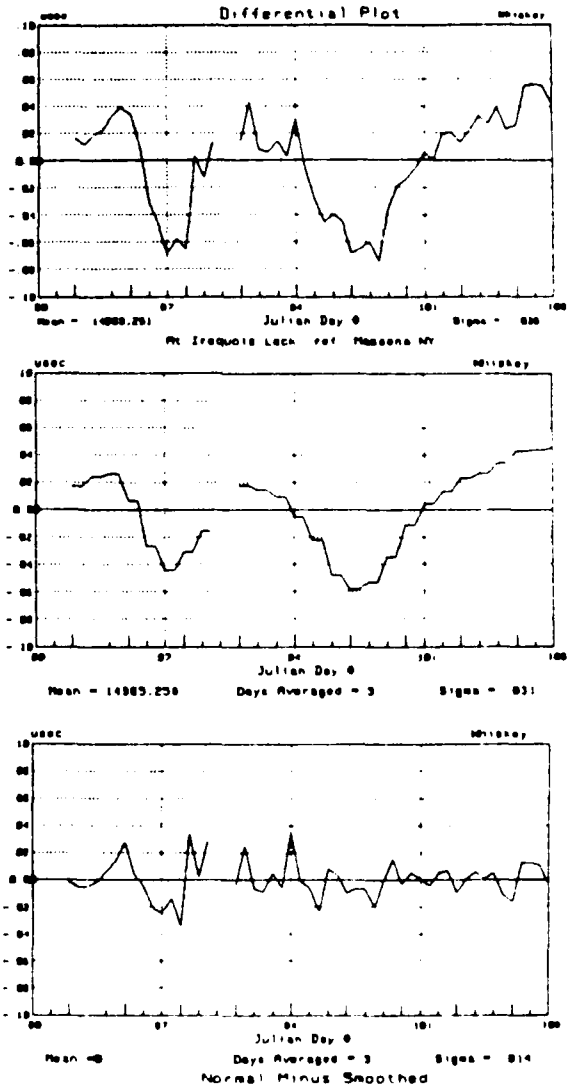

a.

b.

c.

Figure 4-25 Breakdown of 9960-W Differential TD Frequency Components: Iroquois Lock Minus Massena Using 3-Day Smoothing

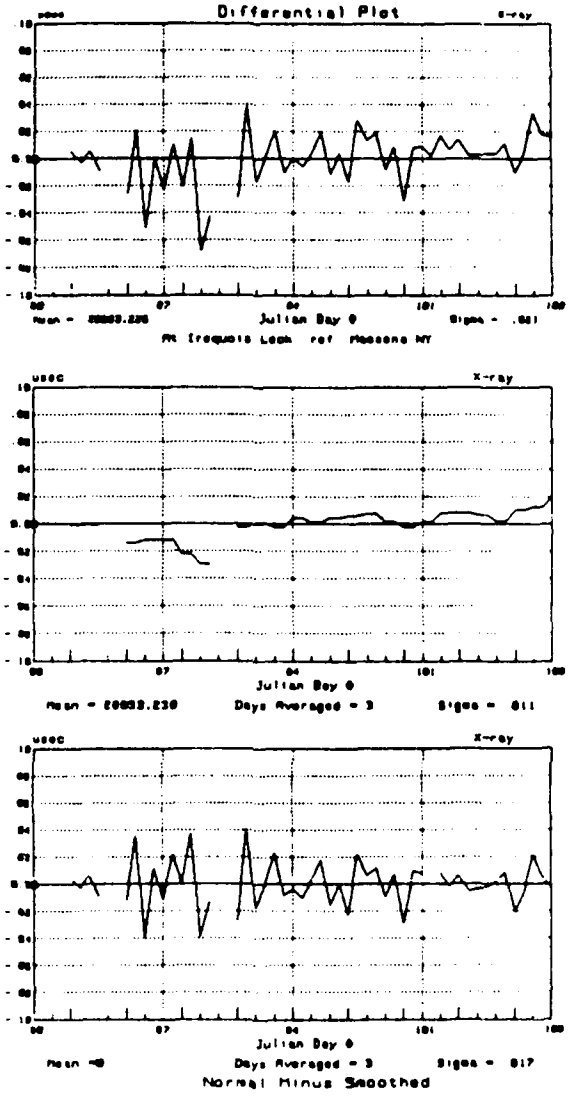

a.

b.

c.

Figure 4-26 Breakdown of 9960-X Differential TD Frequency Components: Iroquois Lock Minus Massena Using 3-Day Smoothing

Several comments immediately come to mind regarding the "raw data" plots in figures 4-25.a. and 4-26.a. First, we note that the 9960-X "sigma" has been reduced to 20 nanoseconds - even without having to remove the "3-day filtered" component. Thus, we have confirmation of our observation in Section 4.3 that, for the 9960-X baseline, the spatially independent component is smaller than we predicted in Section 3. In examining figure 4-26.a. it does not appear there is much room for improvement except for the

period of time surrounding Julian Day 87. The "sigma" of the data in figure 4-26.c. can be reasonably concluded to be an excellent stab at the "bottom line estimate" for the standard deviation of the spatially independent differential Loran-C "remnant." Assigning a value of 11 nanoseconds to this component "before differential corrections" gives us the desired result $11\sqrt{2} = 16$.

In considering the 9960-W data, we note that the plot of figure 4-25.a., the differential "residual" bears a striking resemblance to the original data records for 9960-W at Iroquois Lock and Massena. This both illustrates and confirms the contention of Section 4.3 regarding the "remnant" spatially correlated components after the differential corrections. These components are only removed to a certain percentage (depends on ΔDRD - although we are not yet sure how to compute ΔDRD for both baselines). Noting the "sigma" in figure 4-25.c., we see the standard deviation for the spatially independent component of 9960-W baseline finally agrees with that of the 9960-X baseline.

It is important to note that the ΔDRD from Reach #61 to Reach #74 is 81 km for 9960-W and 40 km for 9960-X (see Table C-3). These reaches span the "critical area of concern" identified previously. We note that the ΔDRD between Massena and Iroquois Lock is 75 km for 9960-W and 50 km for 9960-X. Thus, if "things were linear" between Massena and Tibbetts Point (or at least as far south as Reach #74), we would expect TD records at Reach #61, with corrections from Wellesley Island being applied, to be essentially the same as shown in figures 4-25.a. and 4-26.a. Resulting cross-track error plots are shown for both sites (using Iroquois Lock data in both cases - the geometry and courses are different) in figure 4-27.

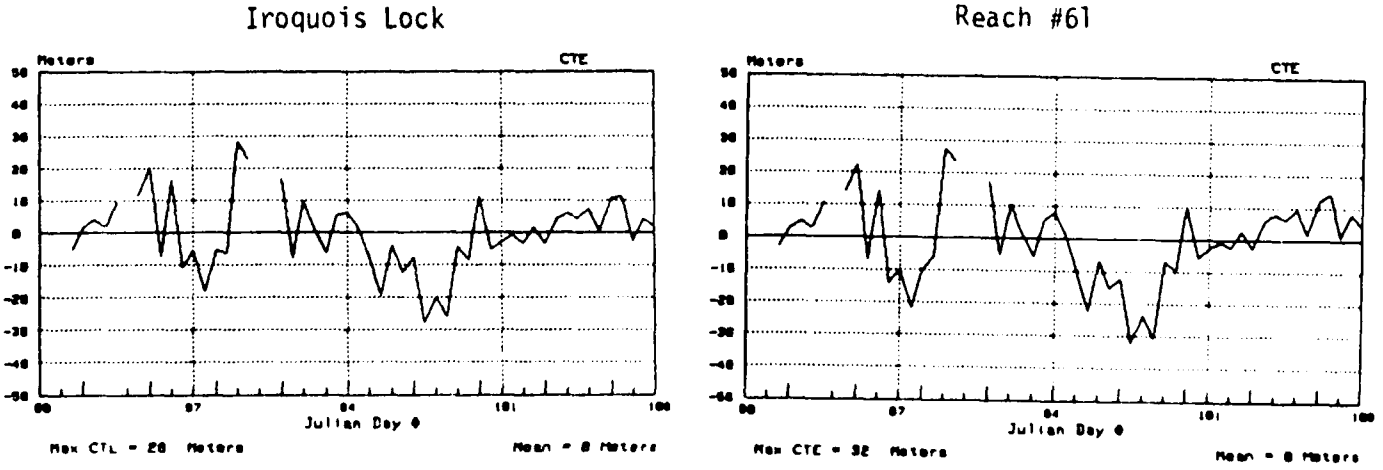

Figure 4-27 CTE Plots Generated by Applying the Data of Figures 4-25 and 4-26 to the Geometry at Iroquois Lock and Reach #61

Some disclaimers are in order. The first is a follow-up on the comment in Section 4.2: "how do we pick the reference point?" For the plots of figure 4-25 and 4-26 and, hence, figure 4-27, the average value over the 30-day period being considered defined the reference point. Since we expect a slight variation in the spatially correlated component from March/April to mid-summer, these figures are optimistic: in practice we only have one "shot" at defining the waypoints. Presumably, since the shipping season starts on 1 April, we would pick reference points halfway between the average values for March/April and those for July/August. Since we do not yet have that data, we must simply note the results indicated by figure 4-27 are optimistic. Here, near the end of our comments on the data, we see an important illustration of the utility of having a model. We do not yet have enough data to draw the final conclusion about performance anywhere. Nevertheless, we have a framework in which to view what we do have. Specifically, the spatially independent component is cheerfully small and the spatially correlated component is still something to be nailed down. We know the performance implications of both of these statements.

The second comment is that it is reasonable, based on what we have seen thus far, to assume what we see at Iroquois Lock, referenced to Massena, is representative of what we would see at Reach #61, referenced to Wellesley Island, for the 9960-W baseline. For the 9960-X baseline, however, what we see at Iroquois Lock is assumed to be optimistic. Although, as in Section 4.3, it is still premature to try to update the predictions, we have gone about as far as we can go in this report. Thus, an update in one specific case is in order.

In figure 4-28, we provide a plot of the 9960-X baseline TD at Tibbetts Point, referenced to Iroquois Lock. We see a standard deviation of 83 nanoseconds - accrued over a Δ DRD of 124 km. If we "remove" a 16 nsec

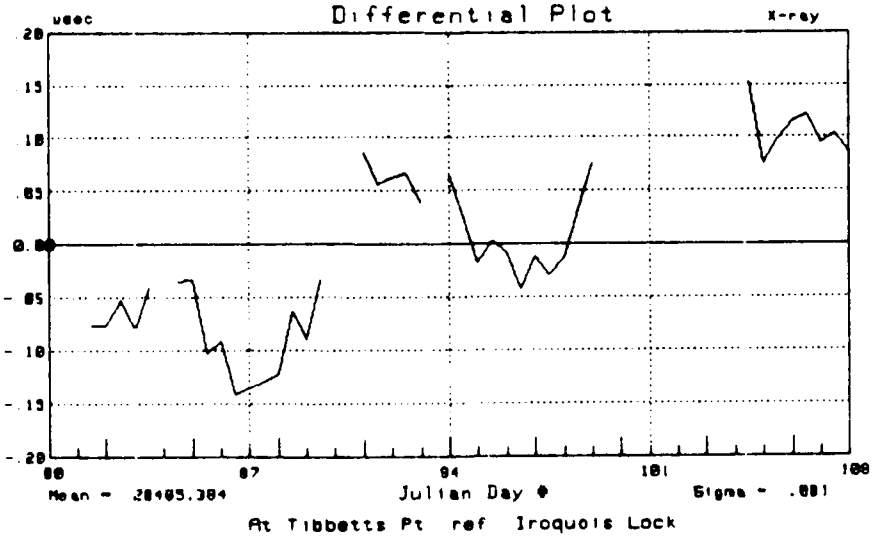

Figure 4-28 9960-X Differential TD Record: Tibbetts Point Minus Iroquois Lock

spatially independent component from this "total sigma" and assume a perfectly linear variation between Tibbetts Point and Iroquois Lock for the spatially correlated component, we would estimate a 26 nsec component at Reach #61, reference to Wellesley Island (a ΔDRD of 40 km). Adding the 16 nsec component back in, we compute a 29 nsec total sigma at Wellesley Island for 9960-X. Combining this with the expected 37 nsec total sigma for 9960-W, and using the math of Appendix C, we compute a "rho" of 0.89. These parameters can be used to generate the 99.9% error ellipse plots of figure 4-29: our current best prediction of the performance at Reaches #61 and 62 with differential corrections from Wellesley Island.

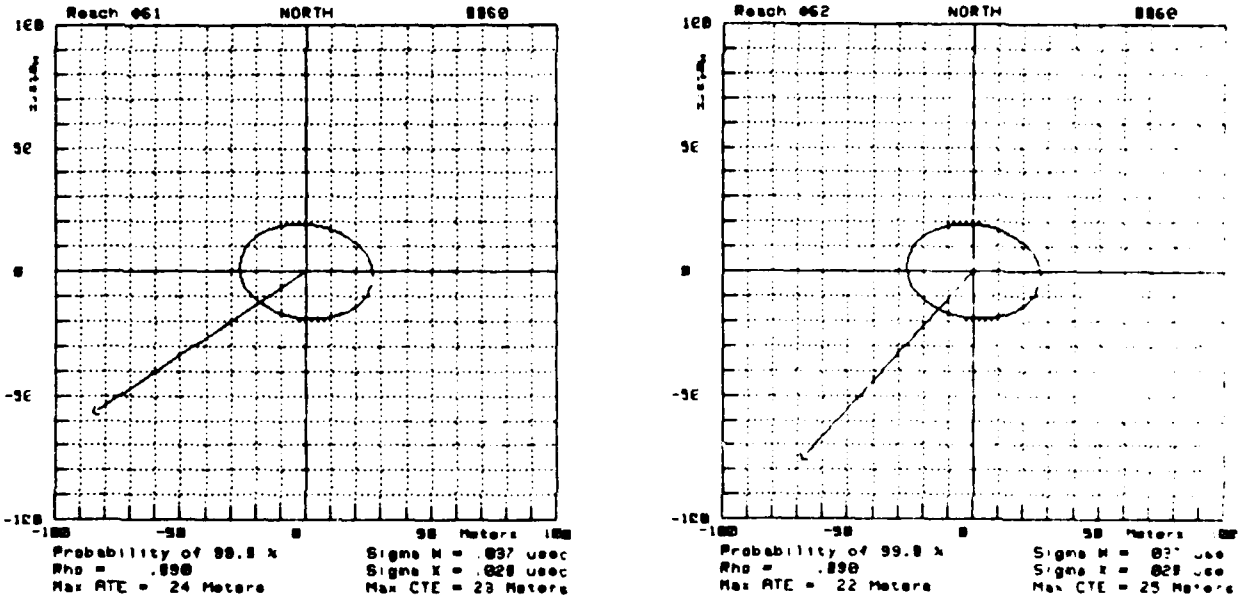

a. b.

Figure 4-29 Predicted 99.9% Differential Error Ellipses at Reaches #61 and 62: Corrections From Wellesley Island

Allowing 17 meters for the vessel "half-width," we are left with 21 (Reach #61) and 19 (Reach #62) meters for guidance error. Although these results look encouraging, we must recall the "reference point" problem. We have just provided predictions which used the mean of the March/April data as the reference point. If we concede our 99.9% error ellipses are representative of "as bad as it gets," we can obtain a better estimate of the year-round situation at these reaches (we cannot do a direct computation because we have no means of computing "March to July" statistics).

First we examine figures 4-12 and 4-13. We see the 9960-W baseline TD looks like it will "steady out" at about 15691.860 usec at Tibbetts Point, with Massena corrections applied. This is 0.258 usec higher than the reference value of figure 4-30.a. - Tibbetts Point minus Massena for the 30-day period. A similar comparison for the 9960-X baseline shows the reference in the summer should be about 0.74 usec above that of figure 4-30.b. Since the shipping season starts in April, the reference values in figure 4-30 should be "as low as we expect" (actually, somewhat lower). Ideal selection of the reference point (for now) can be argued to be midway

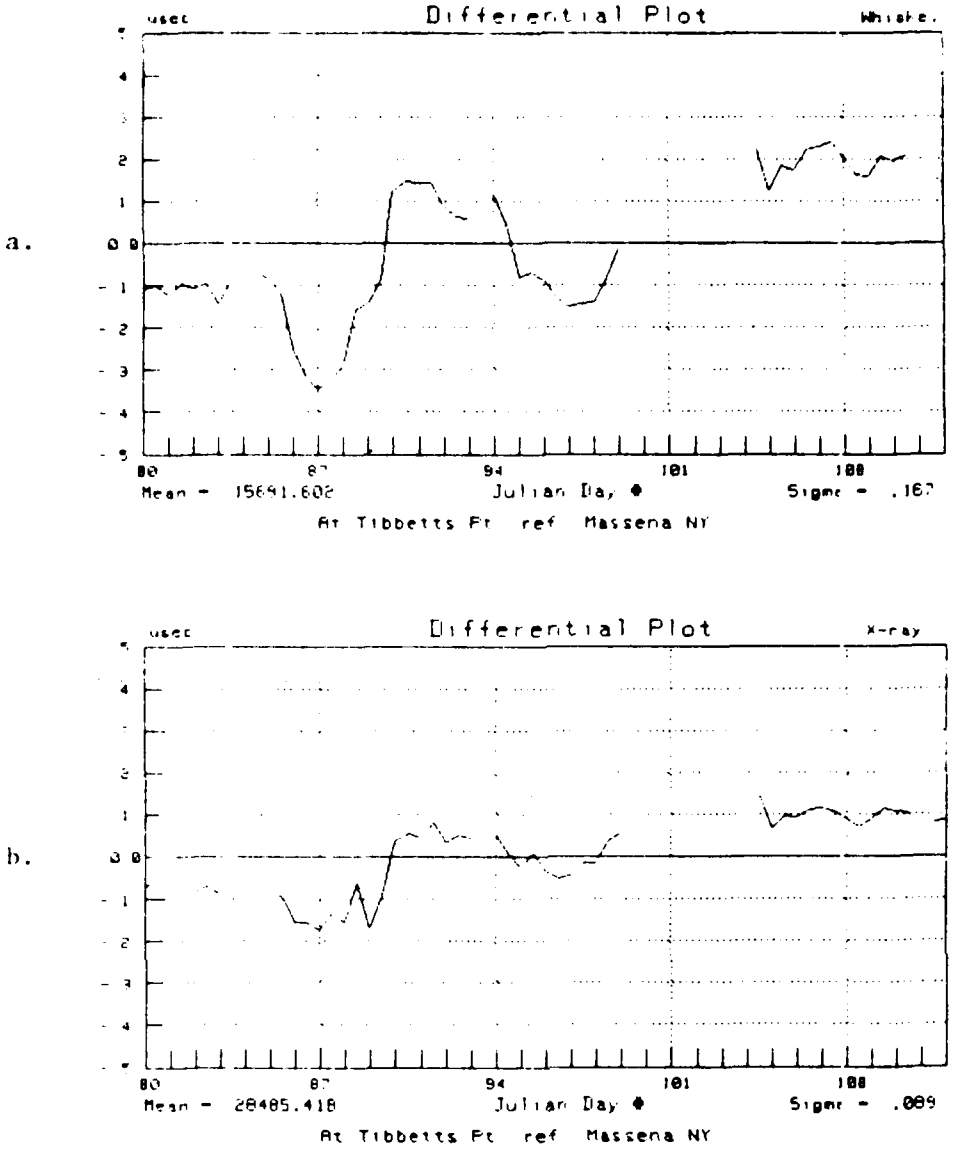

Figure 4-30 9960-W/X Differential TD Record: Tibbetts Point Minus Massena

between these extremes: leaving us with a "reference point drift" of 0.129 usec for 9960-W and 0.037 usec for 9960-X.

To be conservative, however, let us stay with the values of 0.258 and 0.074 usec. This is particularly applicable since we do not yet have a way to pick the ideal reference point. At worst, we would pick the largest value observed in the summer.

Of course, we do not expect to use differential corrections from Massena all the way to Tibbetts Point. We are considering data from these sites because these are the only ones with data records which span the

timeframe required for the desired computation. Data available thus far supports the appropriateness of a linear description of the spatially correlated component of the variation between Massena and Tibbetts Point for the 9960-W baseline. Since the reference point drift is, in full, a spatially correlated phenomenon, we can use this linear model to estimate the drift at Reach #61, with corrections from Wellesley Island, for 9960-W.

In a ΔDRD_W sense, Reach #61 is 81 km from Wellesley Island whereas Tibbetts point is 321 km from Massena. Thus, we expect the reference point will drift 81(258 nsec)/321 = 65 nsec from late March to mid-summer at Reach #61, with corrections from Wellesley Island.

For 9960-X, we have concluded we do not have linear behavior from Massena to Tibbetts Point. Let us again assume that Iroquois Lock "stays with" Massena throughout the year. If so, we would argue the 74 nsec 9960-X drift should be apportioned, in a linear, ΔDRD_X sense, over the distance from Iroquois Lock to Tibbetts Point (124 km - as before). Reach #61 is 40 km from Wellesley Island in the ΔDRD_X sense. Thus, we expect the 9960-X reference point will move 40(74 nsec)/124 = 24 nsec from late March to mid-summer at Reach #61, with corrections from Wellesley Island.

Using the math of Appendix A and appropriate courses, the 65 nsec ΔTD_W and the 24 nsec ΔTD_X values are transformed to a ΔCTE of 8 meters at Reach # 61 and of 6 meters at Reach # 62. These figures "cut into" the 21 and 19 meters we have left for guidance error as shown in figure 4-29. We conclude, however, we are still have room for the somewhat arbitrary 10-meters limit we selected as part of the total error budget.

These results, of course, are still projections from a suboptimal data base: we do not have have data from the desired number of sites and we do not have data from a long enough time period. They may prove to be optimistic but they stand as our best guess at present. We should note there are two ways to improve upon the situation should the need be indicated. First, we can locate a monitor halfway between Reaches #61 and #74. Next, we can be a bit more careful in the selection of our reference point - i.e., try for an approximation to the "ideal" suggested above (i.e., halfway between extremes). Either of these steps will cut the reference point drift in half (together the drift is reduced by a factor of 4). As the figures of the previous paragraph show, however, the total reduction through this mechanism may only be on the order of 6 meters. A larger contribution is made by locating the monitor halfway between the two extremes: it would also reduce the size of the ellipses in figure 4-29. For now, we will simply state that the results look encouraging and note we have "untapped" methods of improvement, should future data prove we have been too optimistic.

The final statement we should make is in regard to the "anomalous" data point indicated in figure 4-20. Recall the data came from the period just before 1 April 1982. It was claimed this was primarily a spatially correlated effect which would have been removed by a closer monitor station. Examination of the "Iroquois minus Massena" data for the same period fully supports this contention.

4.5 Summary of Data.

Observations made at Massena confirm the year-round predictions made by using data obtained at N.E.U.S. coast sites. Importantly, the elliptical pattern of the fixes - oriented with the larger axis perpendicular to the course - is confirmed. By time-domain filtering, we are able to remove part of the spatially correlated component to examine the remnant. The remnant begins to approach the assumed values used in Section 3 for the spatially independent component but too much of the remaining "higher frequency" components appear to be spatially correlated for us to confirm our assumptions. For this, we must have data from another "nearby" site.

In comparing the Tibbetts Point data with the Massena data we can remove more of the spatially correlated components. More importantly, we can remove those components which are identical from one Internav 404 receiver site in the St. Lawrence Seaway to another. Time-domain filtering is again applied to the "Tibbetts Point minus Massena" data to remove the percentage of the spatially correlated components that simply could not be removed because of the large distance from Massena to Tibbetts Point. The result is promising: the remnant, known to still have a spatially correlated portion, is smaller than that assumed in the predictions of Section 3 for the 9960-X baseline and almost as small for the 9960-W baseline. The tie-in between the time-domain filtering and the spatial filtering afforded by differential action is not yet fully justified but we begin to see its applicability.

The criticality of the promising observations regarding the spatially independent component is seen by recalling Section 3 showed the assumed values, given the adverse geometry, yielded performance "too close for comfort" in some reaches. One abnormal data point is noted but it is argued this is a spatially correlated effect.

The Tibbetts Point data, particularly for the 9960-W baseline, also shows variations in the spatially correlated components which are much larger than assumed in Section 3. This is not a critical problem since it can be overcome by appropriate selection of the differential control station site. The contrast in the disagreement with the DRD model at Tibbetts Point with the agreement at Massena, however, suggests a "local non-linearity." Thus, although a solution to the spatially correlated component variation problem exists, it cannot be identified from consideration of just the data from Tibbetts Point and Massena.

Additional data is available for a critical time period at Iroquois Lock. By analyzing the data as before, we finally get agreement between baselines as to the proper estimate for the spatially independent component - about an 11 nsec sigma. An important observation is that the previously noted "anomalous" data point is confirmed to be spatially correlated (thus, "reducible"). We see evidence that the bulk of the non-linearity in the spatially correlated component, for the 9960-W baseline, has occurred "before" Massena. Additional data from the vicinity of Wellesley Island would be useful in confirming this. For the 9960-X baseline, however, we see evidence of local non-linearity in the spatially correlated component.

This is a critical finding and makes data from the vicinity of Wellesley Island crucial.

Finally, we update our predictions at the most critical reaches using all available data. The results look promising - given monitors at Wellesley Island and Massena. We note however, the final conclusions were based, in part, on only 30-days of data and from not enough sites as would be realistically required to draw final conclusions.

5 Considerations on Implementation and Alternatives

5.1. General Statement.

Throughout the report, it has been tacitly assumed that full Differential Loran-C is a system that could possibly satisfy precision navigation requirements in the St. Lawrence Seaway. The prime emphasis of the Steering Committee to date, as well as this report to this point, has been to examine Loran-C system capabilities and Seaway requirements. These areas should continue to receive emphasis but it is time to introduce some feasibility considerations.

Differential Loran-C is a concept. Beyond that we can say it is a concept that has been discussed many times over the years (dinners during symposia, for example, are ideally suited for the discussions). The fact remains that Differential Loran-C has never been implemented as a general navigation system anywhere. Prospects for implementation by the U.S. Coast Guard are, presently, non-existent. One reason for this is the burden of simply establishing the communications network to support the concept. It is unlikely that implementation in one small area (as opposed to all continental U.S. coast waters) would receive acceptance. Thus, for the U.S. Coast Guard, the first step towards government sponsored Differential Loran-C implementation would involve implementation "wherever necessary." Funding to support this substantial increase in service is unlikely.

This does not, however, rule out implementation by other agencies with less direct ties to the basic system. Given the inherent "localized area of interest" of the St. Lawrence Seaway Development Corporation and the St. Lawrence Seaway Authority, the "proliferation" problem is minimized. Moreover, the existing communications network and protocol makes things easier. Feasibility tests can at least be conducted without major installation costs. Having thus alluded to feasibility, two major areas requiring further consideration should be mentioned.

To make the first point, we should point out that Loran-C is a "new" system. We should explain the use of the word "new" when applied to Loran-C. There is a dichotomy involved that is of concern to us as well as, for example, those who would advocate the termination of Loran-C service as soon after the initial availability of GPS as possible. Loran-C is "old" in that signals have been on-air for over 20 years. A benefit of this long "evaluation" period is that many engineering/scientific analyses could be conducted over the years. The "refined" system that replaced Loran-A thus benefitted from these years of study (sadly, in some instances, not enough). For the general user community, however, Loran-C is new. It is just now 5 years that Loran-C has existed at all on the West Coast and Loran-C without "coverage holes" or "charting anomalies" is an even more recent phenomenon on the West Coast. Loran-C for the Great Lakes, Gulf Coast and Canadian East Coast is much less than 5-years old. Although the old "East Coast Loran-C" chain (9930) was operated for about 20 years, its widespread utility for general navigation over even a moderate coverage area

was arguable. Thus, the opportunity for a "good look" at the system by a large group of practical users is a recent occurence.

Several factors are becoming increasingly evident about this "new" system. The major one for our purposes is that a prime advantage of Loran-C, when and/or where Loran-C performance is good, is that it is a "stand-alone" system. This is true about the most modest of user equipment but even more so with those featuring "waypoint navigator" capabilities. These observations come from general users and can be expected to be of even more concern to pilots. Differential Loran-C is a direct contradiction of the "stand-alone" concept.

The second comment involves the degree of difficulty involved in operating and maintaining high quality monitor stations. We can draw upon experience gained in the stability study of this report to underscore the concern. One can envision a "first cut" at planning this study proceding along the following lines. Note the digital storage capacity required for each sample to be obtained. Assume a sampling rate of once per second. Thus multiply by the number of seconds in a year. Multiply by the number of data collection sites. Observe that the resulting storage capacity is well within the capabilites of small systems these days. Observe the fact that Loran-C receivers, of reasonable capabilty, are available on the market. Note that data collection sites are available. Thus, conclude it is a straightforward matter to conduct a Loran-C stability study.

If this report shows nothing else, it should show that the above "plans" are significantly removed from what is truly required to execute a successful study. The harbor monitors have provided reliable data - although not enough of it according to original plans. A reason for the success is that they were developed, over a period of several years and during the course of a study which is similar to this, for the exact purpose of characterizing Loran-C stability. Particularly in the case of the Ad Hoc equipment sets, we see proof that the marketplace is just not ready to directly serve our purposes. As good as the harbor monitor sets are, they are much less than what would be required of an operational system. If a harbor monitor set fails, there is no backup. The failure may go undetected for several days (e.g., if a weekend is involved). Even after discovery of the failure, repair is not completed for several days. This type of performance represents a proper commitment of resources for the purposes of the stability study but is not acceptable under operational conditions.

The above comments can be viewed as implying a negativism regarding Differential Loran-C. The authors, however, intended a simple note of caution which is deemed appropriate to put the preceding sections of the report in perspective. The results of the stability study - those presented herein and those to follow, simply address the capabilty of Differential Loran-C to support St. Lawrence Seaway requirements. A test implementation will provide insights into "the rest of the story." With the above notes of caution we encourage the tests to begin.

5.2 User Generated Corrections.

Guidance equipment developed under USCG R&D studies, as well as many commercially available sets, provide a mechanism for a user to enter corrections for TD biases. The corrections can be entered manually or arrangements can be made, by adding appropriate equipment, to have corrections being broadcast from some shore monitor automatically entered. Guidance equipment with such features are capable of operating in the Differential Loran-C mode. There are, however, alternate means of utilizing this correction capability.

A vessel at the Eisenhower Lock at Massena, for example, has an opportunity to observe the TD's over a reasonably long period of time at a known (tied-into the previously conducted waypoint survey) location. By comparing the observed value to the expected value, the operator obtains a differential correction every bit as good as that to be obtained from some shore-based monitor. Indeed, in applying corrections based on observations made by his own receiver, the operator also removes any TD biases that may occur from receiver to receiver. Thus, these user generated corrections, for a time, are better than those obtained from a shore-based station.

In many areas, this method of correcting for systematic Loran-C variations is entirely adequate. What is typically missing, however, is the opportunity (or willingness) to "sit" in one known location for a reasonable period of time. With an appropriate investment of equipment and allowed system complexity, however, alternate "self-calibration" means can be provided. There are, for example, many small area electronic positioning systems which can provide high accuracy. Like Differential Loran-C, none of these have ever been demonstrated as a practical navigation system. For some, the problem is simply that they cannot cover a large area in a practical way. They may, however, be useful for allowing a periodic "calibration range." Avoiding a deep discussion of practical implementation considerations, let us for the moment simply assume periodic calibrations can be obtained, at specific locations, thus making shore-based differential monitor stations unnecessary.

Under this assumption, it becomes important to ask "for how long and how far" are these "user generated" corrections valid. With the presently available data base, we have a means to address these questions. We take the Massena data records for 9960-W and 9960-X and subtract corresponding records "advanced" 1-day (2 sample periods). This gives us a measure of how well a user who stays in the vicinity of Massena will do with "24-hour old" corrections obtained at Eisenhower Lock. Resulting time difference records are provided in figure 5-1. A scatter plot of the resulting fixes is shown in figure 5-2.

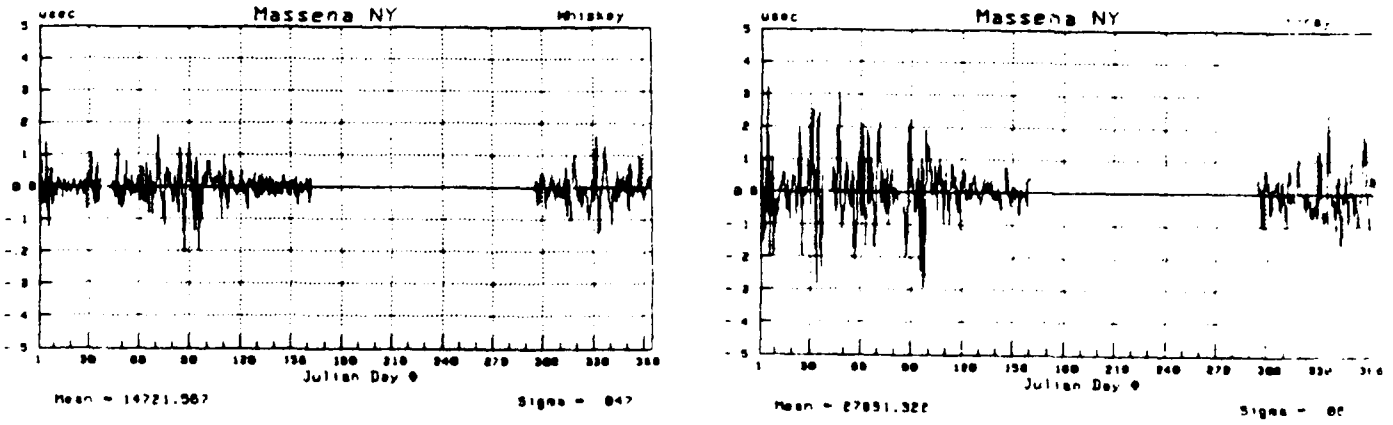

a b

Figure 5-1 9960-W/X TD Records at Massena With 24-Hour Old Corrections

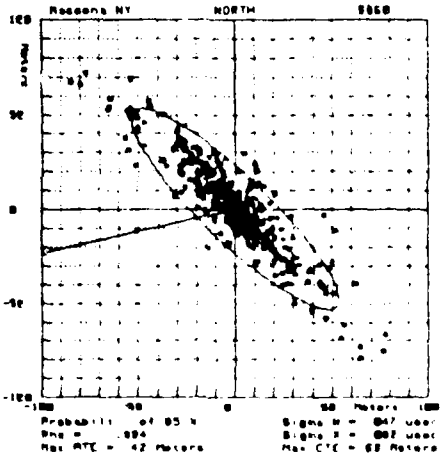

Figure 5-2 Fix Scatter Plot for Data of Figure 5-1

We see that most of the "seasonal structure" of the variations has been removed. Comparing the statistics of the "residuals" with those of the original data record (from figure 4-1, "sigma" is 0.133 usec for 9960-W and 0.248 usec for 9960-X), we see an improvement of about a factor of 3 for both baselines. Although the scatter plot indicates we need more improvement, we note that the TD variations become small shortly after the shipping season starts.

We can generate one level of improvement over the above [illegible] comparing the Massena data with "Massena minus 12 hours" [illegible] are provided in figures 5-3 and 5-4.

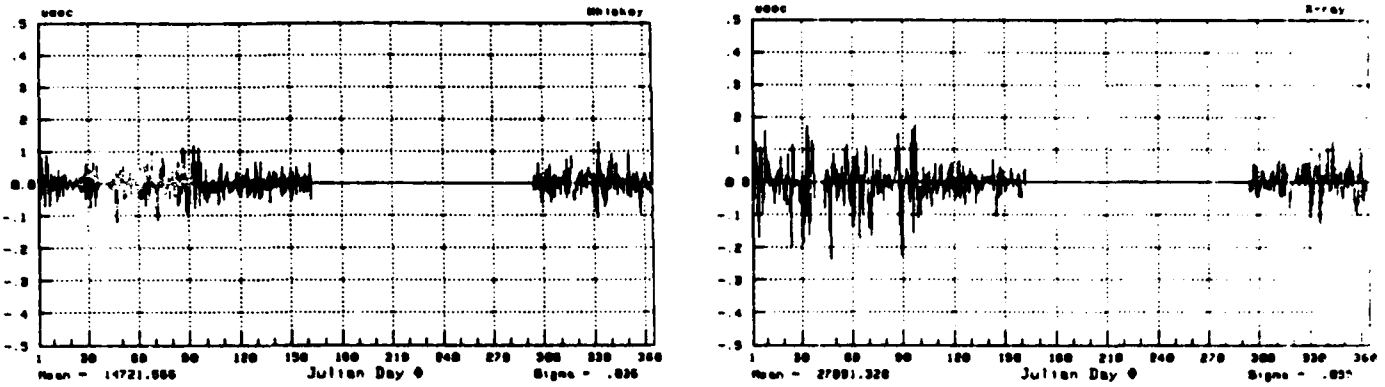

a. b.

Figure 5-3 9960-W/X TD Records at Massena With 12-Hour Old Corrections

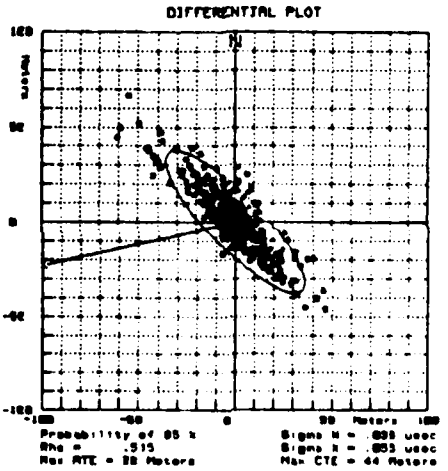

Figure 5-4 Fix Scatter Plot for Data of Figure 5-3

Here we see substantial improvement over the "day old corrections" situation. Particularly with regard to the 9960-W baseline, the variations are approaching the levels which we might consider usable. With "low-density" data, we can go no further in this sequence. At present this is not a significant drawback since we really need to consider what happens someplace away from Massena with the "stale" corrections obtained at Eisenhower Lock. For the 30-day period for which substantial data is available from Iroquois Lock, we can answer the question. From the Iroquois data, we subtract "Massena minus 12-hours" data to obtain the plots of figures 5-5 and 5-6.

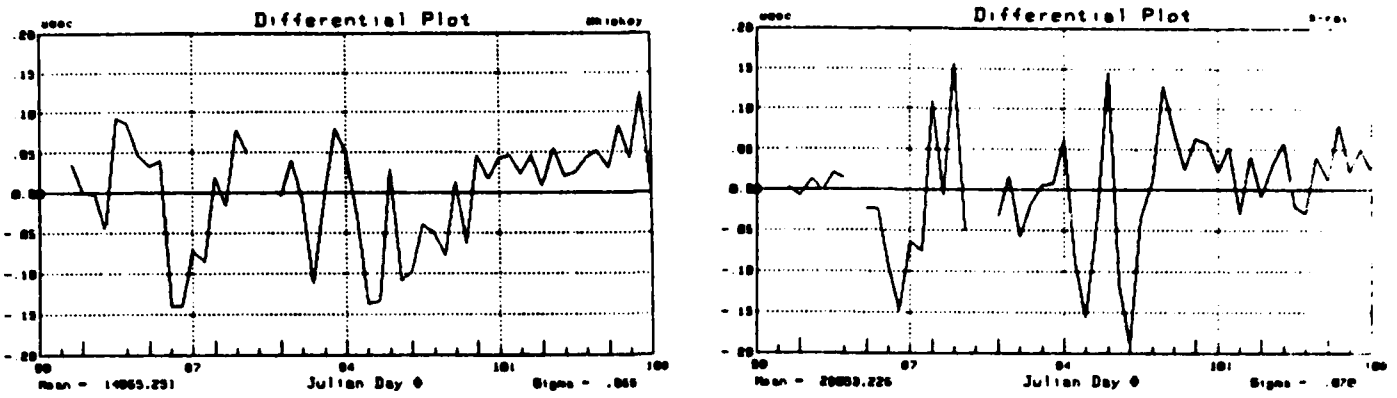

a b

Figure 5-5 9960-W/X TD Records at Iroquois Lock With 12-Hour Old Corrections From Massena

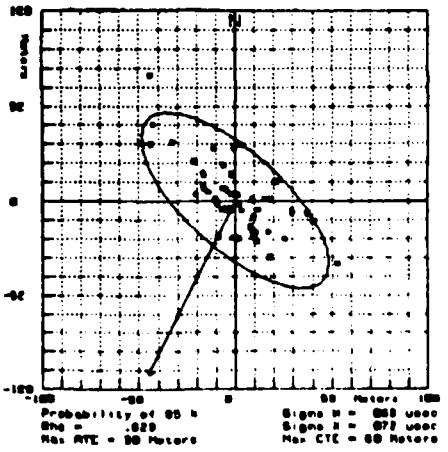

Figure 5-6 Fix Scatter Plot for Data of Figure 5-5

Here we see that there is a small amount of "spatially correlated effects" that has occurred over the period of 12 hours. If we believe what was presented in Section 4, we can say this is what we expected. Notice that by comparing the statistics of figure 5-3 with those of figure 5-5, we see that this has resulted in a substantial increase in the variations for 9960-W but only a mild increase for 9960-X. Again from Section 4, this is the situation we expected for Massena and Iroquois.

Without comparing Massena or Iroquois data to Tibbetts Point data, this is about as far as we can go with this type of analysis. Since Tibbetts Point is so far away and, since the variations seem substantial even at Iroquois, reference to "stale" Massena data, there is no reason for further analysis at this point. We should note, however, that this is a useful correction technique - it might even be all that would be required if the geometry were not so poor. We should continue to examine this form of correction in future studies.

5.3 Changes to Existing Chain Geometry.

Installation and operating costs for Loran-C transmitting stations are substantial. Nevertheless we should examine the implications of our best estimate of what would happen if the geometry could be improved by the addition of another secondary transmitting station. In considering the orientation of the 9960 chain LOP's in the St. Lawrence Seaway, as illustrated in figure 4-19, we see what we really need is a stable LOP oriented at about a course of 225°T. If "a benefactor" were to install and operate a station in the vicinity of North Bay, Ontario (near Lake Nipissing) we would have an LOP with about the desired orientation. If we were able to control the baseline by use of a receiver located at Massena, we would have the stability we seek.

Appendix G contains error ellipses which were obtained by use of the prediction techniques of Section 3 - applied to the 9960-W and 9960-N (North Bay) baselines. To be conservative, we stayed with a spatially independent component "sigma" estimate of 20 nsec. Additionally, we used the 9960-W "pk-pk vs DRD" regression line slope as the basis of 9960-N spatially correlated component predictions. In the Appendix, we begin by assuming no differential corrections are applied. In figure 5-7, we show the resulting error ellipses for several reaches of interest.

As in Section 3, we scale the 95% statistics up to obtain the 99.9% predictions which we will, again, call "conservative." The resulting cross-track error predictions for each reach, along with the error margin and asterisks are shown in Table 5-1.

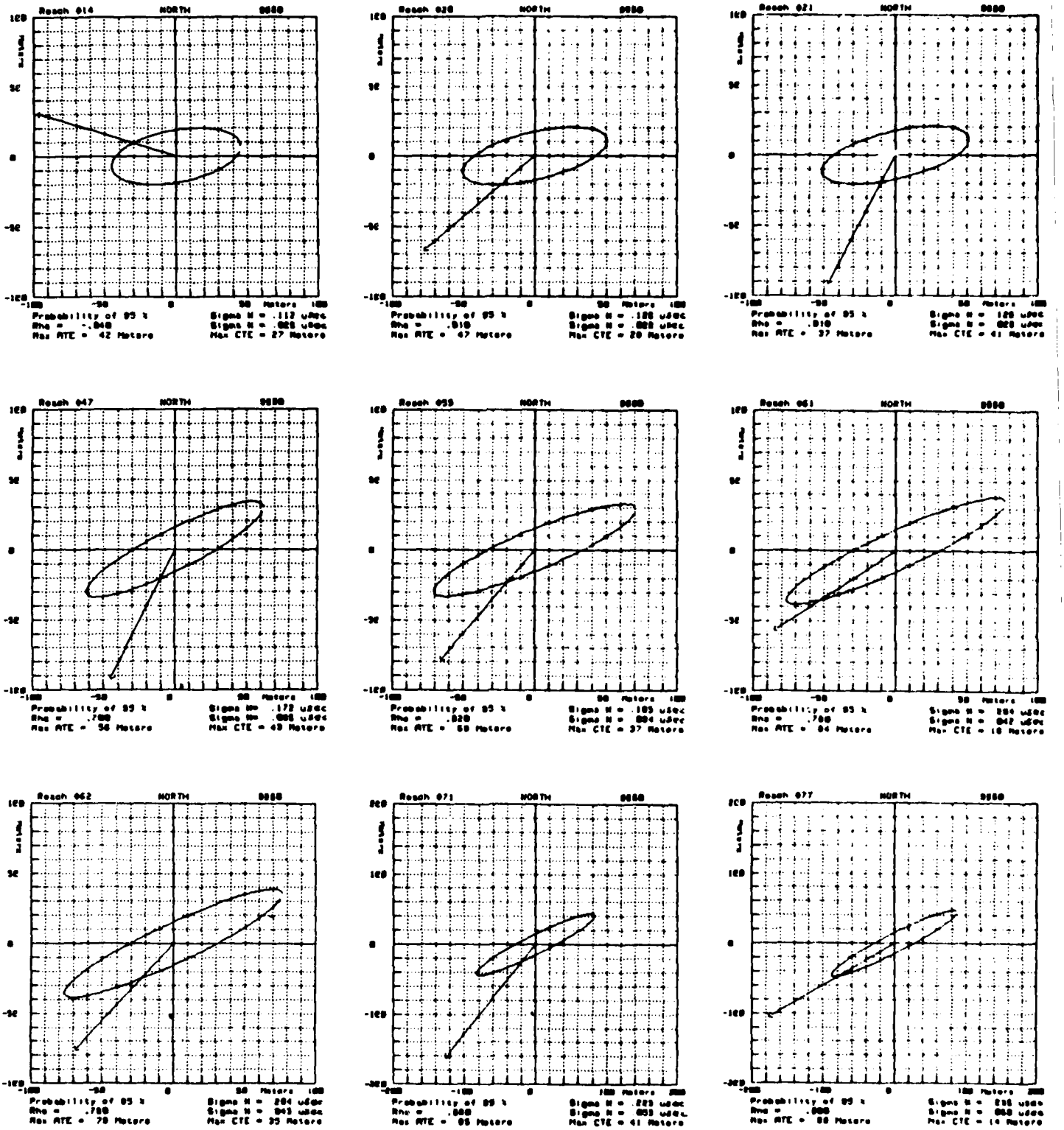

Figure 5-7 9960-W/N Predicted Error Ellipses for Key Reaches

Beach #	Half-Width	"Conservative" Differential CTF Prod.	Error Margin
2	91 m	29 m	62 m
3	91	44	47
4	122	35	87
5	213	48	165
7	91	51	40
8	91	44	47
9	91	36	55
11	91	30	61
12	91	30	61
14	91	41	50
15	68	27	41
16	182	33	149
17	137	59	78
18	99	39	60
19	73	29	44
20	68	42	26 *
21	58	52	6 ***
22	68	47	21 **
23	68	33	35
24	68	27	41
25	68	30	38
26	68	63	5 ***
27	107	35	72
28	68	42	26 *
29	152	38	114
30	91		53
31	107	32	75
33	68	24	44
34	91	24	67
35	93	41	52
36	130	24	106
37	130	27	103
38	111	41	70
39	107	23	84
40	137	60	77
41	91	35	56
42	91	24	67
43	91 m	33 m	58 m
44	114	45	69
45	107	23	84
46	107	26	81
47	76	65	11 ***
49	107	75	32
50	91	45	46
51	91	30	61
52	91	54	37
53	91	29	62
54	114		85
55	96	56	40
56	152	27	125
57	152	51	101
58	152	38	114
59	83	51	32
60	76	33	43
61	61	27	34
62	61	53	8 ***
63	99	62	37
64	93	101	(-) 8 ***
65	93	60	33
66	93		33
67	93	78	15 ***
68	93	45	15 ***
69	93		48
70	93		48
71	91	62	29
72	61		(-) 1 ***
73	68		6 ***
74	68	27	41
75	68		41
76	68		41
77	83	21	62
78	91	41	50
79	111	27	84
80	122+	68	54+

Table 5-1 "Raw" Loran-C 99.9% Probability Cross-Track Error Predictions - 9960-W/N

We see asterisks clustered after Reach #61. Partially, these are due to the suboptimal courses. Primarily, however, they are due to the large 9960-W variations which combine with even the slightest 9960-N variations to produce large ellipses in the southern reaches. The problem areas before Reach #61 are simply the result of suboptimal courses. It is important to emphasize that these results, though they may not be fully satisfactory, are for "raw" Loran-C - with the new baseline. The geometry has improved so much that there may be satisfactory alternatives to full Differential Loran-C. Before exploring the alternatives, we should examine the results we could expect if we were to apply full Differential Loran-C corrections from Massena - for the 9960-W baseline only. In all cases, the results will be better than indicated in Table 5-1. Thus, we need only consider the reaches which are marked with asterisks.

Resulting error ellipses are also provided in Appendix G. Conservative (99.9%) cross-track error predictions and error margins for the problem reaches are listed in Table 5-2.

Reach #	Half-Width	"Conservative" Differential CTE Pred.	Error Margin
20	68 m	24 m	44 m
21	68	23	45
22	68	24	44
26	68	21	47
28	68	23	45
47	76	21	55
62	61	21	40
64	93	22	71
67	93	21	72
68	93	27	66
72	61	20	41
73	68	21	47
81	122 +	27	95 +

Table 5-2 99.9% Probability Cross-Track Error Predictions: 9960-W/N With Differential Corrections from Massena Applied to 9960-W

Here we see we have "solved all problems" (if we believe in predictions): the largest cross-track error is 27 meters. Examining the error margins, which achieve a minimum value of 40 meters at Reach #62, shows that for 17 meter "half-width" vessels, 23 meters is allowed for guidance error. This significantly exceeds our assumed requirements. We have achieved this performance, however, at the expense of requiring a differential monitor station. This is a disadvantage. An advantage over the situation provided by the existing chain is that we only need one monitor station and we have considerable room for error. Careful consideration of the error margin suggests that with the new station, there may be some intermediate step between the "raw 9960-W" and "full differential for 9960-W" situations which would meet our needs. Specifically, we now recall the "factor of 3" improvement over the "raw" data we were able to obtain in the vicinity of Massena with "24-hour old" corrections from Massena and the even greater improvement if the corrections were only 12-hours old.

In Section 5.2, we found that 12-hour old corrections from Massena reduced the standard deviation of 9960-W to 66 nsec - over a "worst case" 30 day period at Iroquois Lock. Such a small variation, combined with the expected 9960-N variation would provide acceptable performance throughout the Seaway. At this point in the experiment, unfortunately, we do not have a database to support further pursuit of this concept. It is introduced, however, as an important thought for future examination.

One final comment should be made to encourage this line of investigation into the implications of the improved performance afforded by the new station. One advantage has already been suggested: we would not be critically dependent upon real-time corrections. Perhaps a more important advantage is that we would not be critically dependent upon data from any <u>one</u> shore-based system. In this regard, recall we are leaning towards a conclusion, for the existing chain, that a monitor at Wellesley Island may not be good enough to allow safe passage of Reach #61. Presumably, a monitor right at Reach #61 would be satisfactory. If, however, there is an equipment failure at that site, the whole system fails.

If we had more room for error, as with the new baseline, we could locate several monitors along the Seaway and deduce an "interpolated" (in, of course, a DRD sense) correction to be used in any reach of interest. (For future reference, such corrections provide what is refered to as "proportional control.") The result would not be as good as if we had a <u>working</u> monitor right at the reach of interest. With the geometry provided by the new station, however, it does not have to be. With the new baseline and this technique, it is hypothesized that we could "lose" all but two, perhaps even one, of the monitor sites and still provide acceptable corrections at any reach along the Seaway. This system "reliability" feature is the significant advantage brought about by the new station. With existing chain geometry, we are simply too sensitive to <u>any</u> increase in errors and thus must demand higher (probably unachievable) reliability.

Future efforts should strive to obtain adequate data bases at Tibbetts Point, Wellesley Island, Iroquois Lock and Massena to further examine the performance of "proportional control corrections" for 9960-W.

6. CONCLUSIONS AND RECOMMENDATIONS

We have commented extensively on data set reliability, the adequacy of the sampling strategy, the nature of Loran-C variations, expected system performance, and actual observations. In summary, the following conclusions can be drawn.

--- The reliability of the harbor monitor sets and the quality of the data base exceeds that obtained in earlier studies in the St. Marys River.

--- Except for a valuable 30-day period at Iroquois Lock, no useful data was obtained from the high density data collection sites. Part of the problem could be remedied if the data could be reviewed in a more timely fashion. This is not practical without some sort of phone line access. Another source of the problem is the enormous size of the data base - errors can be generated almost as fast as they can be detected by the experimenters.

--- Without a reasonable amount of high density data, we cannot make an in-depth comparison of the results of the high density and low density data collection approaches. Careful review of the model presented herein, however, suggests the approaches should yield essentially identical results. The strong agreement between the observations and the predictions which were made using the model stands as the only evidence to support this suggestion.

--- The latest version of the harbor monitor sets (type D) could be used to collect "higher density" data than is used herein.

--- Predictions based on the model described herein, along with data from Northeast U.S. coast sites, indicate "raw" Loran-C from the existing 9960 chain will not yield satisfactory year-round performance in the Seaway. Data from Massena and Tibbetts Point confirms this.

--- Predictions further show that Differential Loran-C, even with several shore sites, will be hard pressed to meet performance requirements. Near "worst case" geometry is the reason.

--- Data to directly confirm the Differential Loran-C predictions is not available. Using an elaborate series of analysis techniques, however, we are able to conclude the spatially independent component of the variations is smaller than predicted. The spatially correlated component is slightly larger than predicted.

--- Available data indicates the spatially correlated component of the 9960-W baseline variations increases as an approximately linear function of double range difference between Massena and Tibbetts Point.

--- Data indicates the spatially correlated component of the 9960-X baseline variations increases in a non-linear fashion between Massena and Tibbetts Point. With the available data, we cannot adequately characterize this non-linearity. This baseline is the prime contributor to cross-track error - the critical performance parameter.

--- Because of the low spatially independent component variations, the data indicates a flawlessly operated and surveyed Differential Loran-C system could provide satisfactory performance. Given the uncertainty regarding the 9960-X spatially correlated component and the scant room for error, we cannot yet say where the shore stations should be located. Another data site in the vicinity of Wellesley Island is needed.

--- Full Differential Loran-C has never been implemented. Since the geometry leaves scant room for error, this would be a rugged area for a first operational deployment. A determination of practical limitations incurred in actual implementation is needed to state the "bottom Line."

--- If a station in the general vicinity of North Bay, Ontario were added to the 9960 chain, the geometry would be improved considerably. "Raw" Loran-C still would not yield satisfactory performance in some reaches.

--- The new station, however, would leave enough room for error so that alternatives to full Differential Loran-C look promising. The periodic application of proportional control corrections is an example of such alternatives.

Based on these conclusions, we offer the following recommendations.

--- Type D harbor monitor sets should be deployed at Brossard, Beauharnois, Massena, Iroquois Lock, Wellesley Island, and Tibbetts Point.

--- Mild increases in the density of the data collection routine should be tried so that continuing fears regarding the inadequacy of the low density data base can be allayed. If the percentage of data available for low density analysis decreases as a result of this attempt to "strain for gnats," however, the density should be decreased.

--- Future data analysis should concentrate on refining the model presented herein and "hardening" the performance estimates.

--- A test implementation of Differential Loran-C in the Seaway should be undertaken.

APPENDIX A

LORAN-C GEOMETRY AND ERROR ELLIPSES

APPENDIX A

LORAN-C GEOMETRY AND ERROR ELLIPSES

Purpose.

There is a large body of literature on geometry considerations pertaining to loran. Much of it is not applicable to our purposes for a variety of reasons. These include:

a. Developed for "standard loran" (Loran-A) not Loran-C
b. Developed for "synchronized" chain operations
c. Developed for chain planning purposes (addresses "global" vic specific questions, uses no "a posteriori" information, etc)
d. Developed to compress two-dimensional information (e.g., along-track/cross-track error) into one number (e.g., drms, CEP, etc)

etc.

The purpose of this appendix is to present the mathematics used for the evaluation of critical loran errors in situations such as the St Lawrence Seaway study. The concepts are not new - simply arranged in the order suited to this report.

Approach.

We begin by describing the "small area" transformation" for Loran-C time difference errors to position errors. From this we can show how to present the positional variations implied by time difference fluctuations. We will consider how to present the results in terms of "north/south" (x,y) or along-track/cross-track error (ATE/CTE) coordinates.

Next, we hypothesize a statistical description of the time difference variations and derive a resultant statistical description of the positional variations. Again, the results will be in terms of (x,y) or (ATE/CTE) coordinates. What results is sensitive only to the assumptions about the time difference statistics as discussed in the main body of the report.

Small Area Transformation

We recognize that the world is "round and lumpy" and that loran LOP's are "warped hyperbolas." Over a small area, however, it is appropriate to consider a so-called "flat earth, linear grid" model (a related discussion may be found in reference 1). In such a case we can represent positional variations in Cartesian coordinate terms - Δx and Δy. Because of the linear grid assumption, we need only consider the slopes of the loran lines at a point. Small loran time difference changes are thus described by the following equations:

$$\Delta TD_1 = \frac{\partial TD_1}{\partial x} \Delta x + \frac{\partial TD_1}{\partial y} \Delta y$$

$$\Delta TD_2 = \frac{\partial TD_2}{\partial x} \Delta x + \frac{\partial TD_2}{\partial y} \Delta y$$

In matrix form, this is

$$\begin{bmatrix} \Delta TD_1 \\ \Delta TD_2 \end{bmatrix} = \begin{bmatrix} \frac{\partial TD_1}{\partial x} & \frac{\partial TD_1}{\partial y} \\ \frac{\partial TD_2}{\partial x} & \frac{\partial TD_2}{\partial y} \end{bmatrix} \begin{bmatrix} \Delta x \\ \Delta y \end{bmatrix} \qquad \text{(A-1)}$$

For Loran-C we have $TD_1 = \gamma_1 + \frac{r_1 - r_m}{v}$

where r_1 = range to secondary station 1 transmitting antenna

r_m = range to master station transmitting antenna

v = speed of signal

γ_1 = baseline emission delay.

Both the emission delay and v are time varying - indeed, such variations cause the need for stability studies and form the basis of the double range difference model as discussed in the report. Emission delay, however, is not related to position of the observer. Hence

$$\frac{\partial \gamma_1}{\partial x} = \frac{\partial \gamma_1}{\partial y} = 0$$

The speed of the signal <u>is</u> a function of position (indeed, this is what makes a survey necessary). Over the small areas considered here, however, (e.g., about 50 meters) we can say

$$\frac{\partial v}{\partial x} \approx \frac{\partial v}{\partial y} \approx 0$$

Thus, we have $\frac{\partial TD_1}{\partial x} = \frac{1}{v}\left[\frac{\partial r_1}{\partial x} - \frac{\partial r_m}{\partial x}\right]$; $\frac{\partial TD_1}{\partial y} = \frac{1}{v}\left[\frac{\partial r_1}{\partial y} - \frac{\partial r_m}{\partial y}\right]$

and (A-1) becomes

$$\begin{bmatrix} \Delta TD_1 \\ \Delta TD_2 \end{bmatrix} = \frac{1}{v} \begin{bmatrix} \frac{\partial r_1}{\partial x} - \frac{\partial r_m}{\partial x} & \frac{\partial r_1}{\partial y} - \frac{\partial r_m}{\partial y} \\ \frac{\partial r_2}{\partial x} - \frac{\partial r_m}{\partial x} & \frac{\partial r_2}{\partial y} - \frac{\partial r_m}{\partial y} \end{bmatrix} \begin{bmatrix} \Delta x \\ \Delta y \end{bmatrix}$$

or

$$\begin{bmatrix} \Delta x \\ \Delta y \end{bmatrix} = v \begin{bmatrix} \frac{\partial r_1}{\partial x} - \frac{\partial r_m}{\partial x} & \frac{\partial r_1}{\partial y} - \frac{\partial r_m}{\partial y} \\ \frac{\partial r_2}{\partial x} - \frac{\partial r_m}{\partial x} & \frac{\partial r_2}{\partial y} - \frac{\partial r_m}{\partial y} \end{bmatrix}^{-1} \begin{bmatrix} \Delta TD_1 \\ \Delta TD_2 \end{bmatrix} \qquad \text{(A-2)}$$

To consider the relationship of an observer (x,y) to a station of a Loran-C baseline we draw the following diagram. We show the observer at point (x,y) and the transmitting antenna at location (x_1,y_1).

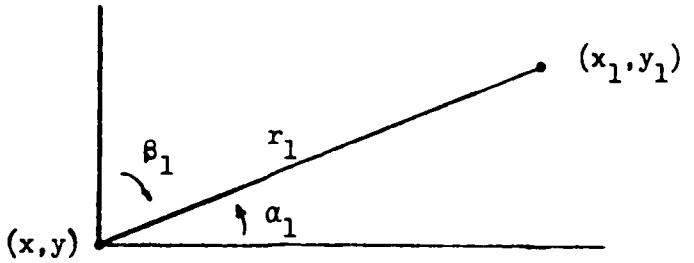

$$r_1 = [\,(x_1 - x)^2 + (y_1 - y)^2\,]^{\frac{1}{2}}$$

so that

$$\frac{\partial r_1}{\partial x} = -(x_1 - x)\,[\,(x_1 - x)^2 + (y_1 - y)^2\,]^{-\frac{1}{2}}$$

$$= -(x_1 - x)/r_1$$

$$= -\cos\alpha_1$$

As shown, $\alpha_1 = 90^\circ - \beta_1$

so $\frac{\partial r_1}{\partial x} = -\cos(90-\beta_1) = -\sin\beta_1$

Similar exercises show:

$$\frac{\partial r_m}{\partial x} = -\sin\beta_m$$

$$\frac{\partial r_2}{\partial x} = -\sin\beta_2$$

$$\frac{\partial r_m}{\partial y} = -\cos\beta_m$$

$$\frac{\partial r_i}{\partial y} = -\cos\beta_i$$

so that (A-2) becomes

$$\begin{bmatrix}\Delta x\\ \Delta y\end{bmatrix} = -v \begin{bmatrix}\sin\beta_1 - \sin\beta_m & \cos\beta_1 - \cos\beta_m\\ \sin\beta_2 - \sin\beta_m & \cos\beta_2 - \cos\beta_m\end{bmatrix}^{-1} \begin{bmatrix}\Delta TD_1\\ \Delta TD_2\end{bmatrix}$$

$$= \underline{B} \begin{bmatrix}\Delta TD_1\\ \Delta TD_2\end{bmatrix} \qquad \text{(A-3)}$$

(A-3) gives us the ability to express TD variations in terms of cartesian coordinates ($\Delta E = \Delta x$, $\Delta N = \Delta y$) - assuming we know the great circle take-off angles from the observer to the stations of the Loran-C chain. A simple algorithm to compute these angles will be presented later. Before proceding with that description, however, we should introduce another general feature. Besides considering the mapping from TD's to x-y, we will want to consider the related coordinate system:

$$\begin{bmatrix}ATE\\ CTE\end{bmatrix} = \underline{w} = \begin{bmatrix}w_1\\ w_2\end{bmatrix}$$

The relationship of concern is $\underline{w} = \underline{L}\,\underline{v}$ where

$$\underline{v} = \begin{bmatrix}v_1\\ v_2\end{bmatrix} = \begin{bmatrix}x\\ y\end{bmatrix}$$

The $\underline{L}$ - matrix is specified by the vessel course and, as shown in the diagram, is a standard "axis-rotation" transformation.

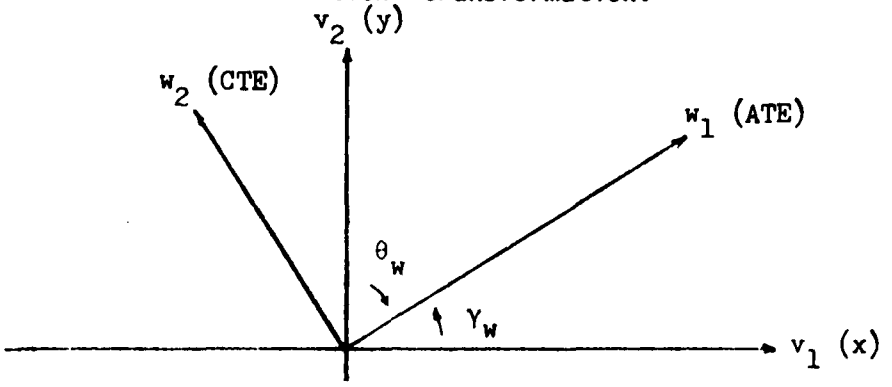

$$\begin{bmatrix} x \\ y \end{bmatrix} = \begin{bmatrix} v_1 \\ v_2 \end{bmatrix} = \begin{bmatrix} \cos\gamma_w & -\sin\gamma_w \\ \sin\gamma_w & \cos\gamma_w \end{bmatrix} \begin{bmatrix} w_1 \\ w_2 \end{bmatrix}$$

or $$\begin{bmatrix} w_1 \\ w_2 \end{bmatrix} = \begin{bmatrix} \cos\gamma_w & -\sin\gamma_w \\ \sin\gamma_w & \cos\gamma_w \end{bmatrix}^{-1} \begin{bmatrix} x \\ y \end{bmatrix} = \underline{L}\,\underline{v}$$

Course is traditionally specified in terms of $\theta_w = 90 - \gamma_w$ so we have

$$\underline{L} = \begin{bmatrix} \sin\theta_w & \cos\theta_w \\ -\cos\theta_w & \sin\theta_w \end{bmatrix} \qquad \text{(A-4)}$$

Thus, given knowledge of the transmitting station locations and the location of the observer, we simply need to compute great circle bearings, as described in the next section, to transform TD variations to position variations. With $\underline{B}$ described by (A-3) and $\underline{L}$ described by (A-4), we have:

$$\begin{bmatrix} \Delta E \\ \Delta N \end{bmatrix} = \underline{B} \begin{bmatrix} \Delta TD_1 \\ \Delta TD_2 \end{bmatrix}$$

and

$$\begin{bmatrix} ATE \\ CTE \end{bmatrix} = \underline{L} \begin{bmatrix} \Delta E \\ \Delta N \end{bmatrix} = \underline{L}\,\underline{B} \begin{bmatrix} \Delta TD_1 \\ \Delta TD_2 \end{bmatrix}$$

Great Circle Bearing Calculations.

The method for computing great circle bearings is fairly common and a derivation need not be presented herein (see, for example, reference 6). Since it is a critical ingredient for computing the Loran-C geometry matrix, however, a simple algorithm for making the calculation will be presented. The derivation assumes the earth is a perfect sphere - an entirely adequate assumption for our purposes.

Due to the form of the spherical triangles considered in the derivations, along with conventions for specifying angles, there are four cases to be considered:

Case I - observer is south and west of the transmitter

Case II - observer is north and west of the transmitter

Case III - observer is south and east of the transmitter

Case IV - observer is north and east of the transmitter

Define the following quantities:

L_1 = latitude of the observer (L_1 is positive for north latitudes)

λ_1 = longitude of the observer (λ_1 is positive for east longitudes)

L_2 = latitude of the transmitter antenna (same sign convention as for L_1)

λ_2 = longitude of the transmitter antenna (same sign convention as for λ_1)

β = great circle bearing from the observer to the transmitter antenna (measured clockwise from north)

Compute:

$$E = \cos L_2 \sin(\lambda_2 - \lambda_1)$$

$$F = \sin L_2 \cos L_1 - \sin L_1 \cos L_2 \cos(\lambda_2 - \lambda_1)$$

$$H = \tan^{-1}(E/F)$$

In case I, $\beta = H$;

In case II, $\beta = H + 180^{o}$;

In case III, $\beta = H + 360^{o}$;

In case IV, $\beta = H + 180^{o}$

A popular algorithm recognizes that F is positive in case I and III and that H is positive in cases I and IV.

Thus, the algorithm features the following steps:

1. Compute E and F
2. Compute H using a single-argument $\tan^{-1}$ function (i.e., $-90^{o} < H < 90^{o}$)
3. Let $\beta = H$
4. If $F < 0$ (i.e., if case II or IV), replace β with $\beta + 180^{o}$
5. If $\beta < 0$ (originally possible only in case II or III. After step 4, possible only in case III) replace β with $\beta + 360^{o}$
6. Done

Statistics.

With the mathematics presented above, we have the ability to transform observations of two time differences into useful 2-dimensional position references. These transformations see heavy use in the body of the report. We will also want to arrive at a statistical description of the positional variations as a function of time difference statistics. If we can then determine a reasonable model for the time difference statistical parameters, and how they vary from site to site, we can extend the results to locations between monitor sites. The first step is to develop a relationship between time difference statistics and position statistics. We will use the notation:

$$\underline{u} = \begin{bmatrix} u_1 \\ u_2 \end{bmatrix} = \begin{bmatrix} \Delta TD_1 \\ \Delta TD_2 \end{bmatrix}$$

As before,

$$\underline{v} = \begin{bmatrix} v_1 \\ v_2 \end{bmatrix} = \begin{bmatrix} \Delta x \\ \Delta y \end{bmatrix}$$

The assumption we will make about the statistics of the TD variations is that they are:

jointly distributed, zero mean, correlated (in general) gaussian random variables with a probability density function:

$$p_{u_1,u_2}(U_1,U_2) = \frac{1}{2\pi\sigma_1\sigma_2(1-\rho^2)^{\frac{1}{2}}} \exp\left[\frac{1}{2(1-\rho^2)}\left(\frac{U_1^2}{\sigma_1^2} - \frac{2\rho U_1 U_2}{\sigma_1\sigma_2} + \frac{U_2^2}{\sigma_1^2}\right)\right]$$

or, in vector form,

$$p_{\underline{u}}(\underline{U}) = \frac{1}{2\pi|\underline{K}|^{\frac{1}{2}}} \exp\left(-\tfrac{1}{2}\,\underline{U}^T\,\underline{K}^{-1}\,\underline{U}\right)$$

where $\underline{K}$ = the covariance matrix = $\begin{bmatrix} \sigma_1^2 & \rho\sigma_1\sigma_2 \\ \rho\sigma_1\sigma_2 & \sigma_2^2 \end{bmatrix}$

$$E[u_1^2] = \sigma_1^2 \qquad E[u_1u_2] = \rho\sigma_1\sigma_2$$

$$E[u_2^2] = \sigma_1^2$$

We have the probability density function for $\underline{u}$ and want to find the probability density function for: $\underline{v} = \underline{g}(\underline{u})$. The procedure is a standard one found in many textbooks (e.g., reference 7). Applying the procedure with

$\underline{v} = \underline{B}\underline{u}$ yields

$$p_{\underline{v}}(\underline{V}) = \frac{1}{|\underline{B}|}\, p_{\underline{u}}(\underline{B}^{-1}\,\underline{V})$$

so that

$$p_{\underline{v}}(\underline{V}) = \frac{1}{2\pi|\underline{B}|\,|\underline{K}|^{\frac{1}{2}}} \exp\left[-\tfrac{1}{2}\,(\underline{B}^{-1}\,\underline{V})^T\,(\underline{K}^{-1})\,(\underline{B}^{-1}\,\underline{V})\right]$$

$$= \frac{1}{2\pi|\underline{B}||\underline{K}|^{\frac{1}{2}}} \exp\left[-\tfrac{1}{2}\,\underline{V}^T(\underline{B}^{-1})^T\,\underline{K}^{-1}\underline{B}^{-1}\underline{V}\right]$$

or $$p_{\underline{V}}(\underline{V}) = \frac{1}{2\pi|\underline{H}|^{\frac{1}{2}}} \exp\left(-\tfrac{1}{2}\,\underline{V}^T\,\underline{H}^{-1}\,\underline{V}\right)$$

where $\underline{H}^{-1} = (\underline{B}^{-1})^T\underline{K}^{-1}\,\underline{B}^{-1}$

Interpretation

Having determined the probability density function for the random vector $\underline{v}$ (subject to the validity of the assumed statistical properties of $\underline{u}$) we need to find how best to use this information. Typical uses (e.g., as per the main body of this report) require us to:

1. find arbitrary equal probability contours $p_{\underline{V}}(\underline{V}) = k$ (so, for example, we can plot the contour)

2. determine the probability of falling within that contour (so, for example, we know what to call what we've plotted -e.g., 50% probability contour, 95% probability contour, etc)

First note that for

$$p_{\underline{V}}(\underline{V}) = k = \frac{1}{2\pi|\underline{H}|^{\frac{1}{2}}} \exp\left(-\tfrac{1}{2}\,\underline{V}^T\,\underline{H}^{-1}\,\underline{V}\right)$$

we have

$$2\pi k|\underline{H}|^{\frac{1}{2}} = \exp[-(1/2)\,\underline{V}^T\,\underline{H}^{-1}\underline{V})$$

or $$\underline{V}^T\,\underline{H}^{-1}\,\underline{V} = -2\ln\left(2\pi k|\underline{H}|^{\frac{1}{2}}\right) = c^2$$

$V^T H^{-1} V = c^2$ is the equation of an ellipse. Thus, we know what to plot. In general, there will be a V_1-V_2 "cross-product" term (due to geometry, a TD correlation, or both) resulting in a rotation of the axes of the ellipse about the V_1-V_2 axes.

Determining what contour we have is another textbook problem. As shown in reference 8 for a 2x2 case, the probability that an error vector lies inside an ellipse whose equation is

$$\underline{A_e}^T \underline{D} \underline{A_e} = c^2 \quad \text{("concentration ellipse")}$$

is

$P = 1 - \exp[-(1/2)c^2]$ .....for normally distributed random variables.

We will be primarily interested in $P = 0.95$

$$0.95 = 1 - \exp[-(1/2)c^2]$$

or $\exp[-(1/2)c^2] = 0.05$

$$c^2 = -2 \ln(0.05)$$

Other concentration ellipses are described by:

$P = 0.50$	$c^2 = -2 \ln (0.50)$
$P = 0.90$	$c^2 = -2 \ln (0.10)$
$P = 0.99$	$c^2 = -2 \ln(0.01)$
$P = 0.999$	$c^2 = -2 \ln(0.001)$

etc...

The main body of the report discusses/illustrates the applicability of the gaussian assumption and how to obtain estimates of σ_1, σ_2 and . . Given the

position of the observer (Lat/Long), knowledge of the chain stations, we now have everything we need to compute

$$\underline{H}^{-1} = (\underline{B}^{-1})^T \underline{K}^{-1} \underline{B}^{-1}$$

Thus we have all we need to plot the error ellipses.

Uses.

We can use the math developed herein as follows:

Scatter/CTE/ATE/Radial Error Plots

1. Store the coordinates of tne transmitter antennas.

2. Store the coordinates of the monitor sites (or any other sites of interest).

3. Identify the site of interest and compute the great circle bearings to form the $\underline{B}$ - matrix.

4. Access the time series TD data for the site of interest.

5. For each element of tne time series vector, compute:

$$\begin{bmatrix} \Delta E \\ \Delta N \end{bmatrix} = \underline{B} \begin{bmatrix} \Delta TD_1 \\ \Delta TD_2 \end{bmatrix}$$

Plotting the resulting series (E = x, N=y) yields the scatter plot

6. For each element of the series resulting in step 5, above, compute $d = [\Delta E^2 + \Delta N^2]^{\frac{1}{2}}$. Plot the result as a function of time to obtain the radial error plot.

7. Identify the course of interest. Compute the $\underline{L}$-matrix. For each element of the series computed in step 5, above, compute:

$$\begin{bmatrix} ATE \\ CTE \end{bmatrix} = \underline{L} \begin{bmatrix} \Delta E \\ \Delta N \end{bmatrix}$$

From the resulting vector, a time series of CTE or ATE can be plotted.

Statistics Plots.

1. For a site of interest, compute the $\underline{B}$-matrix as above.
2. Given estimates of σ_1, σ_2, and ρ, form the $\underline{K}$-matrix.
3. Compute the $\underline{H}^{-1}$ matrix where

   $$\underline{H}^{-1} = (\underline{B}^{-1})^T \underline{K}^{-1} \underline{B}^{-1}$$

4. Specify a desired probability contour, P, and compute:

   $$c^2 = -2 \ln(1-P).$$

5. The error ellipse is specified by the equation

   $$\underline{V}^T \underline{H}^{-1} \underline{V} = c^2$$

To put this in more familiar form, let

$$\underline{H}^{-1} = \underline{F} = \begin{bmatrix} f_{11} & f_{12} \\ f^{21} & f_{22} \end{bmatrix}$$

and note $\underline{v} = \begin{bmatrix} x \\ y \end{bmatrix}$

Thus,

$$c^2 = f_{11} x^2 + (f_{12} + f_{21}) xy + f_{22} y^2$$

APPENDIX B

DOUBLE RANGE DIFFERENCE MODEL

APPENDIX B

DOUBLE RANGE DIFFERENCE MODEL

The so-called double range difference model represents a classic approach to explaining the nature of Loran-C time difference variations. It was the prime model used in the St Marys River Loran-C Mini-Chain Stability Studies reported in reference 4 and several earlier studies. Rather than presenting a full bibliography on the subject, we simply note it has been discussed in references 2 , 9 , and 10. Recent extensions of model applications to areas outside the St Marys River have shown the need to modify the model. The modifications will be discussed in this appendix along with a tutorial on the basic model.

The Basic Model

To begin to examine Loran-C time difference (TD) variations we should examine both the spatial and temporal nature of the processes involved. As will soon become evident, these two aspects are interrelated. They will be separated in the next few paragraphs only for ease of presentation.

Consider the situation illustrated in figure B-1 below.

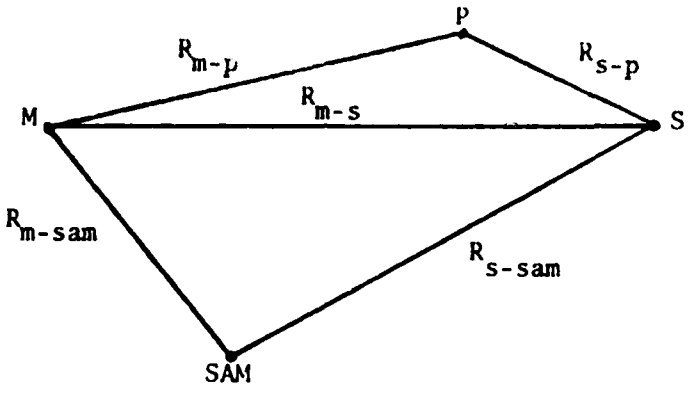

Figure B-1

Define the following quantities:

R_{m-p} = range from the master station to a point of interest

R_{m-sam} = range from the master station to the system area monitor

R_{s-p} = range from the secondary station to the point of interest

R_{s-sam} = range from the secondary station to the system area monitor

v_{m-p} = average signal speed over the path from m to p

v_{m-sam} = average signal speed over the path from m to sam

v_{s-p} = average signal speed over the path from s to p

v_{s-sam} = average signal speed over the path from s to sam

ED = baseline emission delay

From standard Loran-C theory, we have

$$TD_{sam} = ED + R_{s-sam}/v_{s-sam} - R_{m-sam}/v_{m-sam}$$

$$TD_p = ED + R_{s-p}/v_{s-p} - R_{m-p}/v_{s-p}$$

Uniform Propagation Assumption

Let us assume the speed of propagation of the signals is uniform throughout the service area of the baseline. This means:

$v_{s-sam} = v_{m-sam} = v_{s-p} = v_{m-p} = v$ so that

$$TD_{sam} = ED + (R_{s-sam} - R_{m-sam})/v$$

$$TD_p = ED + (R_{s-p} - R_{m-p})/v$$

Now let us assume that the speed of propagation changes from time to time but in a uniform manner. By this we mean that if the speed of propagation at time T_1 is v_1 over some portion of the service area, it is v_1 over all of the service area at T_1. At some other time, T_2, we have some other speed, v_2, everywhere in the service area. Under these circumstances we would have:

At T_1,

$$TD_{1,sam} = ED + (R_{s-sam} - R_{m-sam})/v_1$$

$$TD_{1,p} = ED + (R_{s-p} - R_{m-p})/v_1$$

at T_2,

$$TD_{2,sam} = ED + (R_{s-sam} - R_{m-sam})/v_2$$

$$TD_{2,p} = ED + (R_{s-p} - R_{m-p})/v_2$$

The above equations may seem to imply that the emission delay is held constant and that the TD at the SAM varies from time to time. As a practical matter, Loran-C chains are not operated this way. Control is exerted to adjust the emission delay so that the TD at SAM remains constant (over an averaging period of several hours). Rather than choosing some notation such as ED(t) to imply emission delay is a time-varying function, we will let the quantity ED represent some fixed value which is the true emission delay at some arbitrary point in time and incorporate the term ED + Δ ED in the equations for any other point in time. Thus, taking into account the realities of chain control, but still under the assumption of uniform propagation variations, we have:

At T_1,

$$TD_{1,sam} = ED + (R_{s-sam} - R_{m-sam})/v_1$$

at T_2,

$$TD_{2,sam} = ED + \Delta ED + (R_{s-sam} - R_{m-sam})/v_2$$

Since chain control action forces $TD_{1,sam} = TD_{2,sam}$ = a constant, we have

$$ED + (R_{s-sam} - R_{m-sam})/v_1 = ED + \Delta ED + (R_{s-sam} - R_{m-sam})/v_2$$

or,

$$\Delta ED = (R_{s-sam} - R_{m-sam})\,(1/v_1 - 1/v_2) \qquad (B\text{-}1)$$

Meanwhile, the situation at the point of interest is:

$$TD_{1,p} = ED + (R_{s-p} - R_{m-p})/v_1$$

$$TD_{2,p} = ED + \Delta ED + (R_{s-p} - R_{m-p})/v_2$$

The TD change at the point of interest is ΔTD_p

$$\Delta TD_p = TD_{2,p} - TD_{1,p}$$

$$= \Delta ED + (R_{s-p} - R_{m-p})\,(1/v_2 - 1/v_1)$$

But, $$\Delta ED = -(R_{s-sam} - R_{m-sam})\,(1/v_2 - 1/v_1)$$

so,

$$\Delta TD_p = [(R_{s-p} - R_{m-p}) - (R_{s-sam} - R_{m-sam})]\,(1/v_2 - 1/v_1)$$

The quantity in brackets is a function of <u>two</u> range differences and is the so-called <u>double range difference</u> (DRD_p). Thus,

$$\Delta TD_p = DRD_p\,(1/v_2 - 1/v_1) \qquad \text{(B-2)}$$

where $$DRD_p = (R_{s-p} - R_{m-p}) - (R_{s-sam} - R_{m-sam})$$

We should note an approximation which simplifies the math:

let $v_1 = v$

$v_2 = v + \Delta v$

Then,

$$1/v_2 - 1/v_1 = 1/(v + \Delta v) - 1/v$$

$$= -\Delta v/(v^2 + v\,\Delta v)$$

A large data base shows that for Loran-C, $|\Delta v_{max}| \leq 1\%\ v$ so that,

$$v^2 + v\,\Delta v \approx v^2 = 1/k \quad (\text{a positive constant})$$

so $$\Delta TD_p = -k\,\Delta v\,DRD_p \qquad \text{(B-3)}$$

We should note that if the point of interest is on the same hyperbola as the SAM,

$$R_{s-p} - R_{m-p} = R_{s-sam} - R_{m-sam}$$

so that

$$DRD_p = 0$$

and, with uniform changes in the speed of signal propagation,

$$\Delta TD_p = 0.$$

In practice, the uniform propagation assumption is not entirely valid. Variations on the basic theme, however, can prove extremely useful for explaining a high percentage of observed Loran-C TD variations. Before exploring observations of the actual variations, however, we should finish the theme by presenting some basic rules.

In general, when it gets cold, the signals travel faster. Thus if we establish the summer as our reference time, Δv is positive in the winter.

Under normal circumstances, the location of the SAM is fixed so that

$$DRD_p = (R_{s-p} - R_{m-p}) - (R_{s-sam} - R_{m-sam})$$

$$= R_{s-p} - R_{m-p} - k_1$$

A basic loran feature is that for a fixed speed of propagation, the maximum TD reading is achieved at the master station or on the baseline extension "behind" the master station. The same logic that leads to this result can be applied to the above equation to show that the maximum double range difference is achieved at or "behind" the master station where:

$$DRD_{max} = (R_{s-m} - 0) - k_1 = \beta - k_1$$

where β = baseline length in standard loran notation.

Thus, DRD_m is positive and represents the largest (most positive) value achieved anywhere in the service area.

Similarly, at the secondary,

$$DRD_s = DRD_{min} = -\beta - k_1.$$

This is the smallest (most negative) value achieved.

Since:

$\Delta TD = -k \Delta v \, DRD$ and

DRD is positive at the master, negative at the secondary, and

Δv is positive in the winter,

we expect the TD at the master station to be smaller in the winter than it is in the summer. Similarly, at the secondary station, we expect the TD to be larger in the winter than it is in the summer. Thus, we would expect year long plots of the TD's at either end of the baseline to follow the pattern shown in figure B-2.

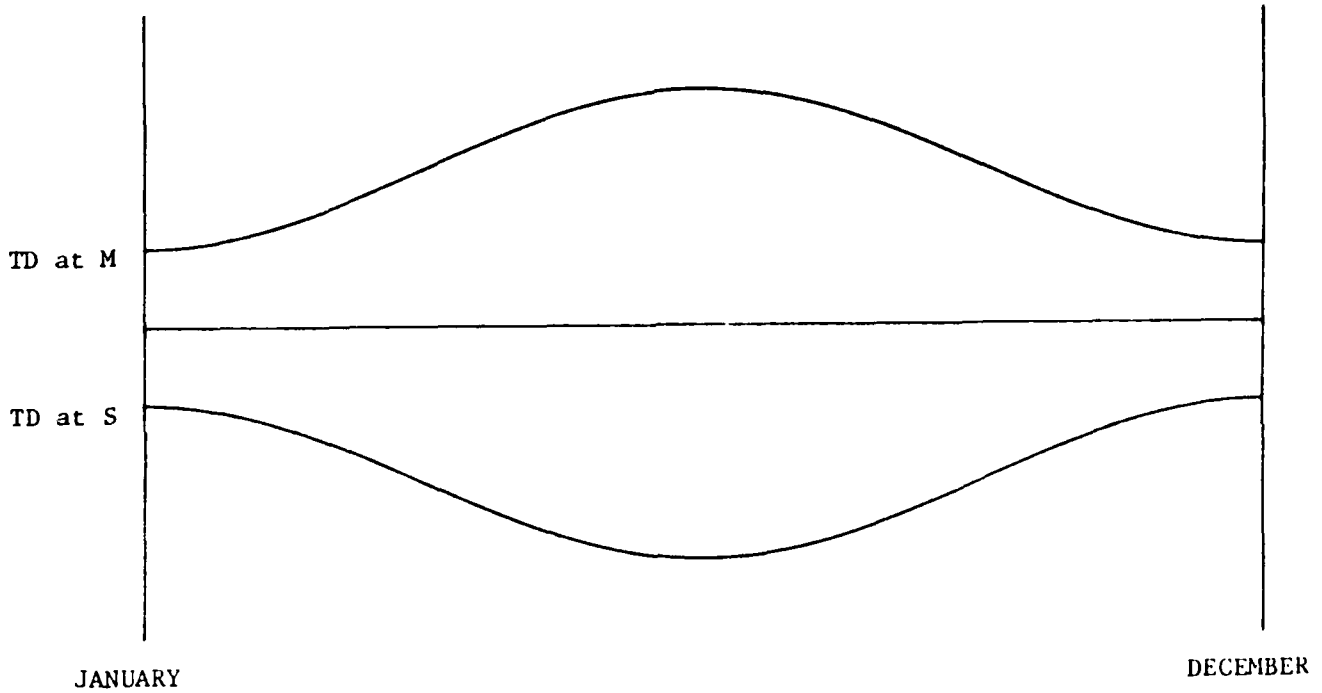

Figure B-2

Of course, temperature is not the only factor affecting signal speed and even if it were, we would not expect to see such "smooth" variations as shown above. Actual TD observation at either end of a baseline, showing a more "ragged" pattern, will be presented later. Before considering these, however, we should examine some other features of the simplified situation shown in figure B-2.

The TD variations presented for the two ends of the baseline in figure B-2 are "equal and opposite." This implies that $TD_m + TD_s$ = a constant value throughout the year. If the uniform propagation assumption were true, it is claimed this would imply the SAM is located on the perpendicular bisector of the baseline as shown in figure B-3. Let us check this claim.

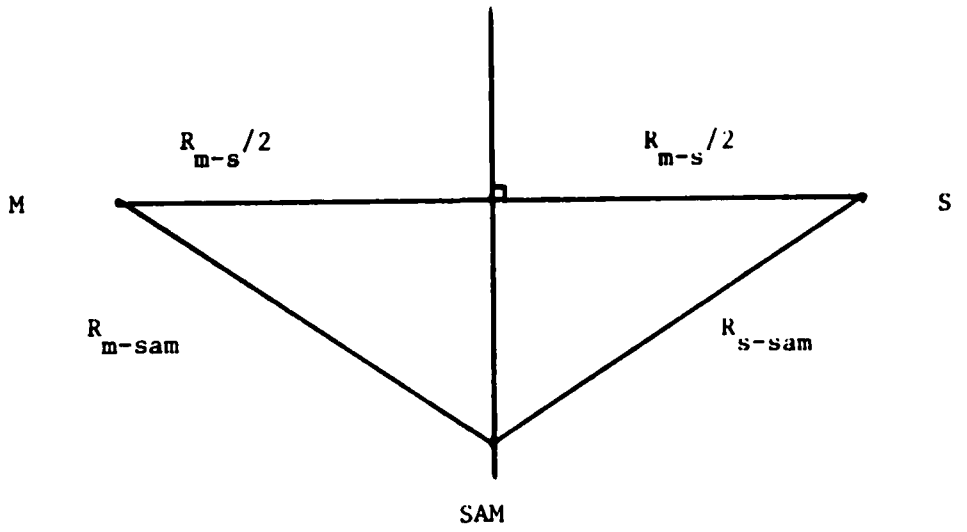

Figure B-3

From (B-1),

$$\Delta ED = (R_{s-sam} - R_{m-sam})(1/v_1 - 1/v_2)$$

$$= 0 \quad \text{for } \underline{\text{any}} \text{ velocity since } R_{s-sam} = R_{m-sam}$$

Thus, under uniform propagation conditions, locating SAM on the baseline perpendicular bisector results in a constant emission delay.

We should note that

$$TD_m = ED + (R_{s-m} - R_{m-m})/v = ED + \Delta ED + R_{s-m}/v$$

and $$TD_s = ED + (R_{s-s} - R_{m-s})/v = ED + \Delta ED - R_{m-s}/v$$

so that

$$(TD_m + TD_s)/2 = (ED + \Delta ED + R_{s-m}/v + ED + \Delta ED - R_{s-m}/v)/2$$

$$= ED + \Delta ED$$

Thus the average of TD_m and TD_s is a direct measure of the emission delay, independent of v, at any point in time. When SAM is on the baseline perpendicular bisector, $\Delta ED = 0$, so that

$(TD_s + TD_m)/2$ = a constant and any TD variations at the master and secondary must be equal in magnitude and of opposite sign as previously claimed.

If the SAM is not on the perpendicular bisector of the baseline, a situation such as shown in figure B-4 occurs.

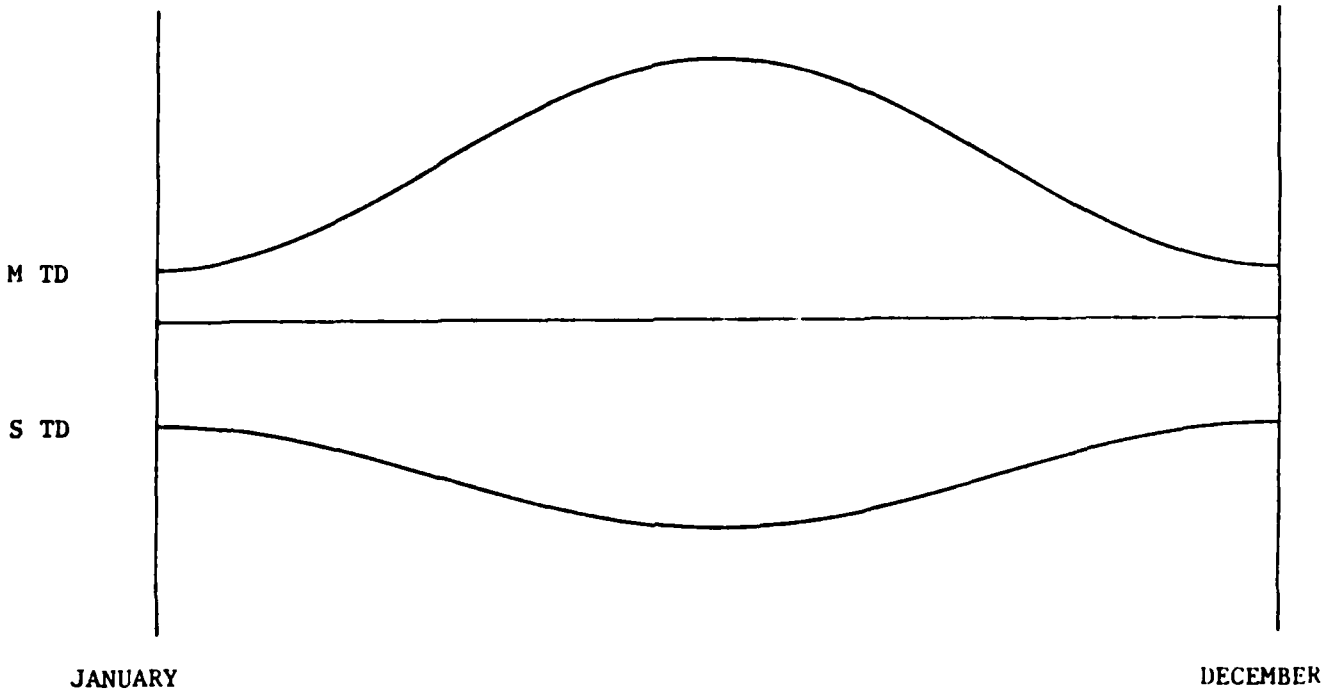

Figure B-4

In generating this example, we placed the SAM on a hyperbola which crosses the baseline at a location 33% of the way from the master to the secondary as shown in figure B-5.

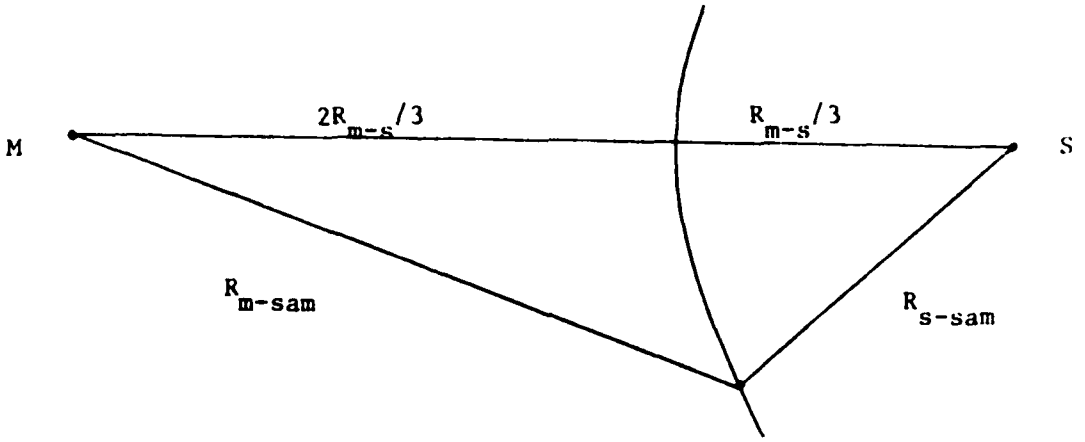

Figure B-5

In figure B-5,

$$(R_{s-sam} - R_{m-sam}) = -R_{m-s}/3 \text{ and}$$

$$\Delta TD_m = -k\Delta v\, DRD_m = -k\Delta v\, [(R_{s-m} - R_{m-m}) - (R_{s-sam} - R_{m-sam})]$$

$$= -k\Delta v\, (R_{m-s} + R_{m-s}/3)$$

$$= -(4/3)\, k\Delta v\, R_{m-s}$$

$$\Delta TD_s = -k\Delta v\, DRD_s = -k\Delta v\, [(R_{s-s} - R_{m-s}) - (R_{s-sam} - R_{m-sam})]$$

$$= -k\Delta v\, (-R_{m-s} + R_{m-s}/3)$$

$$= (2/3)\, k\Delta v\, R_{m-s} = -\Delta TD_m/2$$

In this case,

$$\Delta ED = (\Delta TD_m + \Delta TD_s)/2 = (1/2)\,(-4/3 + 2/3)\, k\Delta v R_{m-s} = (-1/3)\, k\Delta v R_{m-s}$$

At this point we can summarize the conclusions drawn from consideration of smoothed uniform propagation TD plots:

1. By averaging the TD observations at each end of the baseline, we obtain a measure of the baseline emission delay,

$$ED + \Delta ED = (TD_m + TD_s)/2$$

2. With the SAM located on the perpendicular bisector of the baseline, the emission delay is held constant:

$\Delta ED = 0$ when $R_{s-sam} = R_{m-sam}$ and the variations at either end of the baseline are equal and opposite,

$$\Delta TD_m = -\Delta TD_s$$

3. With the SAM located off the perpendicular bisector of the baseline, the emission delay varies, and variations at the end of the baseline closer to the SAM are proportionately smaller than the variations at the other end of the baseline:

for $R_{s-sam} - R_{m-sam} = k_1 R_{m-s}$

$$\Delta TD_m = -(1-k_1)\, k\, \Delta v\, R_{m-s}$$

and

$$\Delta TD_s = (1+k_1)\, k\, \Delta v\, R_{m-s}$$

so that

$$\Delta TD_m = -(1 - k_1)\,\Delta TD_s/(1 + k_1) \qquad \text{(B-4)}$$

and

$$\Delta ED = (\Delta TD_m + \Delta TD_s)/2$$

$$= (-1 + k_1 + 1 + k_1)\, k\, \Delta v\, R_{m-s}/2$$

$$= k_1\, k\, \Delta v\, R_{m-s}$$

$$= -k_1\, TD_m/(1-k_1) = k_1\, \Delta TD_s/(1+k_1)$$

Example:

Suppose SAM is closer to the secondary station and that the difference in distance from the SAM to M and S is 80% of the baseline length. Suppose over the course of a year, the "Baseline Length" (in usec) changes 1.0 usec. Then $k_1 = -0.8$ and $k\,\Delta v\, R_{m-s} = 1.0$ usec so that

$$\Delta TD_m = -1.8 \text{ usec}$$

$$\Delta TD_s = 0.2 \text{ usec}$$

and

$$\Delta ED = -0.8 \text{ usec}$$

Actual Observations.

The foregoing discussions were aimed at presenting the basic considerations in examining Loran-C time difference variations. To be more realistic, however, we must realize that smooth variations such as were shown in figures B-2 and B-5 will not occur since weather variations, the prime cause of TD fluctuations, do not occur in such a smooth fashion over the course of a year. Moreover, if we acknowledge that the signal speed changes from time to time, it is not realistic to claim these changes occur instantaneously, in the same amount, throughout the service area. This, however, is no reason to abandon the model - we need simply acknowledge its shortcomings and take care when making applications. For paths such as are involved in the St Lawrence Seaway, for example, the model can be very useful.

To obtain some of the utility of the model we can simply consider what happens during the coldest month of the year as compared with the warmest month of the year. We thus consider the two extremes and do not get ourselves hopelessly confused trying to account, on a day-to-day, or even week-to-week basis, for what happens in between. Thus, we do not try to predict or model weather in a deterministic sense. We can and should examine the "in-between" periods - but only in a statistical sense.

We begin the consideration of "real observations" with figure B-6. The data was obtained at the master and secondary stations of the 9960-X baseline during calendar year 1981.

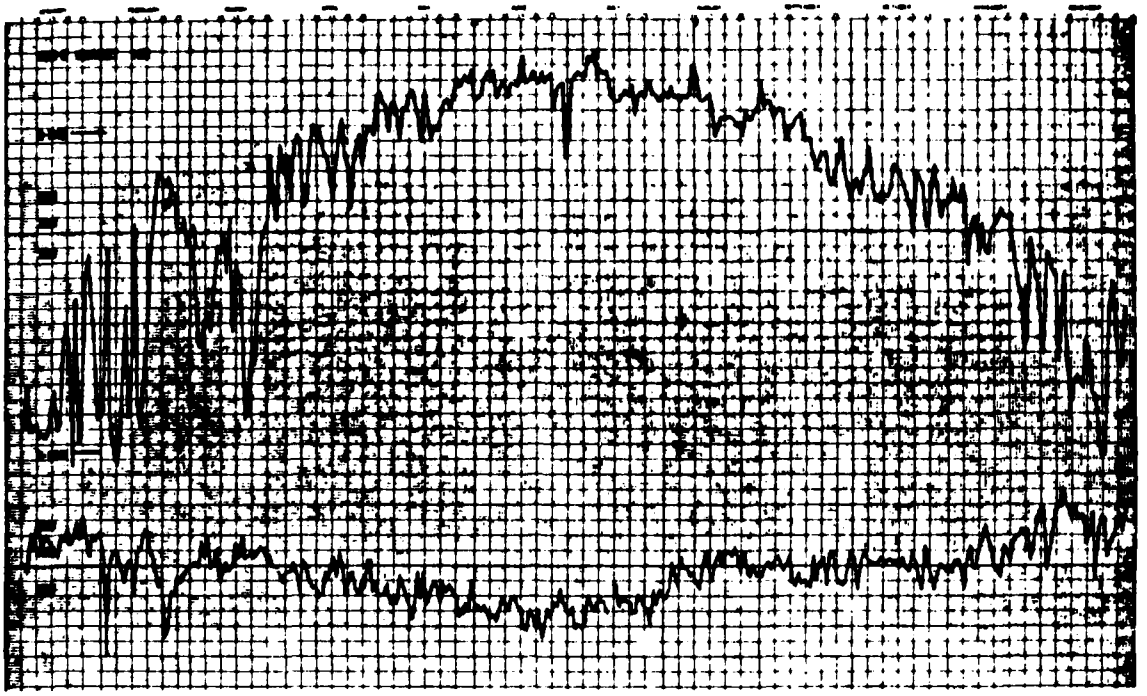

Figure B-6

The "raggedness" of the data records is very much in evidence - most noticeably in the winter months. We note, however, that the underlying trend follows that as shown in figures B-2 and B-5: the master TD's are larger in the summer than in the winter and the secondary TD's are smaller in the summer than in the winter. If we "mark" the January and July average TD's, we see that the change from summer to winter (summer minus winter) is about +1100 nsec at M and about -250 nsec at S. Thus,

$$\Delta TD_m/\Delta TD_s = -1110/25 = -4.40$$

From (B-4) we have

$$\Delta TD_m/\Delta TD_s = -(1-k_1)/(1+k_1)$$

We would thus estimate k_1 as follows,

$$1 - k_1 = 4.40\ (1 + k_1)$$

$$1 - k_1 = 4.4 + 4.4\ k_1$$

$$k_1 = -3.4/5.4 = -0.63$$

so that we estimate $R_{s\text{-}sam} - R_{m\text{-}sam} = -0.63\ R_{m\text{-}s}$

This suggests that SAM is very close, hyperbolically to the secondary. Specifically, we would guess SAM is on a hyperbola which passes through the baseline 18.5% of the baseline length from the secondary and 81.5% of the baseline length from the master as shown in figure B-7. (0.185 - 0.815 = -0.63).

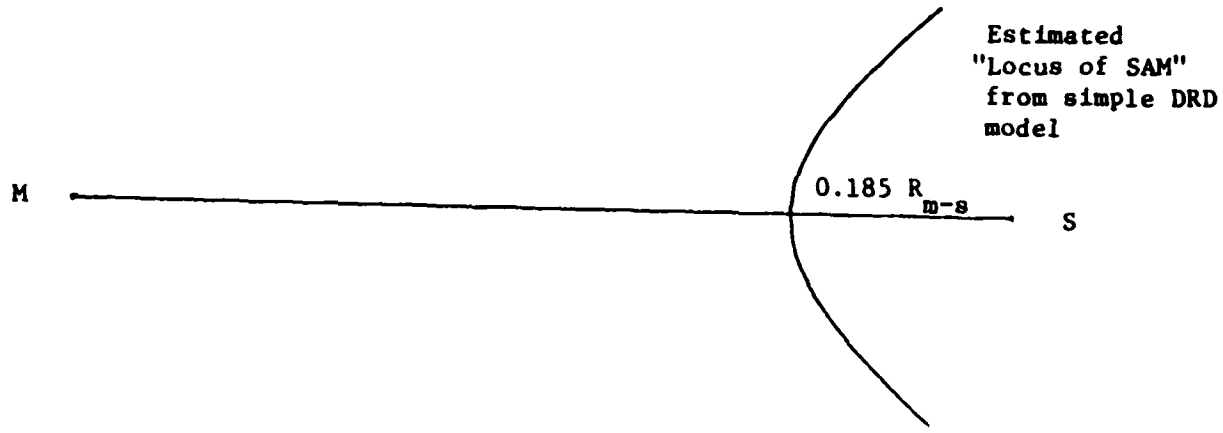

Figure B-7

As it turns out, the actual situation for the 9960-X baseline, with Master at Seneca, N.Y., secondary at Nantucket, Ma, and SAM at Sandy Hook, N.J., is as shown in figure B-8.

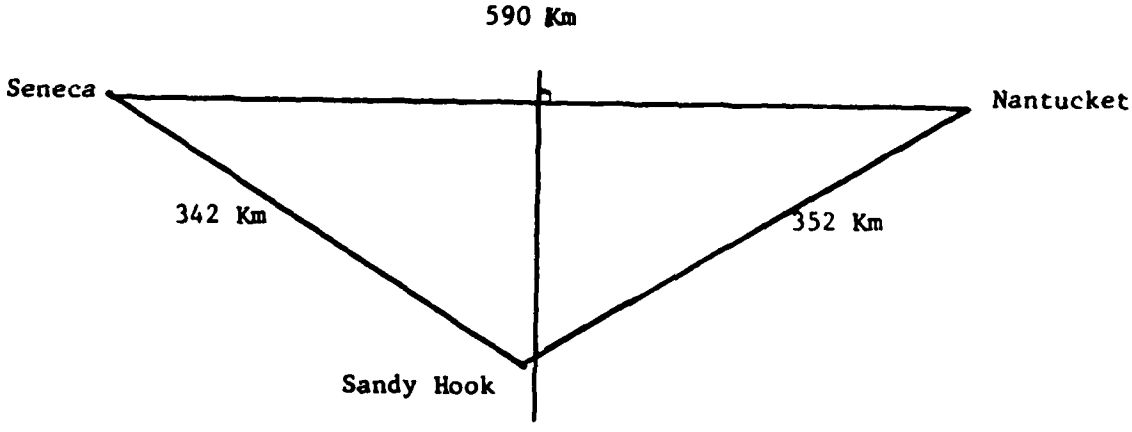

Figure B-8

In actuality, SAM is very nearly on the perpendicular bisector of the baseline:

$$R_{s\text{-}sam} - R_{m\text{-}sam} = 0.02\ R_{m\text{-}s},$$

and our model seems to have failed us.

Closer scrutiny of the situation, however, shows the path from the Master to the Secondary and the path from the Master to the SAM are almost exclusively over land. Moreover, the land paths involved are interior New York State and Massachusetts - areas which normally feature sub-freezing temperatures in mid-winter. The path from the secondary to the SAM, however, is almost entirely comprised of seawater which has a significant moderating effect. The particular effect is that dry, sub-freezing surface temperatures do not occur.

These observations suggest a modification to the double range difference model in cases where paths involve seawater that does not freeze. We have experimented with several modifications and, given the presently available data base, feel the best modification to make is to not count salt water paths at all in calculating ranges (at least in the temperate zones). If we apply this modification to the 9960-X baseline, we find the "modified ranges" of concern are:

Seneca-to-Nantucket = R_{m-s} = 526 km

Seneca to Sandy Hook = R_{m-sam} = 332 km

Nantucket to Sandy Hook = R_{s-sam} = 13

Thus we have

$$(R_{s-sam} - R_{m-sam})/R_{m-s} = -0.60$$

which agrees very closely with the estimated value of -0.63.

Thus, the efficacy of this modification to the DRD-model can be seen. Further evidence can be seen if we tabulate the observations at all available data collection sites for the 9960-X baseline. In table B-1 we show the summer-to-winter variations for each site along with both the "simple DRD" and "modified DRD."

The data is also plotted in figures B-9 and B-10. In figure B-9, the "Peak-Peak seasonal variation" is plotted versus the simple double range difference. In figure B-10, it is plotted versus the modified double range difference. A linear regression analysis shows application of the simple double range difference model reduces the data record variation by about a factor of 5.5. Application of the modified double range difference model yields an additional factor of 3.4 reduction so that the standard deviation of the residuals is only 21 nsec.

Site	TD (Summer - Winter)	Simple DRD	Modified DRD
Seneca, N.Y.	1100 nsec	580 km	843 km
Nantucket, Ma.	-250	-600	-209
Nahant, Ma.	-190	-346	-117
Avery Pt, Ct.	-140	-259	-79
Sandy Hook, N.J.	0	0	0
Cape Elizabeth, Me.	-170	-299	-194

Table B-1

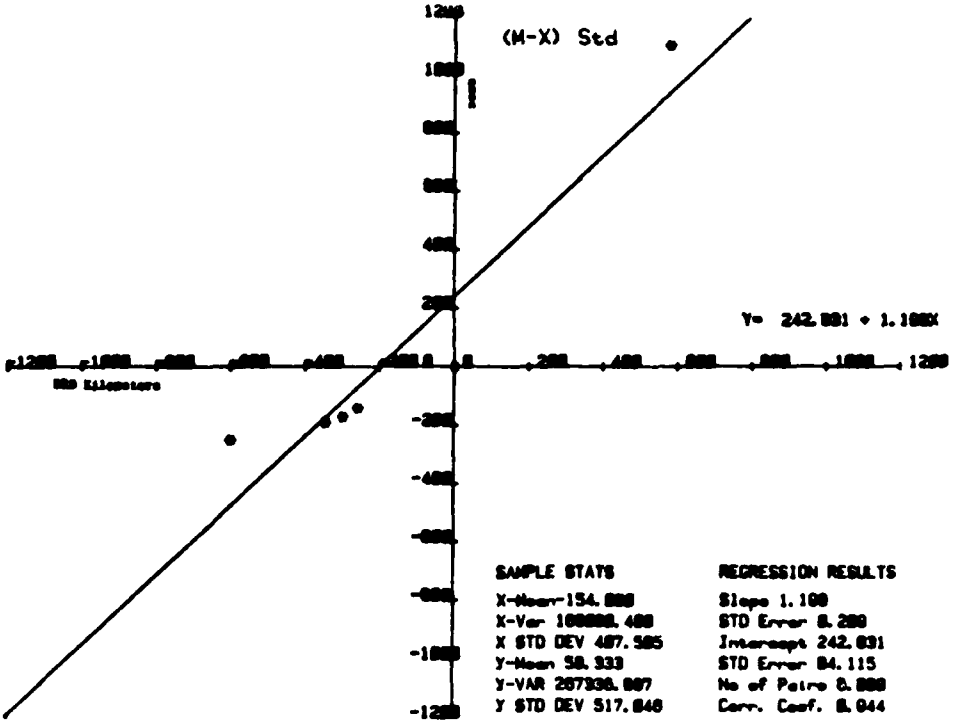

Figure B-9

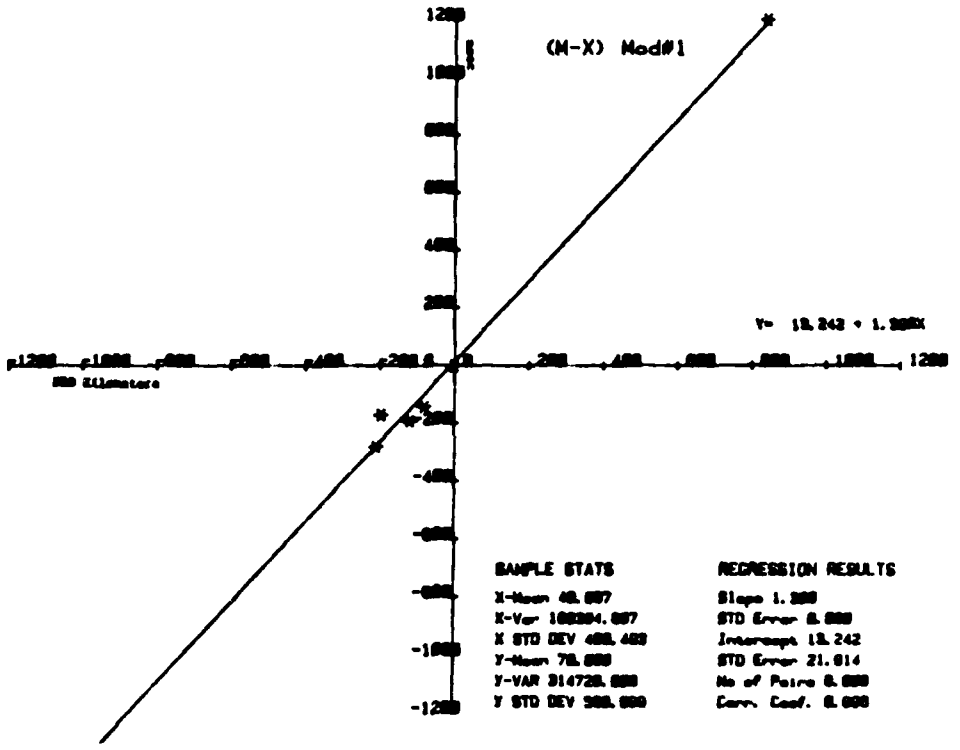

Figure B-10

These results indicate the modified double range difference model is a very good one for the seasonal (i.e., the largest) component of the Loran-C time difference variations. This model is used in the main body of the report to make predictions based on both the 1981 9960-W and 9960-X baseline observations made at harbor monitor sites and from 1981/82 observations made at Massena, N.Y. More detailed application of the simple model was made in reference 4 . At present we are developing modifications to the model to deal more with the statistics of the short term variations than the actual data variations as was done in reference 4 . The underlying concept of this extension is that the "raggedness" of the data records increases as a function of the double range difference just as the peak-peak variation over a year did.

At the time of this writing, we have obtained a full year of Loran-C chain 9960 data in electronic form from only three sites. Thus we feel it would be premature at this time to present the short term variation model. Publication of this further extension of the model is saved for a future report when, in particular, we hope to have a substantial St Lawrence Seaway region Loran-C data base.

APPENDIX C

A PRIORI ESTIMATES OF ST. LAWRENCE SEAWAY LORAN-C STATISTICS

APPENDIX C

A PRIORI ESTIMATES OF ST LAWRENCE SEAWAY LORAN-C STATISTICS

Purpose.

In Appendix A we developed how to generate Loran-C error ellipses and showed how we must first obtain estimates of σ_w, σ_x, and ρ - the standard deviations of the two prime time differences (TD's) in the area and the correlation coefficient between the two TD's. Ultimately, we want to obtain these estimates by direct observations at data collection sites in the Seaway. In section 3 of this report, however, we try to present an a priori assessment of the Loran-C performance to be expected in the Seaway. This serves to focus our attention on the vital statistics to obtain from the stability study and illustrate how these are to be used. From this, the overall experiment strategy can be carefully examined.

Since we do not yet have an adequate data base, the analysis of section 3 must draw statistical parameter estimates from some other source. The double range difference concepts presented in Appendix B can be applied to N.E.U.S. Loran-C station and harbor monitor sites to provide a first-cut estimate of the standard deviations. The methodology to do this, along with a procedure for obtaining first-cut estimates of the correlation coefficients is presented herein.

Formulation - Non-Differential Loran-C.

We begin by noting that section 3 explains that the statistical parameters of interest are time-varying quantities. For our first cut at estimating performance, however, we will ignore this technicality. We say that at any point and at any time, the time difference measurement is a random variable:

$$TD_x = k + x_1 + x_2$$

where k = the non-varying component of the time difference

x_1 = the seasonal component of the time difference, a zero-mean random variable

x_2 = the sum of all shorter term components, a zero-mean random variable

We will assume independence between the varying components so that the total standard deviation, σ_x, is

$$\sigma_x = (\sigma_{x1}^2 + \sigma_{x2}^2)^{\frac{1}{2}}$$

Data obtained at USCG harbor monitor sites suggests that for double-range differences such as those encountered in the St Lawrence region for the 9960-W and X baselines, σ_{x1} is at least 3 or 4 times as large as σ_{x2}.

If $\sigma_{x1} = 3\sigma_{x2}$,

$$\sigma_x = \sigma_{x1} [1 + (1/3)^2]^{1/2} \approx 1.05\ \sigma_{x1} \approx \sigma_{x1}$$

For a "Raw Loran-C" (vice differential Loran-C) analysis, therefore, we can ignore the short-term component in generating a year-round performance prediction.

To obtain an estimate of σ_{x1}, we will simply assume we have pure sinusoidal seasonal components. Thus,

$$\sigma_{x1} = 0.707\ (\text{peak-peak variation})/2$$

(i.e., rms-value of a sinusoid).

By using the results of the double-range difference regression analysis performed using N.E.U.S. chain and harbor monitor site data, we can obtain estimates of σ_w and σ_x at the center of all the St Lawrence Seaway reaches of interest. Appropriate double range differences and resulting "seasonal sigmas" (σ_s) are listed in Table C-1. In the computations, we used:

$$(pk\text{-}pk)_w = 0.993\ DRD_w - 45 \qquad \text{(in nanoseconds)}$$

$$(pk\text{-}pk)_x = 1.316\ DRD_x + 3 \qquad \text{(in nanoseconds)}$$

Reach #	BRD-W	Predicted Seasonal "Sigma-W"	BRD-X	Predicted Seasonal "Sigma-X"
2	275 km	.080 msec	401 km	.187 msec
3	284	.084	381	.190
4	296	.088	414	.194
5	303	.091	420	.196
7	313	.094	423	.198
8	321	.097	429	.201
11	328	.099	435	.204
12	337	.103	444	.208
14	352	.108	462	.215
15	353	.108	463	.216
16	362	.112	472	.221
17	369	.114	478	.224
18	381	.118	486	.227
19	392	.122	495	.232
20	396	.123	499	.233
21	401	.125	801	.234
22	407	.127	504	.236
23	414	.129	809	.238
24	419	.131	513	.240
25	425	.133	519	.242
26	431	.136	522	.244
27	434	.137	523	.244
28	436	.137	527	.246
29	439	.138	529	.247
31	443	.140	533	.249
33	467	.148	554	.259
34	474	.150	558	.260
35	478	.152	562	.263
36	484	.154	566	.264
37	490	.156	570	.266
38	492	.157	572	.267
39	496	.158	574	.268
40	500	.160	576	.269
41	508	.162	578	.270
42	512	.164	881	.272
43	517	.166	586	.274
44	519	.166	588	.275
46	524	.168	590	.276
46	527	.169	593	.277
47	531	.170	595	.278
48	536	.172	597	.279
50	541	.174	600	.280
51	551	.178	606	.283
52	557	.180	610	.285
53	562	.181	612	.286
55	568	.183	616	.288
56	573	.185	619	.289
57	587	.190	628	.293
58	604	.196	638	.298
59	613	.199	644	.301
60	617	.201	646	.302
61	620	.202	647	.302
62	622	.202	649	.304
63	629	.205	652	.304
64	636	.207	653	.305
65	648	.212	658	.307
67	665	.214	661	.309
69	667	.218	667	.311
71	681	.223	674	.315
74	701	.230	683	.319
77	713	.234	694	.324
78	718	.236	695	.324
79	734	.242	697	.325
80	752	.248	706	.330
81	764	.252	712	.332
82	779	.258	718	.335
83	796	.264	727	.339

TABLE C-1

All that remains now is for us to obtain estimates of the correlation coefficients. Note that we have:

$$TD_w = k_w + w_1 + w_2 \qquad TD_x = k_x + x_1 + x_2$$

$$E[TD_w\ TD_x] = \rho \sigma_w \sigma_x$$

Table C-1 lists our estimates for σ_w and σ_x so that ρ is the remaining unknown. As before, we assume the seasonal and short term components are independent so that

$$E[w_1\ w_2] = E[x_1\ x_2] = E[w_1\ x_2] = E[x_1\ w_2] = 0$$

This leaves

$$\rho\ \sigma_w\ \sigma_x = E[TD_w\ TD_x] = \rho_1\ \sigma_{w1}\ \sigma_{x1} + \rho_2\ \sigma_{w2}\ \sigma_{x2} \qquad \text{(C-1)}$$

where

$$\rho_1\ \sigma_{w1}\ \sigma_{x1} = E[w_1\ x_1],$$

and

$$\rho_2\ \sigma_{w2}\ \sigma_{x2} = E[w_2\ x_2]$$

Since we have assumed pure sinusoids for w_1 and x_2 we might as well assume they are perfectly in phase so that $\rho_1 = 1$. (Actually, harbor monitor data suggests this is a valid assumption). The search now focuses on estimating ρ_2. To obtain a useful a priori estimate of ρ_2 we should note the following.

Let

m_{TOA} = short term component of master signal time-of-arrival variation

w_{TOA} = " " " " whisky " " "

x_{TOA} = " " " " xray " " "

Since $w_2 = w_{TOA} - m_{TOA}$ and $x_2 = x_{TOA} - m_{TOA}$,

$$E[w_2\ x_2] = \rho_2\ \sigma_{w2}\ \sigma_{x2} = E[(w_{TOA} - m_{TOA})(x_{TOA} - m_{TOA})]$$

$$= E[w_{TOA}\ x_{TOA}] - E[w_{TOA}\ m_{TOA}] - E[x_{TOA}\ m_{TOA}] + E[m_{TOA}^2]$$

We assume that all short term TOA's measurements are independednt so that.

$$E[w_{TOA}\ x_{TOA}] = E[w_{TOA}\ m_{TOA}] = E[x_{TOA}\ m_{TOA}] = 0$$

Thus,

$$E[w_2\, x_2] = \rho_2\, \sigma_{w2}\, \sigma_{x2} = \sigma_{mTOA}^2$$

But, $\sigma_{w2} = (\sigma_{wTOA}^2 + \sigma_{mTOA}^2)^{1/2}$

and $\sigma_{x2} = (\sigma_{xTOA}^2 + \sigma_{mTOA}^2)^{1/2}$

so,

$$\rho_2 = \frac{\sigma_{mTOA}^2}{\left[(\sigma_{wTOA}^2 + \sigma_{mTOA}^2)\ (\sigma_{xTOA}^2 + \sigma_{mTOA}^2)\right]^{\frac{1}{2}}}$$

Classical treatments assume that short term TOA variations are signal-to-noise ratio dominated. Thus, if the observer is close to the master station, so the argument goes, $\sigma_{mTOA} \ll \sigma_{wTOA}, \sigma_{xTOA}$ so that we can say $\rho_2 \approx 0$. In the middle of the chain coverage area,

$$\sigma_{mTOA} \approx \sigma_{wTOA} \approx \sigma_{xTOA} \approx \sigma$$

so we have

$$\rho = \frac{\sigma^2}{\left[(2\sigma^2)\ (2\sigma^2)\right]^{\frac{1}{2}}} = \frac{1}{2}$$

These treatments thus ignore the effects of imperfections of chain operations, including timing correction granularity, phase modulation, etc. In a more recent treatment (reference 5), Ligon suggests that for the short baseline chains of Canada and CONUS, unless one is truly in a "fringe area," (we are not), it is best to simply assume all short term noise is "transmitter noise" and thus independent of distance to the stations. Thus, we say $\sigma_{mTOA} \approx \sigma_{wTOA} \approx \sigma_{xTOA} \approx \sigma$ and we get $\rho_2 = 1/2$. This assumption is suggested as the most appropriate a priori estimate and the one we will use.

If we let $\sigma_{w1} = k_w\, \sigma_{w2}$

and $\sigma_{x1} = k_x\, \sigma_{x2}$,

we can re-write equation C-1:

$$\rho = \frac{\rho_1\, \sigma_{w1}\, \sigma_{x1} + \rho_2\, \sigma_{w2}\, \sigma_{x2}}{\sigma_w\, \sigma_x}$$

Since

$$\sigma_w = (\sigma_{w1}^2 + \sigma_{w2}^2)^{\frac{1}{2}}, \qquad \sigma_x = (\sigma_{x1}^2 + \sigma_{x2}^2)^{\frac{1}{2}},$$

and

$$\sigma_{w2} = \left(\frac{1}{k_w}\right) \sigma_{w1}, \qquad \sigma_{x2} = \left(\frac{1}{k_x}\right) \sigma_{x1},$$

we have

$$\rho = \frac{\sigma_{w1}\,\sigma_{x1}\left[\rho_1 + \rho_2/(k_w k_x)\right]}{\sigma_{w1}\,\sigma_{x1}\left[(1 + 1/k_w^2)\,(1 + 1/k_x^2)\right]^{\frac{1}{2}}}$$

$$\rho = \frac{\rho_1 k_w k_x + \rho_2}{\left[(k_w^2 + 1)\,(k_x^2 + 1)\right]^{\frac{1}{2}}}$$

For $\rho_1 = 1$ and $\rho_2 = 0.5$,

$$\rho = \frac{k_w k_x + \frac{1}{2}}{\left[(k_w^2 + 1)\,(k_x^2 + 1)\right]^{\frac{1}{2}}}$$

We previously argued it was reasonable to assume $k_w = k_x = 3$ (at least). For these values we have

$$\rho = \frac{9 + 1/2}{9 + 1} = 0.95$$

Alternatively, for $k_w = k_x = 2$, we have

$$\rho = \frac{4 + 1/2}{4 + 1} = 0.90$$

In the St Lawrence, the $\rho = 0.95$ assumption yields smaller errors than the $\rho = 0.90$ assumption. Thus, to be conservative, we will use $\rho = 0.95$ for all reaches. With this final assumption, we have the ability to generate predicted error ellipses for each reach of the seaway and estimate maximum cross-track errors - at some specified probability contour. For a first cut, we use a probability of 0.95 - further discussion on this subject is provided in section 3. Plots of the ellipses are provided in Appendix C - the section called "Raw (Non-Differential) Loran-C Error Ellipses."

Formulation - Differential Loran-C.

If we place a differential monitor site in the St Lawrence Seaway - say at the Eisenhower Locks at Massena, N.Y. - we can considerably reduce the seasonal component of the TD variations observed along the river. The manner in which the variations are reduced - assuming the uniform propagation/double-range difference formulation holds true - is very straightforward. From equation B-3 in Appendix B, we have the change in TD's at any site being represented by:

$$TD_{2,p} - TD_{1,p} = \Delta TD_p = k\,\Delta v\,DRD_p$$

If we call the differential monitor station point d, we have

$$TD_{2,d} - TD_{1,d} = k\,\Delta v\,DRD_d$$

At T_1 (say, the time of the survey), we have

$$TD_{1,p} = k_p + TD_{1,d} \qquad (C\text{-}2)$$

where k_p is some constant value determined by the Loran-C chain numbers and the exact location of the observer - this is all determined during the survey. At T_2, we have

$$TD_{2,p} = TD_{1,p} + k\,\Delta v\,DRD_p$$

$$= k_p + TD_{1,d} + k\,\Delta v\,DRD_p$$

But,

$$TD_{1,d} = TD_{2,d} - k\,\Delta v\,DRD_d$$

so we have

$$TD_{2,p} = k_p + TD_{2,d} - k\,\Delta v\,DRD_d + k\,\Delta v\,DRD_p$$

$$= k_p + TD_{2,d} + k\,\Delta v\,(DRD_p - DRD_d)$$

In utilizing differential Loran-C, an observer at point p computes position based on:

$$TD_{2,p} - \text{differential correction}$$

where $\text{differential correction} = TD_{2,d} - TD_{1,d}$

Thus, the fix is based on

$$TD_{2,p} - TD_{2,d} + TD_{1,d}$$

$$= k_p + TD_{2,d} + k\Delta v\,(DRD_p - DRD_d) - TD_{2,d} + TD_{1,d}$$

$$= [k_p + TD_{1,d}] + k\Delta v\,(DRD_p - DRD_d)$$

The term in brackets, of course, can be seen from equation C-2 above to be simply $TD_{1,p}$. Thus, we have

$$\text{Corrected } TD_{2,p} = TD_{1,p} + k\Delta v\,(DRD_p - DRD_d)$$

and the TD's at point p, with differential corrections applied, vary from time T_1 to T_2 in the manner described below:

$$TD_{p,\,differential} = TD_{2,p,\,differential} - TD_{1,p,differential}$$

$$= k\Delta v\,(DRD_p - DRD_d)$$

Thus, the variations are of the same form as described in Appendix B, we simply have to use what we might call the "differential" double range difference. We pick the proposed monitor site and subtract its double range difference from all other sites of interest.

We expect that the move to differential Loran-C will remove a large portion of the TD variations throughout the St Lawrence Seaway. Thus we can no longer simply assume the seasonal components are so much larger than the shorter term components that they serve as a good estimate of the total variation and we must come up with estimates for the short term variations. There are numerous classical approaches to this problem which relate the short term variation to distance from the transmitting stations. As described earlier in the discussion on short term correlation coefficients these treatments assume atmospheric noise predominates "transmitter noise". Again, we argue this is not an appropriate claim for the St Lawrence Seaway where we assume we are not "atmosperic noise limited." Thus, for this cut, we will choose a single figure to represent the short term standard deviation - for both TD's at all reaches. From harbor monitor experience an estimate of 20 nanoseconds seems most appropriate.

This short term standard deviation must be modified before we can make direct application to the differential Loran-C situation. We must remember that the differential monitor station provides information to the user but it also provides noise. Thus, we assume the short term noise at the monitor is independent of the short term noise the user is encountering so that

after the correction has been applied, the user noise has been increased:

$$\sigma_{p,differential} = (\sigma_p^2 + \sigma_d^2)^{1/2}$$

We assume that $\sigma_p = \sigma_d = 20$ nsec so that $\sigma_{p,diff} = 20\sqrt{2}$. This is the figure we will use for our predictions.

We further assume that the short term and seasonal variations are independent so that

$$\sigma_{total} = [\sigma_s^2 + (20\sqrt{2})^2]^{1/2} \qquad \text{(C-3)}$$

$$= (\sigma_s^2 + 800)^{1/2}$$

where σ_s = the seasonal component standard deviation which is estimated by use of the differential double range difference formulation.

Additionally, with differential Loran-C, we must revise our approach to estimating the correlation coefficient. As before, we will assume the seasonal components are pure sinusoids. Depending on the "sign" of the differential double range differences these sinusoids could be in-phase or 180° out of phase. Due to the nature of the geometry in the St Lawrence, the differential double range differences are always of the same sign. Thus, we will again use $\rho_1 = 1$ and note that if the differential double range differences were of the opposite sign, we would have used $\rho_1 = -1$.

To compute the total correlation coefficient, we re-write equation C-1:

$$\rho = \frac{\rho_1 \sigma_{w1} \sigma_{x1} + \rho_2 \sigma_{w2} \sigma_{x2}}{\sigma_w \sigma_x}$$

Using $\rho_1 = 1$, $\rho_2 = 0.5$ as before, and $\sigma_{w2} = \sigma_{x2} = 20\sqrt{2}$, this combines with equation C-3 to become:

$$\rho = \frac{\sigma_{w1} \sigma_{x1} + 400}{\left[(\sigma_{w1}^2 + 800)(\sigma_{x1}^2 + 800)\right]^{\frac{1}{2}}} \qquad \text{(C-4)}$$

Using equation C-4 and the re-computed double range differences, we can construct Table C-2 which lists the predicted statistics based on a differential monitor site located at Eisenhower Locks. Plots of the resulting error ellipses are presented in Appendix D.

Reach #	DRO-N	Predicted Seasonal "Sigma-N"	Predicted Total "Sigma-N"	DRO-X	Predicted Seasonal "Sigma-X"	Predicted Total "Sigma-X"	Predicted Total "RMO"
2	-183 km	.066 usec	.071 usec	-146 km	.067 usec	.073 usec	0.92
3	-174	.061	.067	-140	.064	.070	0.92
4	-162	.057	.064	-133	.060	.066	0.90
5	-155	.054	.061	-127	.058	.066	0.89
7	-145	.051	.060	-124	.056	.063	0.89
8	-137	.048	.056	-118	.053	.060	0.88
11	-130	.046	.054	-112	.050	.057	0.88
12	-121	.042	.051	-103	.046	.054	0.85
14	-105	.037	.047	-85	.039	.048	0.82
15	-100	.037	.047	-84	.038	.047	0.82
16	-95	.033	.043	-75	.033	.043	0.81
17	-89	.031	.042	-69	.030	.041	0.77
18	-77	.027	.039	-61	.027	.039	0.74
19	-65	.023	.036	-52	.022	.036	0.70
20	-60	.022	.035	-48	.021	.035	0.68
21	-57	.020	.036	-46	.021	.036	0.66
22	-57	.018	.036	-43	.018	.034	0.64
23	-44	.016	.032	-36	.016	.032	0.64
24	-39	.014	.032	-34	.014	.032	0.58
25	-33	.012	.031	-28	.012	.031	0.57
26	-27	.009	.030	-25	.010	.030	0.54
27	-24	.008	.029	-24	.010	.030	0.55
28	-22	.008	.029	-23	.008	.029	0.55
29	-19	.007	.029	-18	.007	.029	0.53
31	-15	.006	.029	-14	.006	.029	0.51
33	9	.003	.028	7	.006	.029	0.51
34	16	.006	.029	11	.006	.029	0.51
35	20	.007	.029	15	.008	.030	0.53
36	25	.009	.030	19	.010	.030	0.54
37	30	.011	.030	23	.012	.031	0.57
38	34	.012	.031	25	.013	.031	0.60
39	38	.013	.031	27	.014	.032	0.60
40	42	.015	.032	29	.015	.032	0.61
41	45	.017	.033	31	.016	.033	0.62
42	54	.019	.034	36	.018	.034	0.64
43	59	.021	.035	39	.020	.035	0.67
44	61	.021	.036	41	.021	.036	0.60
45	65	.023	.035	43	.022	.036	0.70

Reach #	DRO-N	Predicted Seasonal "Sigma-N"	Predicted Total "Sigma-N"	DRO-X	Predicted Seasonal "Sigma-X"	Predicted Total "Sigma-X"	Predicted Total "RMO"
46	69	.024	.037	46	.023	.036	0.71
47	72	.025	.038	48	.024	.037	0.72
48	78	.027	.039	50	.026	.038	0.73
50	83	.029	.041	53	.026	.038	0.74
51	93	.033	.043	59	.029	.041	0.77
52	99	.035	.045	63	.031	.042	0.78
53	104	.036	.046	66	.032	.043	0.78
55	110	.038	.047	69	.034	.044	0.82
56	115	.040	.049	72	.036	.046	0.82
57	129	.045	.053	81	.039	.048	0.85
58	145	.051	.058	91	.044	.052	0.85
59	165	.056	.061	97	.047	.055	0.89
60	169	.056	.063	99	.048	.056	0.88
61	162	.057	.064	101	.048	.056	0.88
62	164	.057	.064	102	.049	.057	0.88
63	171	.060	.065	105	.050	.057	0.90
64	178	.062	.068	105	.051	.058	0.90
65	190	.067	.073	111	.053	.060	0.90
67	197	.069	.076	114	.056	.062	0.90
69	208	.073	.078	120	.057	.064	0.91
71	223	.078	.083	127	.061	.067	0.93
74	243	.085	.089	136	.065	.071	0.93
77	256	.090	.093	147	.070	.076	0.94
78	260	.091	.095	149	.070	.076	0.94
79	276	.097	.101	159	.071	.076	0.95
80	294	.100	.107	159	.076	.081	0.95
81	306	.107	.111	165	.078	.083	0.95
82	321	.113	.116	171	.081	.085	0.96
83	335	.118	.122	180	.086	.090	0.95

Table C-2

Section 3 discusses the situation to be attained if we add a differential monitor site at Wellesley Island. Table C-3 lists the statistics for appropriate reaches with this site providing differential corrections. The data was computed using the same formulation used for Eisenhower Locks. Plots of the resulting error ellipses are also provided in Appendix D.

Reach #	DRD-W	Predicted Seasonal "Sigma-W"	Predicted Total "Sigma-W"	DRD-X	Predicted Seasonal "Sigma-X"	Predicted Total "Sigma-X"	Predicted Total "RHO"
56	-128	.045	.053	-68	.032	.043	0.81
57	-114	.040	.049	-59	.028	.039	0.80
58	-97	.036	.046	-49	.023	.036	0.74
59	-88	.033	.043	-43	.020	.034	0.73
60	-84	.031	.042	-41	.019	.034	0.69
61	-81	.030	.041	-40	.019	.034	0.70
62	-79	.030	.041	-38	.018	.034	0.67
63	-72	.027	.039	-35	.017	.033	0.67
64	-65	.025	.038	-34	.016	.032	0.66
65	-53	.020	.035	-29	.014	.032	0.61
67	-46	.018	.034	-26	.012	.031	0.58
69	-34	.014	.032	-20	.010	.030	0.56
71	-20	.009	.030	-13	.006	.029	0.52
74	0	.000	.028	-4	.002	.028	0.51
77	12	.004	.029	7	.003	.028	0.51
78	17	.006	.029	8	.003	.028	0.51
79	33	.012	.031	10	.004	.029	0.50
80	51	.018	.034	19	.009	.030	0.55
81	63	.022	.036	25	.011	.030	0.59
82	78	.028	.040	31	.014	.032	0.62
83	95	.034	.044	40	.018	.034	0.68

Table C-3

APPENDIX D

ST LAWRENCE SEAWAY PREDICTED LORAN-C ERROR ELLIPSES

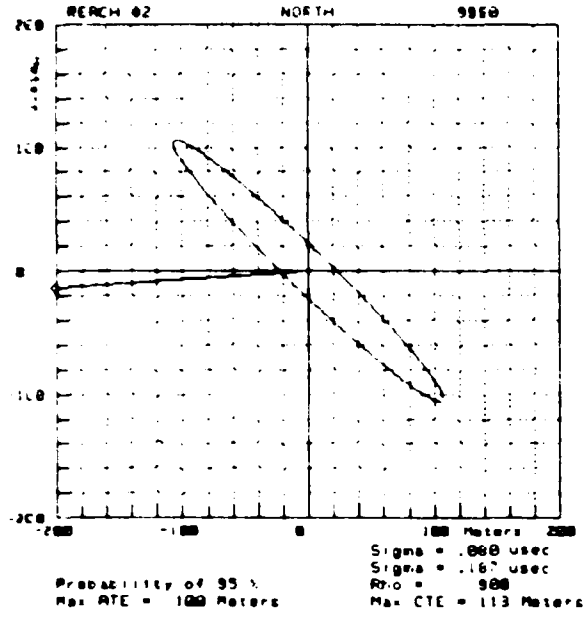
BEACH #2
NORTH
9850
200
100
0
-100
-200
-200
-100
0
100 Meters
200
Sigma = .080 usec
Sigma = .167 usec
Rho = .900
Max CTE = 113 Meters
Probability of 95 %
Max ATE = 100 Meters

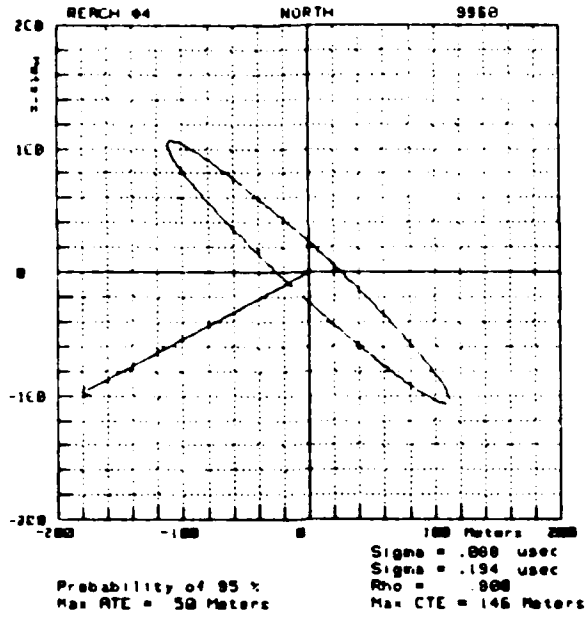
BEACH #4
NORTH
9850
200
100
0
-100
-200
-200
-100
0
100 Meters
200
Sigma = .080 usec
Sigma = .194 usec
Rho = .900
Max CTE = 146 Meters
Probability of 95 %
Max ATE = 50 Meters

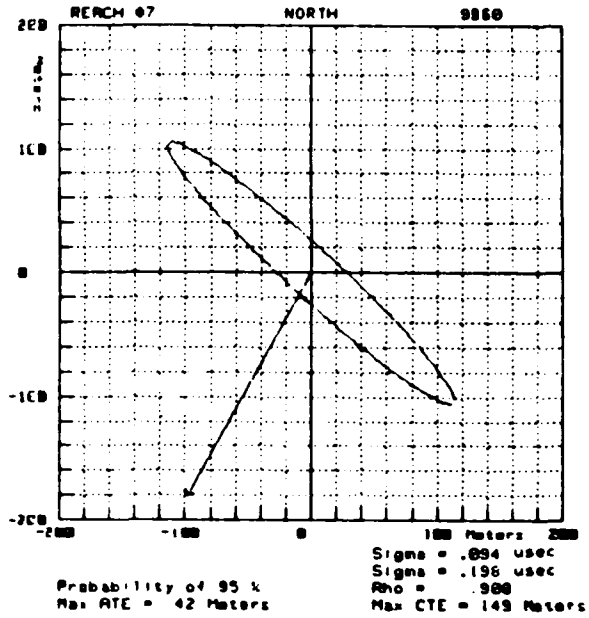
BEACH #7
NORTH
9850
200
100
0
-100
-200
-200
-100
0
100 Meters
200
Sigma = .094 usec
Sigma = .196 usec
Rho = .900
Max CTE = 149 Meters
Probability of 95 %
Max ATE = 42 Meters

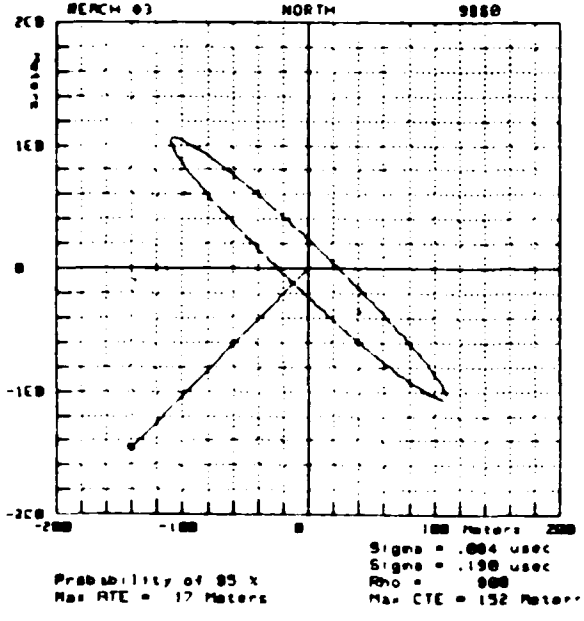
BEACH #3
NORTH
9850
200
100
0
-100
-200
-200
-100
0
100 Meters
200
Sigma = .084 usec
Sigma = .190 usec
Rho = .900
Max CTE = 152 Meters
Probability of 95 %
Max ATE = 17 Meters

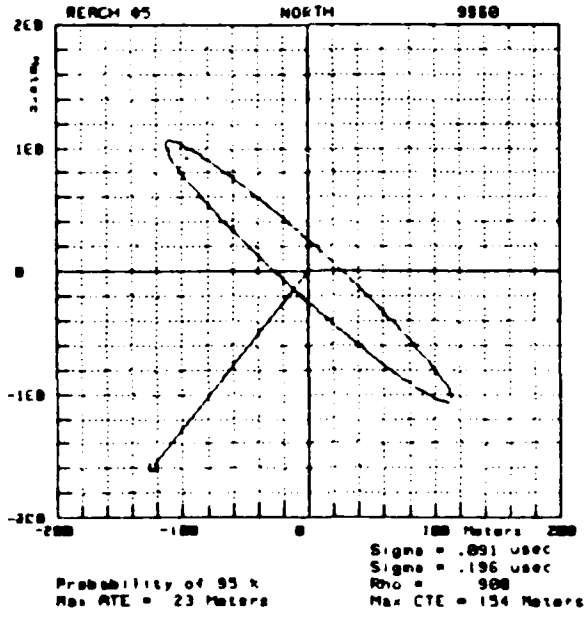
BEACH #5
NORTH
9850
200
100
0
-100
-200
-200
-100
0
100 Meters
200
Sigma = .091 usec
Sigma = .196 usec
Rho = .900
Max CTE = 154 Meters
Probability of 95 %
Max ATE = 23 Meters

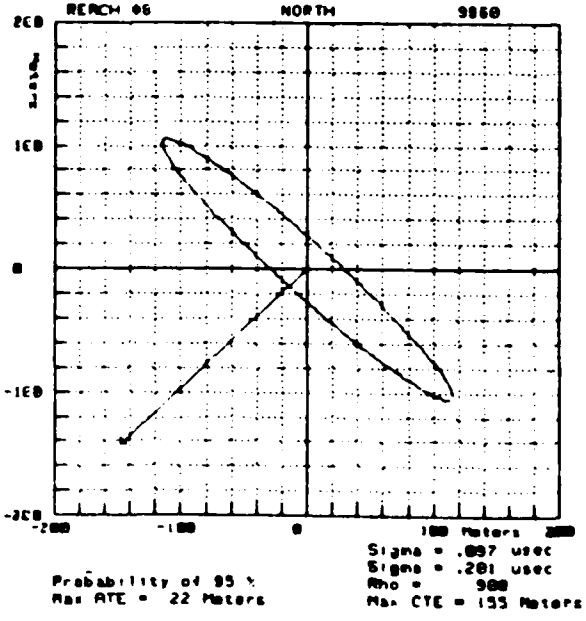
BEACH #6
NORTH
9850
200
100
0
-100
-200
-200
-100
0
100 Meters
200
Sigma = .097 usec
Sigma = .201 usec
Rho = .900
Max CTE = 155 Meters
Probability of 95 %
Max ATE = 22 Meters

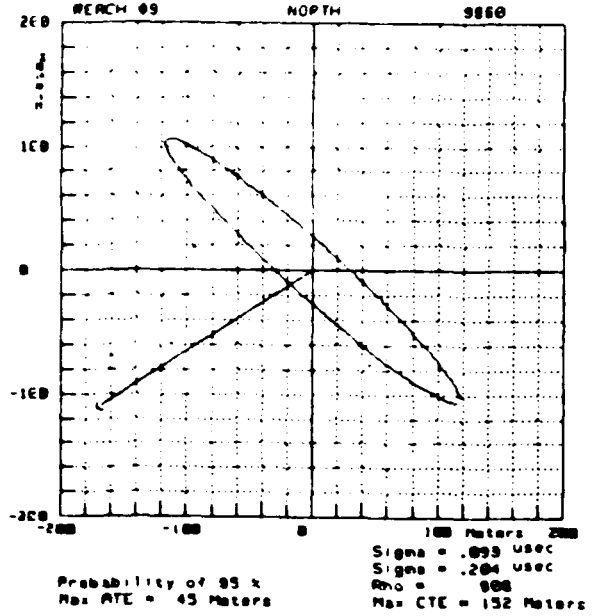

Probability of 95 %
Max ATE = 45 Meters

Sigma = .093 usec
Sigma = .204 usec
Rho = .900
Max CTE = 152 Meters

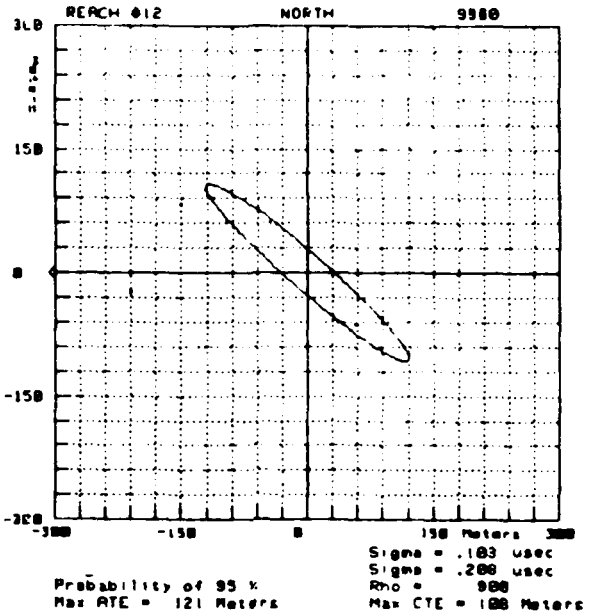

Probability of 95 %
Max ATE = 121 Meters

Sigma = .103 usec
Sigma = .208 usec
Rho = .900
Max CTE = 108 Meters

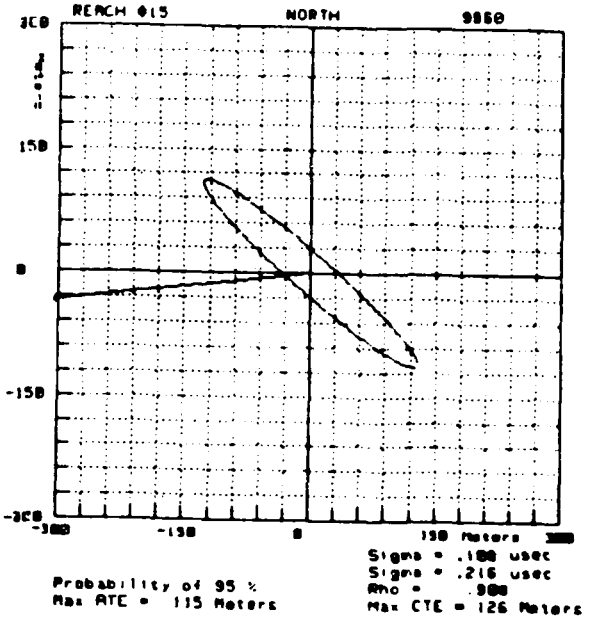

Probability of 95 %
Max ATE = 115 Meters

Sigma = .100 usec
Sigma = .216 usec
Rho = .900
Max CTE = 126 Meters

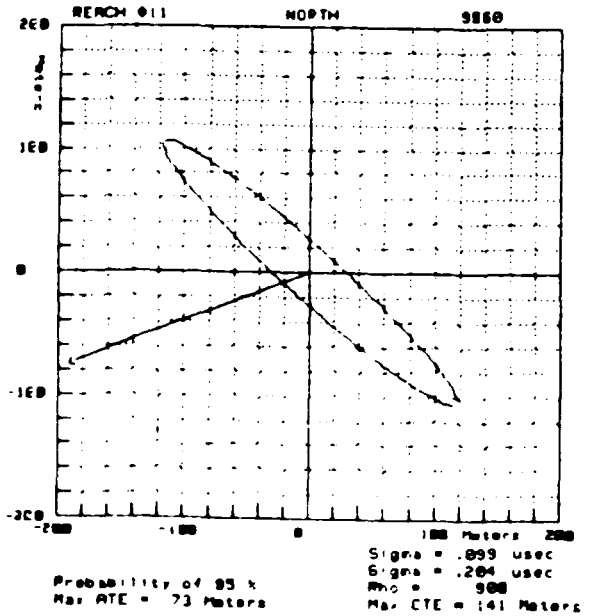

Probability of 95 %
Max ATE = 73 Meters

Sigma = .099 usec
Sigma = .204 usec
Rho = .900
Max CTE = 141 Meters

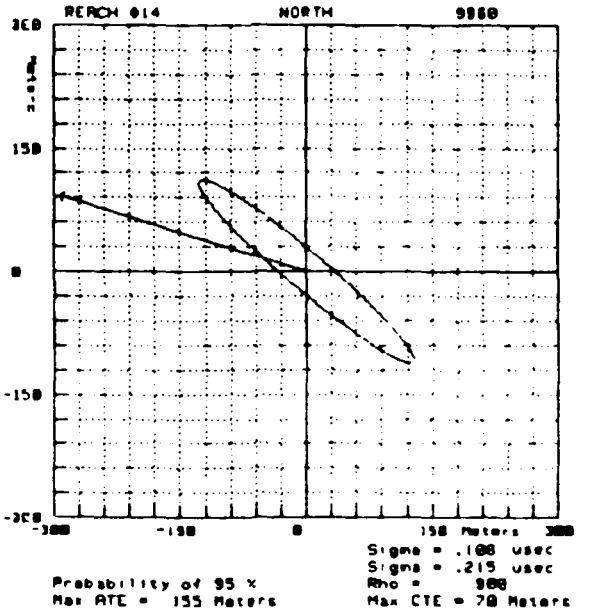

Probability of 95 %
Max ATE = 155 Meters

Sigma = .100 usec
Sigma = .215 usec
Rho = .900
Max CTE = 78 Meters

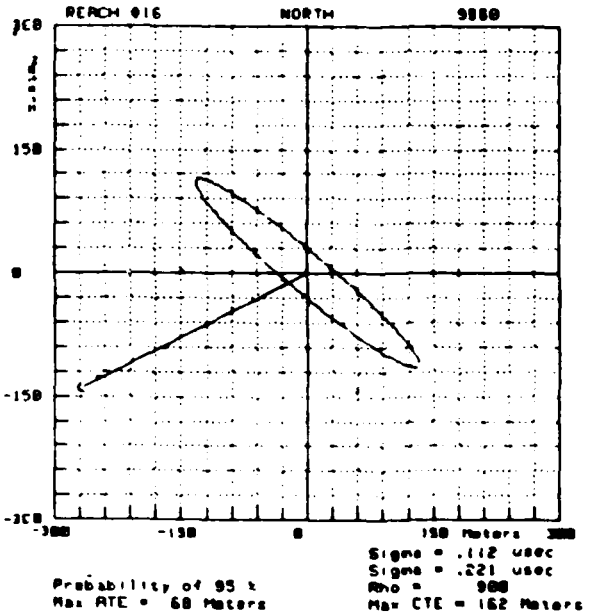

Probability of 95 %
Max ATE = 68 Meters

Sigma = .112 usec
Sigma = .221 usec
Rho = .900
Max CTE = 162 Meters

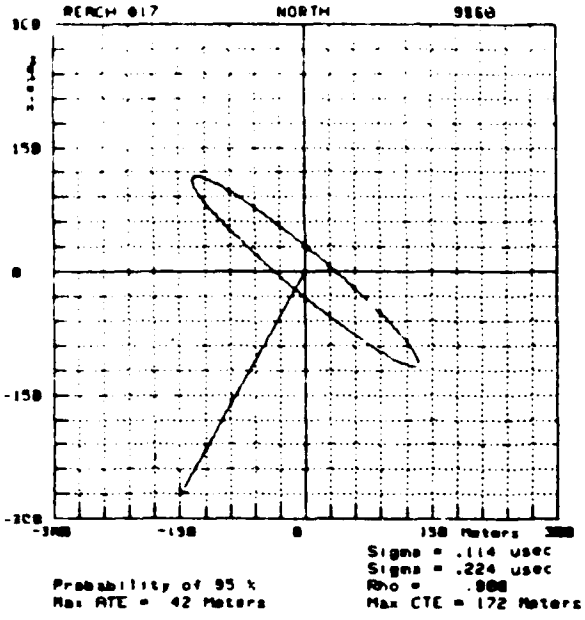
REACH 017
NORTH
9860
300
150
0
-150
-300
-300
-150
0
150 Meters
300
Sigma = .114 usec
Sigma = .224 usec
Rho = .900
Max CTE = 172 Meters
Probability of 95 %
Max ATE = 42 Meters

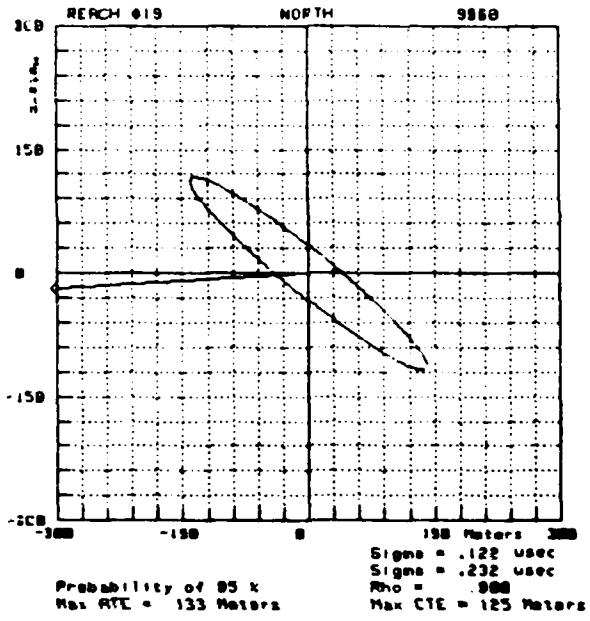
REACH 019
NORTH
9860
300
150
0
-150
-300
-300
-150
0
150 Meters
300
Sigma = .122 usec
Sigma = .232 usec
Rho = .900
Max CTE = 125 Meters
Probability of 95 %
Max ATE = 133 Meters

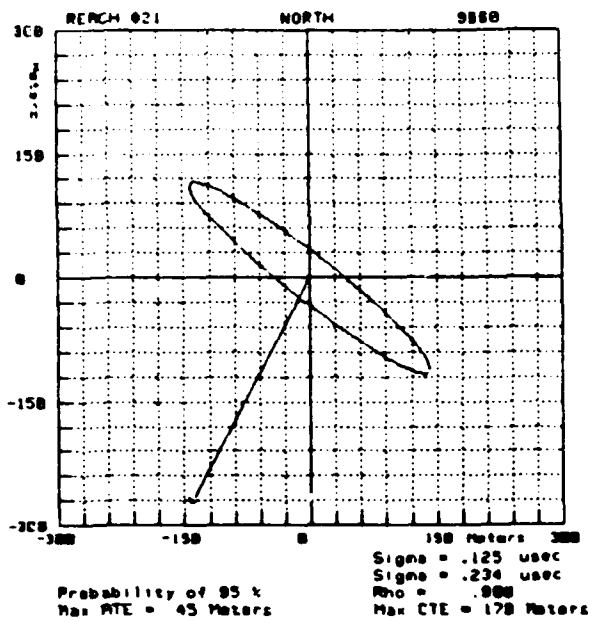
REACH 021
NORTH
9860
300
150
0
-150
-300
-300
-150
0
150 Meters
300
Sigma = .125 usec
Sigma = .234 usec
Rho = .900
Max CTE = 178 Meters
Probability of 95 %
Max ATE = 45 Meters

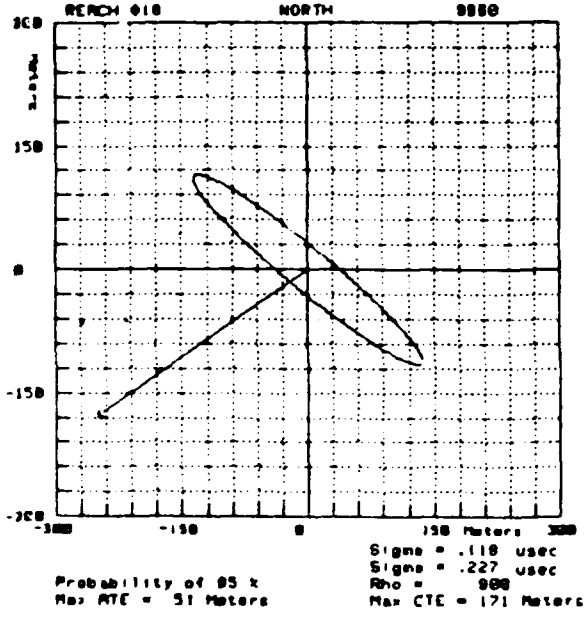
REACH 018
NORTH
9860
300
150
0
-150
-300
-300
-150
0
150 Meters
300
Sigma = .118 usec
Sigma = .227 usec
Rho = .900
Max CTE = 171 Meters
Probability of 95 %
Max ATE = 51 Meters

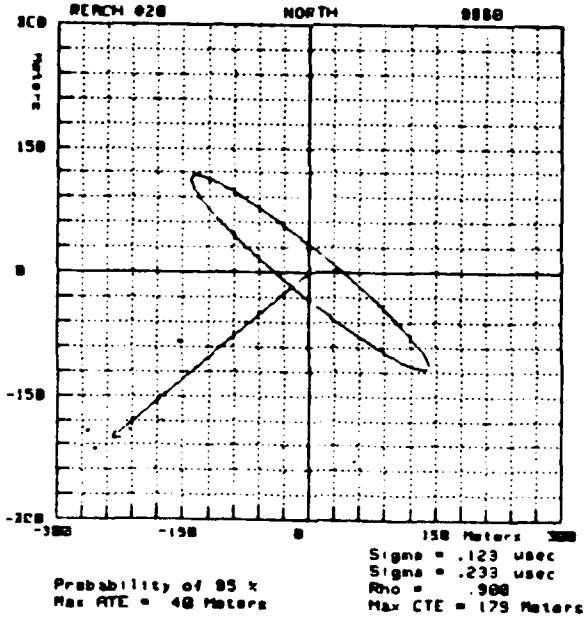
REACH 020
NORTH
9860
300
150
0
-150
-300
-300
-150
0
150 Meters
300
Sigma = .123 usec
Sigma = .233 usec
Rho = .900
Max CTE = 179 Meters
Probability of 95 %
Max ATE = 40 Meters

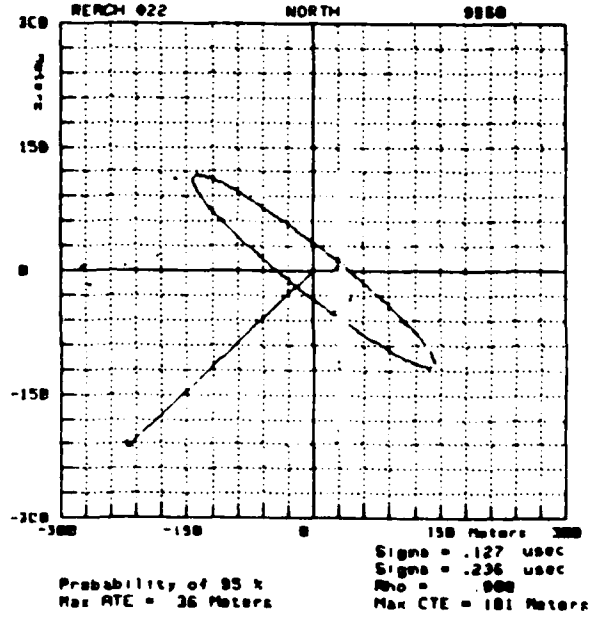
REACH 022
NORTH
9860
300
150
0
-150
-300
-300
-150
0
150 Meters
300
Sigma = .127 usec
Sigma = .236 usec
Rho = .900
Max CTE = 181 Meters
Probability of 95 %
Max ATE = 36 Meters

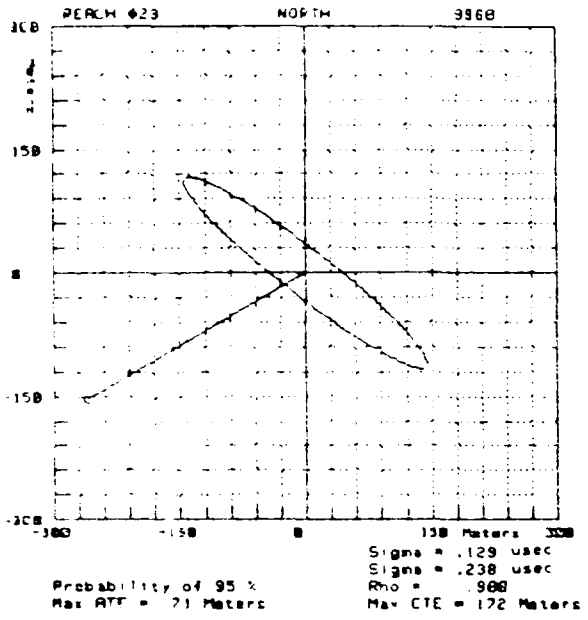

Sigma = .129 usec
Sigma = .238 usec
Rho = .900
Probability of 95 %
Max ATE = 71 Meters
Max CTE = 172 Meters

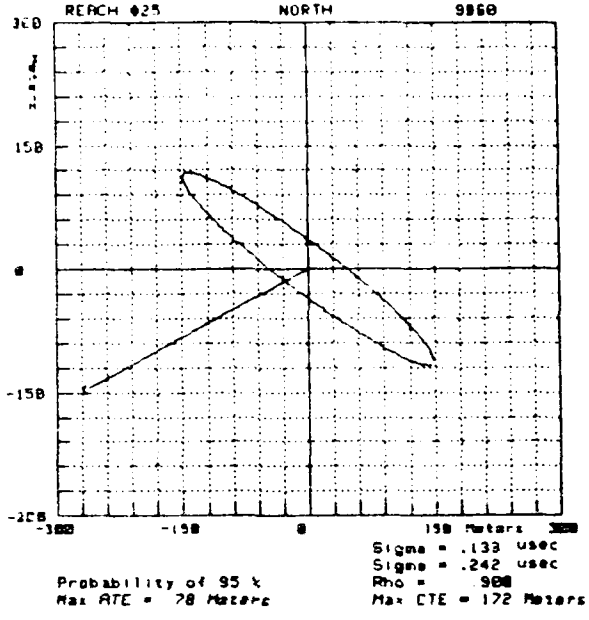

Sigma = .133 usec
Sigma = .242 usec
Rho = .900
Probability of 95 %
Max ATE = 78 Meters
Max CTE = 172 Meters

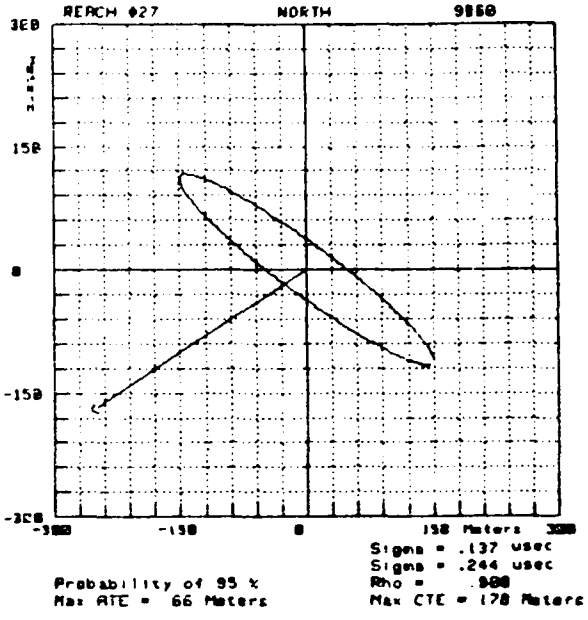

Sigma = .137 usec
Sigma = .244 usec
Rho = .900
Probability of 95 %
Max ATE = 66 Meters
Max CTE = 178 Meters

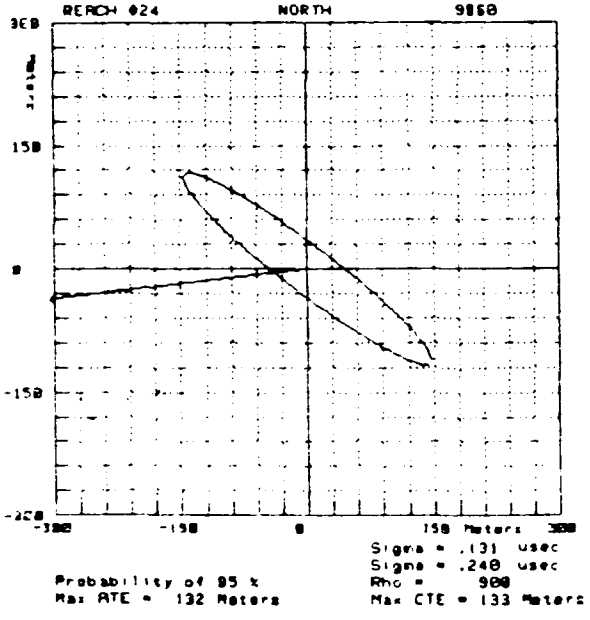

Sigma = .131 usec
Sigma = .240 usec
Rho = .900
Probability of 95 %
Max ATE = 132 Meters
Max CTE = 133 Meters

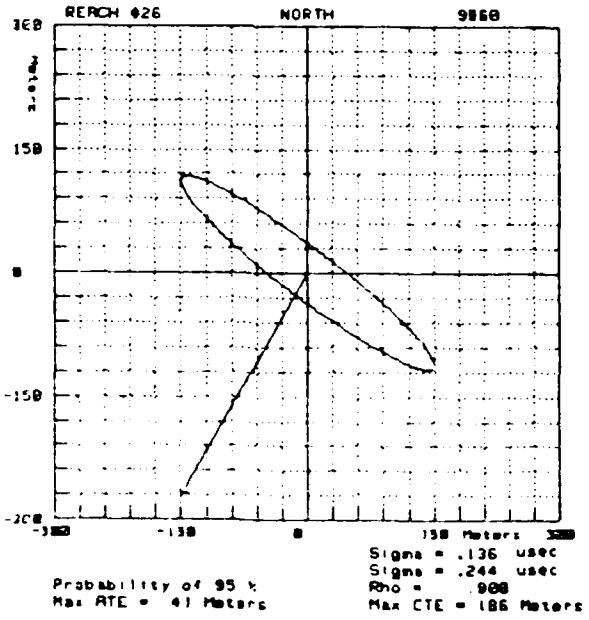

Sigma = .136 usec
Sigma = .244 usec
Rho = .900
Probability of 95 %
Max ATE = 41 Meters
Max CTE = 186 Meters

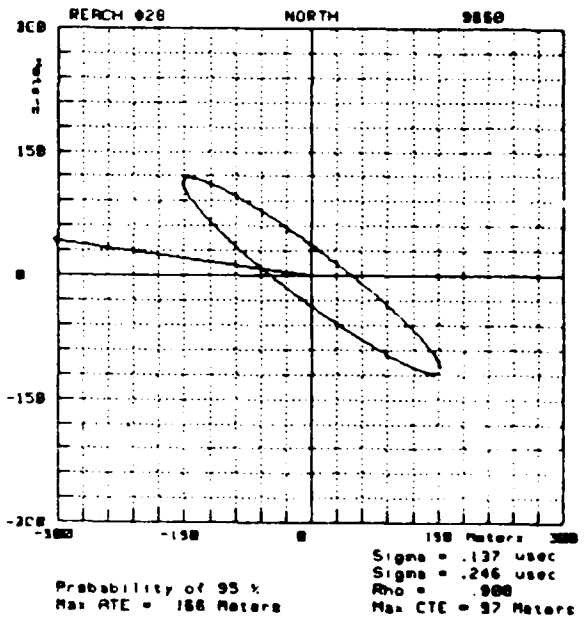

Sigma = .137 usec
Sigma = .246 usec
Rho = .900
Probability of 95 %
Max ATE = 168 Meters
Max CTE = 97 Meters

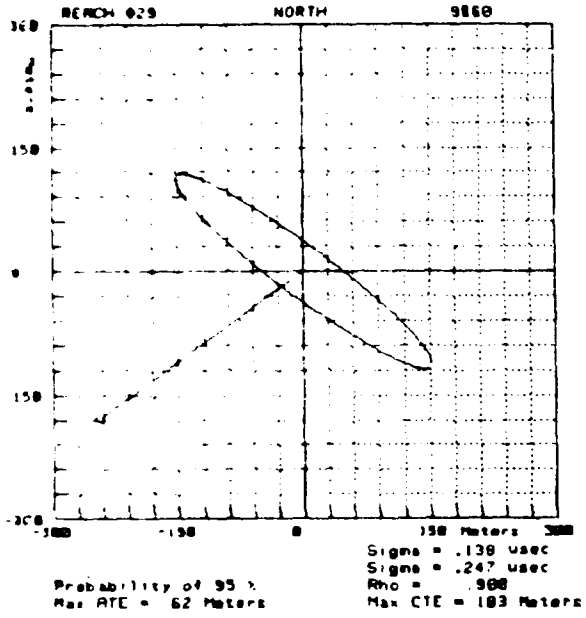
REACH 029
NORTH
9860
Meters
Probability of 95 %
Max ATE = 62 Meters
Sigma = .138 usec
Sigma = .247 usec
Rho = .900
Max CTE = 103 Meters

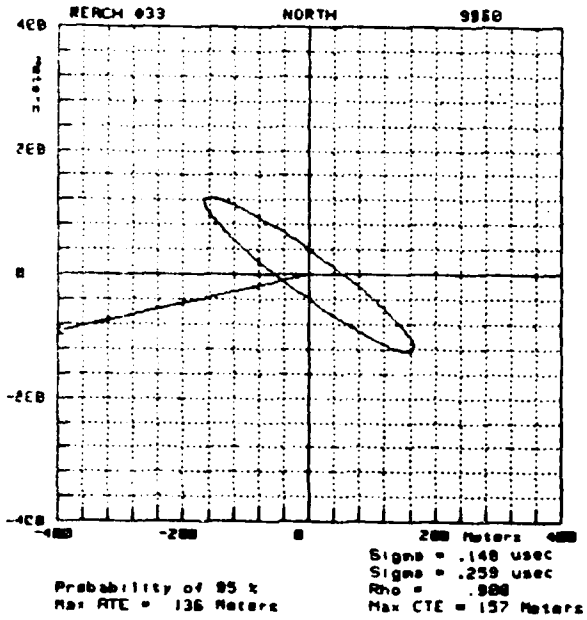
REACH 033
NORTH
9860
Meters
Probability of 95 %
Max ATE = 136 Meters
Sigma = .140 usec
Sigma = .259 usec
Rho = .900
Max CTE = 157 Meters

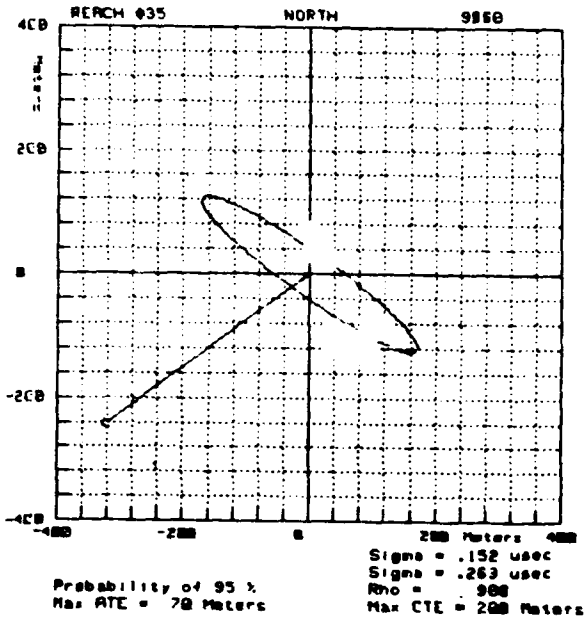
REACH 035
NORTH
9860
Meters
Probability of 95 %
Max ATE = 78 Meters
Sigma = .152 usec
Sigma = .263 usec
Rho = .900
Max CTE = 200 Meters

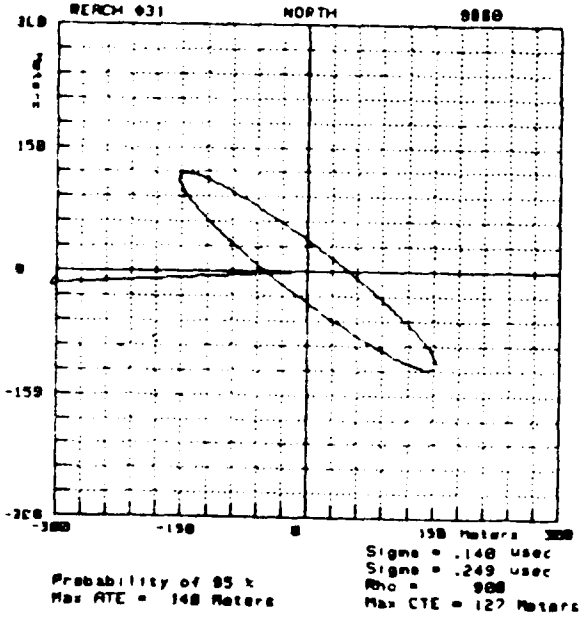
REACH 031
NORTH
9860
Meters
Probability of 95 %
Max ATE = 148 Meters
Sigma = .140 usec
Sigma = .249 usec
Rho = .900
Max CTE = 127 Meters

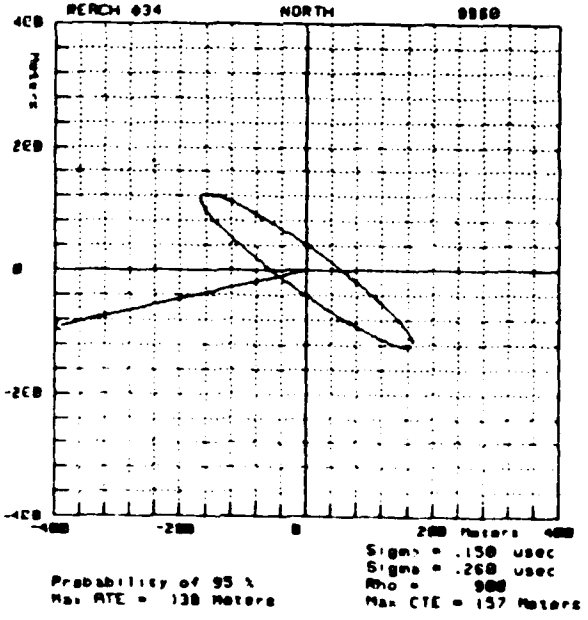
REACH 034
NORTH
9860
Meters
Probability of 95 %
Max ATE = 138 Meters
Sigma = .150 usec
Sigma = .268 usec
Rho = .900
Max CTE = 157 Meters

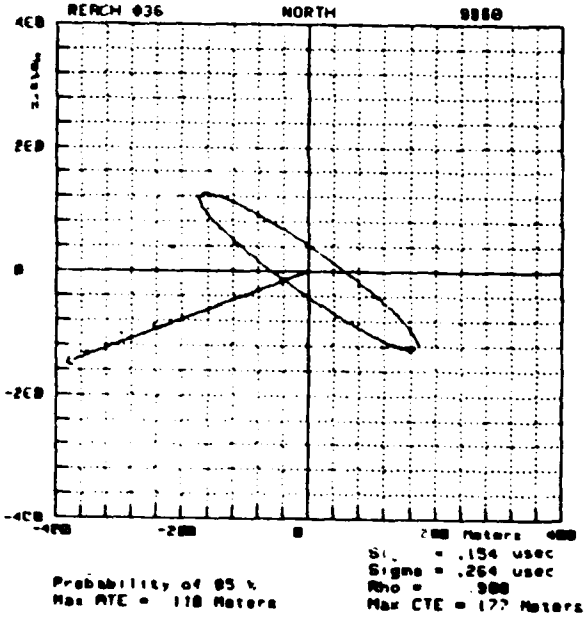
REACH 036
NORTH
9860
Meters
Probability of 95 %
Max ATE = 118 Meters
Sigma = .154 usec
Sigma = .264 usec
Rho = .900
Max CTE = 177 Meters

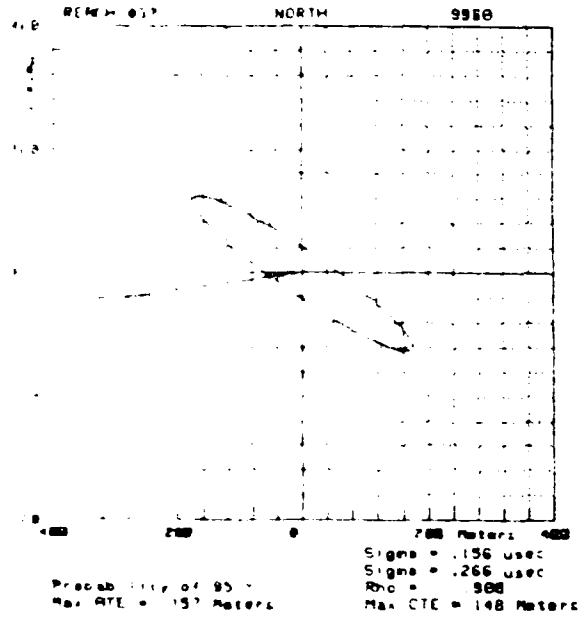
NORTH
9950
Sigma = .156 usec
Sigma = .266 usec
Rho = .900
Max CTE = 148 Meters

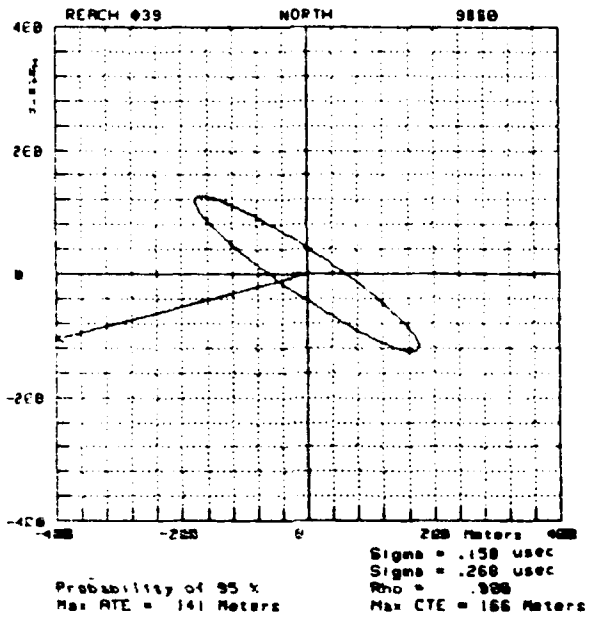
REACH 039
NORTH
9950
Probability of 95 %
Max ATE = 141 Meters
Sigma = .158 usec
Sigma = .268 usec
Rho = .900
Max CTE = 166 Meters

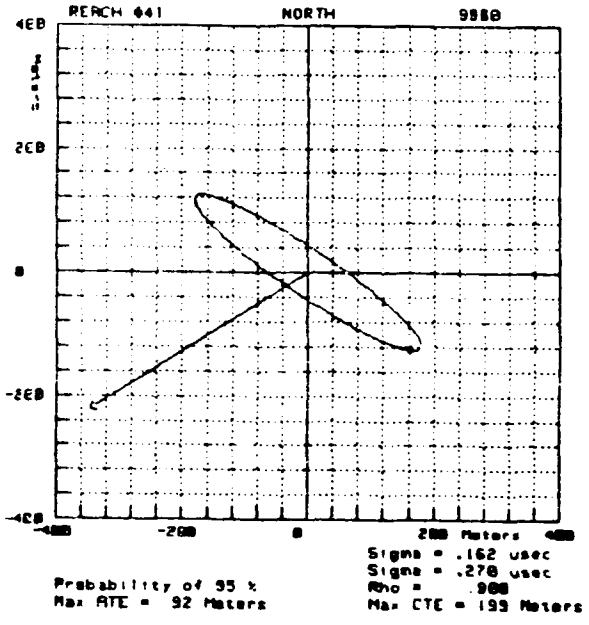
REACH 041
NORTH
9950
Probability of 95 %
Max ATE = 92 Meters
Sigma = .162 usec
Sigma = .270 usec
Rho = .900
Max CTE = 195 Meters

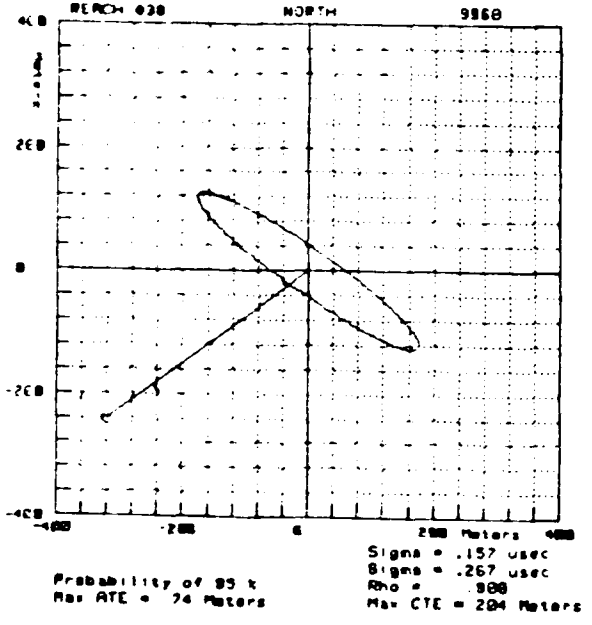
REACH 038
NORTH
9950
Probability of 95 %
Max ATE = 74 Meters
Sigma = .157 usec
Sigma = .267 usec
Rho = .900
Max CTE = 204 Meters

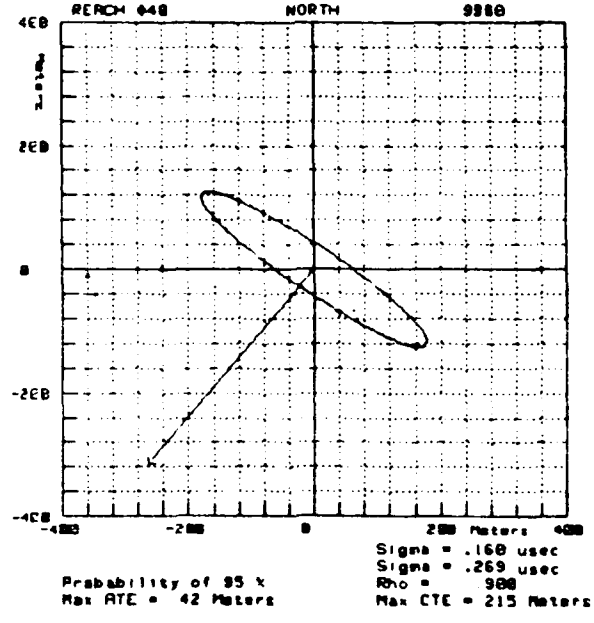
REACH 040
NORTH
9950
Probability of 95 %
Max ATE = 42 Meters
Sigma = .160 usec
Sigma = .269 usec
Rho = .900
Max CTE = 215 Meters

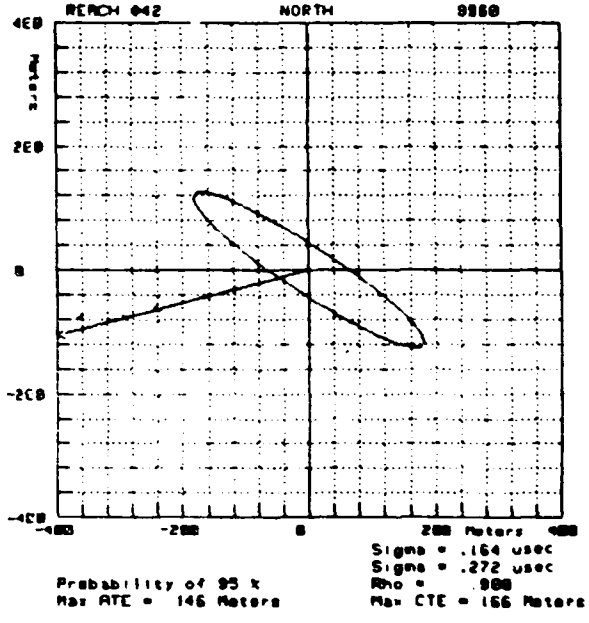
REACH 042
NORTH
9950
Probability of 95 %
Max ATE = 146 Meters
Sigma = .164 usec
Sigma = .272 usec
Rho = .900
Max CTE = 166 Meters

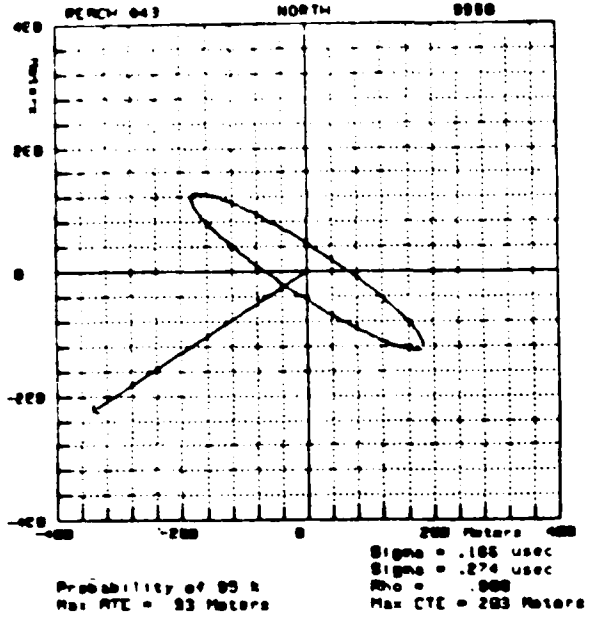
PERCH 043
NORTH
9880
Meters
400
200
0
-200
-400
-400
-200
0
200
400
Meters
Sigma = .185 usec
Sigma = .274 usec
Rho = .900
Probability of 95 %
Max ATE = 93 Meters
Max CTE = 283 Meters

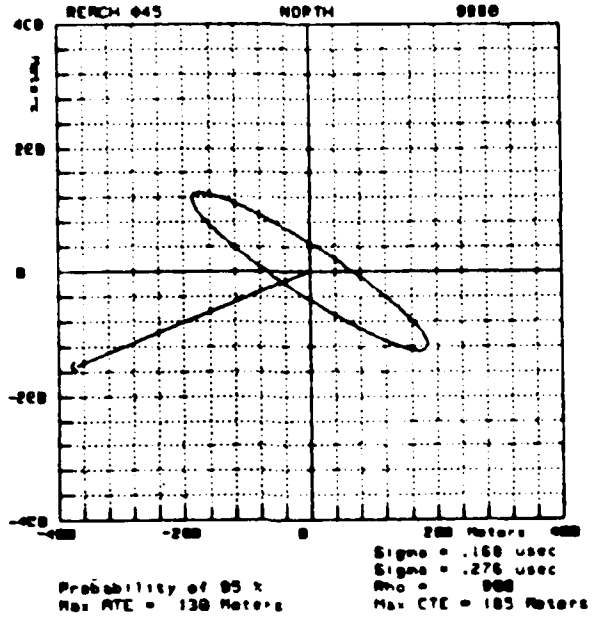
PERCH 045
NORTH
9880
Meters
400
200
0
-200
-400
-400
-200
0
200
400
Meters
Sigma = .168 usec
Sigma = .276 usec
Rho = .900
Probability of 95 %
Max ATE = 130 Meters
Max CTE = 185 Meters

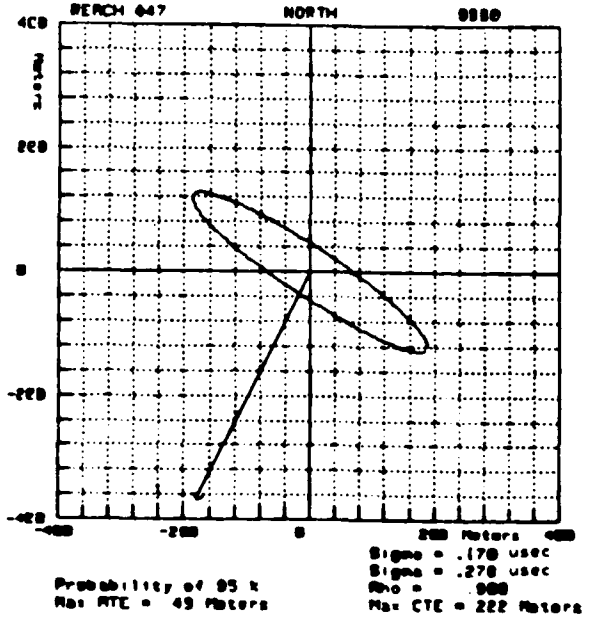
PERCH 047
NORTH
9880
Meters
400
200
0
-200
-400
-400
-200
0
200
400
Meters
Sigma = .170 usec
Sigma = .278 usec
Rho = .900
Probability of 95 %
Max ATE = 49 Meters
Max CTE = 222 Meters

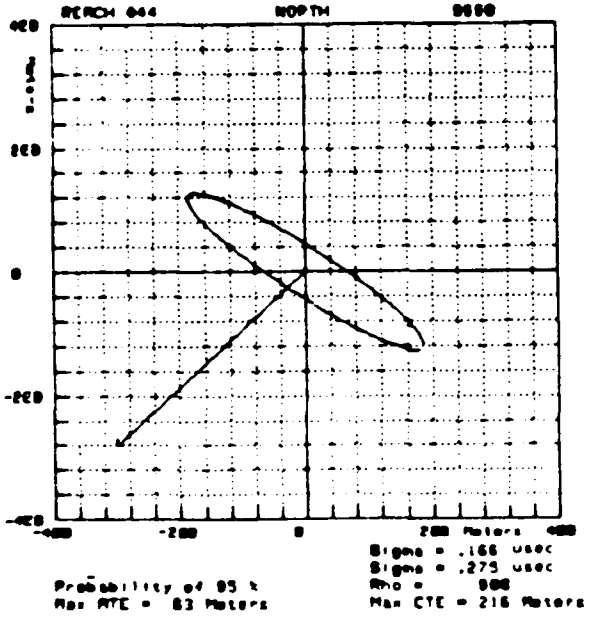
PERCH 044
NORTH
9880
Meters
400
200
0
-200
-400
-400
-200
0
200
400
Meters
Sigma = .166 usec
Sigma = .275 usec
Rho = .900
Probability of 95 %
Max ATE = 83 Meters
Max CTE = 216 Meters

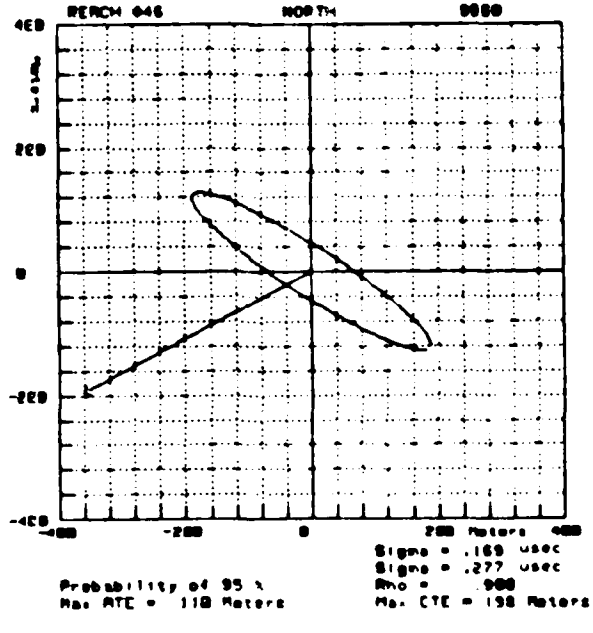
PERCH 046
NORTH
9880
Meters
400
200
0
-200
-400
-400
-200
0
200
400
Meters
Sigma = .169 usec
Sigma = .277 usec
Rho = .900
Probability of 95 %
Max ATE = 110 Meters
Max CTE = 198 Meters

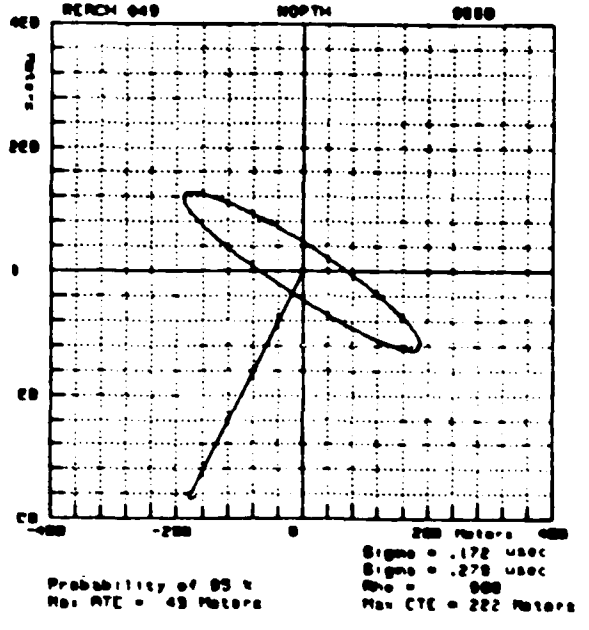
PERCH 049
NORTH
9880
Meters
400
200
0
-200
-400
-400
-200
0
200
400
Meters
Sigma = .172 usec
Sigma = .278 usec
Rho = .900
Probability of 95 %
Max ATE = 49 Meters
Max CTE = 222 Meters

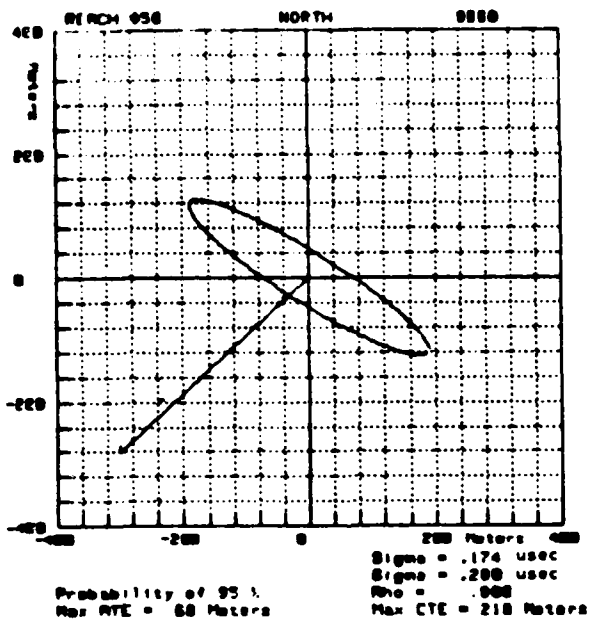

Sigma = .174 usec
Sigma = .200 usec
Rho = .900
Probability of 95 %
Max ATE = 68 Meters
Max CTE = 218 Meters

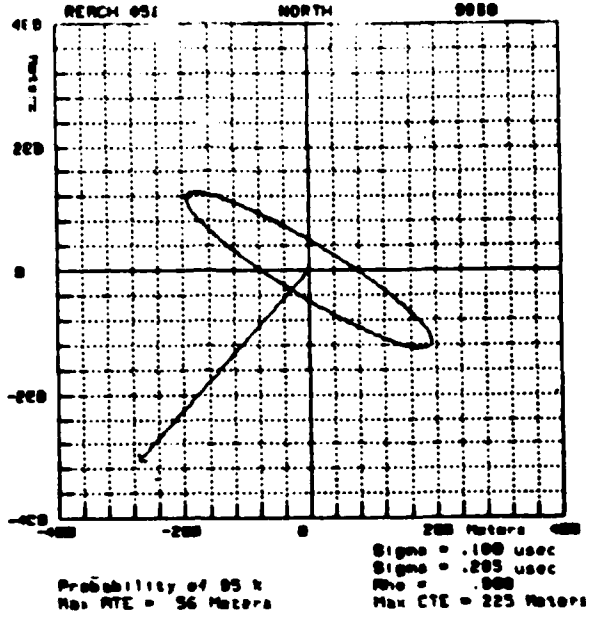

Sigma = .180 usec
Sigma = .205 usec
Rho = .900
Probability of 95 %
Max ATE = 56 Meters
Max CTE = 225 Meters

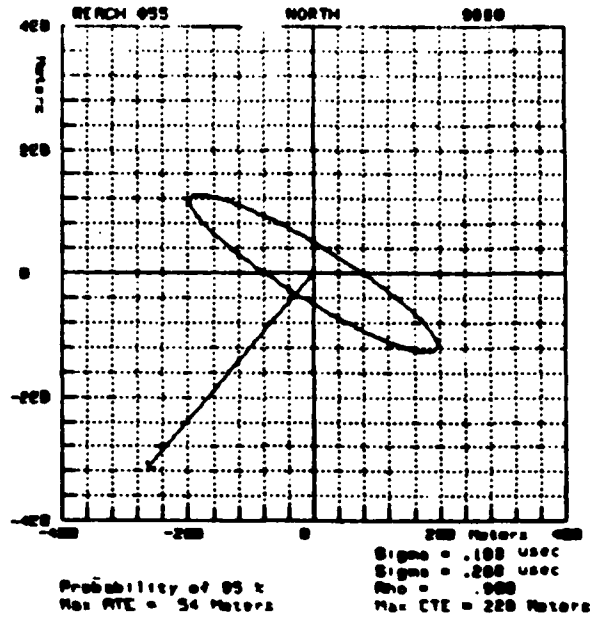

Sigma = .188 usec
Sigma = .208 usec
Rho = .900
Probability of 95 %
Max ATE = 54 Meters
Max CTE = 228 Meters

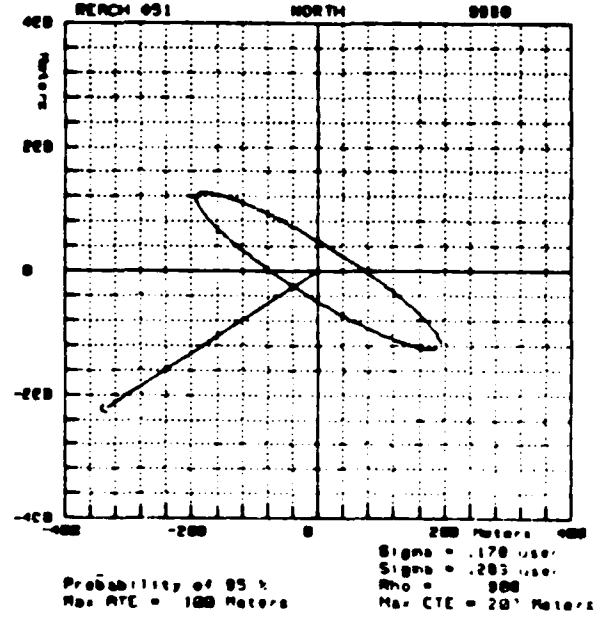

Sigma = .178 usec
Sigma = .203 usec
Rho = .900
Probability of 95 %
Max ATE = 100 Meters
Max CTE = 207 Meters

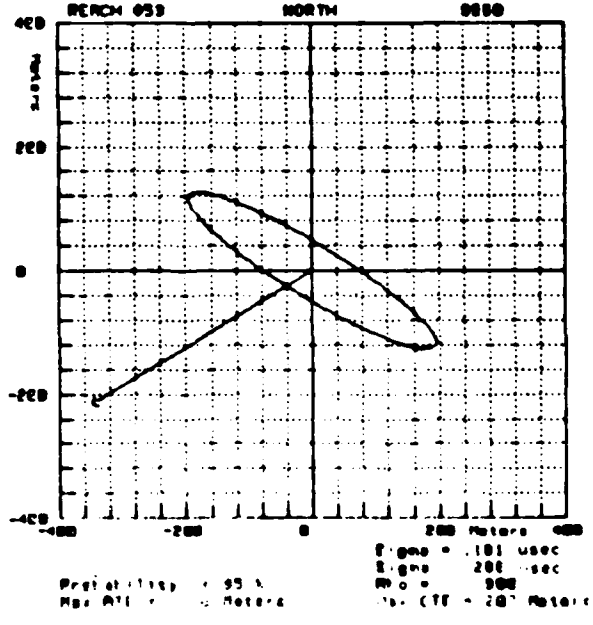

Sigma = .181 usec
Sigma = .206 usec
Rho = .900
Probability of 95 %
Max ATE = 70 Meters
Max CTE = 207 Meters

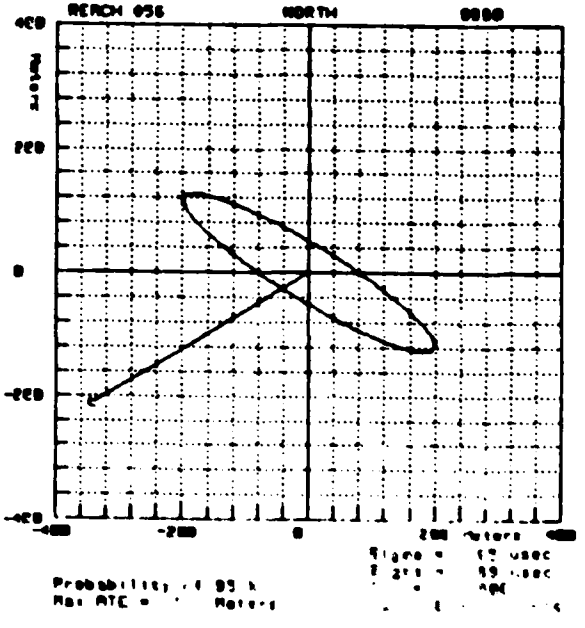

Sigma = .177 usec
Sigma = .199 usec
Rho = .900
Probability of 95 %
Max ATE = 68 Meters
Max CTE = 218 Meters

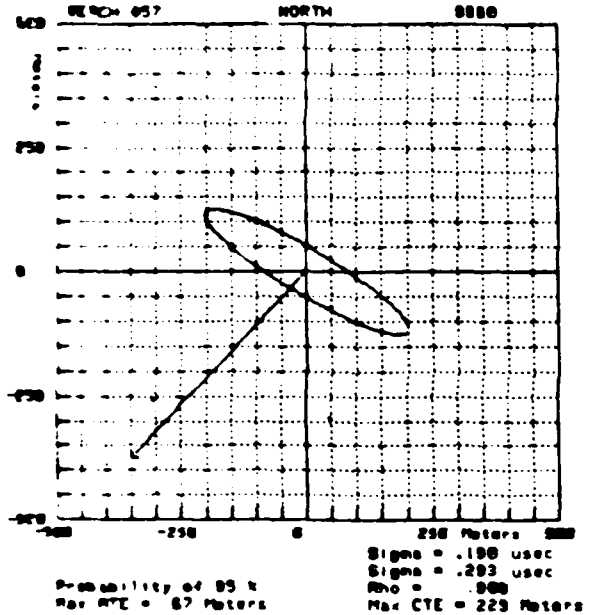

Probability of 95 %
Max ATE = 87 Meters

Sigma = .190 usec
Sigma = .293 usec
Rho = .900
Max CTE = 229 Meters

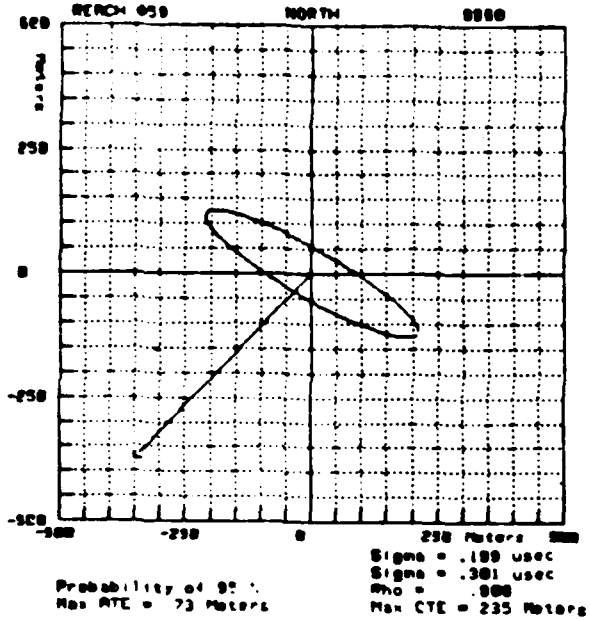

Probability of 95 %
Max ATE = 73 Meters

Sigma = .189 usec
Sigma = .301 usec
Rho = .900
Max CTE = 235 Meters

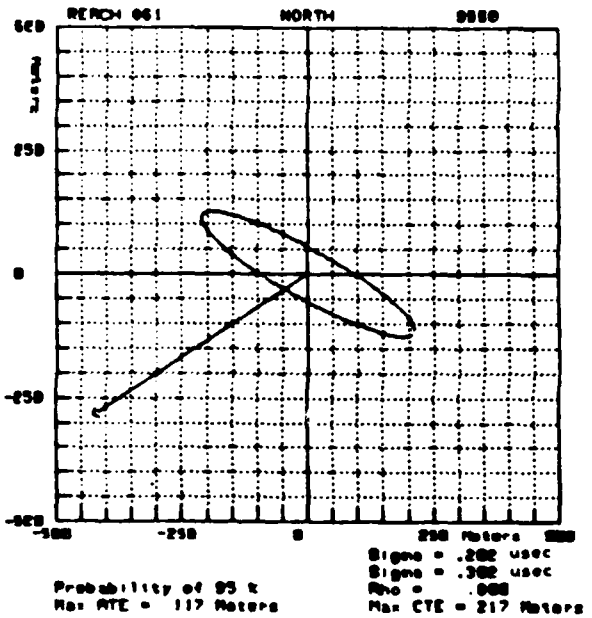

Probability of 95 %
Max ATE = 117 Meters

Sigma = .202 usec
Sigma = .302 usec
Rho = .900
Max CTE = 217 Meters

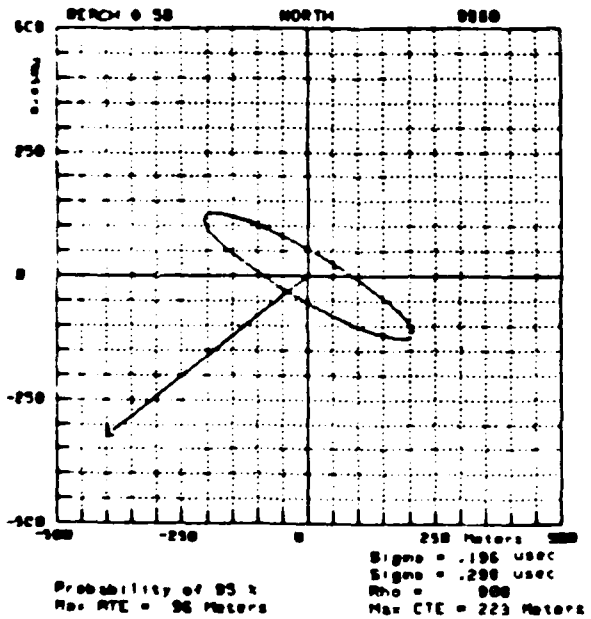

Probability of 95 %
Max ATE = 96 Meters

Sigma = .196 usec
Sigma = .298 usec
Rho = .900
Max CTE = 223 Meters

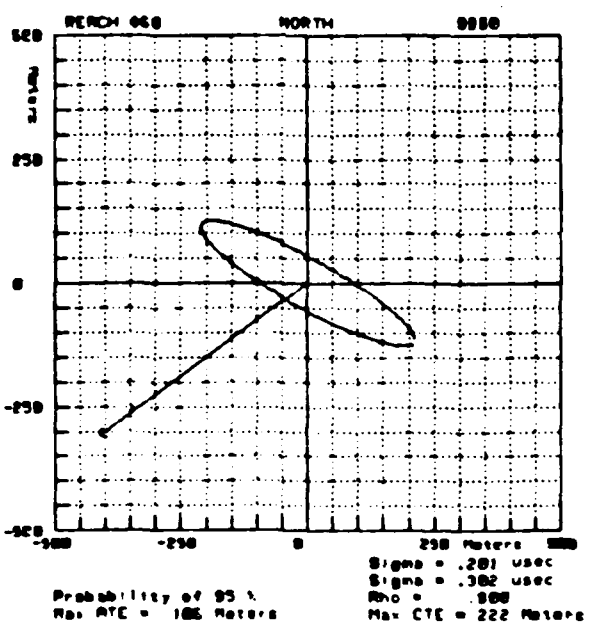

Probability of 95 %
Max ATE = 105 Meters

Sigma = .201 usec
Sigma = .302 usec
Rho = .900
Max CTE = 222 Meters

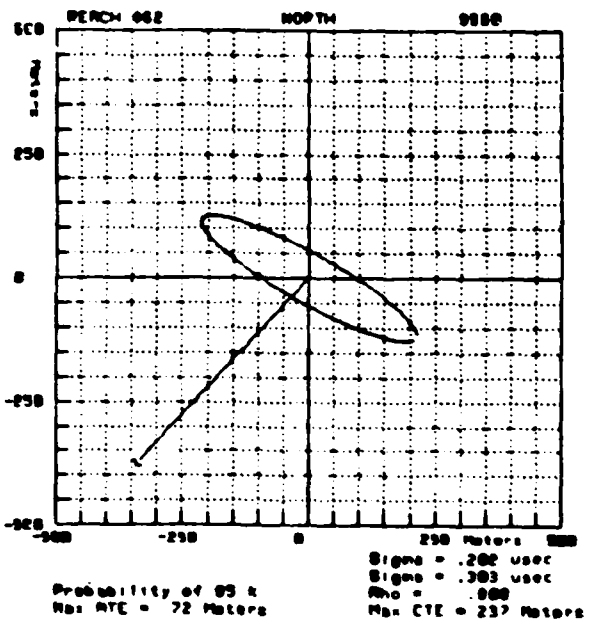

Probability of 95 %
Max ATE = 72 Meters

Sigma = .202 usec
Sigma = .303 usec
Rho = .900
Max CTE = 237 Meters

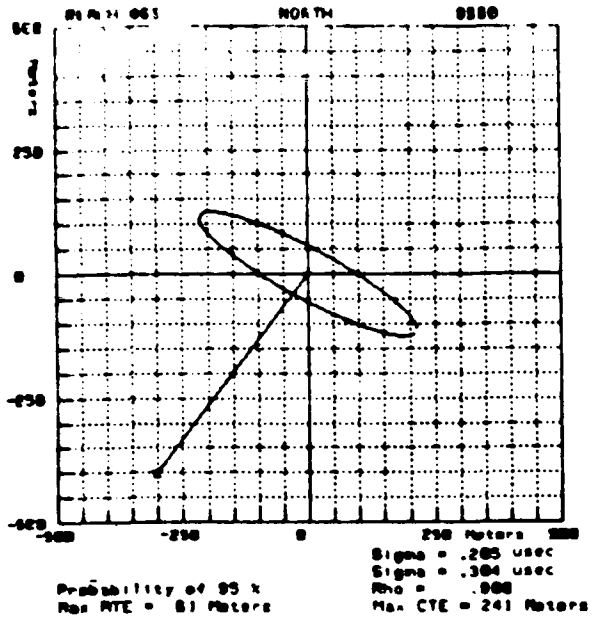
NORTH
Meters
250
0
-250
250 Meters
Sigma = .205 usec
Sigma = .304 usec
Rho = .900
Probability of 95 %
Max ATE = 81 Meters
Max CTE = 241 Meters

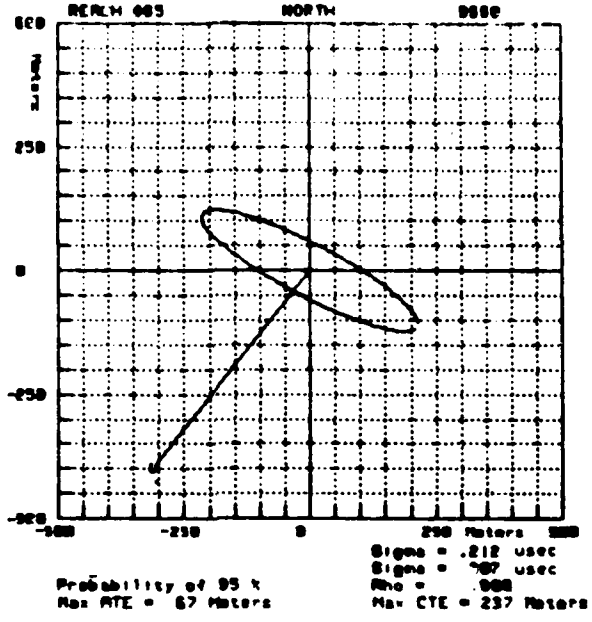
RERCH 065
NORTH
Meters
250
0
-250
250 Meters
Sigma = .212 usec
Sigma = .307 usec
Rho = .900
Probability of 95 %
Max ATE = 87 Meters
Max CTE = 237 Meters

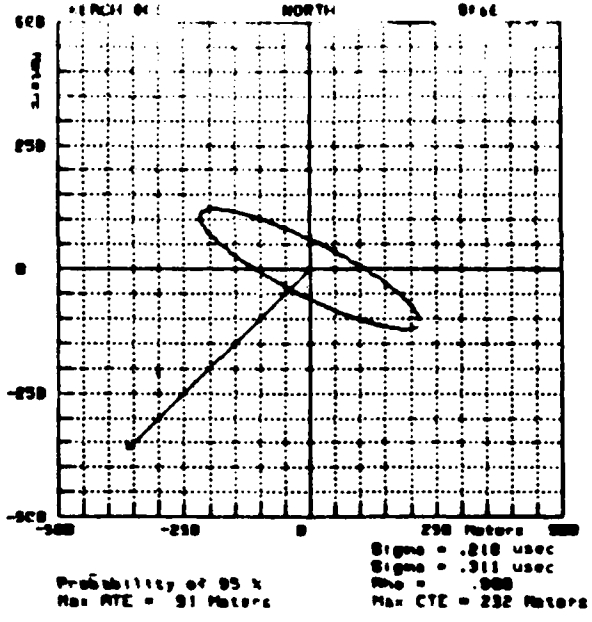
NORTH
Meters
250
0
-250
250 Meters
Sigma = .218 usec
Sigma = .311 usec
Rho = .900
Probability of 95 %
Max ATE = 91 Meters
Max CTE = 232 Meters

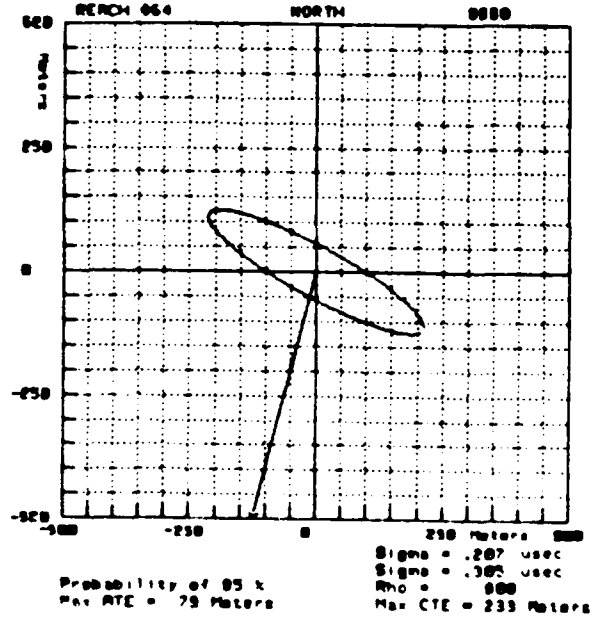
RERCH 064
NORTH
Meters
250
0
-250
250 Meters
Sigma = .207 usec
Sigma = .305 usec
Rho = .900
Probability of 95 %
Max ATE = 79 Meters
Max CTE = 233 Meters

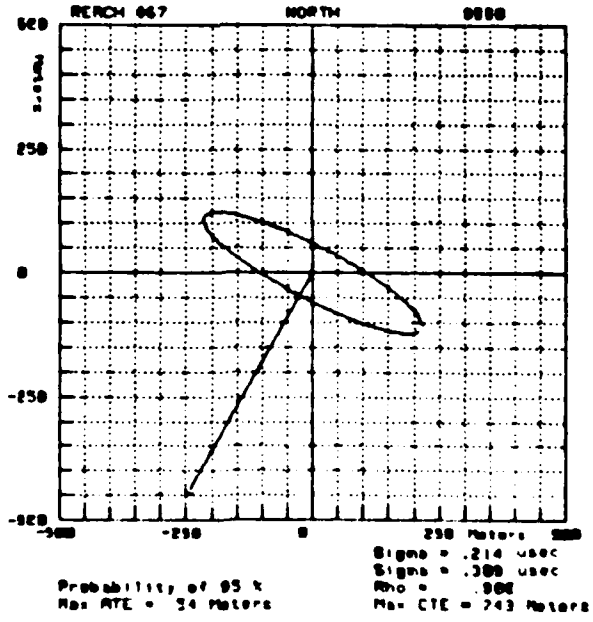
RERCH 067
NORTH
Meters
250
0
-250
250 Meters
Sigma = .214 usec
Sigma = .308 usec
Rho = .900
Probability of 95 %
Max ATE = 84 Meters
Max CTE = 243 Meters

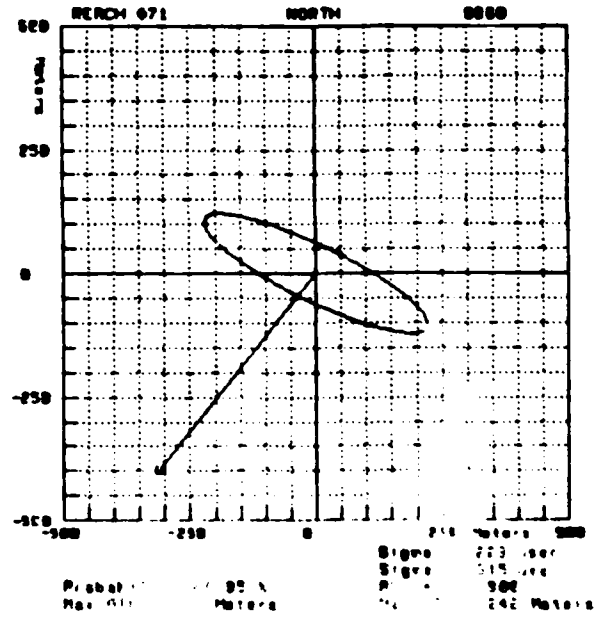
NORTH
Meters
250
0
-250
Rho = .900

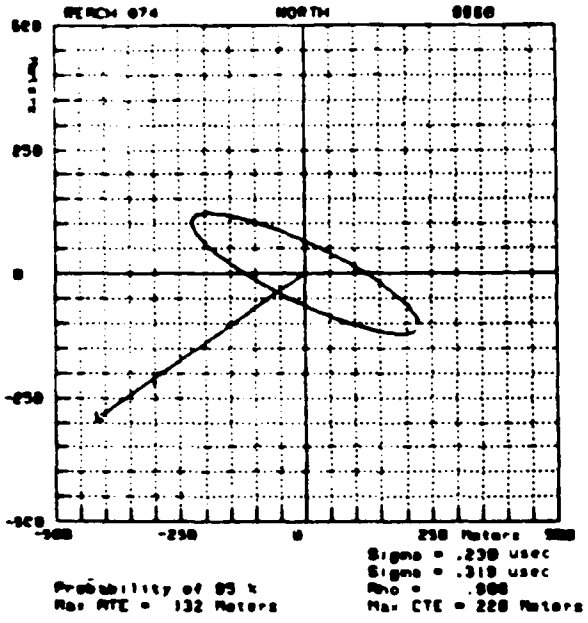
REACH 074
NORTH
9850
250
0
-250
-500
-250
0
250 Meters
Sigma = .230 usec
Sigma = .319 usec
Rho = .988
Probability of 95 %
Max ATE = 132 Meters
Max CTE = 220 Meters

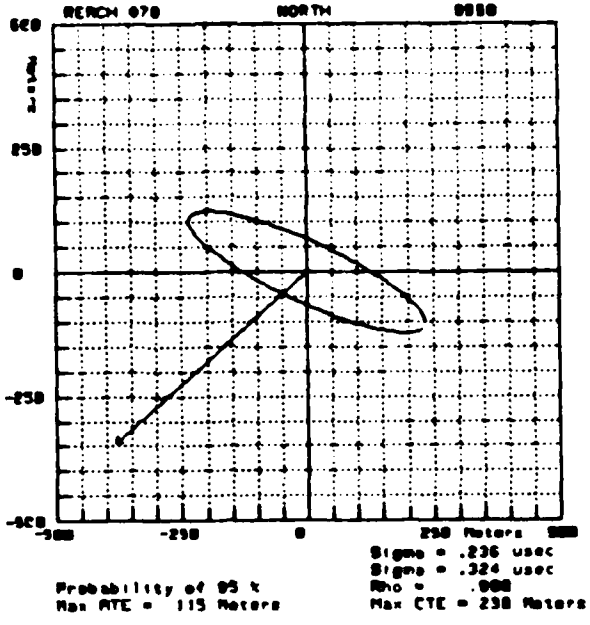
REACH 078
NORTH
9850
250
0
-250
-500
-250
0
250 Meters
Sigma = .236 usec
Sigma = .324 usec
Rho = .988
Probability of 95 %
Max ATE = 115 Meters
Max CTE = 238 Meters

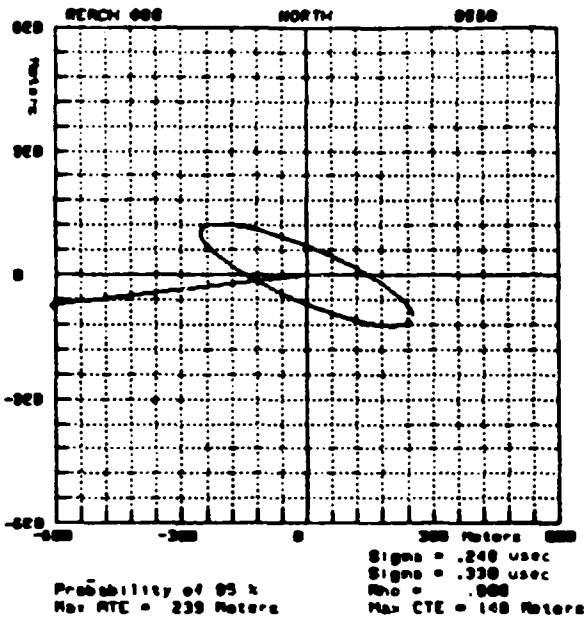
REACH 080
NORTH
9850
250
0
-250
-500
-250
0
250 Meters
Sigma = .240 usec
Sigma = .330 usec
Rho = .988
Probability of 95 %
Max ATE = 239 Meters
Max CTE = 148 Meters

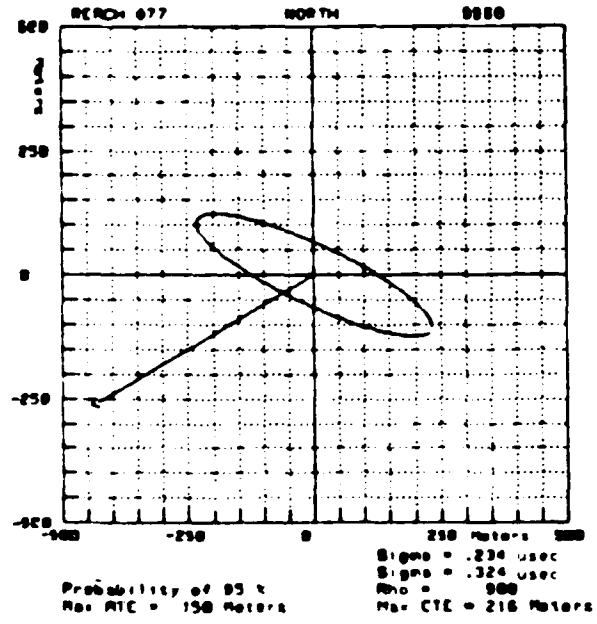
REACH 077
NORTH
9850
250
0
-250
-500
-250
0
250 Meters
Sigma = .234 usec
Sigma = .324 usec
Rho = .988
Probability of 95 %
Max ATE = 150 Meters
Max CTE = 216 Meters

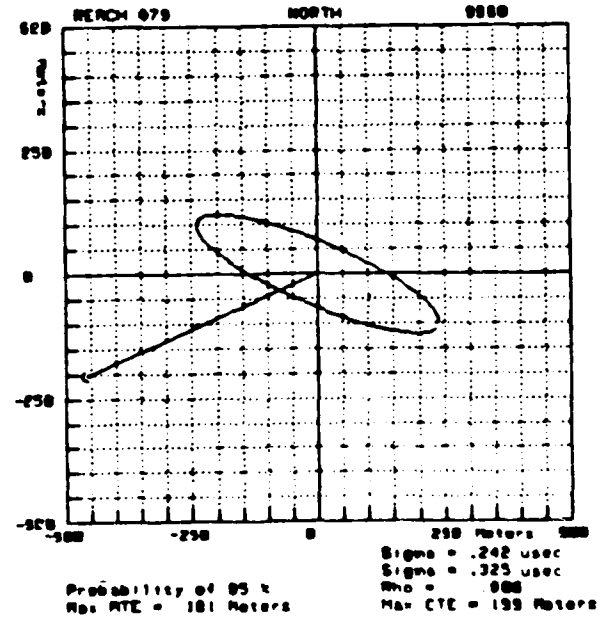
REACH 079
NORTH
9850
250
0
-250
-500
-250
0
250 Meters
Sigma = .242 usec
Sigma = .325 usec
Rho = .988
Probability of 95 %
Max ATE = 181 Meters
Max CTE = 199 Meters

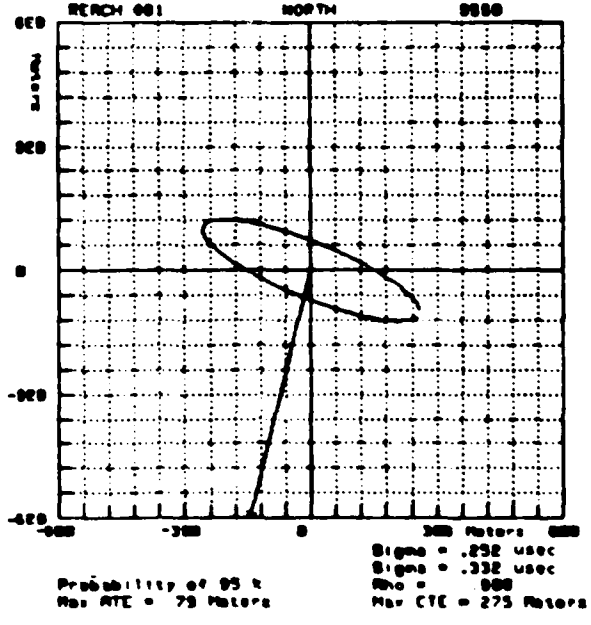
REACH 081
NORTH
9850
250
0
-250
-500
-250
0
250 Meters
Sigma = .252 usec
Sigma = .332 usec
Rho = .988
Probability of 95 %
Max ATE = 79 Meters
Max CTE = 275 Meters

DIFFERENTIAL LORAN-C - RELATIVE TO MASSENA

PREDICTED ERROR ELLIPSE PLOTS

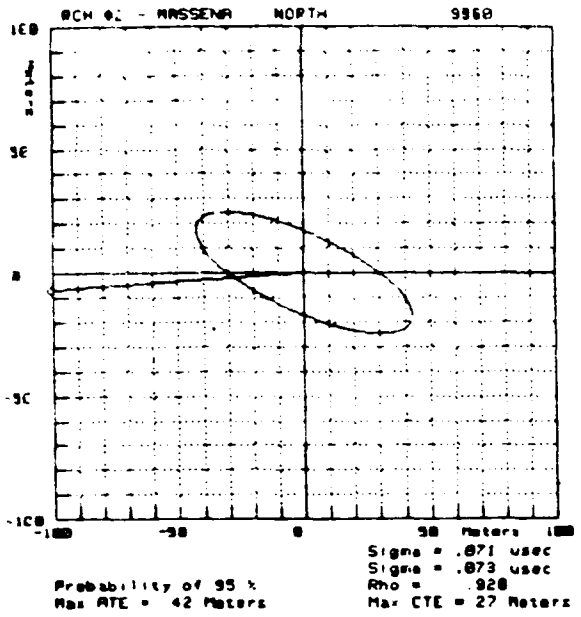
RCH 02 - MASSENA NORTH 9860
100
50
0
-50
-100
-100
-50
0
50
100
Meters
Sigma = .071 usec
Sigma = .073 usec
Rho = .928
Probability of 95 %
Max ATE = 42 Meters
Max CTE = 27 Meters

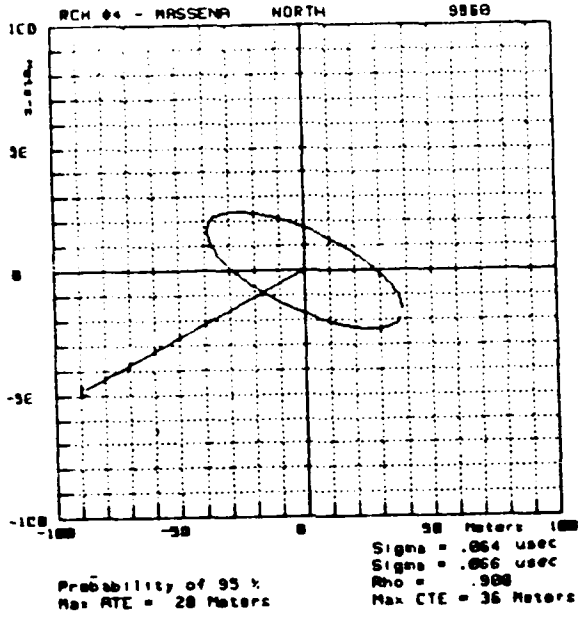
RCH 04 - MASSENA NORTH 9860
100
50
0
-50
-100
-100
-50
0
50
100
Meters
Sigma = .064 usec
Sigma = .066 usec
Rho = .908
Probability of 95 %
Max ATE = 28 Meters
Max CTE = 36 Meters

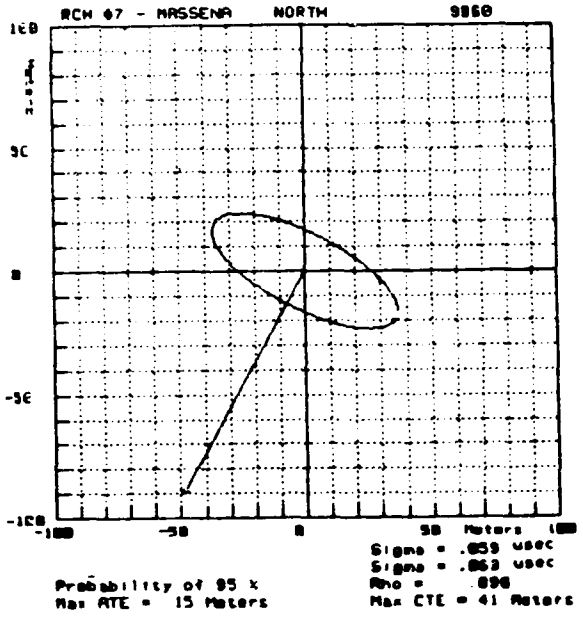
RCH 07 - MASSENA NORTH 9860
100
50
0
-50
-100
-100
-50
0
50
100
Meters
Sigma = .059 usec
Sigma = .063 usec
Rho = .896
Probability of 95 %
Max ATE = 15 Meters
Max CTE = 41 Meters

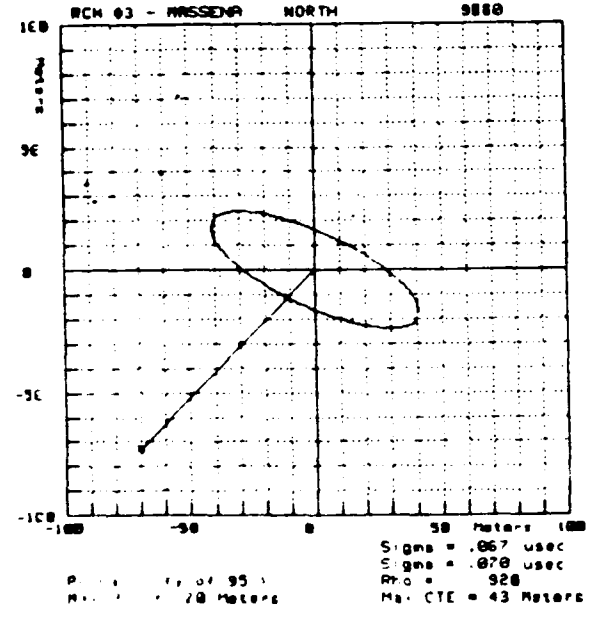
RCH 03 - MASSENA NORTH 9860
100
50
0
-50
-100
-100
-50
0
50
100
Meters
Sigma = .067 usec
Sigma = .070 usec
Rho = .928
Max CTE = 43 Meters

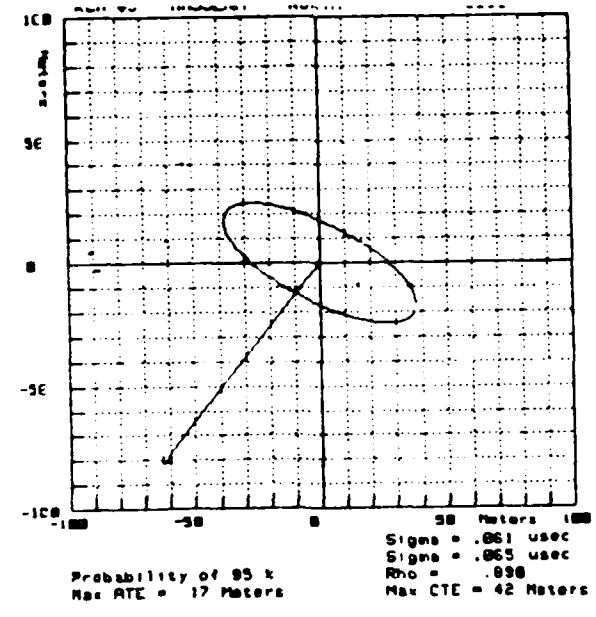
100
50
0
-50
-100
-100
-50
0
50
100
Meters
Sigma = .061 usec
Sigma = .065 usec
Rho = .898
Probability of 95 %
Max ATE = 17 Meters
Max CTE = 42 Meters

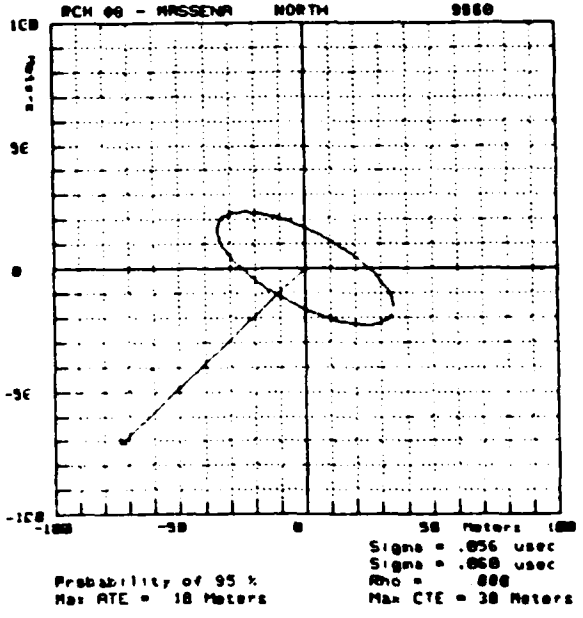
RCH 08 - MASSENA NORTH 9860
100
50
0
-50
-100
-100
-50
0
50
100
Meters
Sigma = .056 usec
Sigma = .060 usec
Rho = .886
Probability of 95 %
Max ATE = 18 Meters
Max CTE = 38 Meters

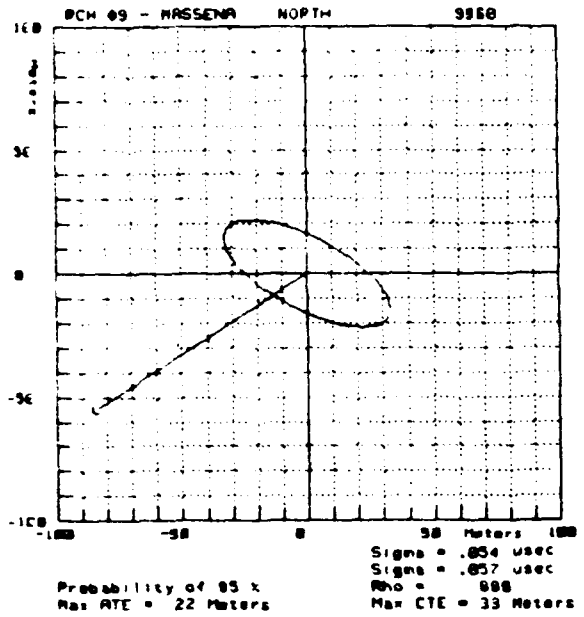
RCH 09 - MASSENA NORTH 9960
100
50
0
-50
-100
-1000
-50
0
50
Meters
1000
Probability of 95 %
Max ATE = 22 Meters
Sigma = .054 usec
Sigma = .057 usec
Rho = .888
Max CTE = 33 Meters

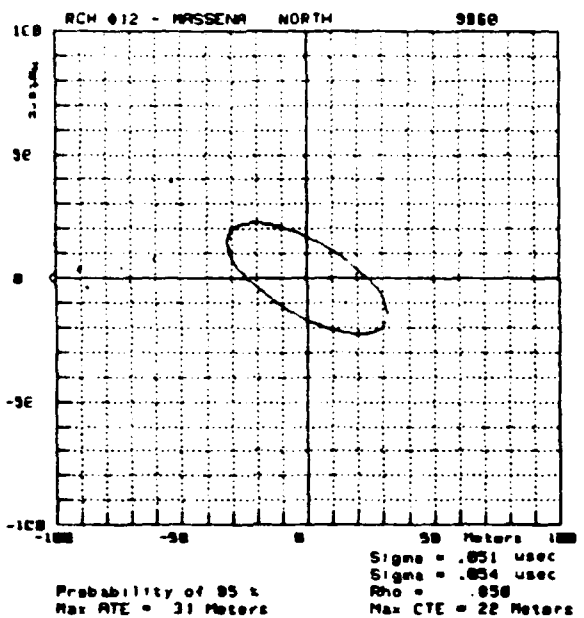
RCH 12 - MASSENA NORTH 9960
100
50
0
-50
-100
-1000
-50
0
50
Meters
1000
Probability of 95 %
Max ATE = 31 Meters
Sigma = .051 usec
Sigma = .054 usec
Rho = .858
Max CTE = 22 Meters

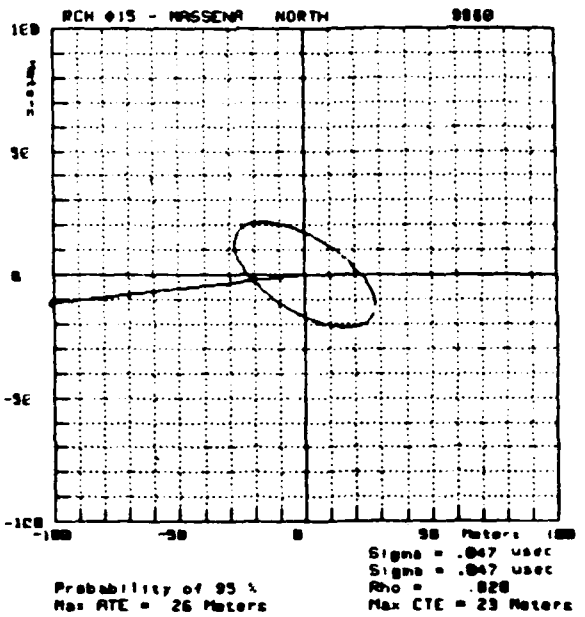
RCH 15 - MASSENA NORTH 9960
100
50
0
-50
-100
-1000
-50
0
50
Meters
1000
Probability of 95 %
Max ATE = 26 Meters
Sigma = .047 usec
Sigma = .047 usec
Rho = .828
Max CTE = 23 Meters

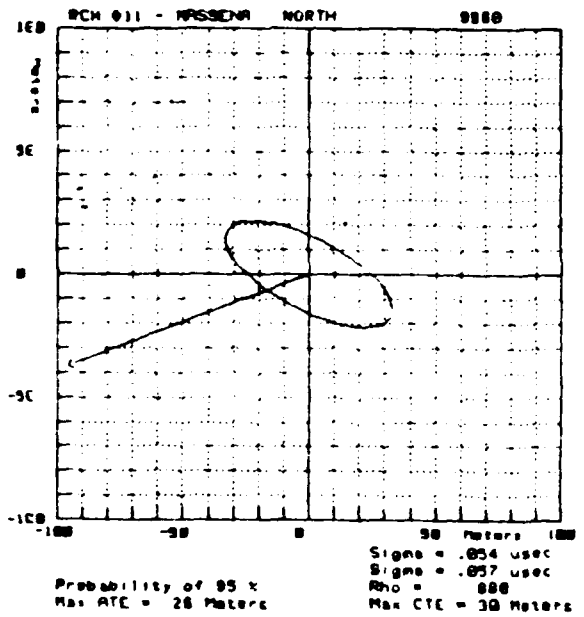
RCH 11 - MASSENA NORTH 9960
100
50
0
-50
-100
-1000
-50
0
50
Meters
1000
Probability of 95 %
Max ATE = 28 Meters
Sigma = .054 usec
Sigma = .057 usec
Rho = .888
Max CTE = 30 Meters

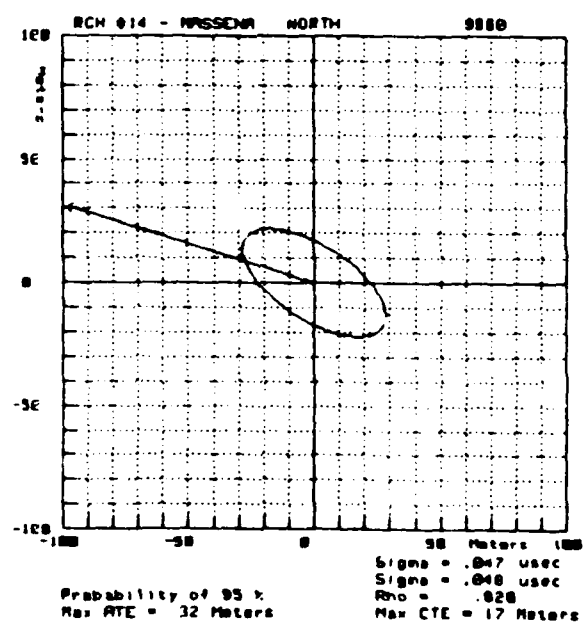
RCH 14 - MASSENA NORTH 9960
100
50
0
-50
-100
-1000
-50
0
50
Meters
1000
Probability of 95 %
Max ATE = 32 Meters
Sigma = .047 usec
Sigma = .048 usec
Rho = .828
Max CTE = 17 Meters

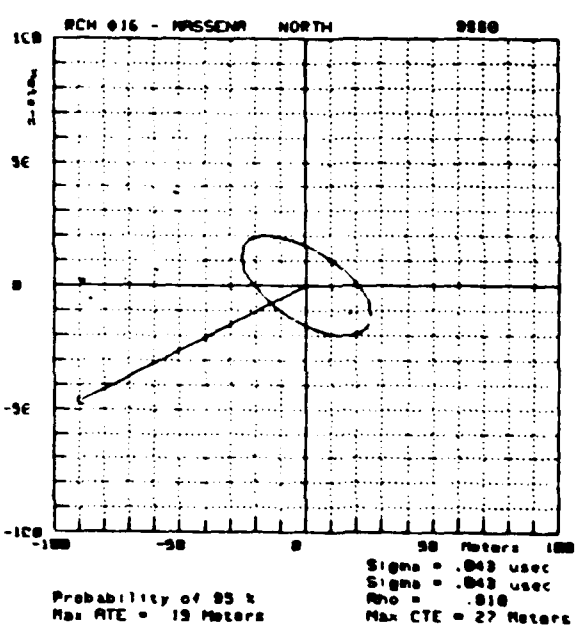
RCH 16 - MASSENA NORTH 9960
100
50
0
-50
-100
-1000
-50
0
50
Meters
1000
Probability of 95 %
Max ATE = 19 Meters
Sigma = .043 usec
Sigma = .043 usec
Rho = .818
Max CTE = 27 Meters

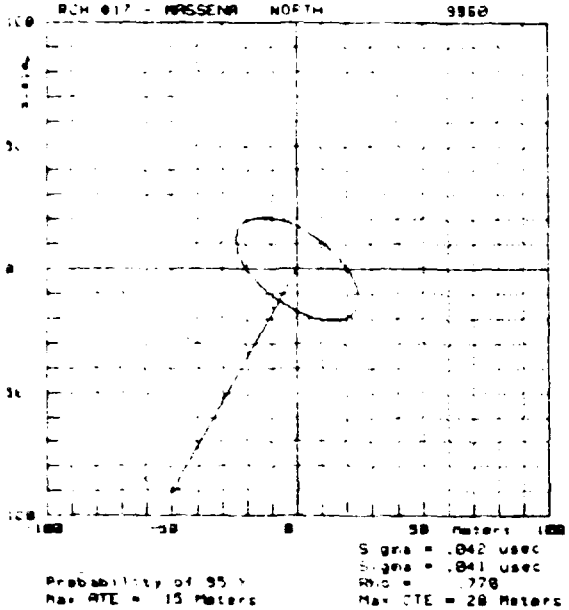
RCH 017 - MASSENA NORTH 9960
Sigma = .042 usec
Sigma = .041 usec
Rho = .778
Max CTE = 28 Meters
Probability of 95 %
Max ATE = 15 Meters

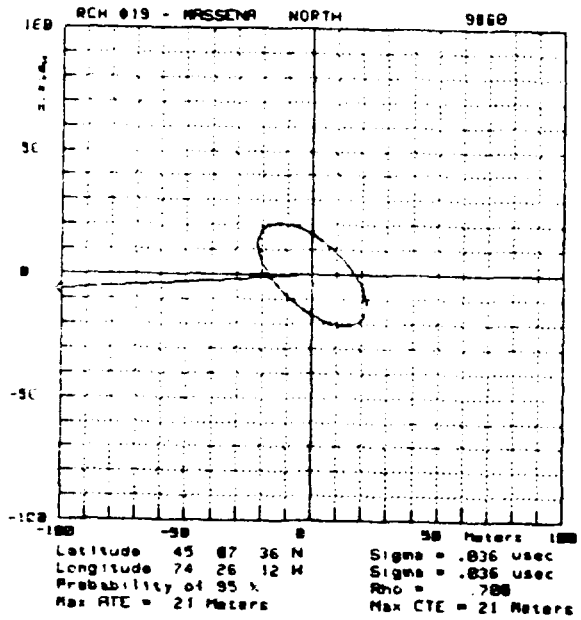
RCH 019 - MASSENA NORTH 9960
Latitude 44 57 36 N
Longitude 74 26 12 W
Probability of 95 %
Max ATE = 21 Meters
Sigma = .036 usec
Sigma = .036 usec
Rho = .788
Max CTE = 21 Meters

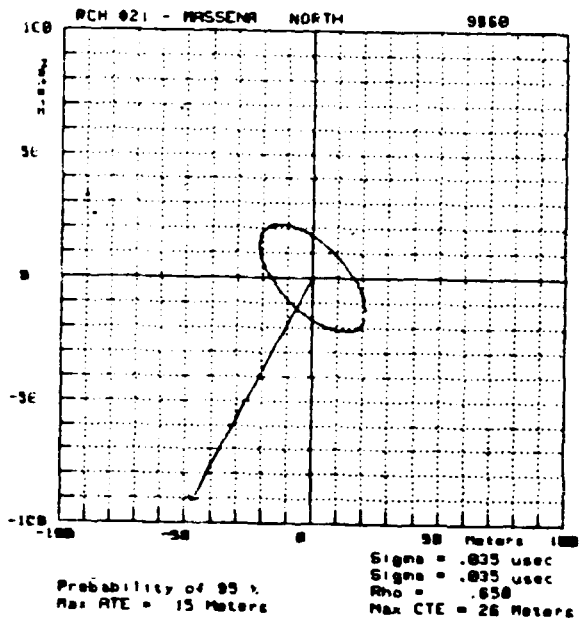
RCH 021 - MASSENA NORTH 9960
Probability of 95 %
Max ATE = 15 Meters
Sigma = .035 usec
Sigma = .035 usec
Rho = .858
Max CTE = 26 Meters

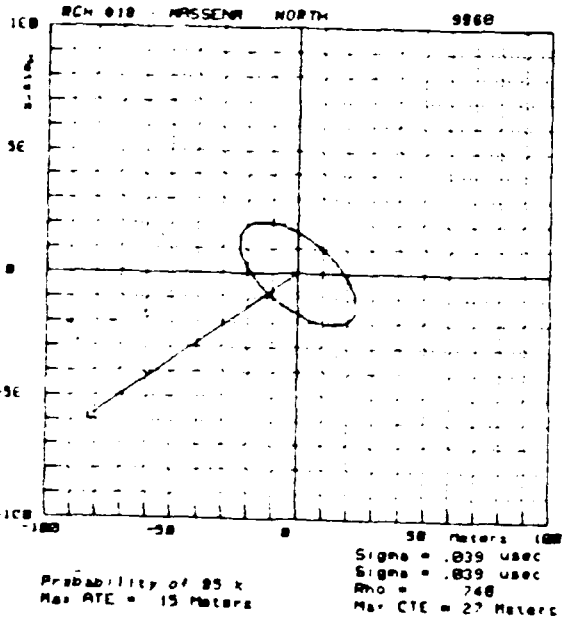
RCH 018 - MASSENA NORTH 9960
Probability of 95 %
Max ATE = 15 Meters
Sigma = .039 usec
Sigma = .039 usec
Rho = .748
Max CTE = 27 Meters

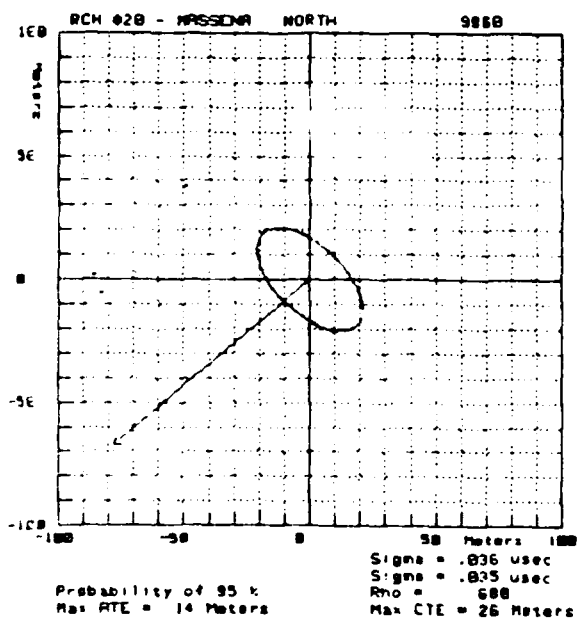
RCH 020 - MASSENA NORTH 9960
Probability of 95 %
Max ATE = 14 Meters
Sigma = .036 usec
Sigma = .035 usec
Rho = .688
Max CTE = 26 Meters

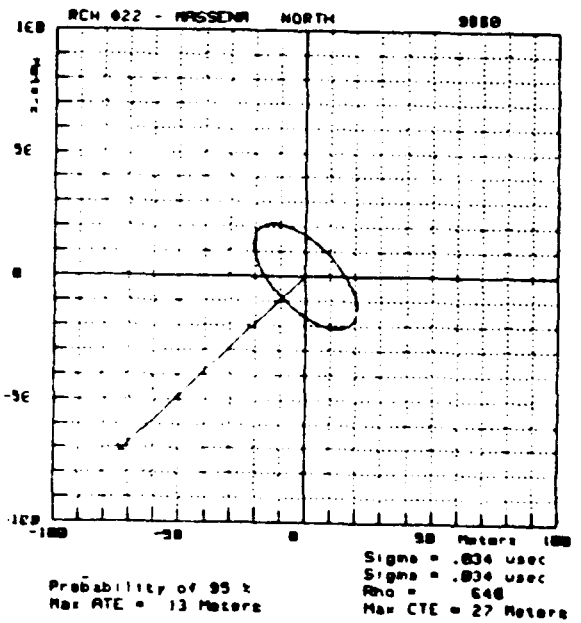
RCH 022 - MASSENA NORTH 9960
Probability of 95 %
Max ATE = 13 Meters
Sigma = .034 usec
Sigma = .034 usec
Rho = .648
Max CTE = 27 Meters

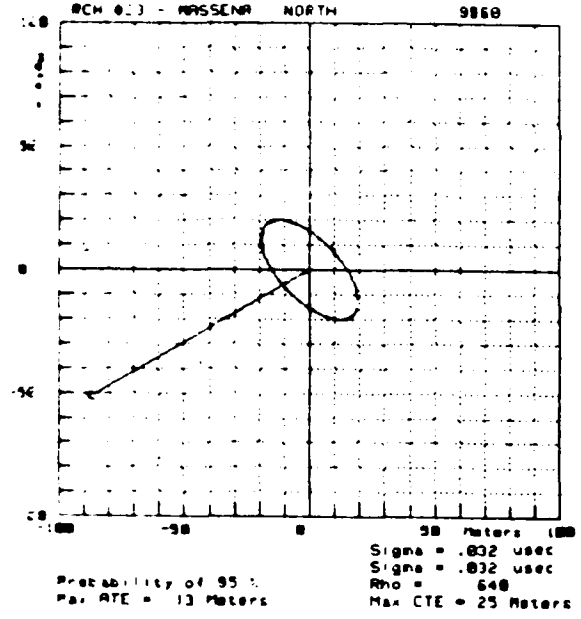
RCH 023 - MASSENA NORTH 9860
Meters
Probability of 95 %
Max ATE = 13 Meters
Sigma = .032 usec
Sigma = .032 usec
Rho = .648
Max CTE = 25 Meters

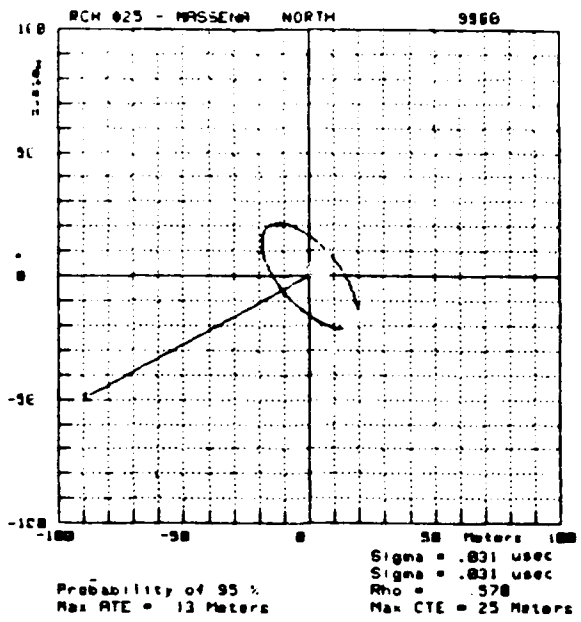
RCH 025 - MASSENA NORTH 9860
Meters
Probability of 95 %
Max ATE = 13 Meters
Sigma = .031 usec
Sigma = .031 usec
Rho = .578
Max CTE = 25 Meters

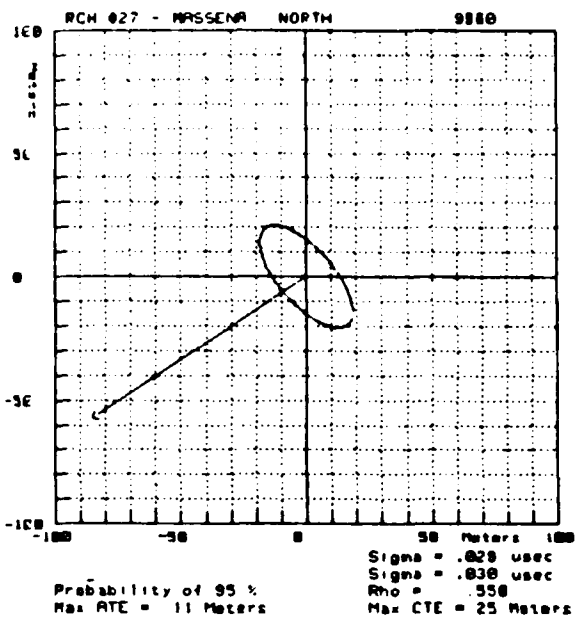
RCH 027 - MASSENA NORTH 9860
Meters
Probability of 95 %
Max ATE = 11 Meters
Sigma = .029 usec
Sigma = .030 usec
Rho = .558
Max CTE = 25 Meters

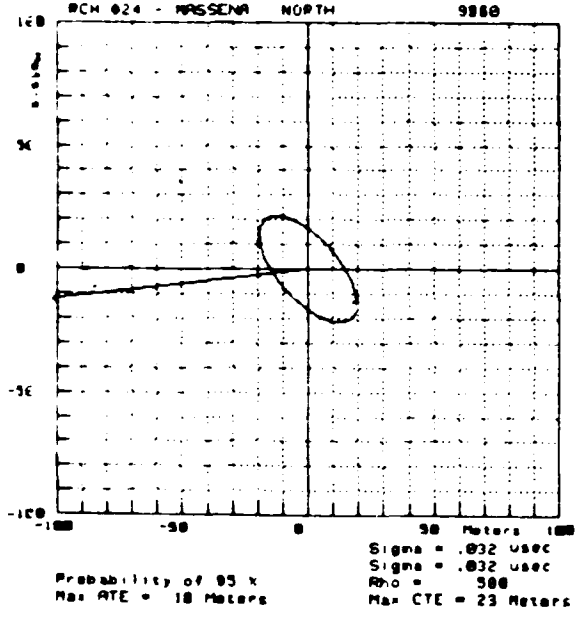
RCH 024 - MASSENA NORTH 9860
Meters
Probability of 95 %
Max ATE = 18 Meters
Sigma = .032 usec
Sigma = .032 usec
Rho = .588
Max CTE = 23 Meters

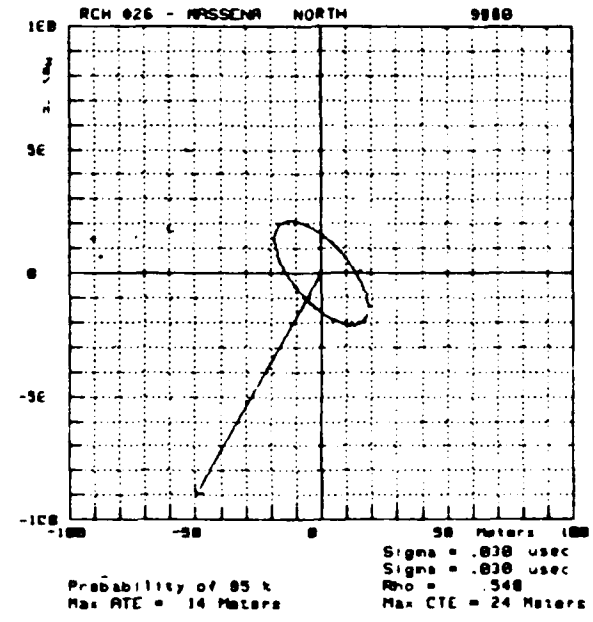
RCH 026 - MASSENA NORTH 9860
Meters
Probability of 95 %
Max ATE = 14 Meters
Sigma = .030 usec
Sigma = .030 usec
Rho = .548
Max CTE = 24 Meters

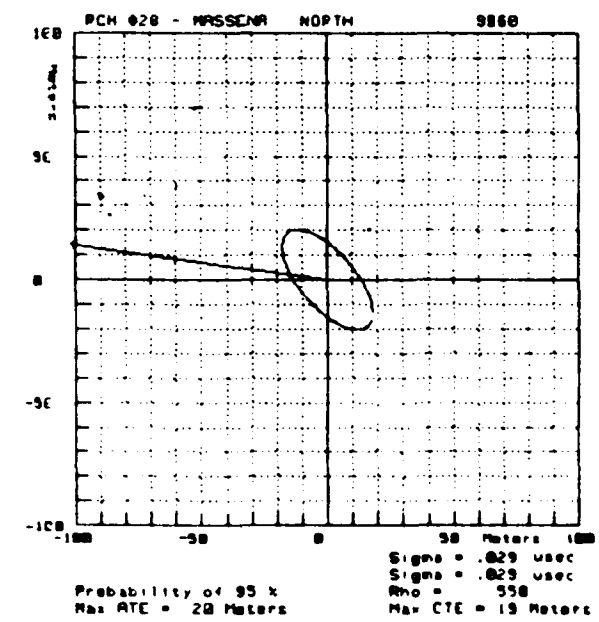
RCH 028 - MASSENA NORTH 9860
Meters
Probability of 95 %
Max ATE = 20 Meters
Sigma = .029 usec
Sigma = .029 usec
Rho = .558
Max CTE = 19 Meters

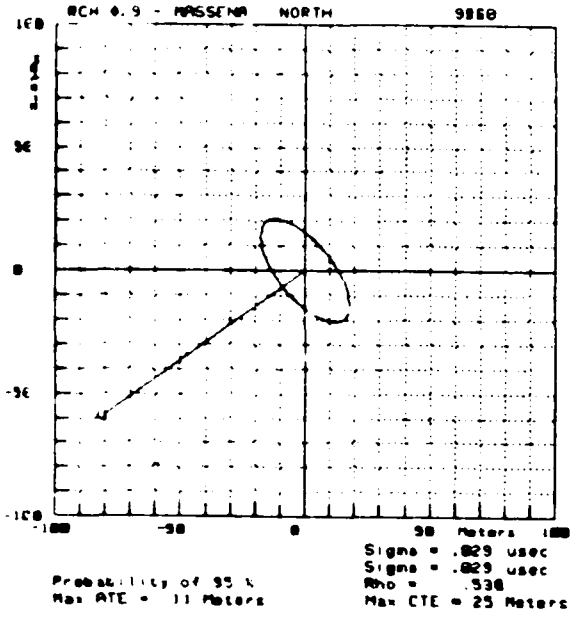
RCH 0.9 - MASSENA NORTH 9860
100
50
0
-50
-100
-100
-50
0
50
Meters
100
Probability of 95 %
Max ATE = 11 Meters
Sigma = .029 usec
Sigma = .029 usec
Rho = .538
Max CTE = 25 Meters

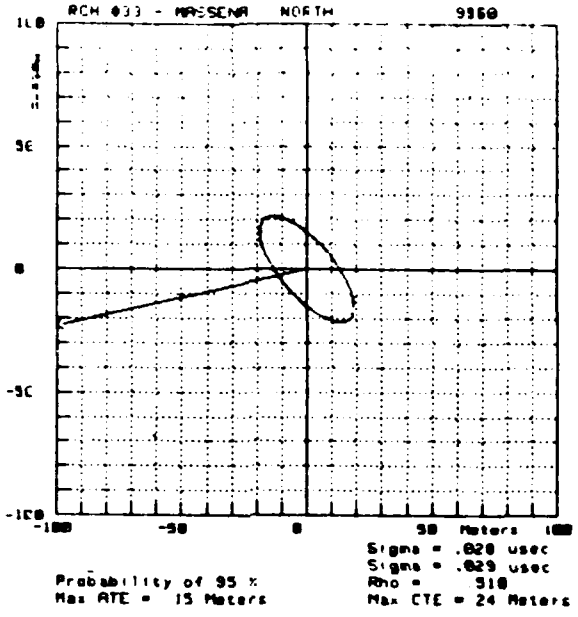
RCH 033 - MASSENA NORTH 9860
100
50
0
-50
-100
-100
-50
0
50
Meters
100
Probability of 95 %
Max ATE = 15 Meters
Sigma = .028 usec
Sigma = .029 usec
Rho = .518
Max CTE = 24 Meters

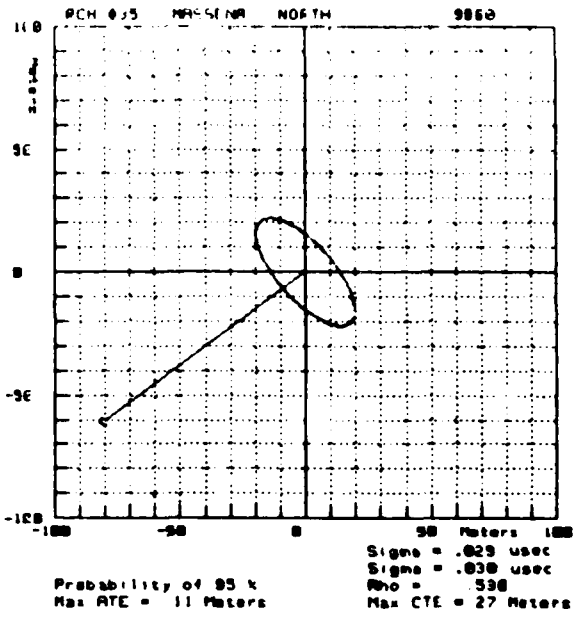
RCH 035 MASSENA NORTH 9860
100
50
0
-50
-100
-100
-50
0
50
Meters
100
Probability of 95 %
Max ATE = 11 Meters
Sigma = .029 usec
Sigma = .030 usec
Rho = .538
Max CTE = 27 Meters

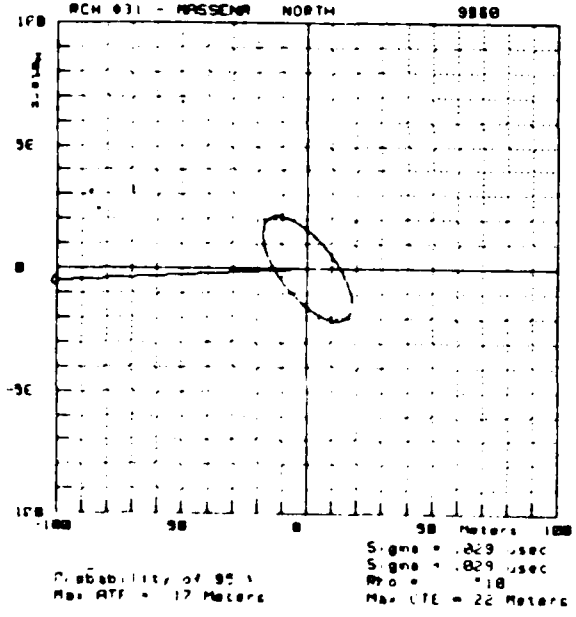
RCH 031 - MASSENA NORTH 9860
100
50
0
-50
-100
-100
-50
0
50
Meters
100
Probability of 95 %
Max ATE = 17 Meters
Sigma = .029 usec
Sigma = .029 usec
Rho = .518
Max CTE = 22 Meters

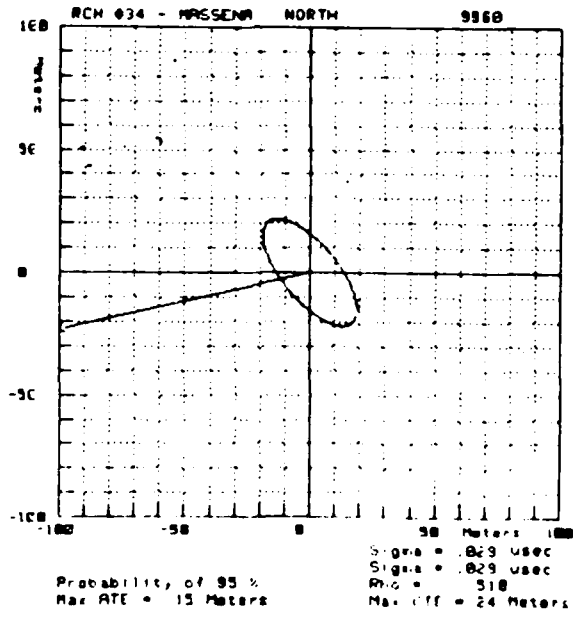
RCH 034 - MASSENA NORTH 9860
100
50
0
-50
-100
-100
-50
0
50
Meters
100
Probability of 95 %
Max ATE = 15 Meters
Sigma = .029 usec
Sigma = .029 usec
Rho = .518
Max CTE = 24 Meters

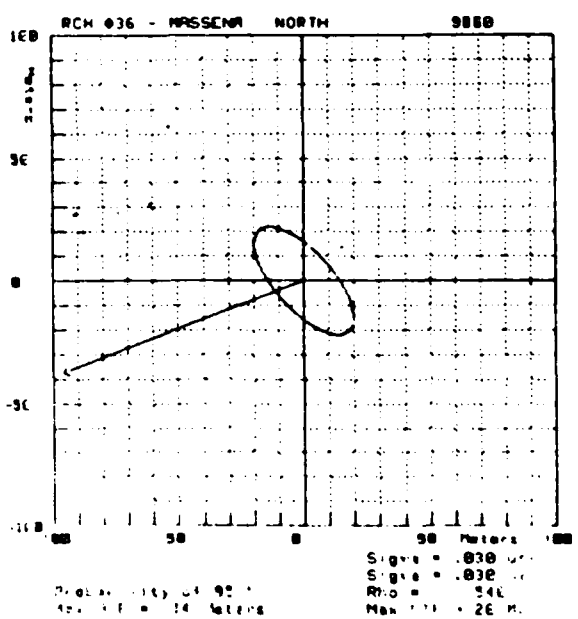
RCH 036 - MASSENA NORTH 9860
100
50
0
-50
-100
-100
-50
0
50
Meters
100
Sigma = .030
Sigma = .030
Rho = .546
Max CTE = 26 M

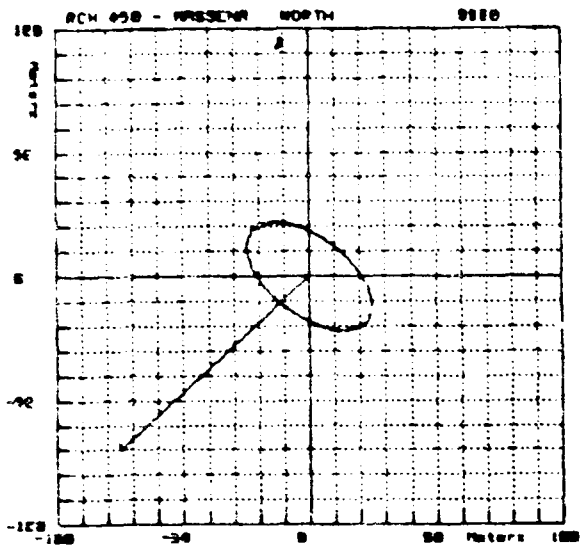

Sigma = .041 usec
Sigma = .038 usec
Rho = .748
Probability of 95 %
Max ATE = 16 Meters
Max CTE = 29 Meters

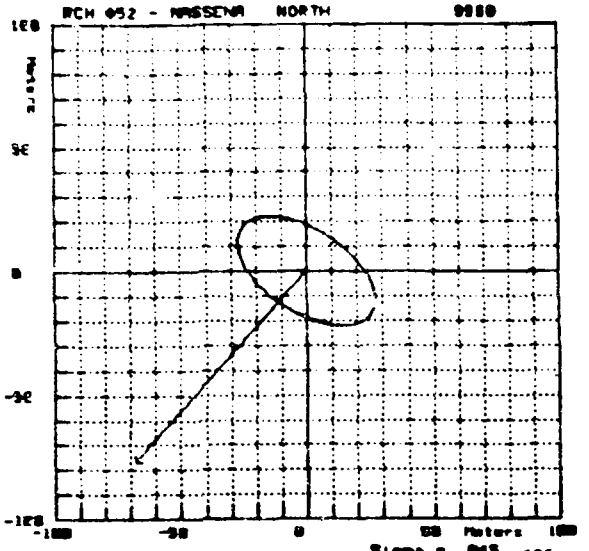

Sigma = .045 usec
Sigma = .042 usec
Rho = .708
Probability of 95 %
Max ATE = 17 Meters
Max CTE = 31 Meters

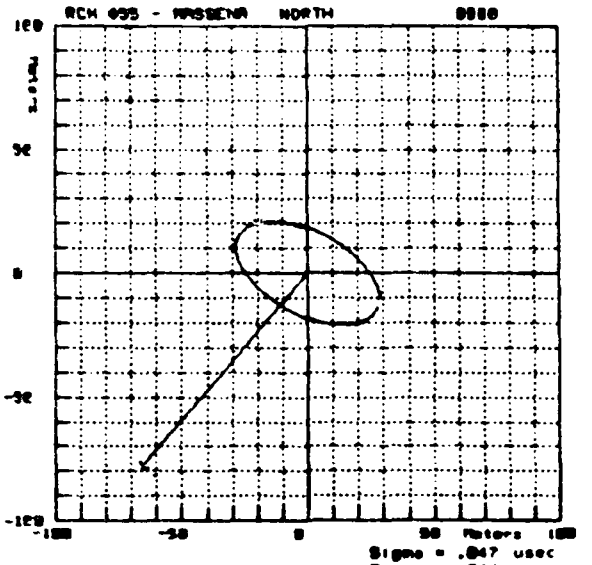

Sigma = .047 usec
Sigma = .044 usec
Rho = .828
Probability of 95 %
Max ATE = 17 Meters
Max CTE = 31 Meters

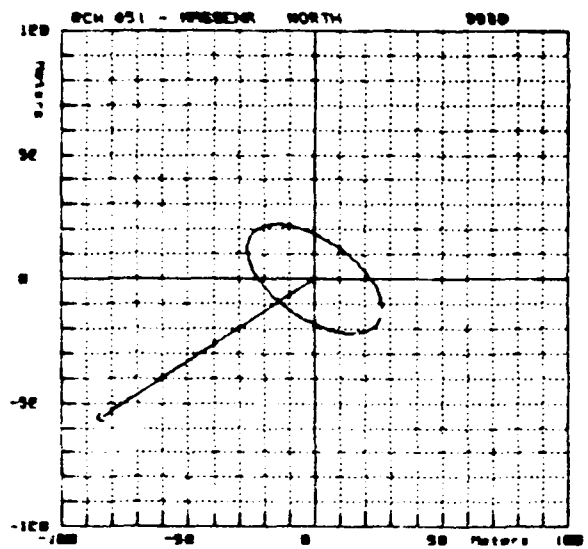

Sigma = .042 usec
Sigma = .041 usec
Rho = .778
Probability of 95 %
Max ATE = 19 Meters
Max CTE = 29 Meters

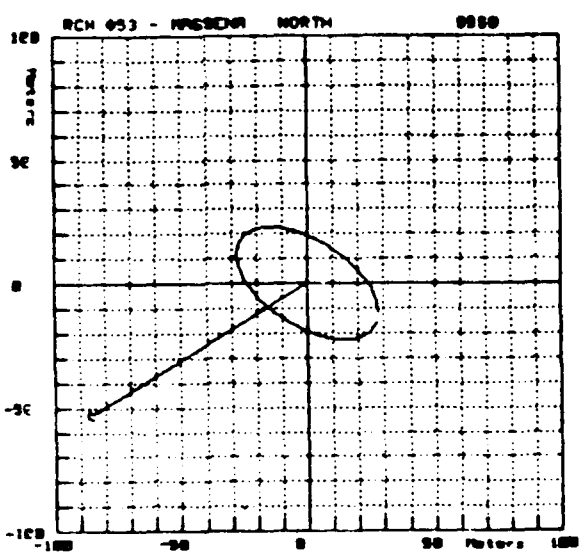

Sigma = .046 usec
Sigma = .043 usec
Rho = .708
Probability of 95 %
Max ATE = 28 Meters
Max CTE = 38 Meters

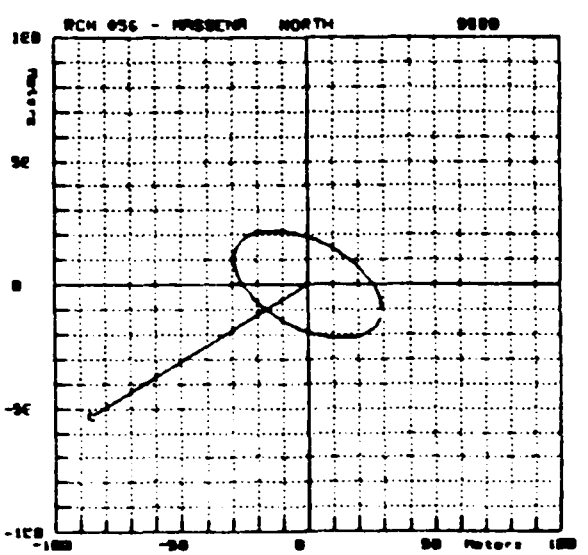

Sigma = .049 usec
Sigma = .045 usec
Rho = .828
Probability of 95 %
Max ATE = 22 Meters
Max CTE = 25 Meters

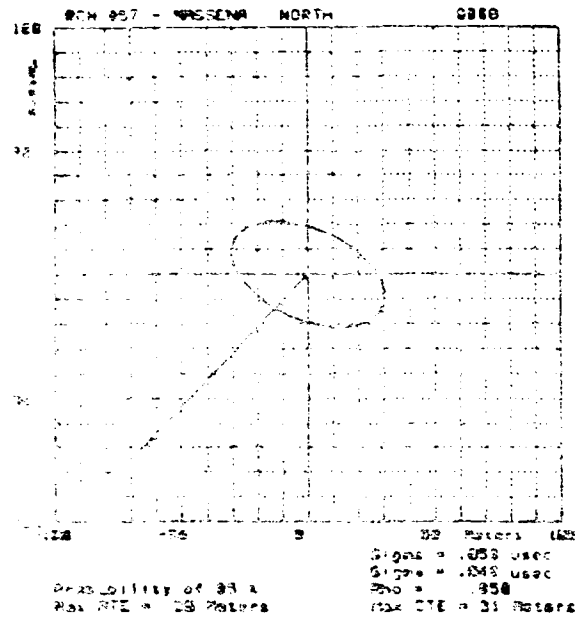
RCH 957 - MASSENA NORTH 0860
Sigma = .058 usec
Sigma = .049 usec
Rho = .850
Probability of 95 %
Max ATE = 28 Meters
Max CTE = 31 Meters

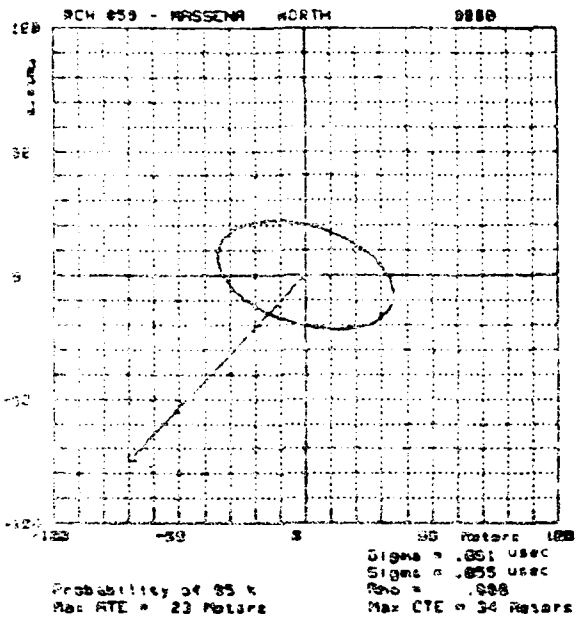
RCH 959 - MASSENA NORTH 0880
Sigma = .061 usec
Sigma = .055 usec
Rho = .898
Probability of 95 %
Max ATE = 23 Meters
Max CTE = 34 Meters

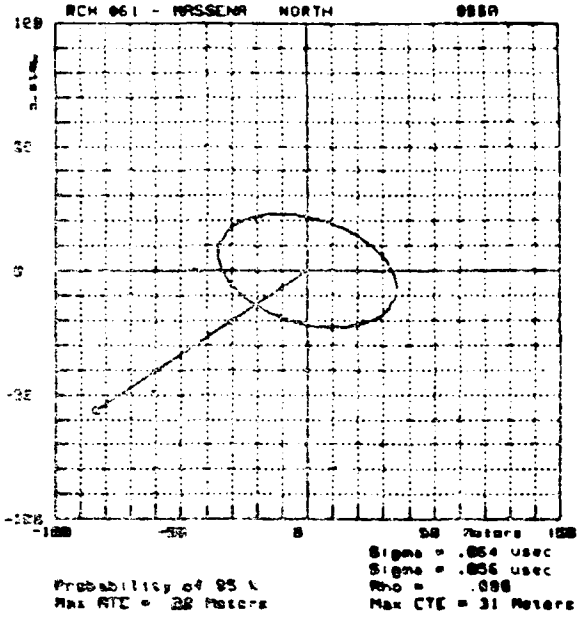
RCH 961 - MASSENA NORTH 0880
Sigma = .054 usec
Sigma = .056 usec
Rho = .898
Probability of 95 %
Max ATE = 28 Meters
Max CTE = 31 Meters

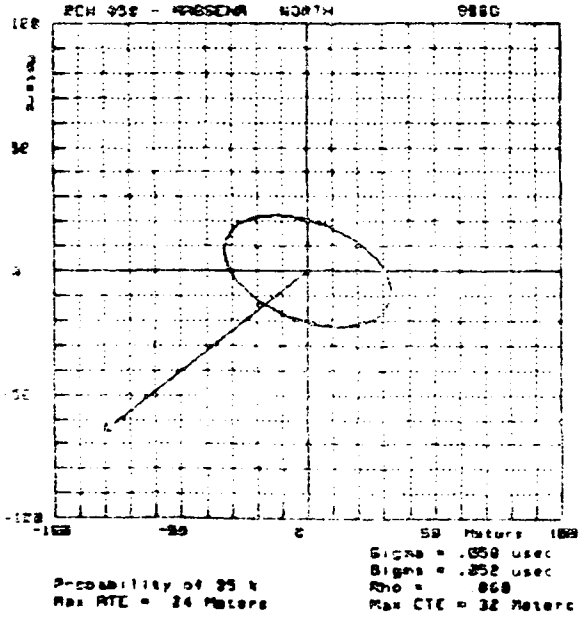
RCH 958 - MASSENA NORTH 0880
Sigma = .058 usec
Sigma = .052 usec
Rho = .868
Probability of 95 %
Max ATE = 24 Meters
Max CTE = 32 Meters

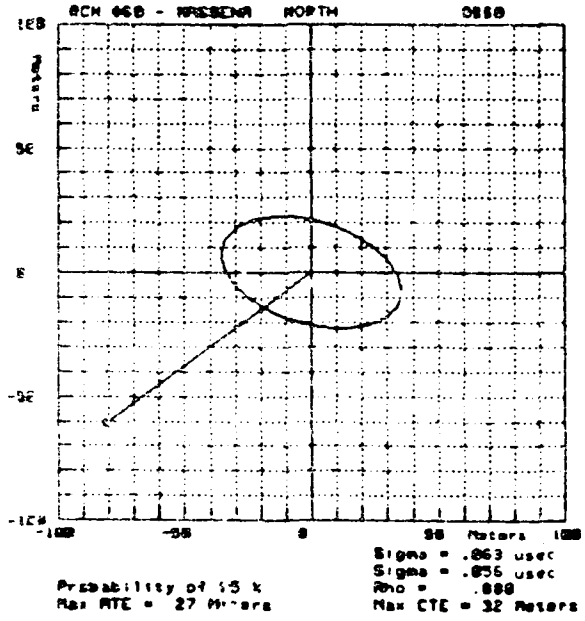
RCH 960 - MASSENA NORTH 0880
Sigma = .063 usec
Sigma = .056 usec
Rho = .888
Probability of 95 %
Max ATE = 27 Meters
Max CTE = 32 Meters

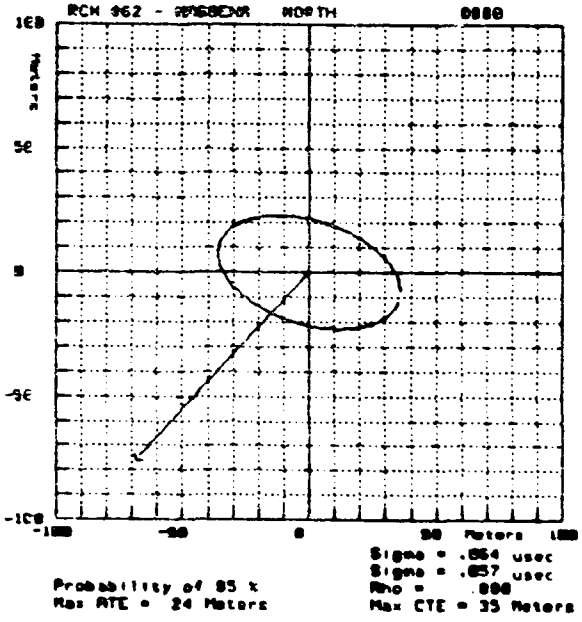
RCH 962 - MASSENA NORTH 0880
Sigma = .054 usec
Sigma = .057 usec
Rho = .898
Probability of 95 %
Max ATE = 24 Meters
Max CTE = 35 Meters

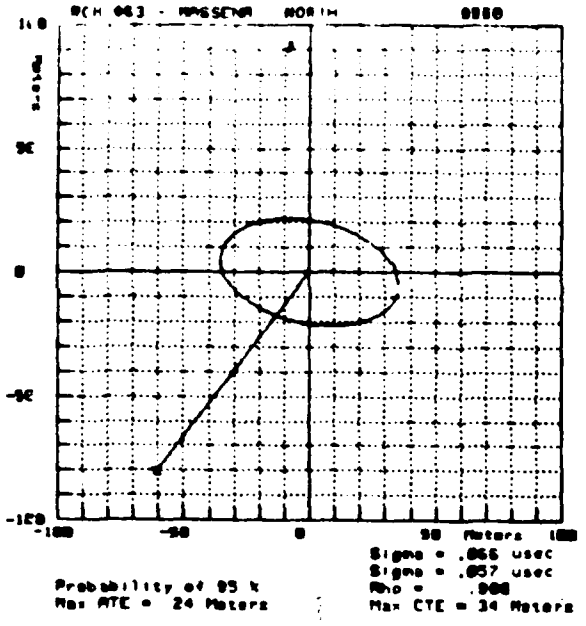
RCH 063 - MASSENA NORTH 9880
Meters
100
50
0
-50
-100
-100
-50
0
50
100
Meters
Sigma = .066 usec
Sigma = .057 usec
Rho = .900
Max CTE = 34 Meters
Probability of 95 %
Max ATE = 24 Meters

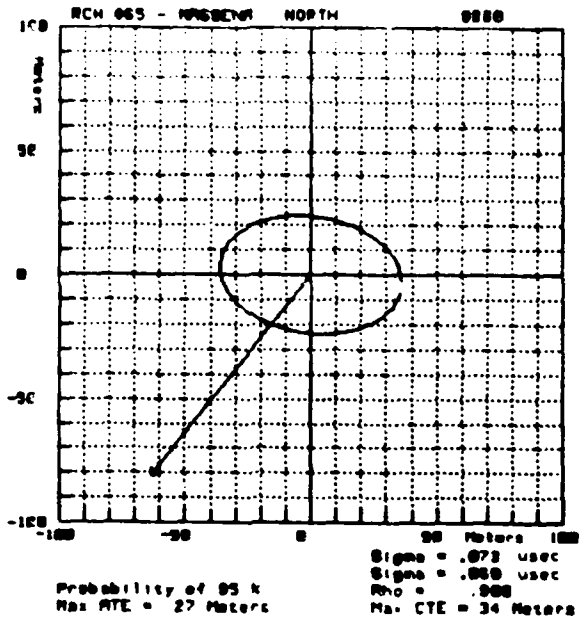
RCH 065 - MASSENA NORTH 9880
Meters
100
50
0
-50
-100
-100
-50
0
50
100
Meters
Sigma = .073 usec
Sigma = .060 usec
Rho = .900
Max CTE = 34 Meters
Probability of 95 %
Max ATE = 27 Meters

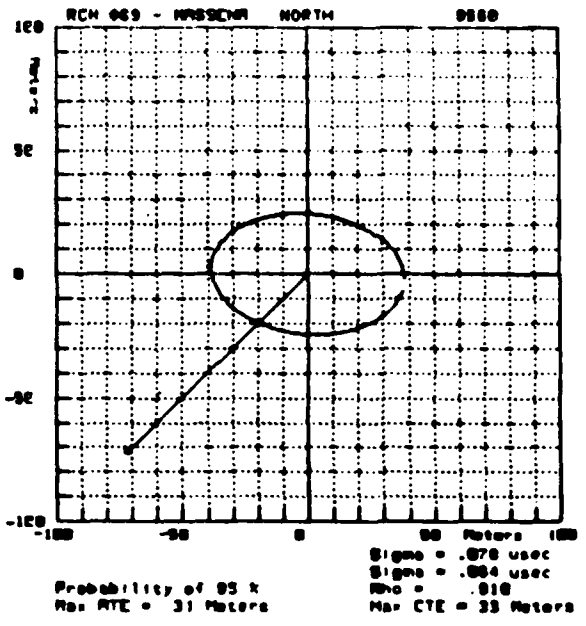
RCH 069 - MASSENA NORTH 9880
Meters
100
50
0
-50
-100
-100
-50
0
50
100
Meters
Sigma = .078 usec
Sigma = .064 usec
Rho = .910
Max CTE = 33 Meters
Probability of 95 %
Max ATE = 31 Meters

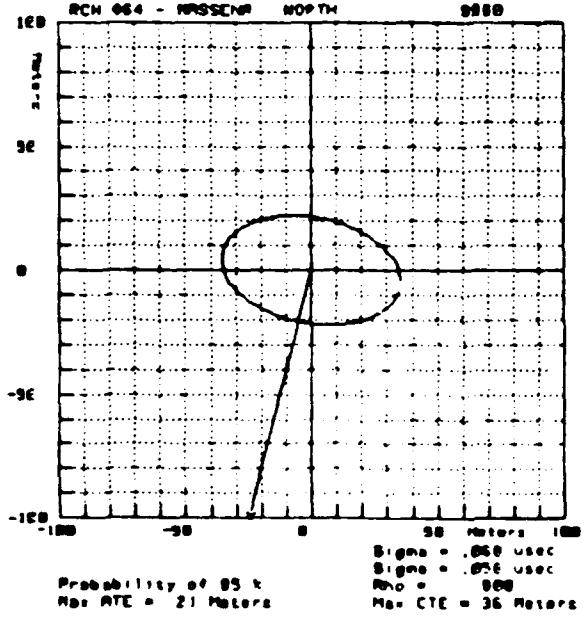
RCH 064 - MASSENA NORTH 9880
Meters
100
50
0
-50
-100
-100
-50
0
50
100
Meters
Sigma = .068 usec
Sigma = .056 usec
Rho = .900
Max CTE = 36 Meters
Probability of 95 %
Max ATE = 21 Meters

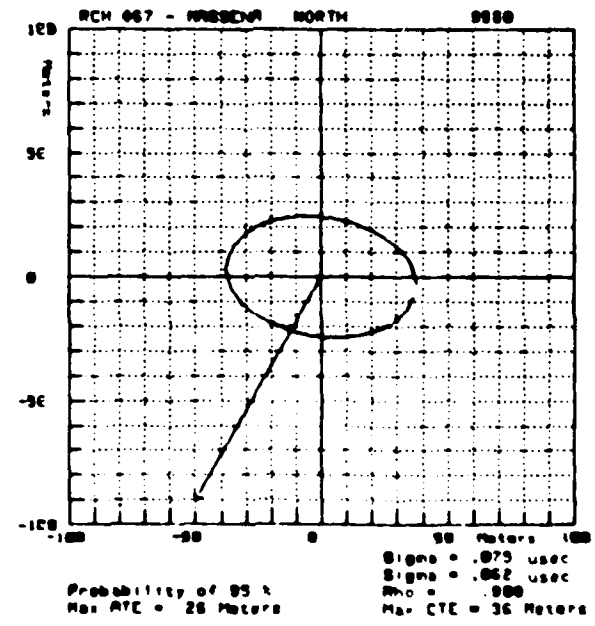
RCH 067 - MASSENA NORTH 9880
Meters
100
50
0
-50
-100
-100
-50
0
50
100
Meters
Sigma = .075 usec
Sigma = .062 usec
Rho = .900
Max CTE = 36 Meters
Probability of 95 %
Max ATE = 28 Meters

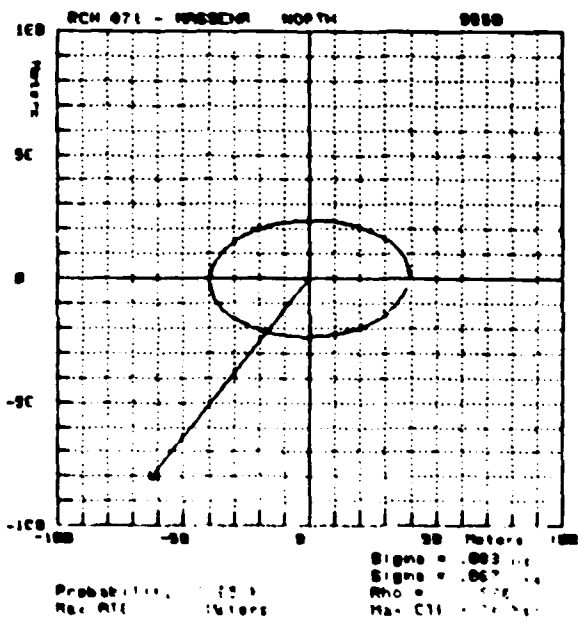
RCH 071 - MASSENA NORTH 9880
Meters
100
50
0
-50
-100
-100
-50
0
50
100
Meters

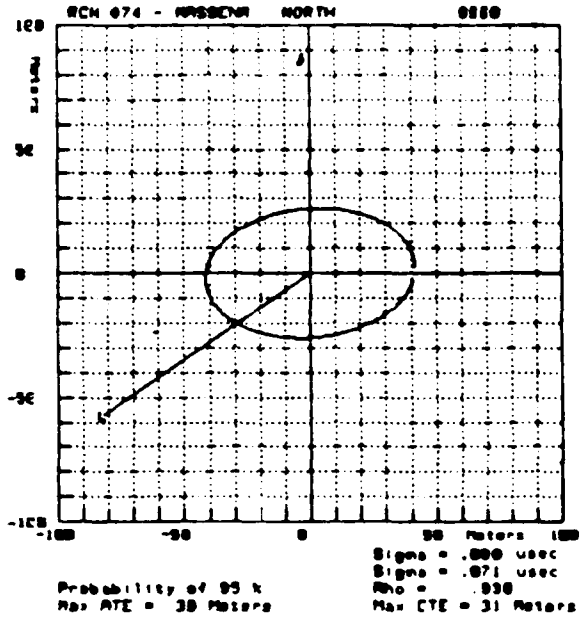
RCH 074 - MASSENA NORTH 9880
100
Meters
50
0
-50
-100
-100
-50
0
50
Meters
100
Probability of 95 %
Max ATE = 38 Meters
Sigma = .080 usec
Sigma = .071 usec
Rho = .930
Max CTE = 31 Meters

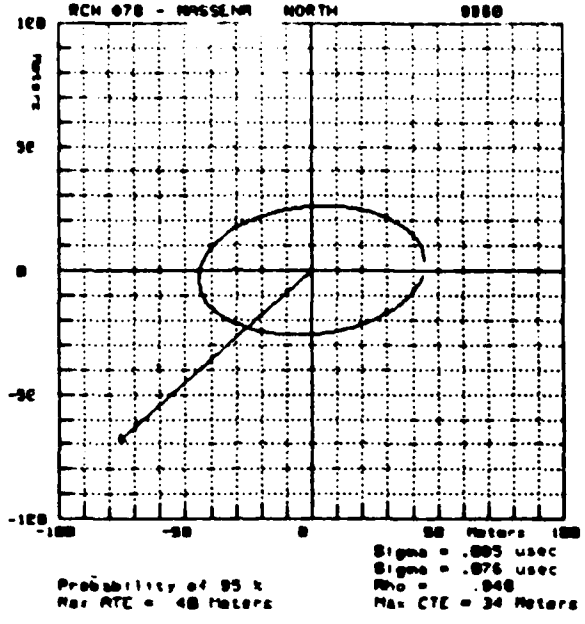
RCH 078 - MASSENA NORTH 9880
100
Meters
50
0
-50
-100
-100
-50
0
50
Meters
100
Probability of 95 %
Max ATE = 48 Meters
Sigma = .085 usec
Sigma = .076 usec
Rho = .940
Max CTE = 34 Meters

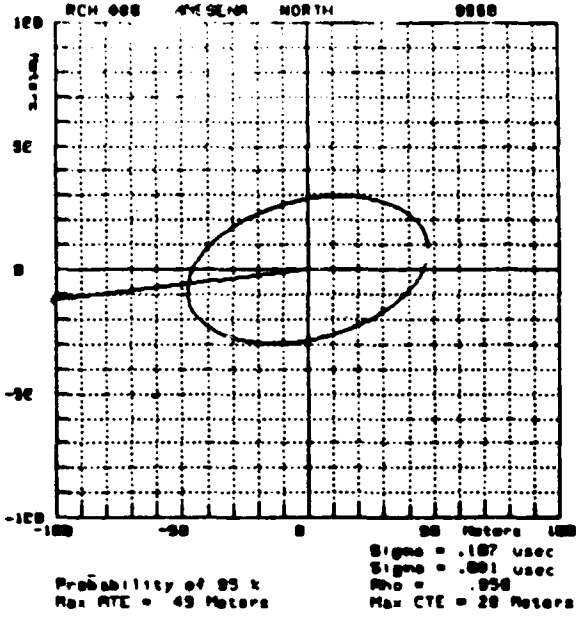
RCH 088 - MASSENA NORTH 9880
100
Meters
50
0
-50
-100
-100
-50
0
50
Meters
100
Probability of 95 %
Max ATE = 49 Meters
Sigma = .107 usec
Sigma = .081 usec
Rho = .950
Max CTE = 28 Meters

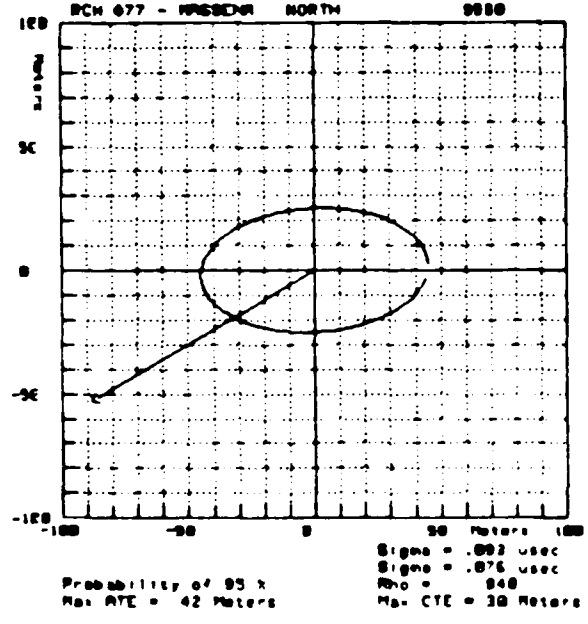
RCH 077 - MASSENA NORTH 9880
100
Meters
50
0
-50
-100
-100
-50
0
50
Meters
100
Probability of 95 %
Max ATE = 42 Meters
Sigma = .083 usec
Sigma = .076 usec
Rho = .940
Max CTE = 38 Meters

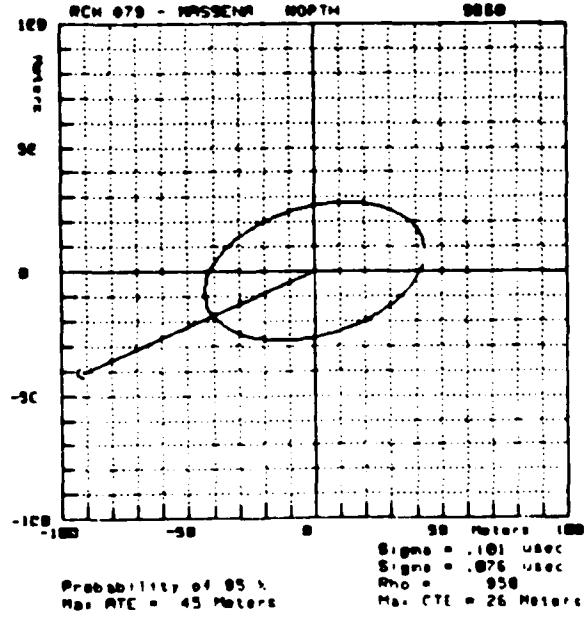
RCH 079 - MASSENA NORTH 9880
100
Meters
50
0
-50
-100
-100
-50
0
50
Meters
100
Probability of 95 %
Max ATE = 45 Meters
Sigma = .101 usec
Sigma = .076 usec
Rho = .950
Max CTE = 26 Meters

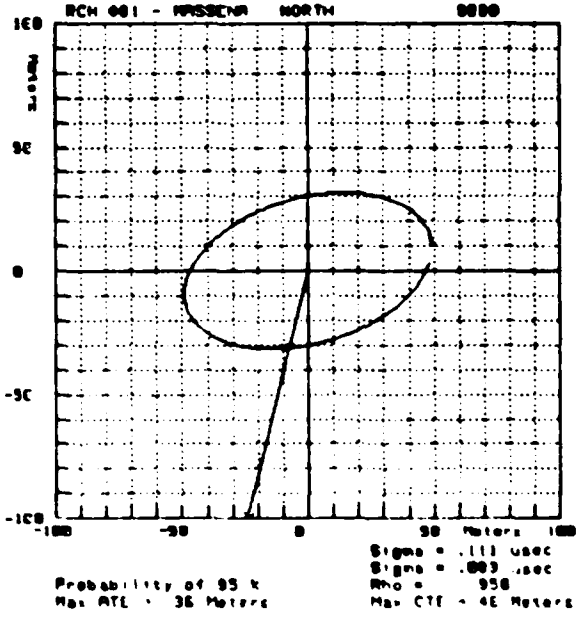
RCH 081 - MASSENA NORTH 9880
100
Meters
50
0
-50
-100
-100
-50
0
50
Meters
100
Probability of 95 %
Max ATE = 36 Meters
Sigma = .111 usec
Sigma = .083 usec
Rho = .950
Max CTE = 46 Meters

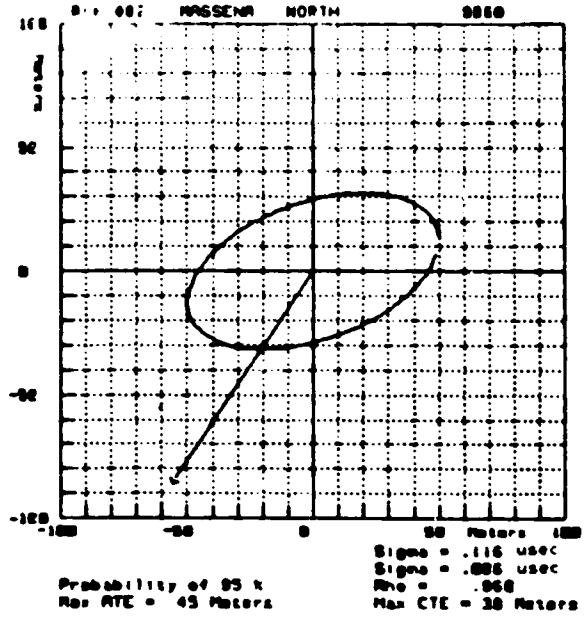
RASSENA
NORTH
9860
Meters
Sigma = .116 usec
Sigma = .086 usec
Rho = .068
Max CTE = 38 Meters
Probability of 95 %
Max RTE = 45 Meters

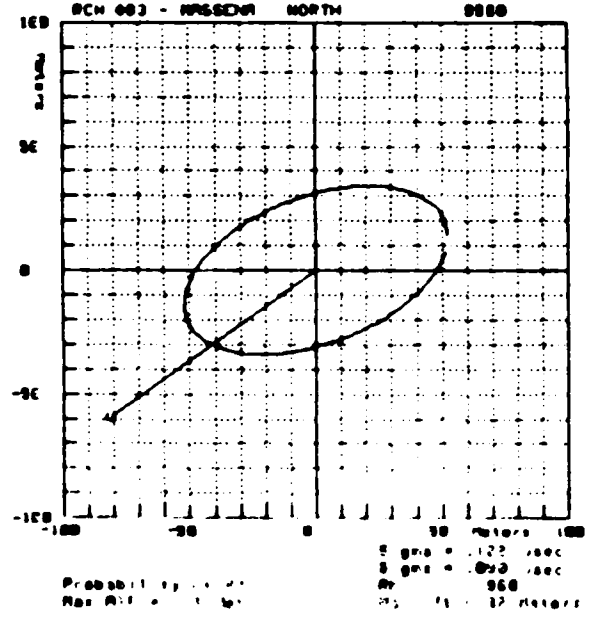
RASSENA
NORTH
9860
Meters

DIFFERENTIAL LORAN-C - RELATIVE TO WELLESLEY IS

PREDICTED ERROR ELLIPSE PLOTS

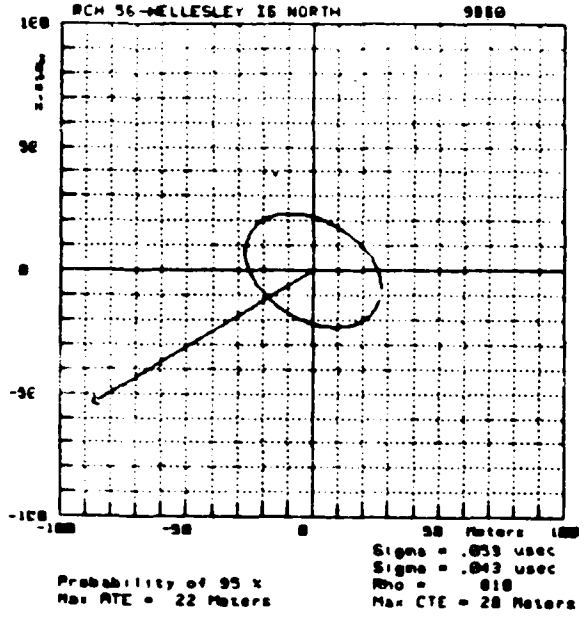
RCH 56→WELLESLEY IS NORTH 9880
Meters
Probability of 95 %
Max ATE = 22 Meters
Sigma = .053 usec
Sigma = .043 usec
Rho = .810
Max CTE = 28 Meters

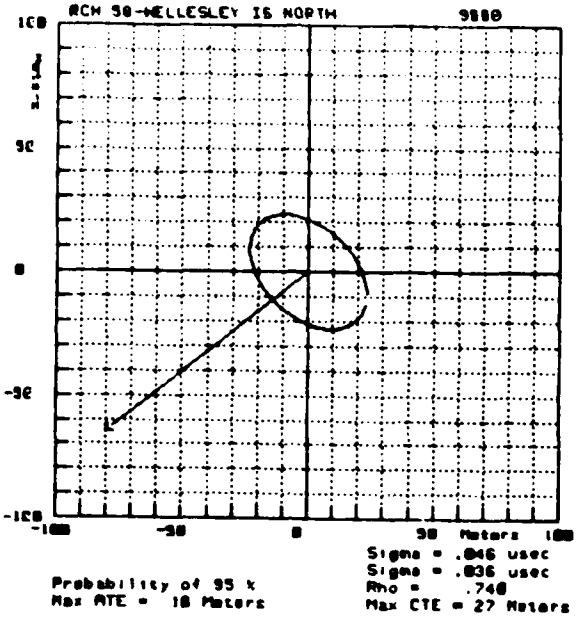
RCH 58→WELLESLEY IS NORTH 9880
Meters
Probability of 95 %
Max ATE = 18 Meters
Sigma = .046 usec
Sigma = .036 usec
Rho = .748
Max CTE = 27 Meters

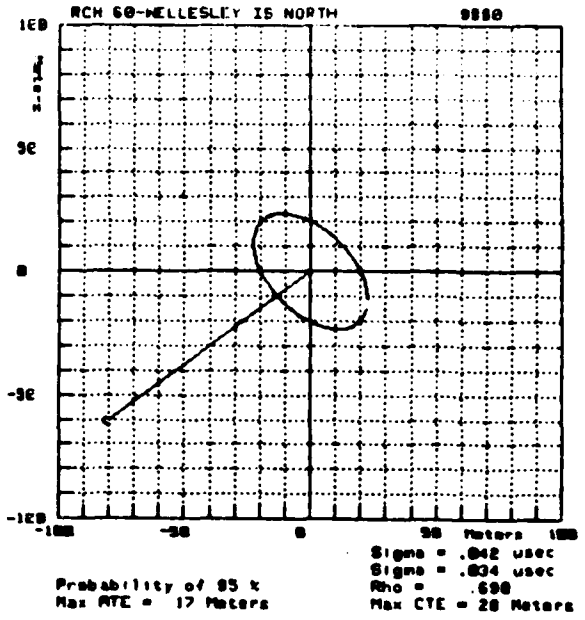
RCH 60→WELLESLEY IS NORTH 9880
Meters
Probability of 95 %
Max ATE = 17 Meters
Sigma = .042 usec
Sigma = .034 usec
Rho = .698
Max CTE = 28 Meters

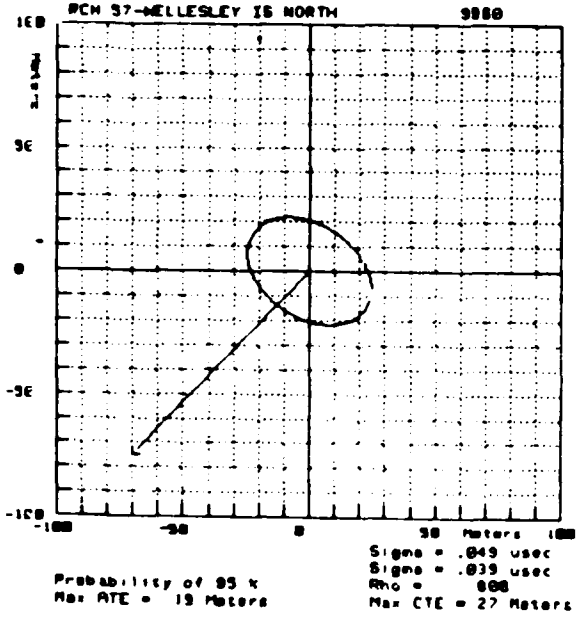
RCH 57→WELLESLEY IS NORTH 9880
Meters
Probability of 95 %
Max ATE = 19 Meters
Sigma = .049 usec
Sigma = .039 usec
Rho = .808
Max CTE = 27 Meters

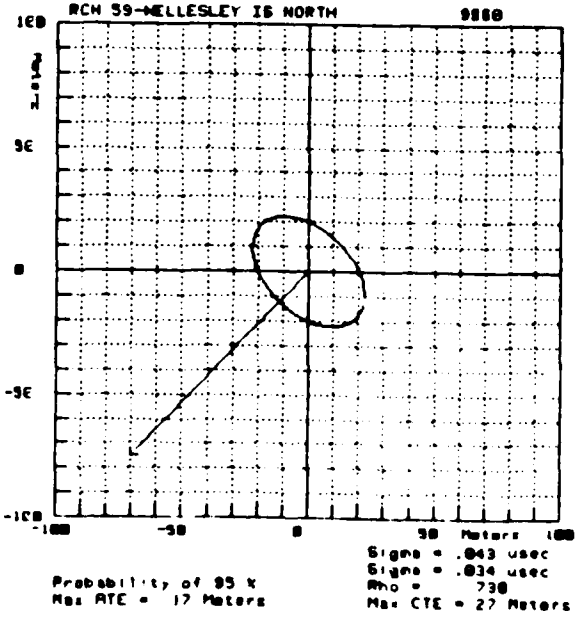
RCH 59→WELLESLEY IS NORTH 9880
Meters
Probability of 95 %
Max ATE = 17 Meters
Sigma = .043 usec
Sigma = .034 usec
Rho = .738
Max CTE = 27 Meters

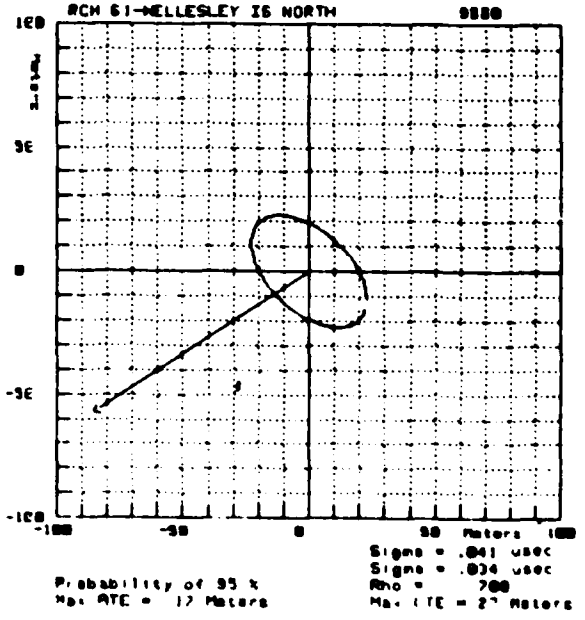
RCH 61→WELLESLEY IS NORTH 9880
Meters
Probability of 95 %
Max ATE = 17 Meters
Sigma = .041 usec
Sigma = .034 usec
Rho = .708
Max CTE = 27 Meters

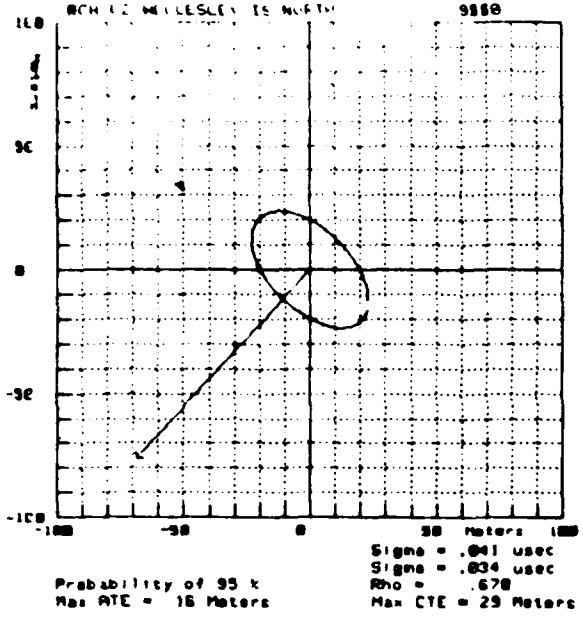
RCH 62-WELLESLEY IS NORTH
9880
Meters
Sigma = .041 usec
Sigma = .034 usec
Rho = .670
Probability of 95 %
Max ATE = 16 Meters
Max CTE = 29 Meters

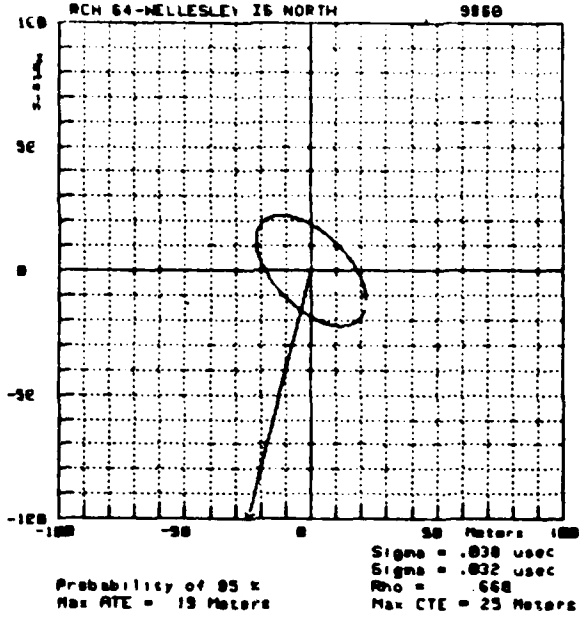
RCH 64-WELLESLEY IS NORTH
9880
Meters
Sigma = .038 usec
Sigma = .032 usec
Rho = .668
Probability of 95 %
Max ATE = 19 Meters
Max CTE = 25 Meters

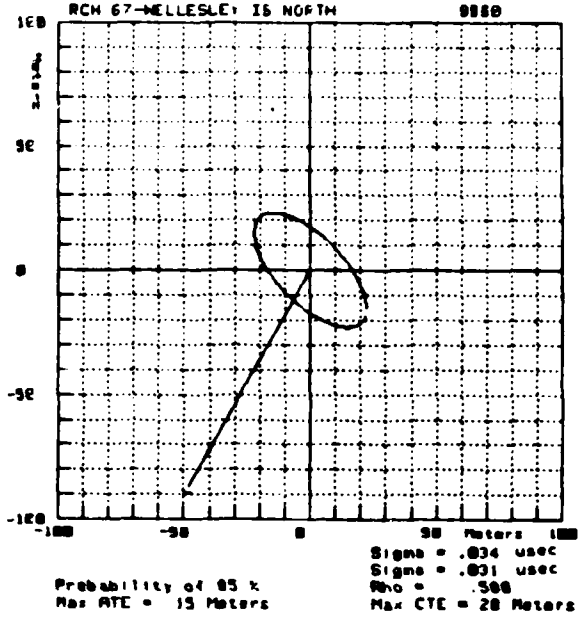
RCH 67-WELLESLEY IS NORTH
9880
Meters
Sigma = .034 usec
Sigma = .031 usec
Rho = .588
Probability of 95 %
Max ATE = 15 Meters
Max CTE = 28 Meters

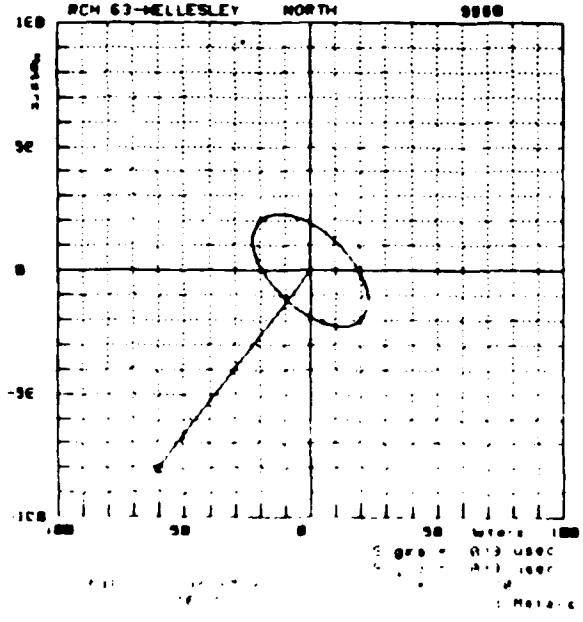
RCH 63-WELLESLEY NORTH
9880
Meters

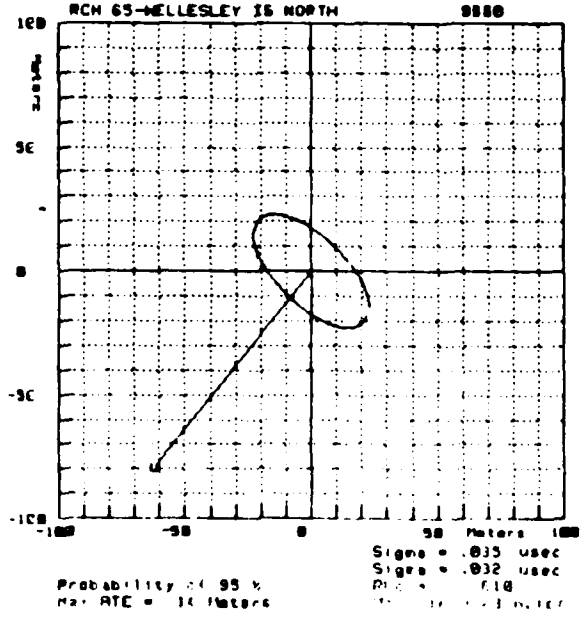
RCH 65-WELLESLEY IS NORTH
9880
Meters
Sigma = .035 usec
Sigma = .032 usec
Max ATE = 16 Meters

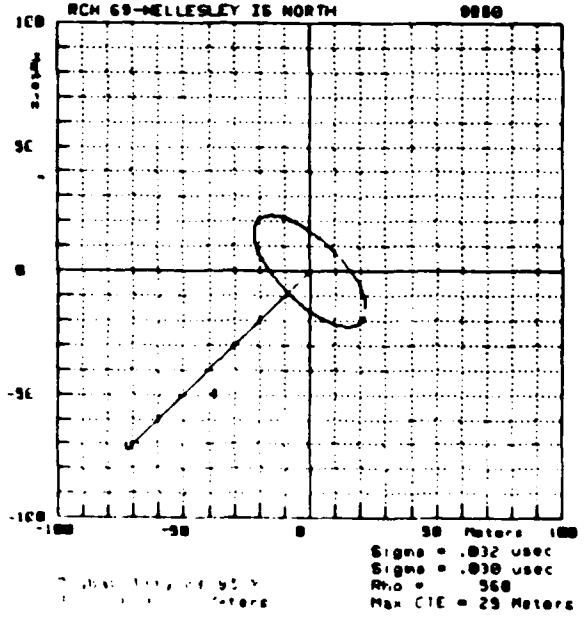
RCH 69-WELLESLEY IS NORTH
9880
Meters
Sigma = .032 usec
Sigma = .030 usec
Rho = .568
Max CTE = 29 Meters

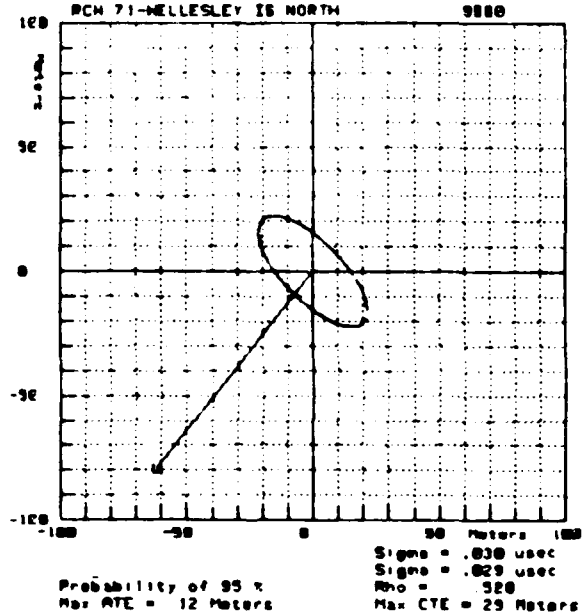
RCH 71-WELLESLEY IS NORTH
9880
Meters
100
50
0
-50
-100
-100
-50
0
50
100
Meters
Probability of 95 %
Max ATE = 12 Meters
Sigma = .030 usec
Sigma = .029 usec
Rho = .520
Max CTE = 29 Meters

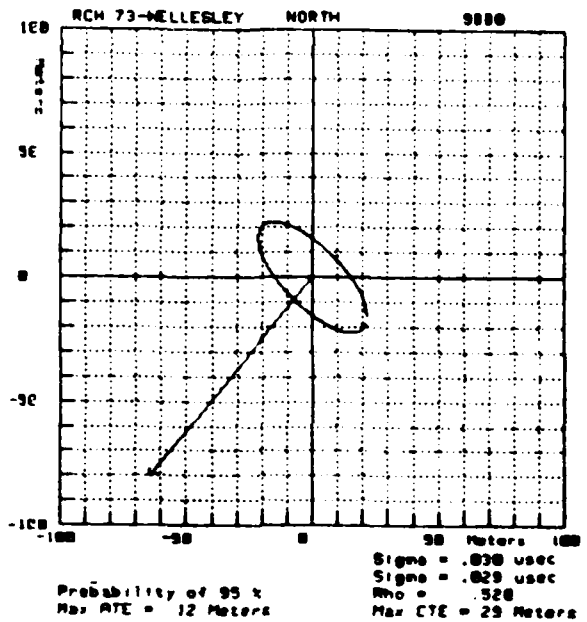
RCH 73-WELLESLEY NORTH
9880
Meters
100
50
0
-50
-100
-100
-50
0
50
100
Meters
Probability of 95 %
Max ATE = 12 Meters
Sigma = .030 usec
Sigma = .029 usec
Rho = .520
Max CTE = 29 Meters

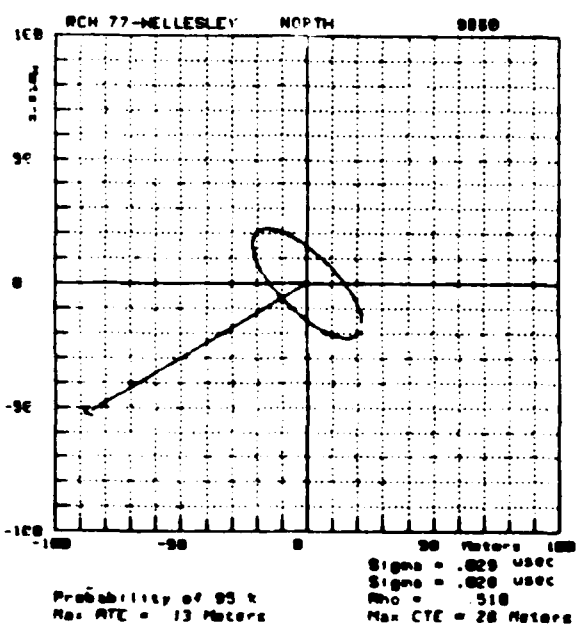
RCH 77-WELLESLEY NORTH
9880
Meters
100
50
0
-50
-100
-100
-50
0
50
100
Meters
Probability of 95 %
Max ATE = 13 Meters
Sigma = .029 usec
Sigma = .028 usec
Rho = .518
Max CTE = 28 Meters

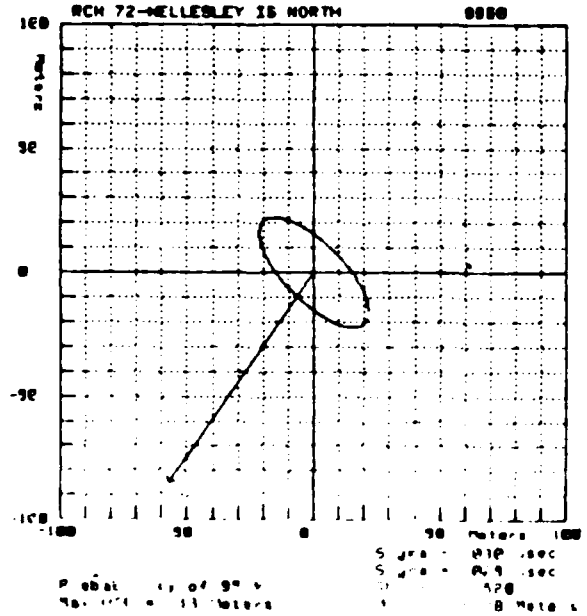
RCH 72-WELLESLEY IS NORTH
9880
Meters
100
50
0
-50
-100
-100
-50
0
50
100
Meters

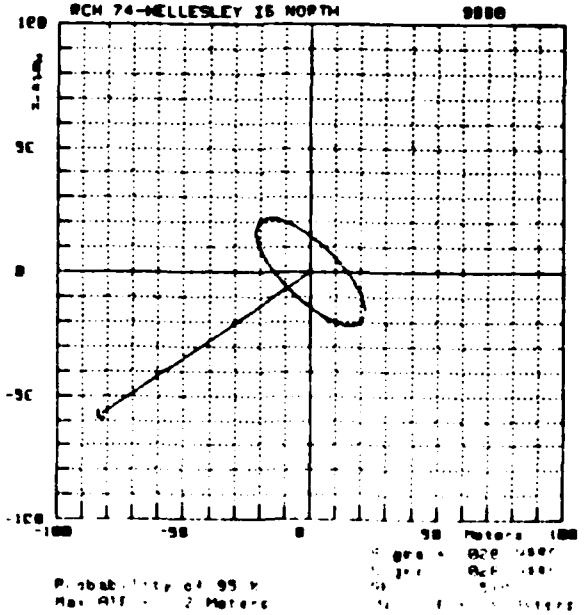
RCH 74-WELLESLEY IS NORTH
9880
Meters
100
50
0
-50
-100
-100
-50
0
50
100
Meters

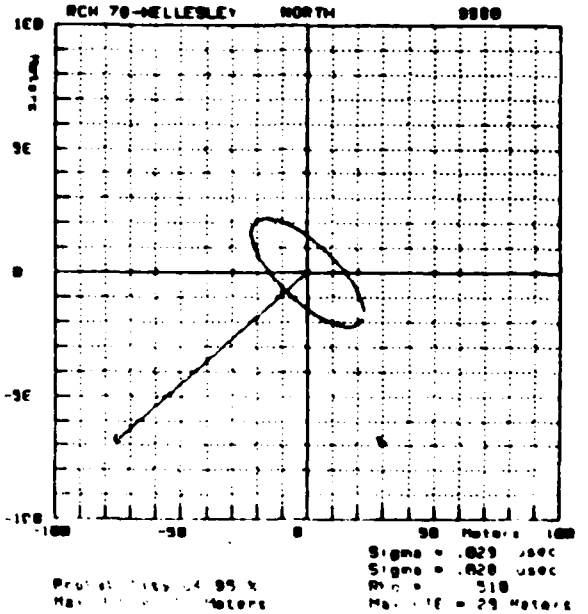
RCH 78-WELLESLEY NORTH
9880
Meters
100
50
0
-50
-100
-100
-50
0
50
100
Meters
Sigma = .029 usec
Sigma = .028 usec
Rho = .518
Max CTE = 29 Meters

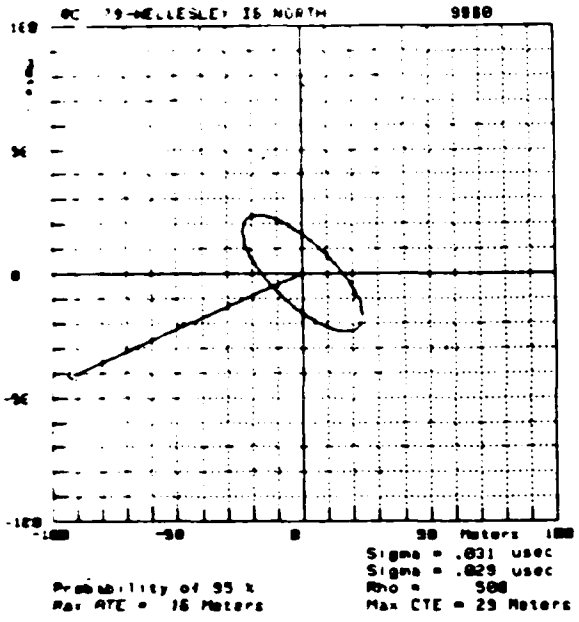
RCH 79→WELLESLEY IS NORTH
9880
Meters
Sigma = .031 usec
Sigma = .029 usec
Rho = .508
Probability of 95 %
Max ATE = 16 Meters
Max CTE = 29 Meters

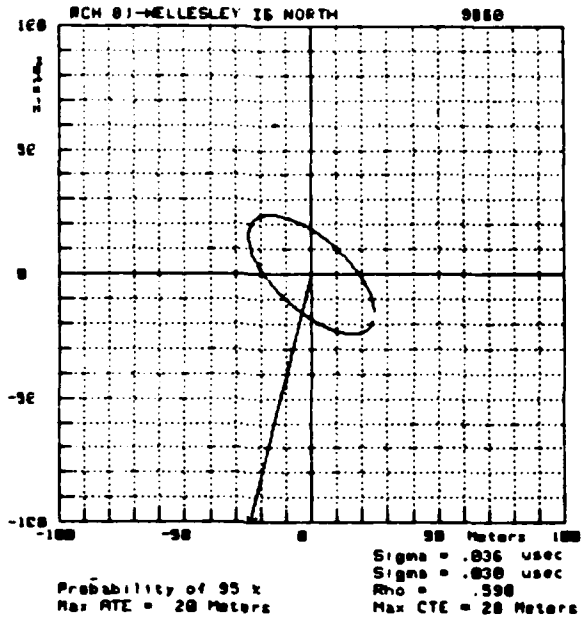
RCH 81→WELLESLEY IS NORTH
9880
Meters
Sigma = .036 usec
Sigma = .030 usec
Rho = .590
Probability of 95 %
Max ATE = 20 Meters
Max CTE = 28 Meters

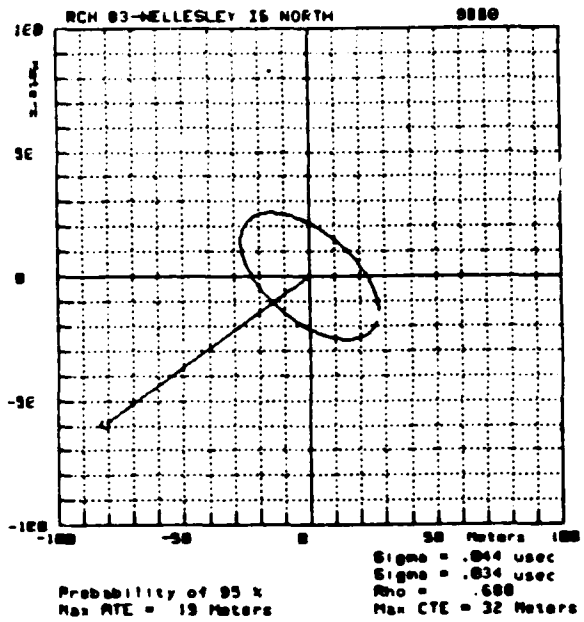
RCH 83→WELLESLEY IS NORTH
9880
Meters
Sigma = .044 usec
Sigma = .034 usec
Rho = .688
Probability of 95 %
Max ATE = 19 Meters
Max CTE = 32 Meters

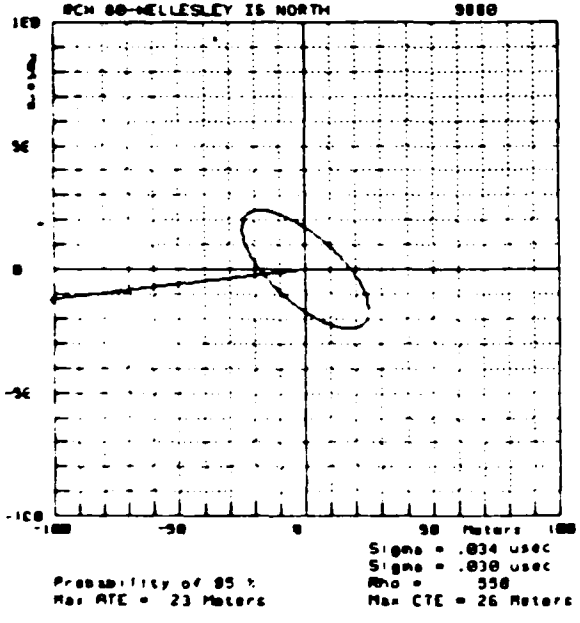
RCH 80→WELLESLEY IS NORTH
9880
Meters
Sigma = .034 usec
Sigma = .030 usec
Rho = .550
Probability of 95 %
Max ATE = 23 Meters
Max CTE = 26 Meters

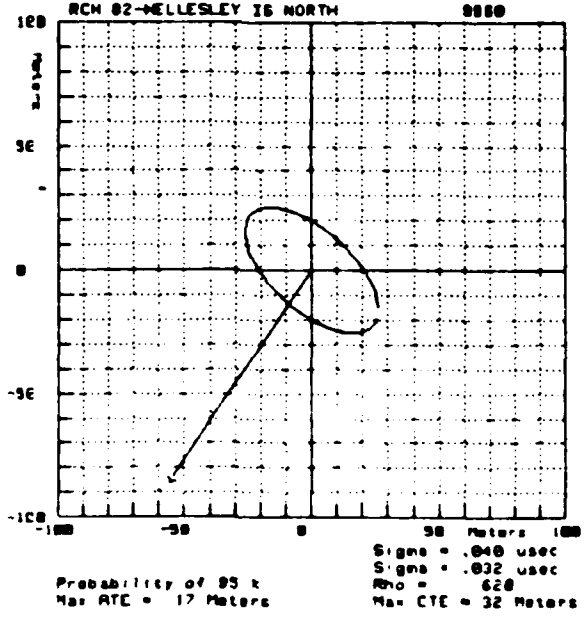
RCH 82→WELLESLEY IS NORTH
9880
Meters
Sigma = .040 usec
Sigma = .032 usec
Rho = .620
Probability of 95 %
Max ATE = 17 Meters
Max CTE = 32 Meters

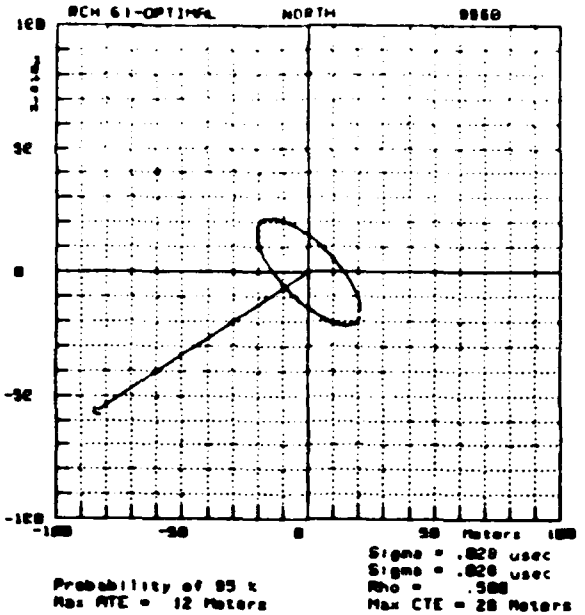
RCH 61-OPTIMAL
NORTH
9860
100
50
0
-50
-100
-100
-50
0
50
Meters
100
Sigma = .020 usec
Sigma = .020 usec
Rho = .500
Max CTE = 28 Meters
Probability of 95 %
Max ATE = 12 Meters

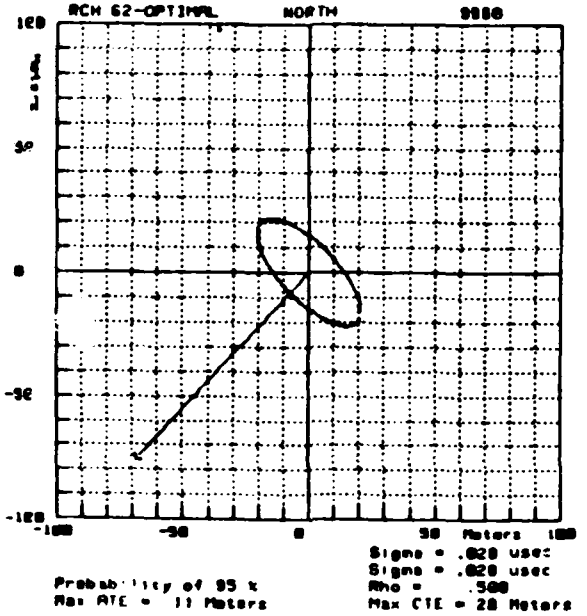
RCH 62-OPTIMAL
NORTH
9860
100
50
0
-50
-100
-100
-50
0
50
Meters
100
Sigma = .020 usec
Sigma = .020 usec
Rho = .500
Max CTE = 28 Meters
Probability of 95 %
Max ATE = 11 Meters

APPENDIX E

DESCRIPTIONS OF ST. LAWRENCE SEAWAY REACHES

REACH DESCRIPTION # 1

MARCH 1982 UTILIZATION OF ARCTEC 1978 REPORT

DESCRIPTION OF SEAWAY REACHES

PILOTING REQUIREMENTS

Reach Description	Reach Number	Upbound Channel Bearing (°T)	+ = R - = L Turns	Channel Mileage* Begin	End	Length	Channel Width (ft)	(m)	Cross Track Req.(1) ±(m)	Nav Aids Adequate Y
Montreal Harbor	1	167	0	0	1.3	1.3	200	61.0	7.2	
Cartier Bridge	2	167	0	1.3	1.3	0	200	61.0	7.2	Y
South Shore Canal	3	167	0	1.3	3	1.7	225	68.6	8.7	Y
St. Lambert Lock	4	167	0	3	3.25	0.25	80	24.4	N/A	Y
Vertical Lift Bridge	5	167	- 2	3.25	3.25	0	80	24.4	N/A	Y
South Shore Canal	6	165	-12	3.25	4	0.75	280	85.3	12.1	Y
	7	157	+20	4	5.25	1.25	280	85.3	12.1	Y
	8	177	+22	5.25	7.85	2.60	280	85.3	12.1	Y
	9	199	+22	7.85	8.5	0.65	280	85.3	12.1	Y
	10	221	+20	8.5	9.25	0.75	280	85.3	12.1	Y
	11	241	+19	9.25	10	0.75	280	85.3	12.1	Y
	12	260	+ 9	10	10.5	0.5	280	85.3	12.1	Y
	13	269	0	10.5	11.75	1.25	280	85.3	12.1	Y
St. Catherine Lock	14	269	0	11.75	12	0.25	80	24.4	N/A	Y

*STATUTE MILES

(1) Kroon, (0.2w-5) meters

DESCRIPTION OF SEAWAY REACHES

PILOTING REQUIREMENTS

Reach Description	Reach Number	Upbound Channel Bearing (°T)	+ = R - = L Turns	Channel Mileage* Begin	End	Length	Channel Width (ft)	(m)	Cross Track Req.(1) ±(m)	Nav Aids Adequate Y
South Shore Canal	15	269	-14	12	13.25	1.25	250	76.2	10.2	Y
	16	255	+22	13.25	14.75	1.50	250	76.2	10.2	Y
	17	277	+26	14.75	15.75	1.00	250	76.2	10.2	Y
	18	303	-26	15.75	17.37	1.62	250	76.2	10.2	Y
	19	278	-29	17.37	18	0.63	225	68.6	8.7	Y
South Shore Canal	20	249	+17	18	20	2	250	76.2	10.2	Y
Entrance to Lake St. Louis	21	266	-43	20	22.3	2.3	500	152.4	25.5	
	22	223	+28.3	22.3	27	4.7	650	198.1	34.6	
	23	241.3	-23.3	27	30	3	750	228.6	40.72	
	24	218	- 8.7	30	31.5	1.5	1400	426.7	80.3	
Beauharnois and Melocheville Locks	25	209.3	0	31.5	32.5	1	80	24.4	N/A	Y
Beauharnois Canal	26	209.3	+16.7	32.5	36	3.5	590	179.8	31.0	
	27	226	+11	36	38.5	2.5	590	179.8	31.0	
	28	237	0	38.5	39	0.5	590	179.8	31.0	
St. Louis Bridge	29	237	+11.3	38.5	38.5	0	180	54.9	6.0	
	30	248.3	+21.7	39	40.5	1.5	590	179.8	31.0	
	31	270	+17	40.5	44.5	4	590	179.8	31.0	

PILOTING REQUIREMENTS

Reach Description	Reach Number	Upbound Channel Bearing (°T)	+ = R - = L Turns	Channel Mileage* Begin	End	Length	Channel Width (ft)	(m)	Cross Track Req.(1) ±(m)	Nav Aids Adequate Y
Valley Field Bridge	32	[illegible]	0	44.5	44.5	0	180	54.9	6.0	
	33	[illegible]	-24	44.5	47	2.5	590	179.8	31.0	
	34	263	-20.6	47.0	51.4	4.4	500	152.4	25.5	
Lake St. Francis	35	242.4	-33.4	51.4	54.2	2.8	1160	353.6	65.7	
	36	209	+25	54.2	56.4	2.2	1160	353.6	65.7	
	37	234	+32	56.4	63	6.6	1160	353.6	65.7	
	38	266	-37.8	63	64.2	1.2	480	146.3	24.3	
Lancaster Bar	39	228.2	-21	64.2	66.4	2.2	450	137.2	22.4	
	40	207.2	+18.35	66.4	67.8	1.4	450	137.2	22.4	
	41	225.55	+13.6	67.8	70.3	2.5	450	137.2	22.4	
	42	239.15	+23.35	70.3	72.5	2.2	460	140.2	23.0	
	43	262.5	-21.4	72.5	73.6	1.1	480	146.3	24.3	
Glengary Anchorage	44	241.1	-32.1	73.6	77.1	3.5	650	198.1	34.6	
Cornwall and St. Regis Island	45	209	+27	77.1	78	.9	460	140.2	23.0	
Turn Cornwall Island	46	236	+42	78	79	1	700	213.4	37.7	
	47	278	-44	79	80	1	460	140.2	23.0	
Turn Seaway International Bridge (Polly's Gut)	48	234	+33	80	82	2	460	140.2	23.0	
	49	267	0	82	82	0	600	182.9	31.6	
	50	267	0	82	83	1	700	213.4	37.7	
	51	267	+ 5	83	84	1	700	213.4	37.7	

DESCRIPTION OF SEAWAY REACHES

PILOTING REQUIREMENTS

Reach Description	Reach Number	Upbound Channel Bearing (°T)	+ = R - = L Turns	Channel Mileage* Begin	End	Length	Channel Width (ft)	(m)	Cross Track Req.(1) ±(m)	Nav Aids Adequate Y
Snell Lock	52	272	-11	84	84	0	80	24.4	N/A	Y
Intermediate Pool	53	261	- 1	84	87.5	3.5	442	134.7	21.9	Y
Eisenhower Lock	54	260	- 3	87.5	87.5	0	80	24.4	N/A	Y
	55	257	0	87.5	90.5	3	442	134.7	21.9	
Wiley-Dondero Channel	56	257	0	90.5	92.5	2	442	134.7	21.9	
	57	257	-24	92.5	95	2.5	442	134.7	21.9	
Cat Island Shoal	58	233	+15	95	96	1	610	185.9	32.2	
Morrisburg Section	59	248	+14.15	96	99	3	730	222.5	39.5	
	60	262.15	-29.15	99	100	1	730	222.5	39.5	
	61	233	+22	100	101	1	730	222.5	39.5	
	62	255	-35	101	102	1	730	222.5	39.5	
	63	220	+17	102	104	2	730	222.5	39.5	
	64	237	+18.25	104	106	2	600	182.9	31.6	
	65	255.25	-18.25	106	108	2	630	192.0	33.4	
	66	237	-10	108	109	1	610	185.9	32.2	
	67	227	+21	109	110	1	600	182.9	31.6	
	68	248	-5.5	110	110.75	.75	600	182.9	31.6	
	69	242.5	-36.35	110.75	112	1.25	580	176.8	30.4	
	70	206.15	+2.85	112	112.5	.5	400	121.9	19.4	

DESCRIPTION OF SEAWAY REACHES

PILOTING REQUIREMENTS

Reach Description	Reach Number	Upbound Channel Bearing (°T)	+ = R - = L Turns	Channel Mileage* Begin	End	Length	Channel Width (ft)	(m)	Cross Track Req.(1) ±(m)	Nav Aids Adequate Y
Iroquois Lock	71	209	0	112.5	112.75	.25	80	24.4	N/A	Y
Rolling Lift Bridge	72	209	0	112.75	112.75	0	80	24.4	N/A	Y
	73	209	+18.2	112.75	114	1.25	840	256.0	46.2	
	74	227.2	+ 9.8	114	117.5	3.5	500	152.4	25.5	
	75	237	-15.55	117.5	119.5	2	400	121.9	19.4	
	76	221.45	+16.9	119.5	121	1.5	400	121.9	19.4	
	77	238.35	0	121	123	2	450	137.2	22.4	
Ogdensburg-Prescott Bridge	78	238.35	-18.35	123	123	0	550	167.6	28.5	
	79	220	+18	123	124.75	1.75	630	192.0	33.4	
	80	238	-15	124.75	126.5	1.75	730	222.5	39.5	
	81	223	+ 8	126.5	133.5	7	730	222.5	39.5	
	82	231	-11	133.5	136.5	3	730	222.5	39.5	
McNair Island	83	220	+12	136.5	138.25	1.75	730	222.5	39.5	
Skeleton Island	84	232	+ 4	138.25	139	.75	400	121.9	19.4	
Smith Island	85	236	-14	139	140	1	300	91.4	13.3	
Brockville Narrows	86	222	- 5	140	142	2	300	91.4	13.3	
	87	217	-23	142	144	2	550	167.6	28.5	

PILOTING REQUIREMENTS

Reach Description	Reach Number	Upbound Channel Bearing (°T)	+ = R - = L Turns	Channel Mileage* Begin	End	Length	Channel Width (ft)	(m)	Cross Track Req.(1) ±(m)	Nav Aids Adequate Y
Whaleback Shoals	88	194	+24	144	146.5	2.5	610	185.9	32.2	
	89	218	- 9	146.5	151	4.5	610	185.9	32.2	
	90	209	+16	151	154	3	610	185.9	32.2	
	91	225	- 7	154	157	3	600	182.9	31.6	
American Narrows	92	218	- 4	157	159	2	600	182.9	31.6	
	93	214	+ 5	159	160	1	450	137.2	22.4	
	94	219	+16	160	162	2	450	137.2	22.4	
	95	235	0	162	164.5	2.5	450	137.2	22.4	
Thousand Island Bridge	96	235	- 4	164.5	164.5	0	450	137.2	22.4	
	97	231	+ 8	164.5	167	2.5	450	137.2	22.4	
	98	239	-11	167	169.5	2.5	610	185.9	32.2	
	99	228	+18	169.5	170.5	1	610	185.9	32.2	
	100	246	+17	170.5	178	7.5	730	222.5	39.5	
	101	263	-69.8	178	182	4	730	222.5	39.5	
	102	193.2	-40.8	182	186	4	730	222.5	39.5	
Tibbetts Point	103	234		186	190	4	730	222.5	39.5	

REACH DESCRIPTION # 2

Prepared by:

The St. Lawrence Seaway Authority

Operational Services Division

May 1982

GEOMETRIC DESCRIPTION OF SEAWAY REACHES
PILOTING REQUIREMENTS

Reach Description	Reach Number	Upbound Channel Bearing (°T)	+ = R - = L Turns	Channel Length Stat.Miles	Channel Width (ft)	Channel Width (m)	Cross Track Requirements (± from C.L.)	Nav Aids Adequate
CIP2 - Entrance to Lake St.Louis	1	This section is ± 20 miles long. It consists of a confined waterway having two locks. It is considered that nav. aids (lighting, etc) in this reach are adequate and no other system will be required.						
Entrance to Lake St. Louis	2	266	- 42	2.3	600	182		
	3	224	+17.5	4.7	600	182		
	4	241.5	- 23.5	3.0	800	243		
	5	218		1.2	1400	426		
Beauharnois Locks	6	This section is 2.2 miles long. It consists of two locks and an intermediate pool. It is considered that nav. aids in this area are adequate and no other system will be required. Channel bearing is 209.3°.						
Beauharnois Canal	7	208.5	+17.5	2.6	600	182		
	8	226	+11	2.5	600	182		
	9	237	0	0.4	600	182		
St.Louis Bridge	10	237	+11.5	0	180	54		
	11	248.5	+21.5	1.5	600	182		
	12	270.0	+17.5	4.1	600	182		
Valleyfield Bridge	13	287.5	0	0	180	54		
	14	287.5	- 24	2.4	600	182		

GEOMETRIC DESCRIPTION OF SEAWAY REACHES
PILOTING REQUIREMENTS

Reach Description	Reach Number	Upbound Channel Bearing (°T)	+ = R - = L Turns	Channel Length Stat.Miles	Channel Width (ft)	(m)	Cross Track Requirements (± from C.L.)	Nav Aids Adequate
Valleyfield Bridge	15	263.5		4.4	450	137		
			- 21					
Lake St.Francis	16	242.5		2.8	1200	365		
			- 33.5					
	17	209		2.2	900	274		
			+25.5					
	18	234.5		6.6	650	198		
			+32					
	19	266.5		1.2	480	146		
			-37.5					
Lancaster Bar	20	229		2.2	450	137		
			-21.5					
	21	207.5		1.4	450	137		
			+19.5					
	22	226		2.5	450	137		
			+13.5					
	23	239.5		2.2	450	137		
			+23.5					
	24	263		1.1	450	137		
			-22					
Glengarry Anchorage	25	241		3.5	450	137		
			-32					
CWL & St.Regis Island	26	209		.9	450	137		
			+27					
Turn CWL Island	27	236		1	700	213		
			+42					
	28	278		1	450	137		
			-44					
Turn Seaway Int. Bridge	29	234		2	1000	304		
			+33					
	30	267		0	600	182		
			0					
	31	267		0.75	700	213		

GEOMETRIC DESCRIPTION OF SEAWAY REACHES
PILOTING REQUIREMENTS

Reach Description	Reach Number	Upbound Channel Bearing (°T)	+ = R - = L Turns	Channel Length Stat.Miles	Channel Width (ft)	Channel Width (m)	Cross Track Requirements (± from C.L.)	Nav Aids Adequate
Snell & Eisenhower Locks	32	This section is 7.75 miles long. It consists of two locks and an intermediate pool. It is considered that nav. aids in this area are adequate and no other system will be required.						
Wiley-Dondero Canal	33	257		2	450	137		
			0					
	34	257		2.5	600	182		
			-24					
Cat Island Shoal	35	233		1	610	185		
			+15.5					
Morrisburg Section	36	248.5		3	850	259		
			+13.5					
	37	262		1	850	259		
			-29					
	38	233		1	730	222		
			+22					
	39	255		1	700	213		
			-35					
	40	220		2	900	274		
			+17.5					
	41	237.5		2	600	182		
			+17.5					
	42	255		2	600	182		
			-18					
	43	237		1	600	182		
			-10					
	44	227		1	750	228		
			+21					
	45	248		.75	700	213		
			-6.5					
	46	241.5		1.25	700	213		
			-35.5					
	47	206		.5	500	152		

GEOMETRIC DESCRIPTION OF SEAWAY REACHES
PILOTING REQUIREMENTS

Reach Description	Reach Number	Upbound Channel Bearing (°T)	+ = R - = L Turns	Channel Length Stat.Miles	Channel Width (ft)	(m)	Cross Track Requirements (± from C.L.)	Nav Aids Adequate
Iroquois Lock	48	This Section is about 1.1 miles long. It consists of one lock. It is considered that nav. aids in this area are adequate and no other system will be required. Channel bearing is 206°						
	49	206	+21	.7	700	213		
	50	227	+9.5	3.5	600	182		
	51	236.5	-15	2	600	182		
	52	221.5	+16.5	1.5	600	182		
	53	238	0	1.5	600	182		
Ogdensburg/Prescott Bridge	54	238	-18	0	750	228		
	55	220	+18	2.25	630	192		
	56	238	-15	1.75	1000	304		
	57	223	+8	7	1000	304		
	58	231	-8	3	1000	304		
McNair Island	59	223	+10	1.75	550	167		
Skeleton Island	60	233	+4	.75	500	152		
Smith Island	61	236	-14	1	400	121		
Brockville Narrows	62	222	-5	2	400	121		
	63	217	+23	2	650	198		

GEOMETRIC DESCRIPTION OF SEAWAY REACHES

PILOTING REQUIREMENTS

Reach Description	Reach Number	Upbound Channel Bearing (°T)	+ = R - = L Turns	Channel Length Stat. Miles	Channel Width (ft)	(m)	Cross Track Requirements (± from C.L.)	Nav Aids Adequate
Whaleback Shoal	64	194		2.5	610	185		
			+24					
	65	218		1.4	610	185		
			-2					
Superior Shoal	66	216		3.1	610	185		
			-7					
	67	209		1.9	610	185		
			-2					
Sister Island	68	207		1.1	610	185		
			+18					
	69	225		1.2	610	185		
			+3					
Whiskey Island Shoal	70	228		1.8	610	185		
			-10					
American Narrows	71	218		2	600	182		
			-4					
	72	214		1	400	121		
			+5					
	73	219		2	450	137		
			+16					
	74	235		2.5	450	137		
			0					
1000 Island Bridge	75	235		0	450	137		
			-4					
	76	231		2.5	450	137		
			+8					
	77	239		2.5	550	167		
			-11					
	78	228		1	600	182		
			+18					
	79	246		7.5	730	222		
			+17					
	80	263		4	800+	243+		
			-69.5					

GEOMETRIC DESCRIPTION OF SEAWAY REACHES
PILOTING REQUIREMENTS

Reach Description	Reach Number	Upbound Channel Bearing (°T)	+ = R - = L Turns	Channel Length Stat.Miles	Channel Width (ft)	(m)	Cross Track Requirements (± from C.L.)	Nav Aids Adequate
1000 Island Bridge	81	193.5	+19.5	4	800+	243+		
	82	213	+21	1.5	1080	329		
	83	234		3.5	2500	762		

APPENDIX F

EXAMPLES OF DATA COLLECTION PROBLEMS

Comments on Examples

Example	Comment
Figure F-1	The printout is from the Cote Ste. Catherine site Ad Hoc equipment. The column labeled "GRI" provides a measure of the receiver oscillator stability. It should be very steady at some value in the range 99600.00 +/- 0.20. The significant variation in this measure of oscillator performance is reflected in the unstable time difference readings. This malfunction was the major cause of lost data at Cote Ste. Catherine.
Figure F-2	The printout is from the Iroquois Lock site Ad Hoc equipment. (Note the stable oscillator readings.) Receiver estimated signal-to-noise ratios for the M, W, X, Y, and Z signals are listed in the last five columns, respectively. Notice how the SNR's periodically drop substantially and then return to normal. Related fluctuations in the time differences (columns 2 through 5) can be seen. At present, the cause of these fluctuations is unknown.
Figures F-3 and F-4	The printouts are from the Prescott Buoy Auditing equipment sets. The data of figure F-3 was obtained on Julian Day 116. The column labeled "DB" represents the deviation of the 9960-X average from the nominal value of 28130.93 in tens of nanoseconds. The column labeled "SDB" represents the standard deviation of the time differences, also in tens of nanoseconds, over the period for which the average value in column "DB" was computed. The fluctuations in the averages are extraordinarily high as are the standard deviations. At this point, it could have been concluded there was a receiver problem. Figure F-4 shows the data from the same site 2 weeks later. The receiver is still abnormal. The two figures, taken together, illustrate the major characteristic of the data bases from the high density data collection sites: 2 weeks after the problem was first evident, it still has not been detected and corrected. (The receiver was eventually changed on Julian Day 159 - more than 6 weeks after the problems were evident.)

Comments on Examples (con't)

Example	Comment
Figure F-5	The printout is from the Beauharnois site Ad Hoc equipment set. Two problems are illustrated. Notice the third column. The correct 9960-X time difference reading is about 27579. usec. The receiver is tracking on the wrong cycle (thus the reading is about 10 usec low). Later it is tracking on the correct cycle (the heading "INTERNAV..... ....300 BAUD" means an operator intervened). Still later it is again tracking 10 usec low. The second problem is "when did this all occur?" In the heading, the notation "00/00/00 00:00" means "it is now midnight on the 0th day of the 0th month of the 0th year." (Should a star have been visible in the midnight clear or did that happen a year later?) After seven more readings are taken, and, after data collection was interrupted for some indeterminate amount of time, we are again led to believe it is still midnight on the same day. These unknown times of observation make the data unusable for Differential Loran-C analysis purposes.
Figure F-5	The data here was also obtained at Beauharnois. The two sets of data show a substantial offset. This is not a "seasonal effect" nor is it the result of an equipment problem. Careful investigation by the authors revealed the antenna was moved to a new location during this period (Loran-C works!)

INTERNAV LC404 00/00/00 00:00 06020 GRI SPACING 300 BAUD

GRI	ATD	BTD	CTD	DTD	MSN	ASN	BSN	CSN	DSN
99600.07	14015.64	27464.65	.	.	+06	+05	-01		
99600.17	14015.41	27464.61	.	.	+07	+05	-03		
99600.07	14015.50	27464.62	.	.	+06	+04	-05		
99600.17	14015.46	27464.49	.	.	+06	+03	-07		
99600.07	14015.69	27464.93	.	.	+06	+04	-06		
99600.07	14015.43	27464.74	.	.	+07	+05	-05		
99600.08	14015.44	27464.74	.	.	+07	+04	-06		
99599.97	14015.54	27464.95	.	.	+07	+04	-07		
99600.07	14015.76	27464.89	.	.	+06	+04	-05		
99600.16	14015.54	27464.77	.	.	+06	+04	-05		
99600.17	14015.44	27464.44	45250.46	.	+06	+04	-08		
99600.06	14015.55	27464.62	45282.31	.	+06	+04	-07	-20	
99600.17	14015.45	27464.37	45281.69	.	+06	+04	-07	-17	
99600.07	14015.75	27464.73	45282.44	.	+06	+03	-07	-20	
99599.97	14015.66	27464.66	45282.24	.	+06	+04	-07	-20	
99600.06	14015.47	27464.46	45282.43	.	+07	+06	-05	-20	
99600.07	14015.64	27464.66	45282.21	.	+07	+05	-05	-19	

Figure F-1

99600.06	14965.29	28053.28	45401.36	60098.34	+08	+06	+03	+03	+04
99600.05	14965.28	28053.31	45401.39	60098.41	+08	+06	+03	+04	+04
99600.05	14965.30	28053.29	45401.41	60098.42	+05	+00	-03	-03	-03
99600.06	14965.30	28053.29	45401.42	60098.38	+08	+05	+03	+03	+04
99600.05	14965.27	28053.30	45401.43	60098.43	+02	-06	-13	-15	-14
99600.06	14965.31	28053.28	45401.42	60098.34	+05	-02	-06	-05	-05
99600.04	14965.33	28053.31	45401.34	60098.37	+08	+05	+04	+04	+05
99600.06	14965.33	28053.32	45401.34	60098.34	+07	+01	-03	-03	-03
99600.05	14965.28	28053.33	45401.25	60098.20	+09	+06	+04	+04	+05
99600.05	14965.31	28053.31	45401.27	60098.28	+09	+06	+04	+04	+05
99600.05	14965.30	28053.31	45401.30	60098.31	+09	+06	+04	+04	+04
99600.06	14965.30	28053.31	45401.41	60098.32	+09	+06	+05	+05	+05
99600.05	14965.30	28053.31	45401.46	60098.30	+08	+05	+03	+04	+05
99600.04	14965.28	28053.41	45401.48	60098.34	+05	-03	-10	-10	-09
99600.05	14965.43	28053.18	45401.19	60098.39	+02	-10	-20	-20	-20
99600.06	14965.29	28053.30	45401.56	60098.21	+08	+06	+03	+03	+04
99600.05	14965.32	28053.29	45401.58	60098.25	+08	+06	+04	+03	+04
99600.06	14965.35	28053.34	45401.62	60098.25	+08	+06	+03	+04	+04
99600.06	14965.28	28053.35	45401.59	60098.23	+08	+06	+03	+03	+04
99600.06	14965.32	28053.29	45401.55	60098.23	+08	+06	+02	+03	+04
99600.06	14965.32	28053.33	45401.53	60098.18	+08	+06	+03	+04	+04
99600.06	14965.33	28053.30	45401.56	60098.18	+08	+06	+03	+04	+04
99600.05	14965.35	28053.29	45401.52	60098.17	+08	+06	+03	+03	+04

Figure F-2

LORAN-C @ PRESCOTT CG BASE
SAMPLE SIZE 100
TIME 9: 8:35 JULIAN DAY: 116/365 YEAR: 1982
TD-A 15097.89 TD-B 28130.93 TD-C 45411.35 TD-D 60095.14
RX#1 (FOR TD A,B) S/N: 1006 RX#2 (FOR TD C,D) S/N: 1017

TIME	! NA	DA	SDA	! NB	DB	SDB	! NC	DC	SDC	! ND	DD	SDD
9:12: 8	!100	12	1	!100	11	2	! 99	19	2	!100	4	2
9:15:31	!100	13	2	!100	13	4	!100	18	3	!100	6	2
9:18:54	!100	11	3	! 99	17	3	!100	19	3	!100	7	2
9:22:17	!100	12	3	! 99	13	3	!100	19	2	!100	4	2
9:25:40	!100	11	2	! 99	10	2	!100	17	2	!100	5	2
9:29: 3	!100	12	3	!100	12	2	!100	18	3	!100	6	2
9:32:27	!100	11	4	!100	15	7	!100	19	6	!100	4	4
9:35:50	!100	12	7	! 99	24	7	!100	19	5	!100	8	4
9:39:13	!100	10	3	!100	15	4	! 91	20	4	! 91	5	4
9:42:36	!100	14	3	! 99	16	3	!100	20	4	!100	7	2
9:45:59	!100	15	3	!100	15	4	!100	21	3	!100	6	3
9:49:23	!100	18	3	!100	7	6	!100	20	3	!100	6	3
9:52:46	!100	18	3	!100	12	4	!100	21	3	!100	8	2
9:56: 9	!100	18	2	!100	14	3	!100	22	2	!100	7	2
9:59:32	!100	19	2	!100	18	4	!100	20	3	!100	8	2

Figure F-3

LORAN-C @ PRESCOTT C.G. BASE
SAMPLE SIZE 100
TIME 22:31: 6 JULIAN DAY: 130/365 YEAR: 1982
TD-A 15097.89 TD-B 28130.93 TD-C 45411.35 TD-D 60095.14
RX#1 (FOR TD A,B) S/N: 1006 RX#2 (FOR TD C,D) S/N: 1017

TIME	! NA	DA	SDA	! NB	DB	SDB	! NC	DC	SDC	! ND	DD	SDD
22:34:37	!100	7	3	!100	14	4	! 0	9999	•••	! 0	9999	•••
22:37:59	!100	5	4	!100	14	5	! 0	9999	•••	! 0	9999	•••
22:41:21	!100	6	3	!100	18	4	! 0	9999	•••	! 0	9999	•••
22:44:43	!100	5	3	!100	13	4	! 0	9999	•••	! 0	9999	•••
22:48: 5	!100	5	3	!100	6	3	! 0	9999	•••	! 0	9999	•••
22:51:28	!100	4	3	!100	11	6	! 0	9999	•••	! 0	9999	•••
22:54:50	!100	5	3	!100	4	8	! 0	9999	•••	! 0	9999	•••
22:58:12	!100	4	5	!100	15	10	! 0	9999	•••	! 0	9999	•••
23: 1:34	!100	5	3	!100	13	5	! 0	9999	•••	! 0	9999	•••
23: 4:56	!100	5	4	!100	12	4	! 0	9999	•••	! 0	9999	•••
23: 8:19	!100	8	4	!100	14	4	! 0	9999	•••	! 0	9999	•••
23:11:41	!100	5	3	!100	14	6	! 0	9999	•••	! 0	9999	•••
23:15: 3	!100	9	3	!100	12	5	! 0	9999	•••	! 0	9999	•••
23:18:25	!100	9	4	!100	12	9	! 0	9999	•••	! 0	9999	•••
23:21:47	!100	5	3	!100	16	12	! 0	9999	•••	! 0	9999	•••
23:25: 9	!100	8	3	!100	9	4	! 0	9999	•••	! 0	9999	•••
23:28:32	!100	4	4	!100	19	5	! 0	9999	•••	! 0	9999	•••

Figure F-4

```
99599.92 14209.13 27569.30 45318.92 60151.02   +08 +07 +03 +00 +02
99599.92 14209.13 27569.23 45318.90 60150.97   +08 +06 +05 +02 +04
99599.92 14209.16 27569.24 45318.85 60151.04   +08 +06 +05 +01 +03
99599.92 14209.11 27569.30 45318.86 60150.96   +08 +06 +04 +02 +03
99599.93 14209.13 27569.21 45318.79 60150.94   +08 +07 +05 +02 +03
99599.92 14209.14 27569.26 45318.78 60150.94   +08 +06 +04 +02 +04
99599.93 14209.13 27569.30 45318.82 60150.99   +08 +06 +04 +03 +04
99599.92 14209.13 27569.24 45318.87 60151.04   +08 +06 +04 +03 +04
99599.93 14209.11 27569.24 45318.96 60151.10   +08 +07 +04 +02 +04
99599.92 14209.13 27569.23 45319.04 60151.08   +08 +07 +00 -03 -01
  INTERNAV    LC404    00/00/00    00:00   06020 GRI SPACING   300 BAUD

  GRI       ATD       BTD       CTD       DTD       MSN ASN BSN CSN DSN
99599.93 14209.12 27579.47         .         .     +08 +06 +04
99599.92 14209.14 27579.50         .         .     +08 +07 +04
99599.92 14209.18 27579.52         .         .     +08 +07 +04
99599.92 14209.12 27579.46         .         .     +08 +07 +05
99599.92 14209.15 27579.52         .         .     +08 +07 +05
99599.93 14209.10 27579.47         .         .     +08 +07 +05
99599.92 14209.15 27579.48 45308.97 60151.13   +08 +07 +05 -07 -0
  INTERNAV    LC404    00/00/00    00:00   06020 GRI SPACING   300 BAUD

  GRI       ATD       BTD       CTD       DTD       MSN ASN BSN CSN DSN
99599.93 14209.08 27569.31 45319.18 60151.17   +08 +07 +00 -03 -01
99599.92 14209.07 27569.22 45309.11 60151.05   +08 +07 +01 -07 -01
99599.92 14209.11 27569.28 45309.06 60151.12   +08 +07 +00 -07 -02
99599.92 14209.11 27569.25 45309.13 60151.11   +08 +07 +00 -07 -0
99599.92 14209.02 27569.26 45308.66 60151.10   +08 +06 +01 -14 -0
99599.93 14209.12 27569.33 45309.01 60151.06   +08 +06 +00 -0
99599.94 14209.15 27569.31 45309.08 60150.85   +08 +06 +01 -0
99599.93 14209.12 27569.30 45309.03 60150.68   +08 +06 +00 -07 -0
99599.93 14209.13 27569.30 45308.95 60150.75   +08 +06 +00 -0
99599.91 14209.04 27569.23 45308.91 60150.59   +08 +07 +00 -0
99599.91 14209.13 27569.25 45308.93 60150.67   +08 +07 +01 -07 -
99599.94 14209.13 27569.23 45308.95 60150.66   +08 +07 +00 -0
```

Figure F-5

```
99599.87 14209.62 27579.17         .         .     +08 +06 +05
99599.88 14209.62 27579.19         .         .     +08 +07 +04
99599.87 14209.63 27579.16         .         .     +09 +07 +05
99599.87 14209.61 27579.18         .         .     +08 +06 +05
99599.87 14209.62 27579.17         .         .     +08 +06 +05
99599.87 14209.63 27579.20         .         .     +08 +07 +05
99599.87 14209.61 27579.22         .         .     +08 +07 +05
99599.87 14209.65 27579.15         .       99.92 14208.93 27579.07 -
  +13 +07 +05 -08      00 00 00 00 45
  INTERNAV    LC404    01/20/82    15:55   06020 GRI SPACING   300 BAUD

  GRI       ATD       BTD       CTD       DTD       MSN ASN BSN CSN DSN
99599.90 14208.98 27579.06 45308.51 55396.05   +13 +06 +05 -07
99599.90 14208.94 27579.10 45308.53 55308.05   +11 +06 +05 -
99599.88 14208.97 27579.10 45308.50 55000.06   +10 +06 +05 -08
99599.89 14208.97 27579.07 45308.46 55836.05   +11 +06 +05 -0
99599.89 14208.93 27579.06 45308.46 55407.05   +11 +07 +04 -0
99599.89 14208.94 27579.10 45308.43 56067.05   +12 +07 +05 -
99599.90 14208.95 27579.08 45308.47 56078.04   +13 +07 +04 -0
99599.91 14208.95 27579.10 45308.39 55352.04   +12 +07 +04 -0
99599.92 14208.99 27579.09 45308.50 55220.04   +13 +06 +04 -0
99599.92 14208.97 27579.10 45308.51 55935.04   +11 +06 +04 -
99599.91 14208.99 27579.06 45308.49 55605.04   +11 +06 +04 -
```

Figure F-6

APPENDIX G

ERROR ELLIPSES FOR NEW CONFIGURATION

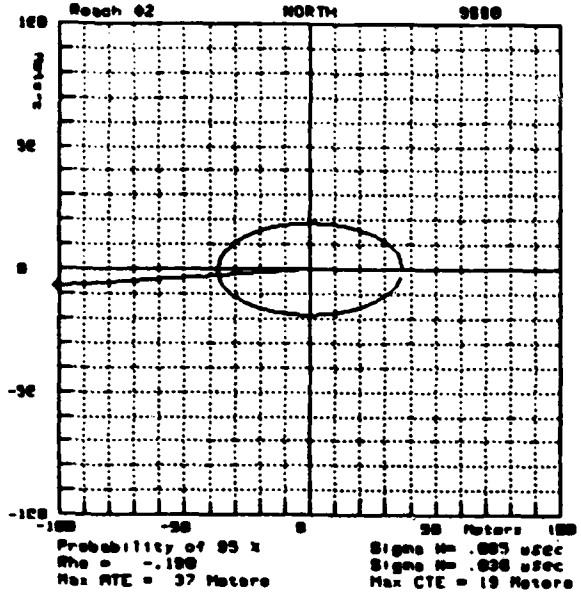
Reach 02
NORTH
9880
100
50
0
-50
-100
-100
-50
0
50
100
Meters
Probability of 95 %
Rho = -.190
Max ATE = 37 Meters
Sigma N= .085 usec
Sigma E= .036 usec
Max CTE = 19 Meters

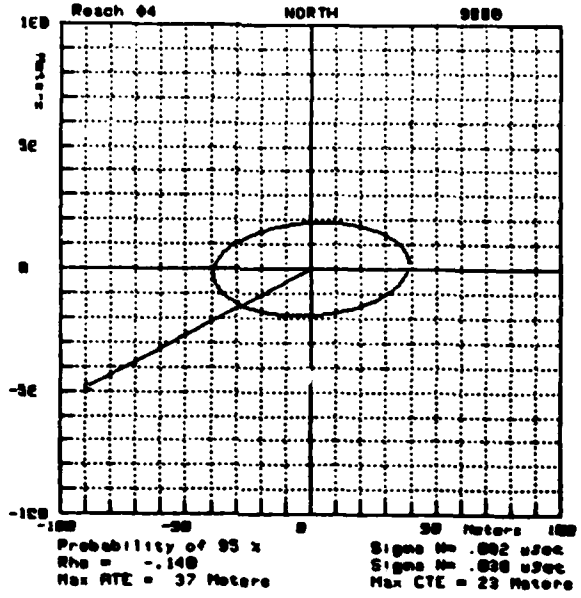
Reach 04
NORTH
9880
100
50
0
-50
-100
-100
-50
0
50
100
Meters
Probability of 95 %
Rho = -.140
Max ATE = 37 Meters
Sigma N= .082 usec
Sigma E= .030 usec
Max CTE = 23 Meters

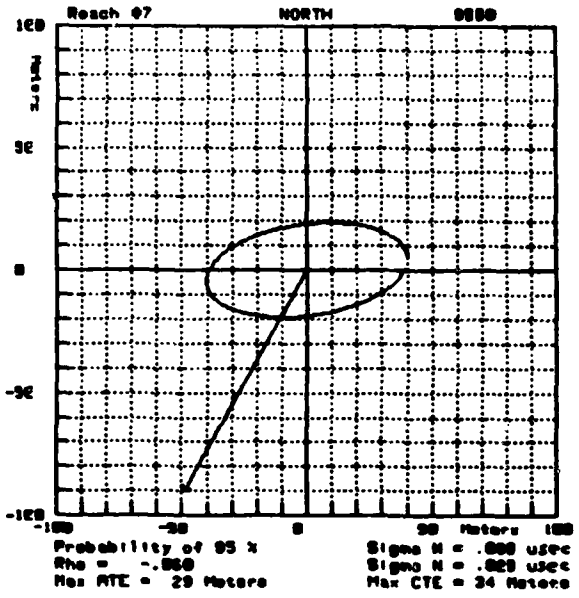
Reach 07
NORTH
9880
100
50
0
-50
-100
-100
-50
0
50
100
Meters
Probability of 95 %
Rho = -.060
Max ATE = 29 Meters
Sigma N = .088 usec
Sigma N = .029 usec
Max CTE = 34 Meters

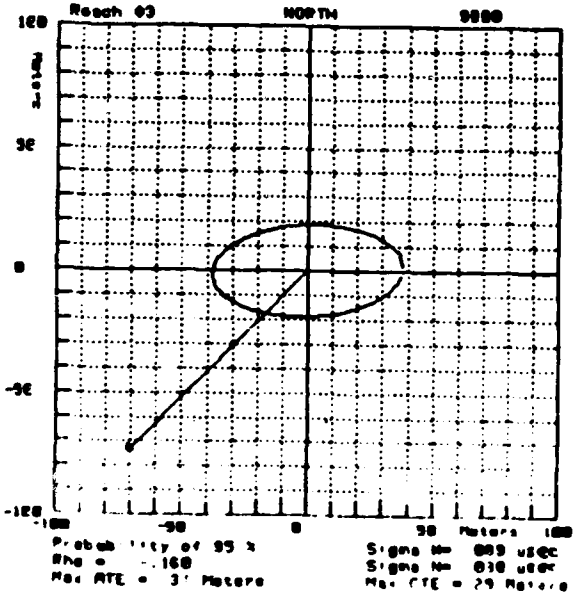
Reach 03
NORTH
9880
100
50
0
-50
-100
-100
-50
0
50
100
Meters
Probability of 95 %
Rho = -.160
Max ATE = 31 Meters
Sigma N= 089 usec
Sigma E= 030 usec
Max CTE = 29 Meters

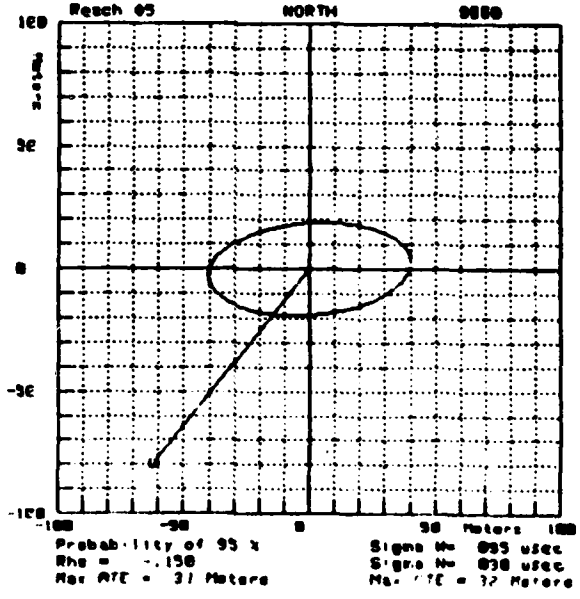
Reach 05
NORTH
9880
100
50
0
-50
-100
-100
-50
0
50
100
Meters
Probability of 95 %
Rho = -.150
Max ATE = 31 Meters
Sigma N= 095 usec
Sigma E= 030 usec
Max CTE = 32 Meters

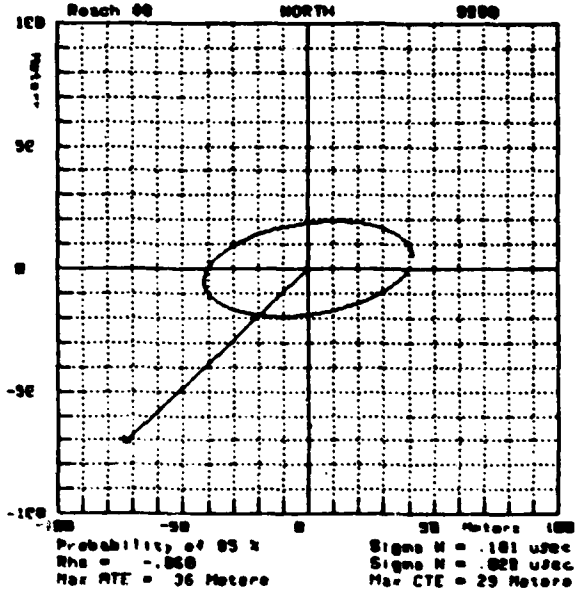
Reach 08
NORTH
9880
100
50
0
-50
-100
-100
-50
0
50
100
Meters
Probability of 95 %
Rho = -.060
Max ATE = 36 Meters
Sigma N = .101 usec
Sigma E = .029 usec
Max CTE = 29 Meters

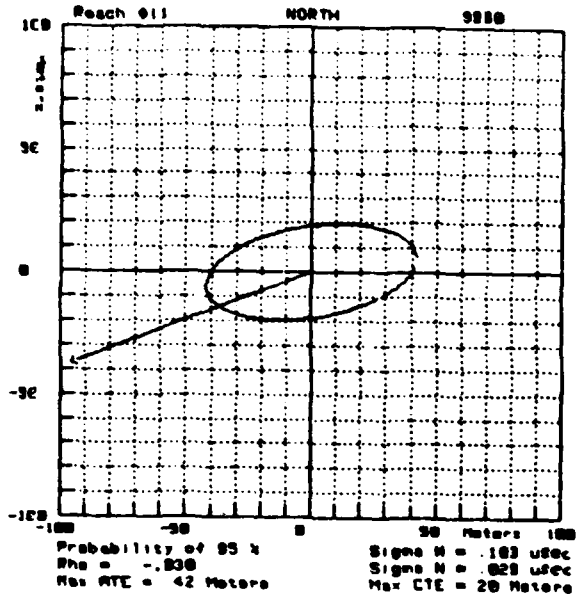
Reach #11
NORTH
9880
100
50
0
-50
-100
-100
-50
0
50
100
Meters
Probability of 95 %
Rho = -.838
Max ATE = 42 Meters
Sigma N = .103 usec
Sigma N = .028 usec
Max CTE = 20 Meters

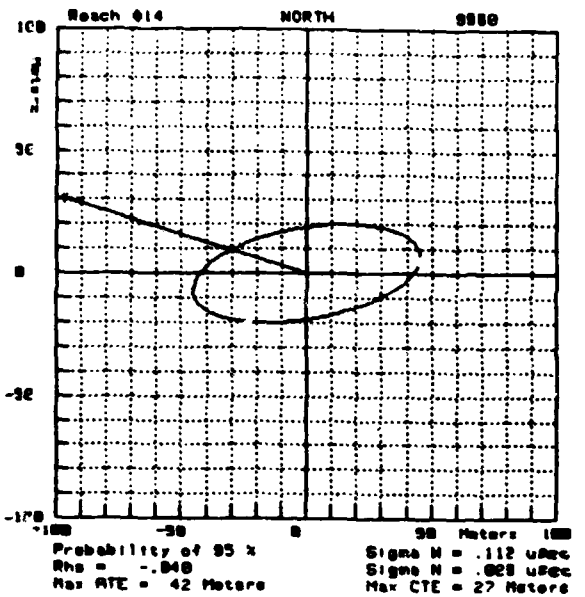
Reach #14
NORTH
9880
100
50
0
-50
-100
-100
-50
0
50
100
Meters
Probability of 95 %
Rho = -.840
Max ATE = 42 Meters
Sigma N = .112 usec
Sigma N = .028 usec
Max CTE = 27 Meters

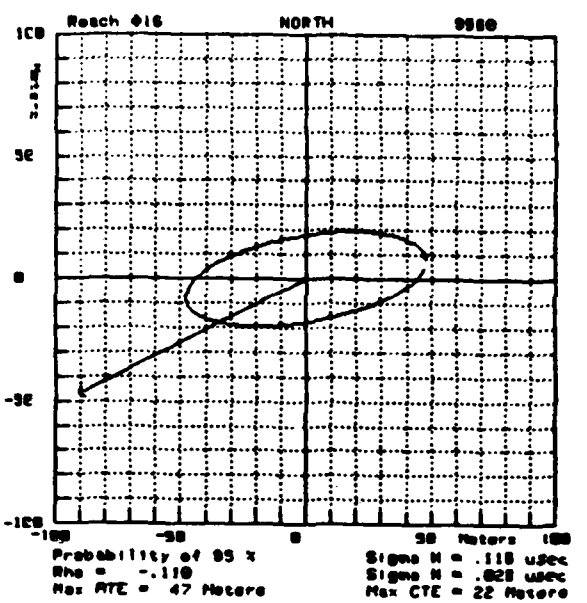
Reach #16
NORTH
9880
100
50
0
-50
-100
-100
-50
0
50
100
Meters
Probability of 95 %
Rho = -.110
Max ATE = 47 Meters
Sigma N = .118 usec
Sigma N = .028 usec
Max CTE = 22 Meters

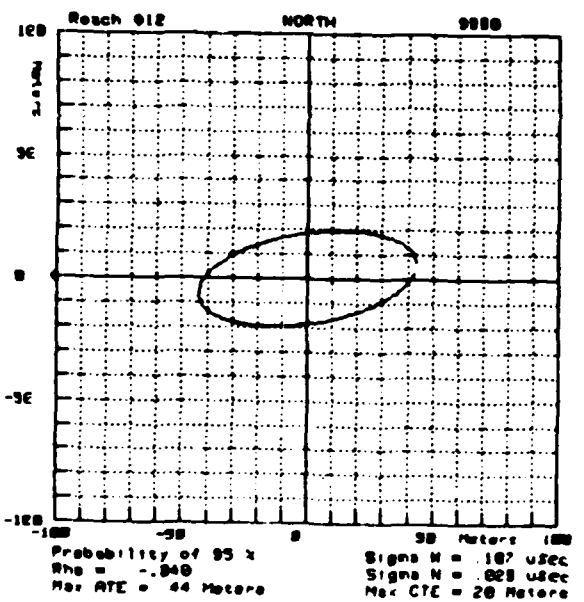
Reach #12
NORTH
9880
100
50
0
-50
-100
-100
-50
0
50
100
Meters
Probability of 95 %
Rho = -.840
Max ATE = 44 Meters
Sigma N = .107 usec
Sigma N = .028 usec
Max CTE = 20 Meters

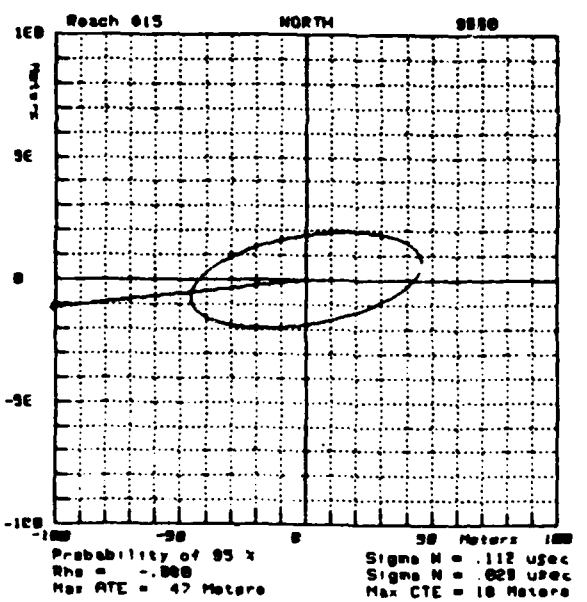
Reach #15
NORTH
9880
100
50
0
-50
-100
-100
-50
0
50
100
Meters
Probability of 95 %
Rho = -.888
Max ATE = 47 Meters
Sigma N = .112 usec
Sigma N = .028 usec
Max CTE = 18 Meters

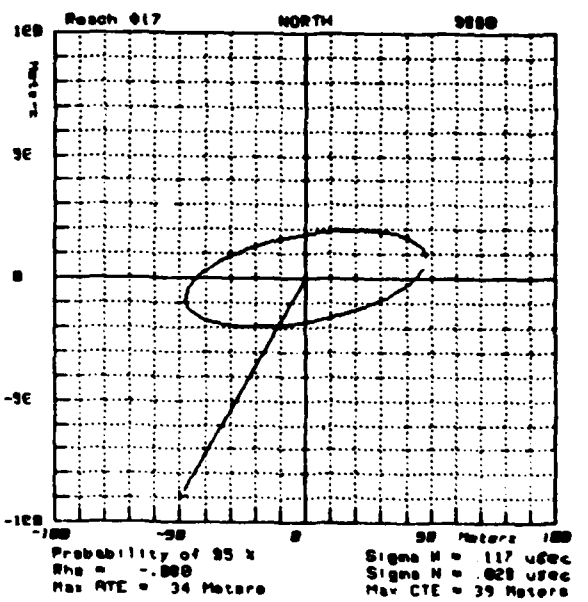
Reach #17
NORTH
9880
100
50
0
-50
-100
-100
-50
0
50
100
Meters
Probability of 95 %
Rho = -.880
Max ATE = 34 Meters
Sigma N = .117 usec
Sigma N = .028 usec
Max CTE = 39 Meters

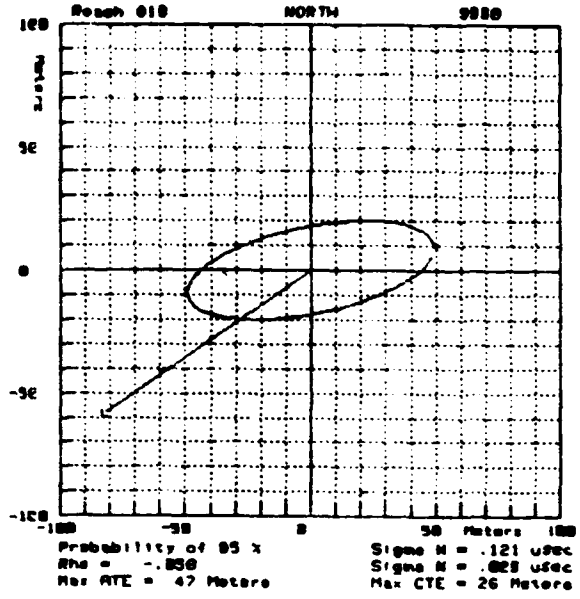
Reach 018
NORTH
9950
Meters
100
50
0
-50
-100
-100
-50
0
50
Meters
100
Probability of 95 %
Rho = -.850
Max ATE = 47 Meters
Sigma N = .121 usec
Sigma N = .028 usec
Max CTE = 26 Meters

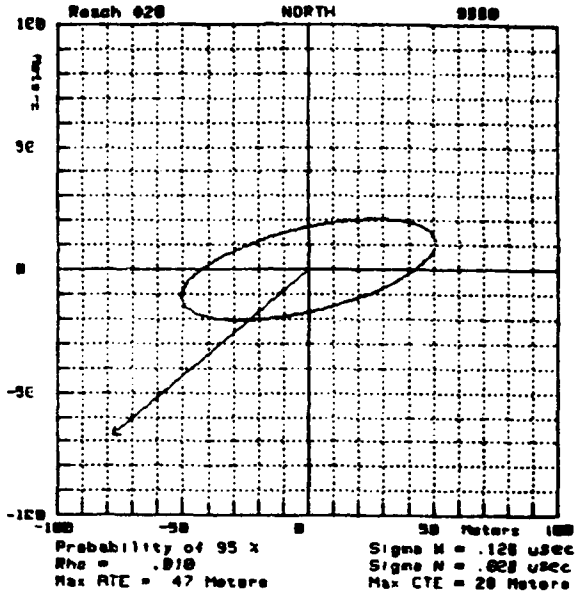
Reach 020
NORTH
9950
Meters
100
50
0
-50
-100
-100
-50
0
50
Meters
100
Probability of 95 %
Rho = .910
Max ATE = 47 Meters
Sigma N = .128 usec
Sigma N = .028 usec
Max CTE = 28 Meters

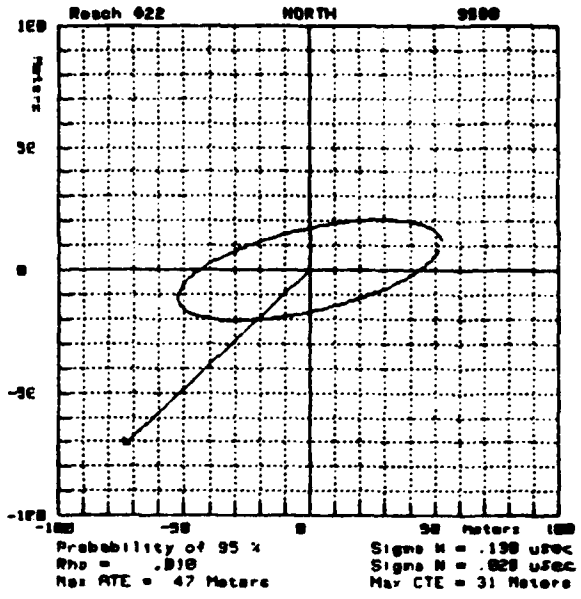
Reach 022
NORTH
9950
Meters
100
50
0
-50
-100
-100
-50
0
50
Meters
100
Probability of 95 %
Rho = .910
Max ATE = 47 Meters
Sigma N = .130 usec
Sigma N = .028 usec
Max CTE = 31 Meters

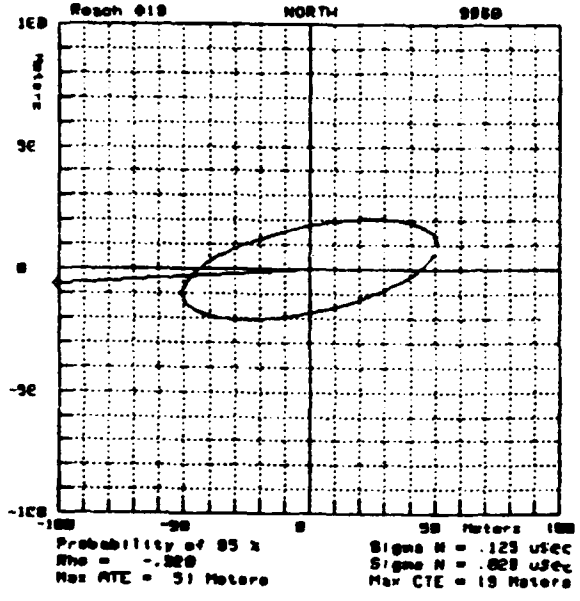
Reach 019
NORTH
9950
Meters
100
50
0
-50
-100
-100
-50
0
50
Meters
100
Probability of 95 %
Rho = -.920
Max ATE = 51 Meters
Sigma N = .123 usec
Sigma N = .028 usec
Max CTE = 19 Meters

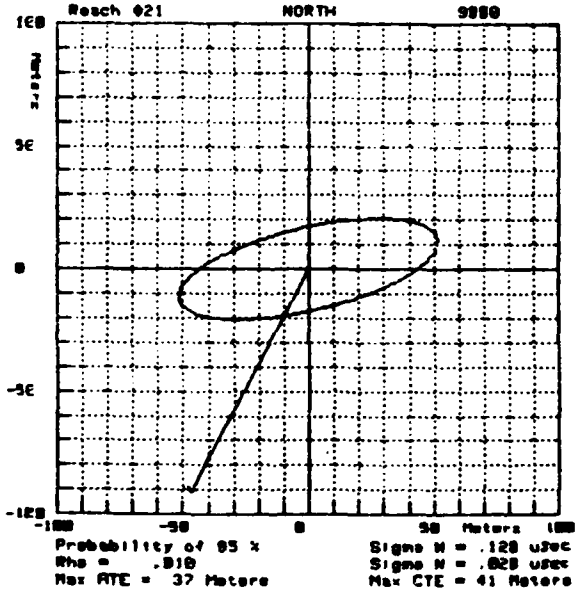
Reach 021
NORTH
9950
Meters
100
50
0
-50
-100
-100
-50
0
50
Meters
100
Probability of 95 %
Rho = .910
Max ATE = 37 Meters
Sigma N = .128 usec
Sigma N = .028 usec
Max CTE = 41 Meters

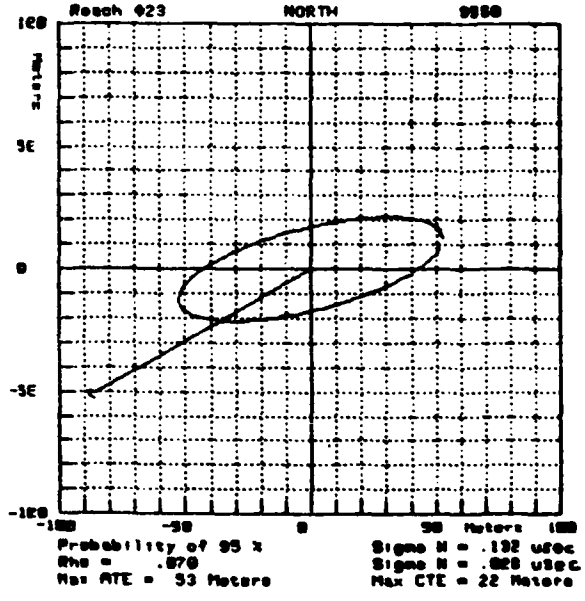
Reach 023
NORTH
9950
Meters
100
50
0
-50
-100
-100
-50
0
50
Meters
100
Probability of 95 %
Rho = .870
Max ATE = 53 Meters
Sigma N = .132 usec
Sigma N = .028 usec
Max CTE = 22 Meters

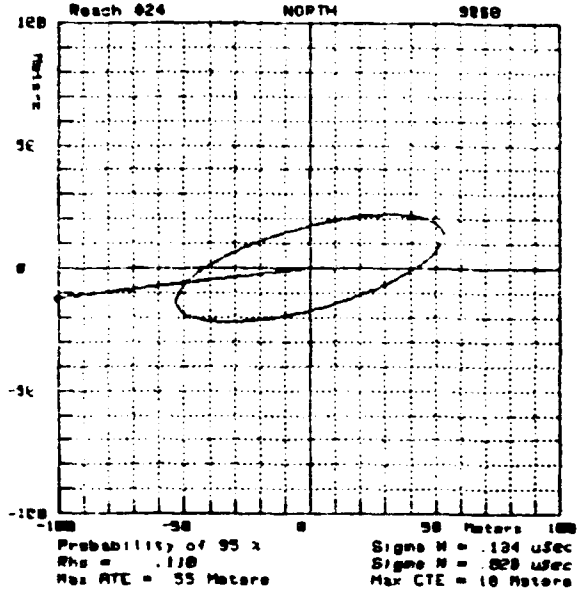
Reach 024
NORTH
9880
Meters
100
50
0
-50
-100
-100
-50
0
50
100
Meters
Probability of 95 %
Rho = .110
Max ATE = 55 Meters
Sigma N = .134 usec
Sigma N = .828 usec
Max CTE = 10 Meters

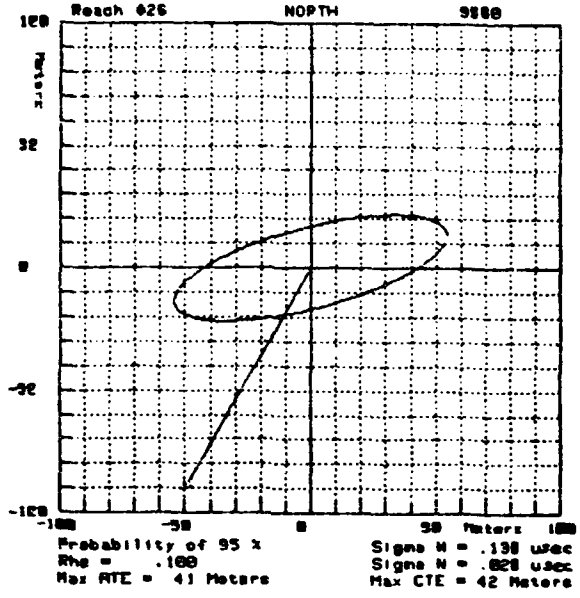
Reach 026
NORTH
9880
Meters
100
50
0
-50
-100
-100
-50
0
50
100
Meters
Probability of 95 %
Rho = .100
Max ATE = 41 Meters
Sigma N = .138 usec
Sigma N = .828 usec
Max CTE = 42 Meters

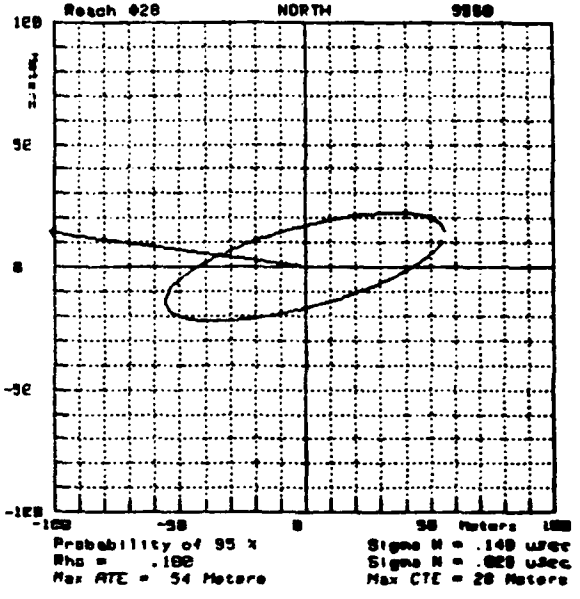
Reach 028
NORTH
9880
Meters
100
50
0
-50
-100
-100
-50
0
50
100
Meters
Probability of 95 %
Rho = .100
Max ATE = 54 Meters
Sigma N = .140 usec
Sigma N = .828 usec
Max CTE = 28 Meters

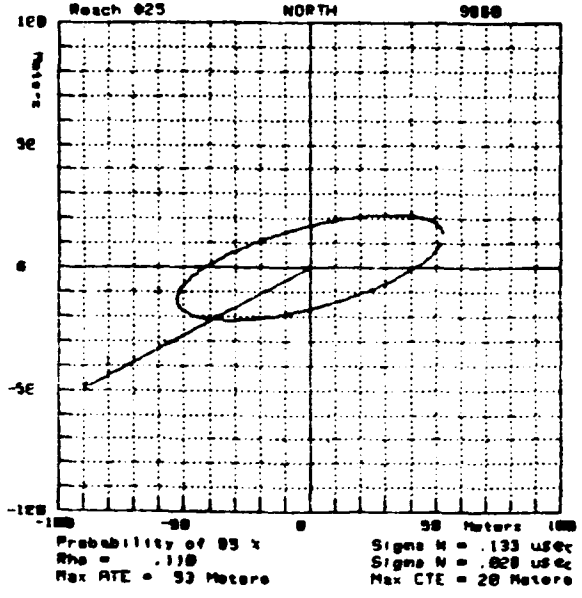
Reach 025
NORTH
9880
Meters
100
50
0
-50
-100
-100
-50
0
50
100
Meters
Probability of 95 %
Rho = .110
Max ATE = 93 Meters
Sigma N = .133 usec
Sigma N = .828 usec
Max CTE = 20 Meters

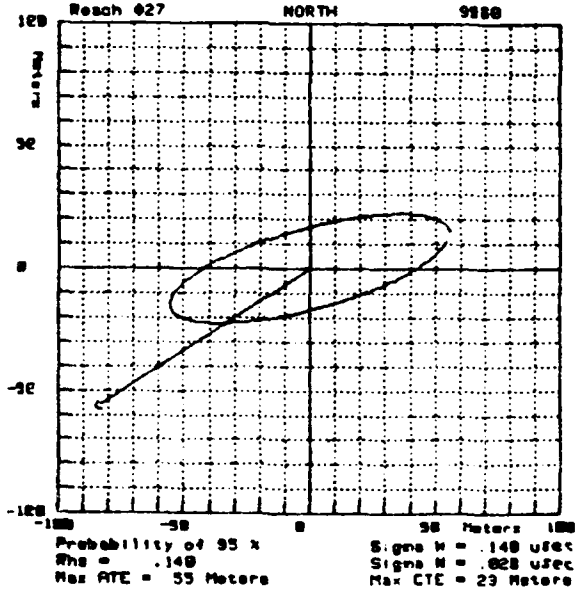
Reach 027
NORTH
9880
Meters
100
50
0
-50
-100
-100
-50
0
50
100
Meters
Probability of 95 %
Rho = .140
Max ATE = 55 Meters
Sigma N = .140 usec
Sigma N = .828 usec
Max CTE = 23 Meters

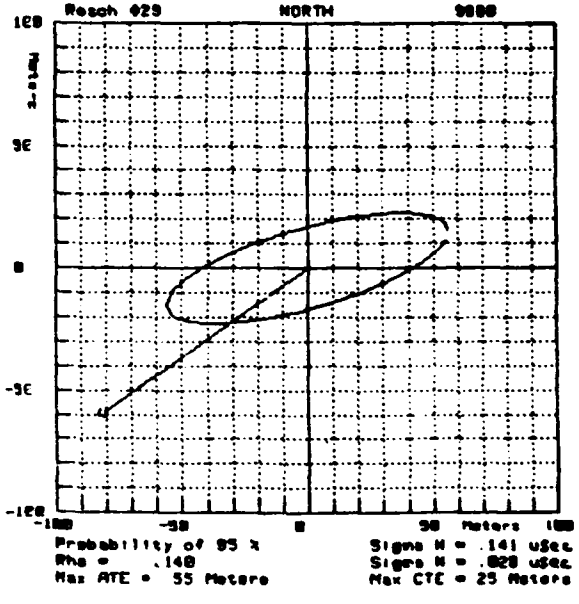
Reach 029
NORTH
9880
Meters
100
50
0
-50
-100
-100
-50
0
50
100
Meters
Probability of 95 %
Rho = .140
Max ATE = 55 Meters
Sigma N = .141 usec
Sigma N = .828 usec
Max CTE = 25 Meters

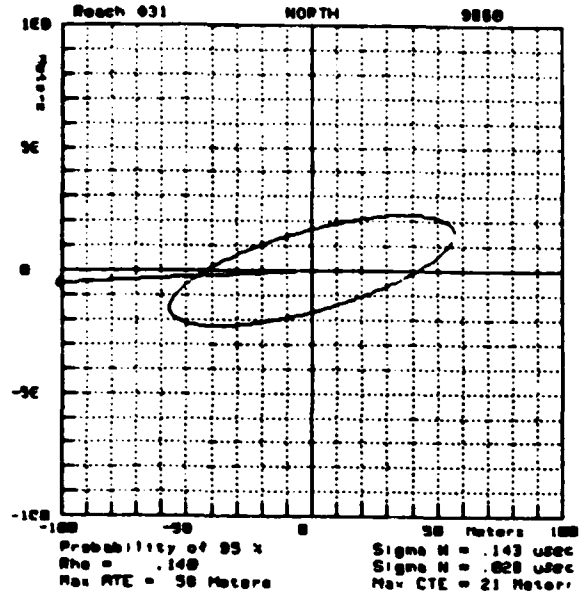
Reach 031
NORTH
9880
100
50
0
-50
-100
-100
-50
0
50
100
Meters
Probability of 95 %
Rho = .140
Max ATE = 58 Meters
Sigma N = .143 usec
Sigma N = .028 usec
Max CTE = 21 Meters

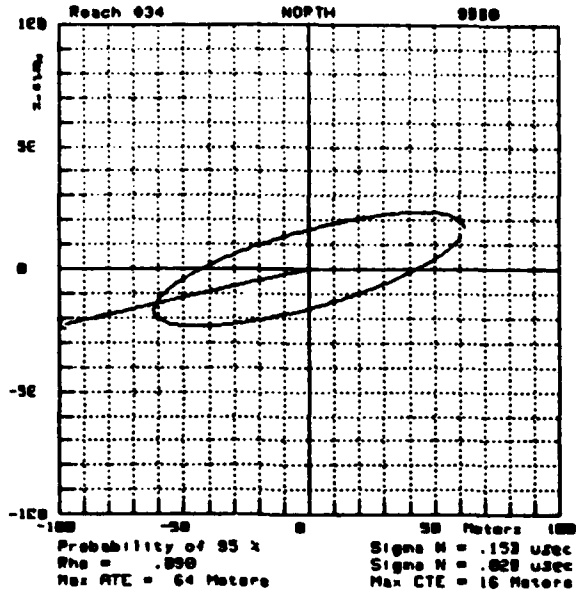
Reach 034
NORTH
9880
100
50
0
-50
-100
-100
-50
0
50
100
Meters
Probability of 95 %
Rho = .090
Max ATE = 64 Meters
Sigma N = .153 usec
Sigma N = .028 usec
Max CTE = 16 Meters

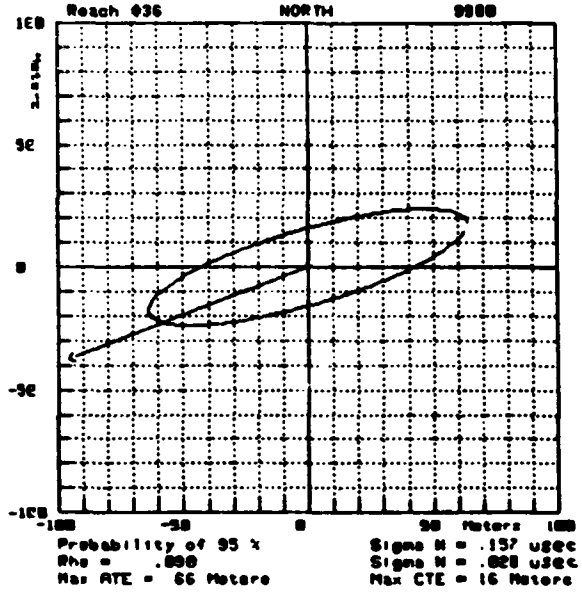
Reach 036
NORTH
9880
100
50
0
-50
-100
-100
-50
0
50
100
Meters
Probability of 95 %
Rho = .090
Max ATE = 66 Meters
Sigma N = .157 usec
Sigma N = .028 usec
Max CTE = 16 Meters

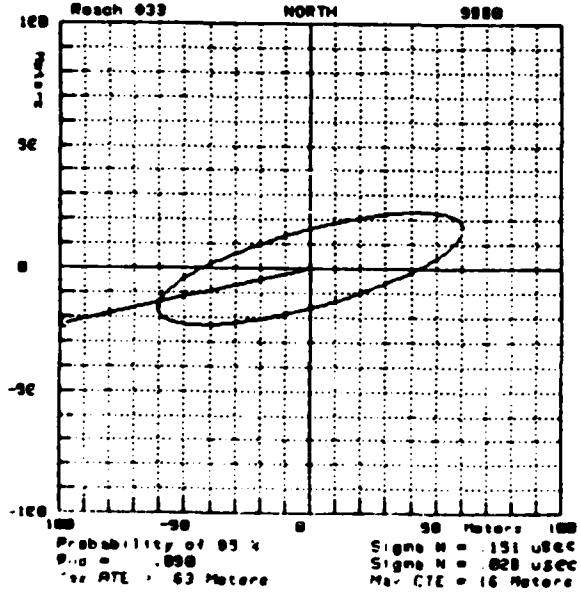
Reach 033
NORTH
9880
100
50
0
-50
-100
-100
-50
0
50
100
Meters
Probability of 95 %
Sigma N = .151 usec
Sigma N = .028 usec
Max CTE = 16 Meters

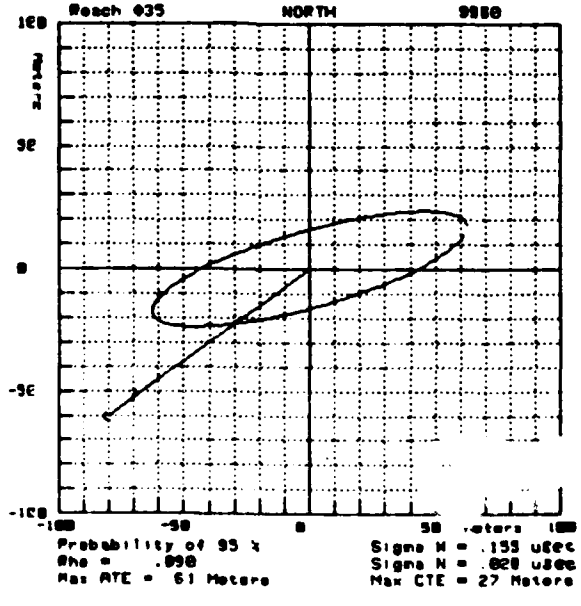
Reach 035
NORTH
9880
100
50
0
-50
-100
-100
-50
0
50
100
Meters
Probability of 95 %
Rho = .090
Max ATE = 61 Meters
Sigma N = .153 usec
Sigma N = .028 usec
Max CTE = 27 Meters

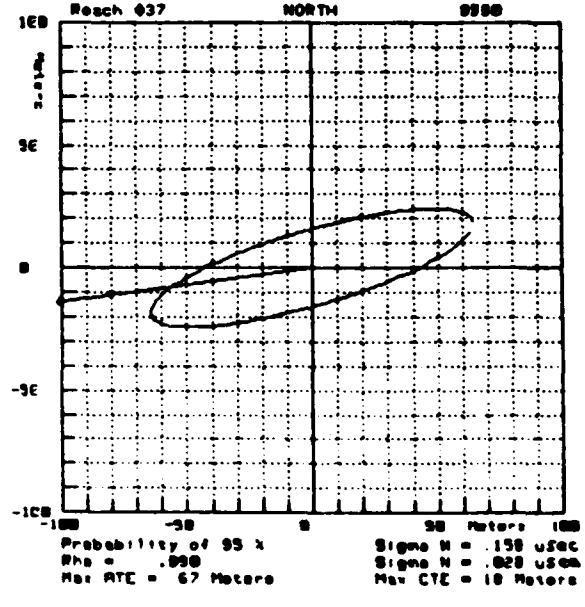
Reach 037
NORTH
9880
100
50
0
-50
-100
-100
-50
0
50
100
Meters
Probability of 95 %
Rho = .090
Max ATE = 67 Meters
Sigma N = .158 usec
Sigma N = .028 usec
Max CTE = 18 Meters

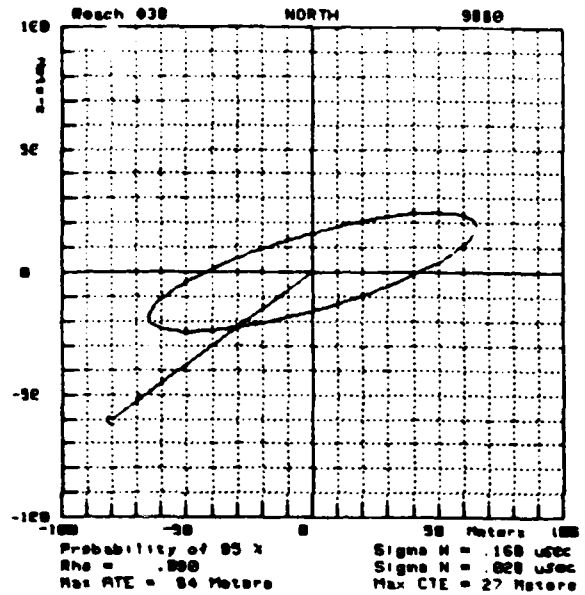
Reach 038
NORTH
9880
Meters
100
50
0
-50
-100
-100
-50
0
50
100
Meters
Probability of 95 %
Rho = .890
Max ATE = 84 Meters
Sigma N = .168 usec
Sigma N = .028 usec
Max CTE = 27 Meters

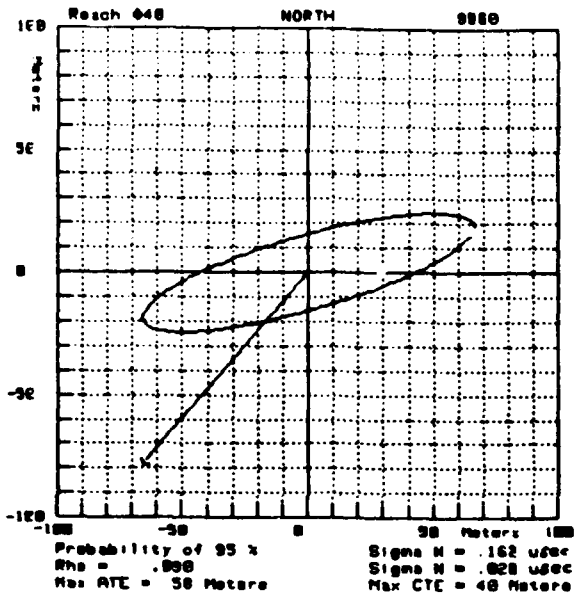
Reach 040
NORTH
9880
Meters
100
50
0
-50
-100
-100
-50
0
50
100
Meters
Probability of 95 %
Rho = .890
Max ATE = 58 Meters
Sigma N = .162 usec
Sigma N = .028 usec
Max CTE = 40 Meters

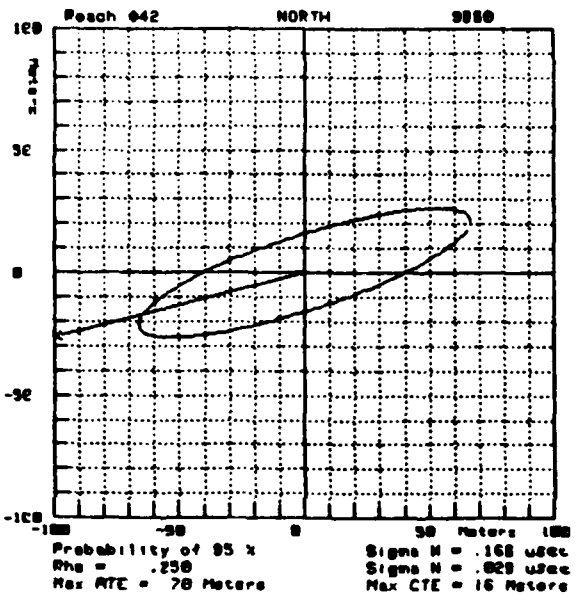
Reach 042
NORTH
9880
Meters
100
50
0
-50
-100
-100
-50
0
50
100
Meters
Probability of 95 %
Rho = .250
Max ATE = 78 Meters
Sigma N = .168 usec
Sigma N = .029 usec
Max CTE = 16 Meters

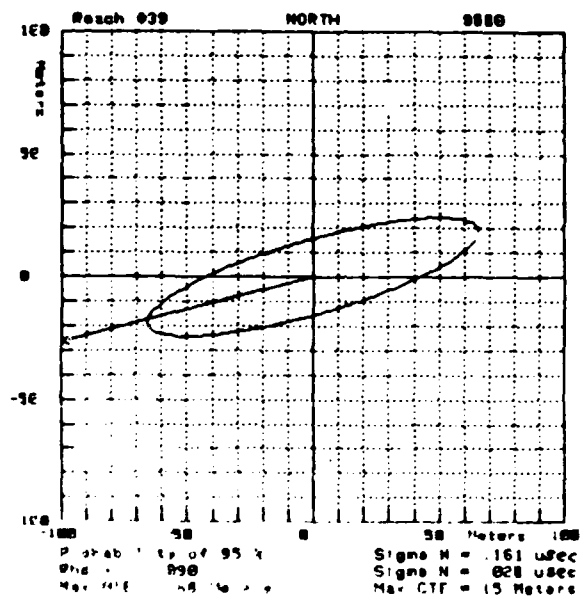
Reach 039
NORTH
9880
Meters
100
50
0
-50
-100
-100
-50
0
50
100
Meters
Sigma N = .161 usec
Sigma N = .028 usec
Max CTE = 15 Meters

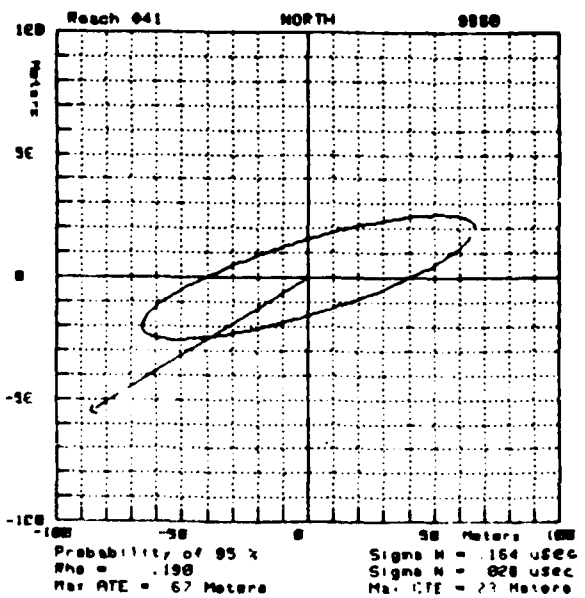
Reach 041
NORTH
9880
Meters
100
50
0
-50
-100
-100
-50
0
50
100
Meters
Probability of 95 %
Rho = .190
Max ATE = 67 Meters
Sigma N = .164 usec
Sigma N = .028 usec

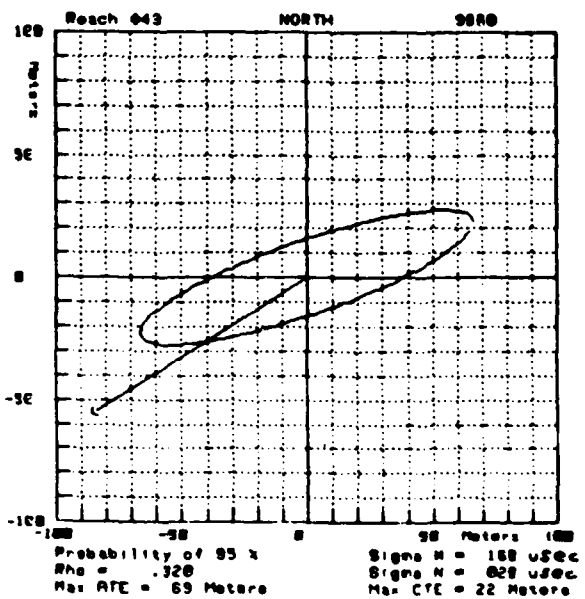
Reach 043
NORTH
9880
Meters
100
50
0
-50
-100
-100
-50
0
50
100
Meters
Probability of 95 %
Rho = .320
Max ATE = 69 Meters
Sigma N = .168 usec
Sigma N = .029 usec
Max CTE = 22 Meters

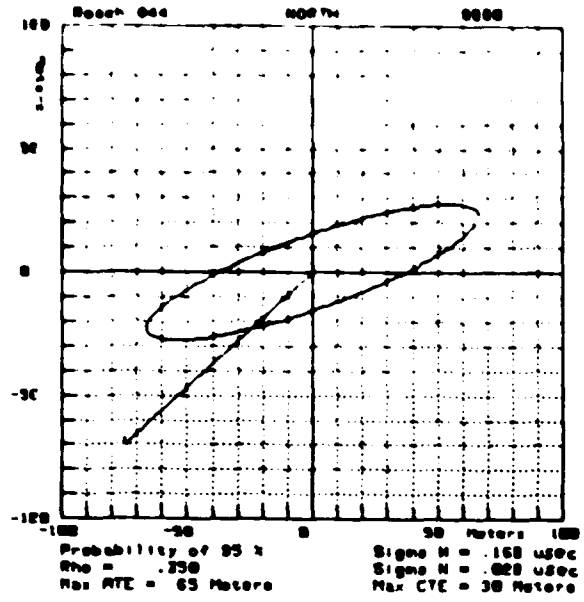
Reach 044
NORTH
9880
Probability of 95 %
Rho = .350
Max ATE = 65 Meters
Sigma N = .168 uSec
Sigma N = .028 uSec
Max CTE = 30 Meters

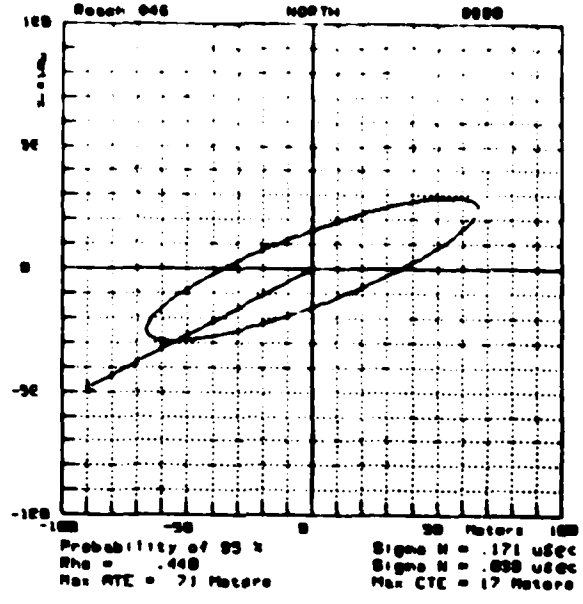
Reach 046
NORTH
9880
Probability of 95 %
Rho = .440
Max ATE = 71 Meters
Sigma N = .171 uSec
Sigma N = .030 uSec
Max CTE = 17 Meters

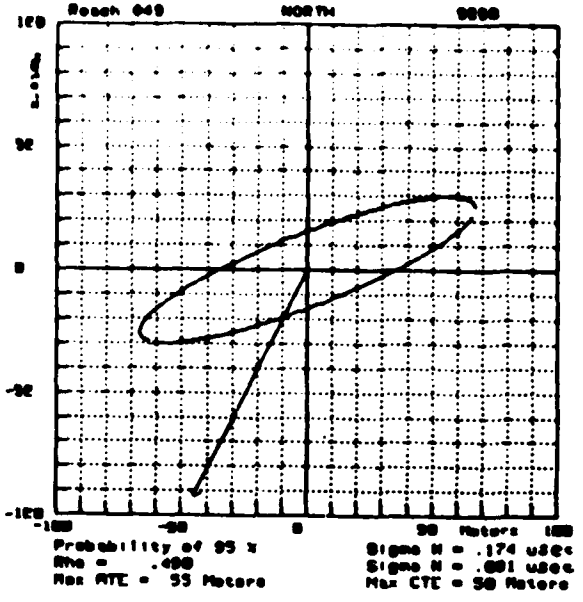
Reach 049
NORTH
9880
Probability of 95 %
Rho = .490
Max ATE = 55 Meters
Sigma N = .174 uSec
Sigma N = .031 uSec
Max CTE = 50 Meters

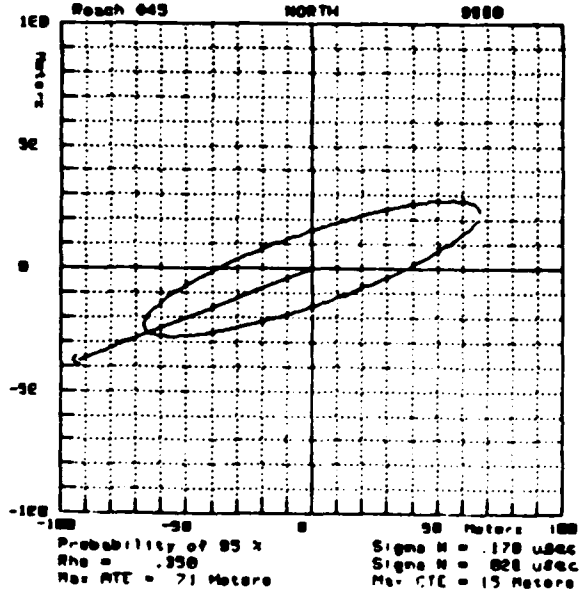
Reach 045
NORTH
9880
Probability of 95 %
Rho = .350
Max ATE = 71 Meters
Sigma N = .170 uSec
Sigma N = .028 uSec
Max CTE = 15 Meters

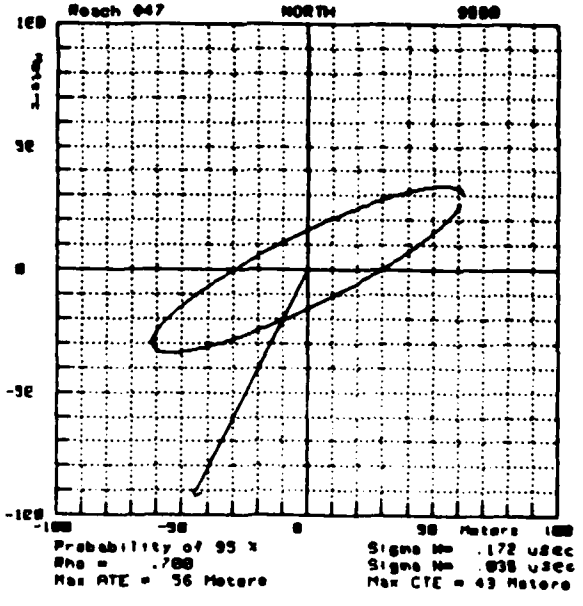
Reach 047
NORTH
9880
Probability of 95 %
Rho = .700
Max ATE = 56 Meters
Sigma Nn .172 uSec
Sigma Nn .030 uSec
Max CTE = 43 Meters

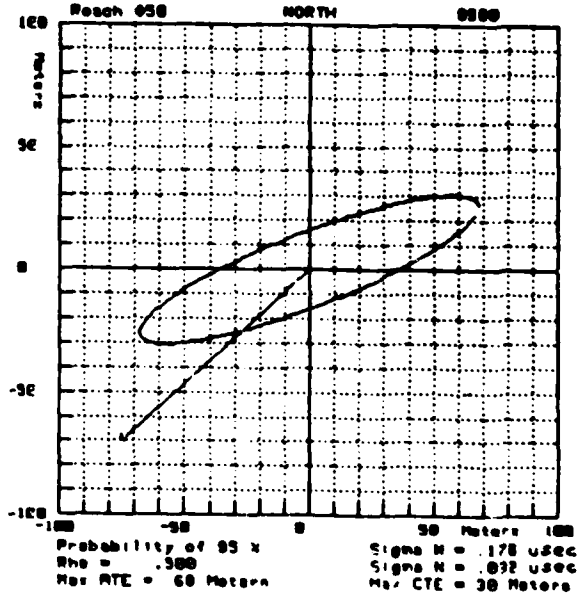
Reach 050
NORTH
9880
Probability of 95 %
Rho = .500
Max ATE = 60 Meters
Sigma N = .178 uSec
Sigma N = .032 uSec
Max CTE = 30 Meters

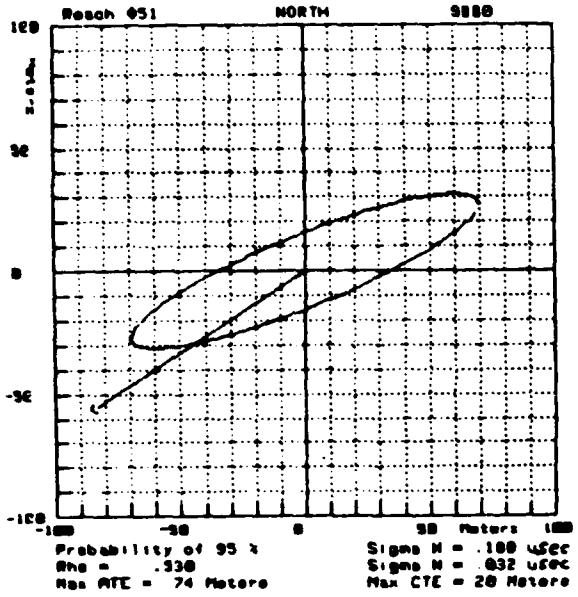
Reach 051
NORTH
9880
100
50
0
-50
-100
-100
-50
0
50
Meters
100
Probability of 95 %
Rho = .930
Max ATE = 74 Meters
Sigma N = .100 usec
Sigma N = .032 usec
Max CTE = 28 Meters

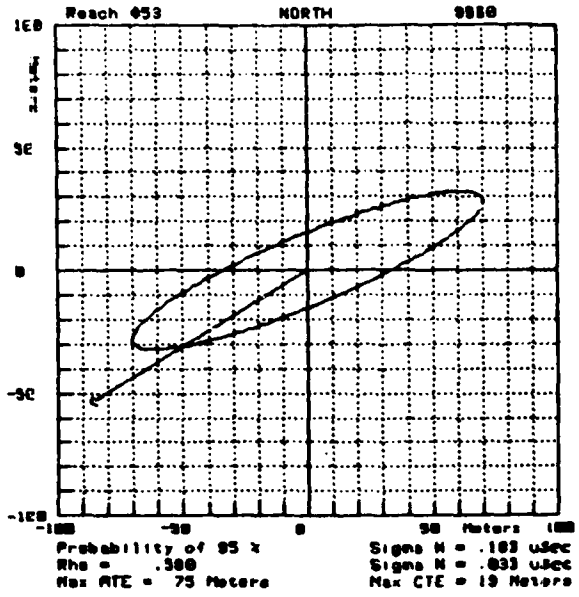
Reach 053
NORTH
9880
100
50
0
-50
-100
-100
-50
0
50
Meters
100
Probability of 95 %
Rho = .980
Max ATE = 75 Meters
Sigma N = .103 usec
Sigma N = .033 usec
Max CTE = 19 Meters

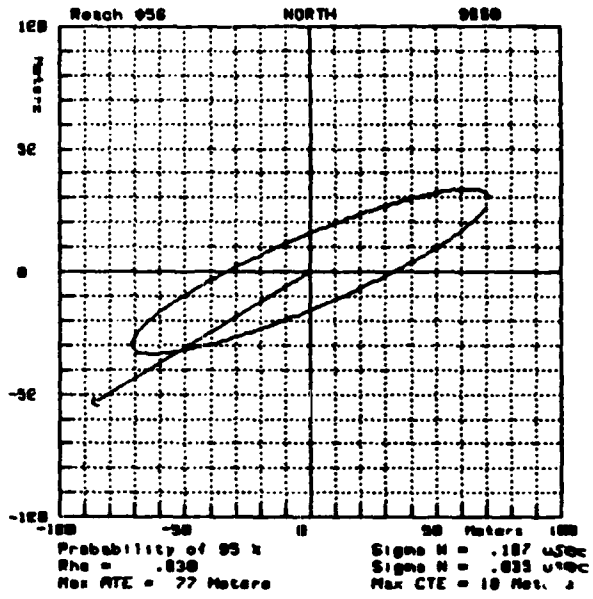
Reach 056
NORTH
9880
100
50
0
-50
-100
-100
-50
0
50
Meters
100
Probability of 95 %
Rho = .830
Max ATE = 77 Meters
Sigma N = .107 usec
Sigma N = .033 usec
Max CTE = 18 Meters

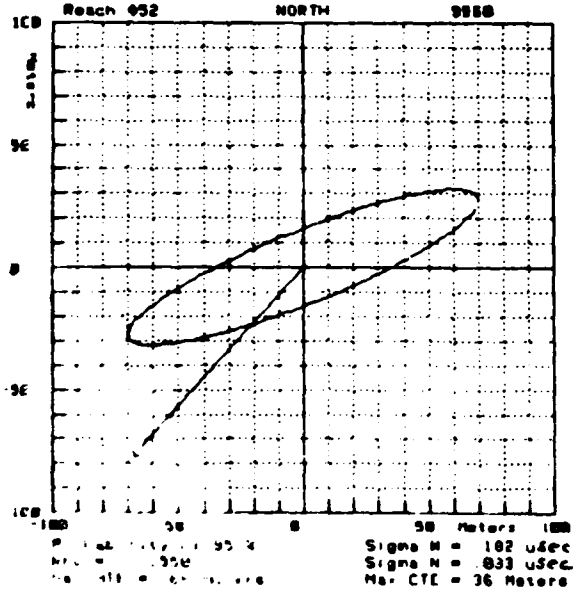
Reach 052
NORTH
9880
100
50
0
-50
-100
-100
-50
0
50
Meters
100
Sigma N = .102 usec
Sigma N = .033 usec
Max CTE = 36 Meters

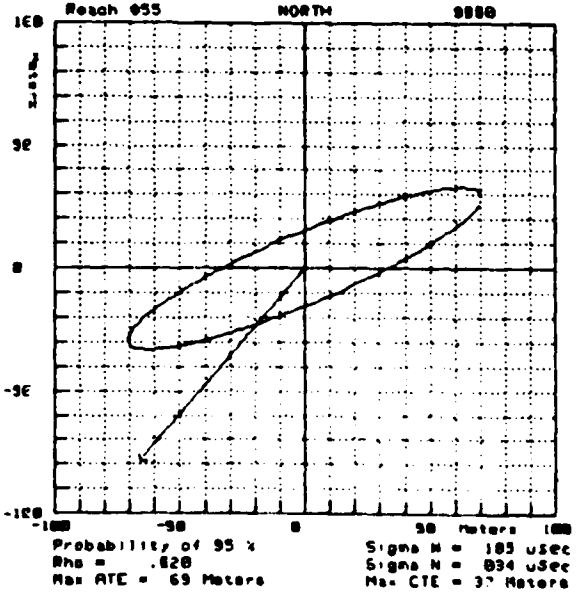
Reach 055
NORTH
9880
100
50
0
-50
-100
-100
-50
0
50
Meters
100
Probability of 95 %
Rho = .820
Max ATE = 69 Meters
Sigma N = .105 usec
Sigma N = .034 usec
Max CTE = 37 Meters

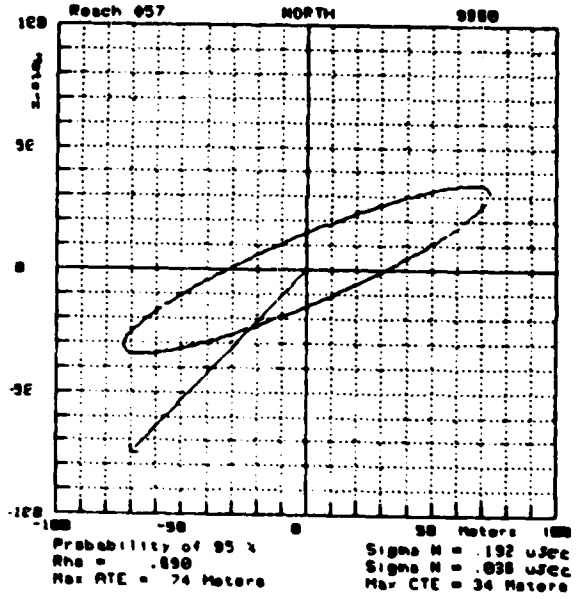
Reach 057
NORTH
9880
100
50
0
-50
-100
-100
-50
0
50
Meters
100
Probability of 95 %
Rho = .890
Max ATE = 74 Meters
Sigma N = .102 usec
Sigma N = .038 usec
Max CTE = 34 Meters

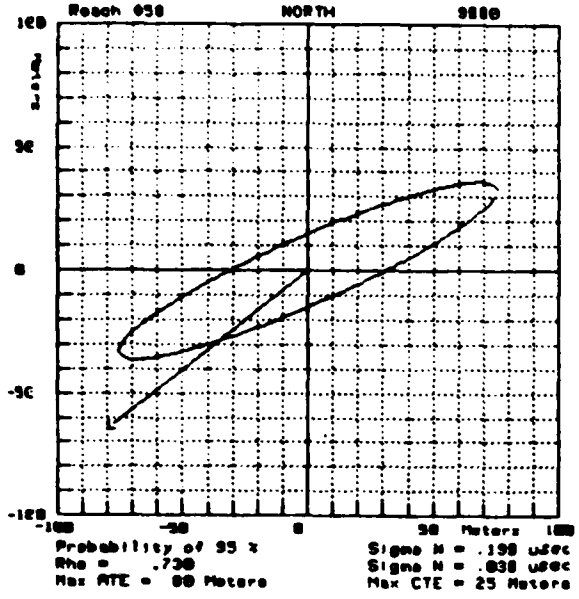
Reach 058
NORTH
9880
100
50
0
-50
-100
-100
-50
0
50
100
Meters
Probability of 95 %
Rho = .730
Max ATE = 80 Meters
Sigma N = .198 usec
Sigma N = .838 usec
Max CTE = 25 Meters

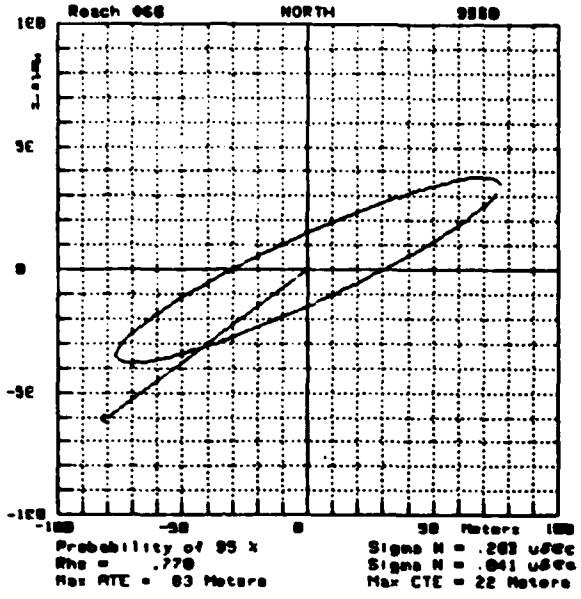
Reach 060
NORTH
9880
100
50
0
-50
-100
-100
-50
0
50
100
Meters
Probability of 95 %
Rho = .770
Max ATE = 83 Meters
Sigma N = .203 usec
Sigma N = .841 usec
Max CTE = 22 Meters

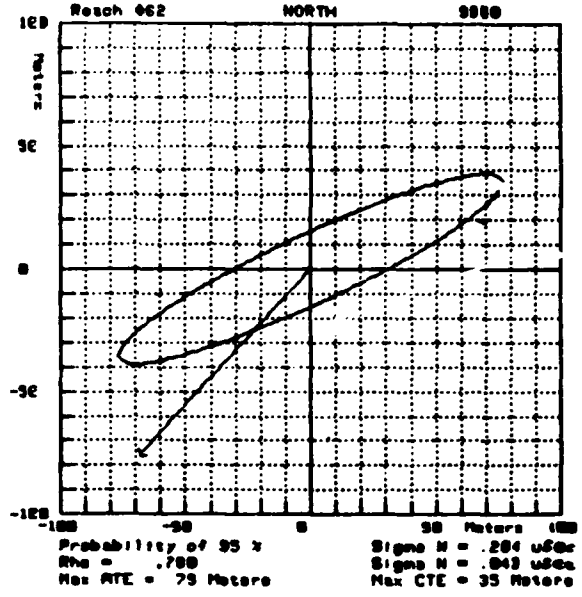
Reach 062
NORTH
9880
100
50
0
-50
-100
-100
-50
0
50
100
Meters
Probability of 95 %
Rho = .780
Max ATE = 79 Meters
Sigma N = .204 usec
Sigma N = .843 usec
Max CTE = 35 Meters

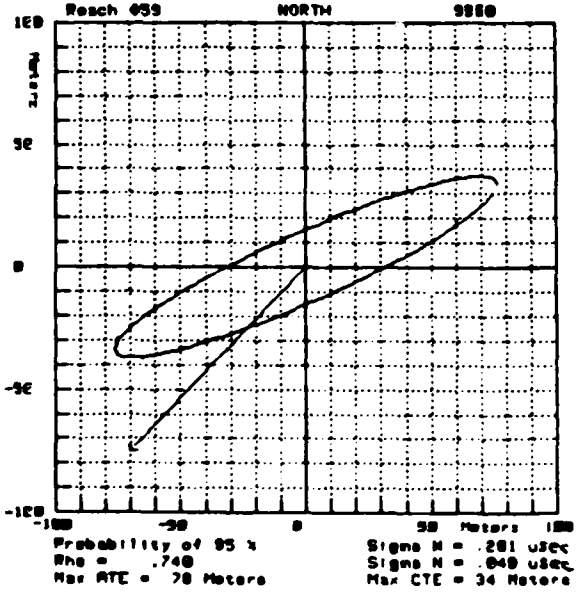
Reach 059
NORTH
9880
100
50
0
-50
-100
-100
-50
0
50
100
Meters
Probability of 95 %
Rho = .740
Max ATE = 78 Meters
Sigma N = .201 usec
Sigma N = .849 usec
Max CTE = 34 Meters

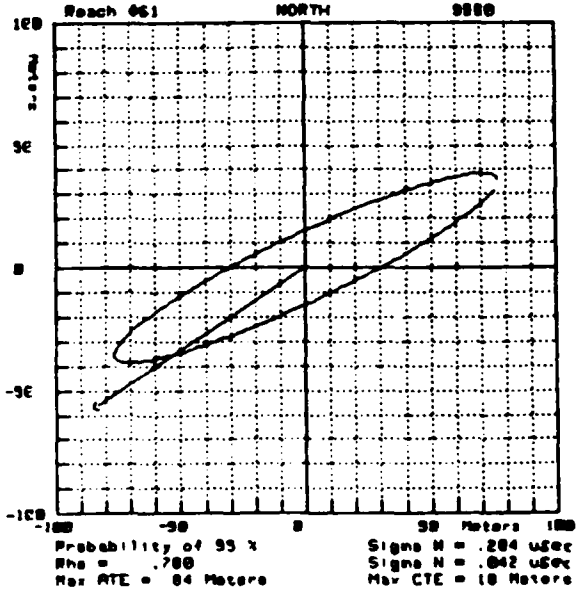
Reach 061
NORTH
9880
100
50
0
-50
-100
-100
-50
0
50
100
Meters
Probability of 95 %
Rho = .780
Max ATE = 84 Meters
Sigma N = .204 usec
Sigma N = .842 usec
Max CTE = 18 Meters

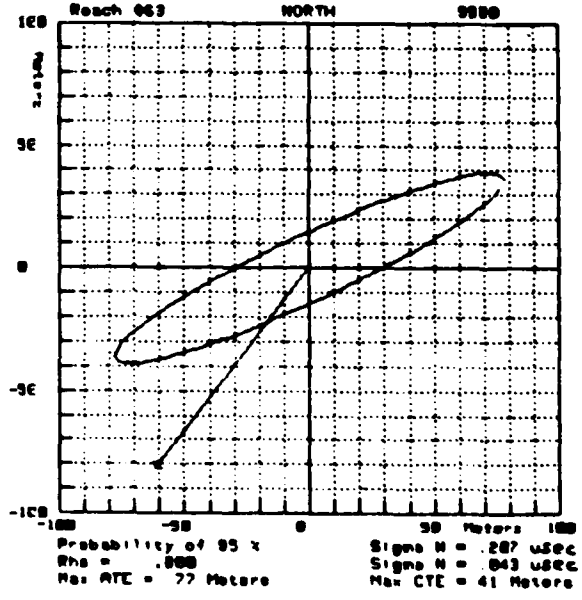
Reach 063
NORTH
9880
100
50
0
-50
-100
-100
-50
0
50
100
Meters
Probability of 95 %
Rho = .800
Max ATE = 77 Meters
Sigma N = .207 usec
Sigma N = .843 usec
Max CTE = 41 Meters

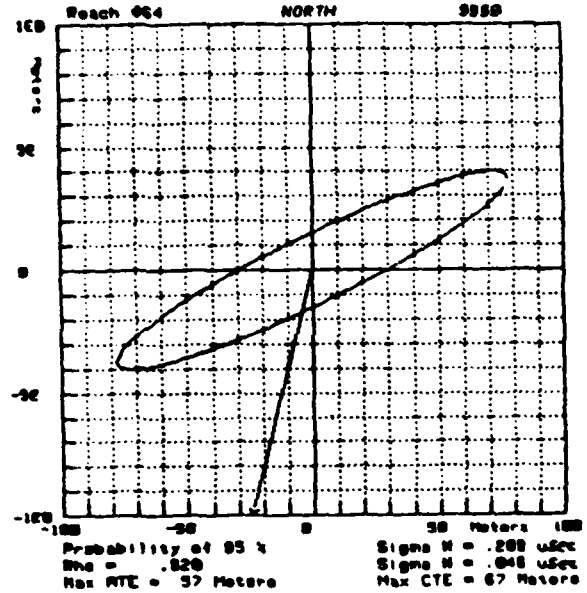
Reach 064
NORTH
9880
Meters
100
50
0
-50
-100
-100
-50
0
50
Meters
100
Probability of 95 %
Rho = .820
Max ATE = 57 Meters
Sigma N = .208 usec
Sigma N = .048 usec
Max CTE = 67 Meters

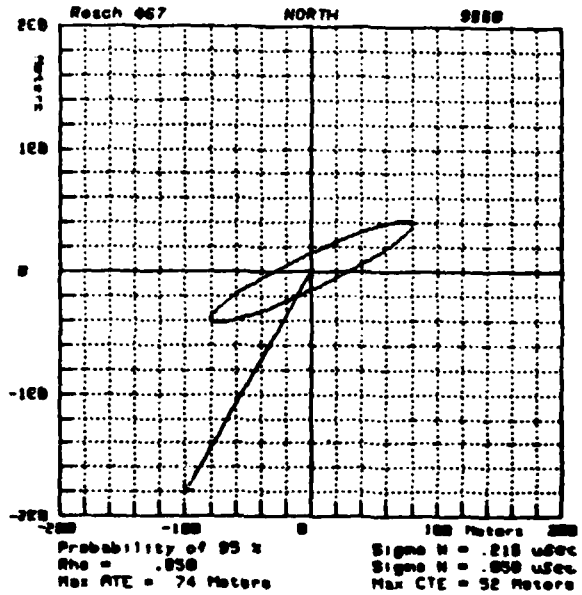
Reach 067
NORTH
9880
Meters
200
100
0
-100
-200
-200
-100
0
100
Meters
200
Probability of 95 %
Rho = .850
Max ATE = 74 Meters
Sigma N = .218 usec
Sigma N = .050 usec
Max CTE = 52 Meters

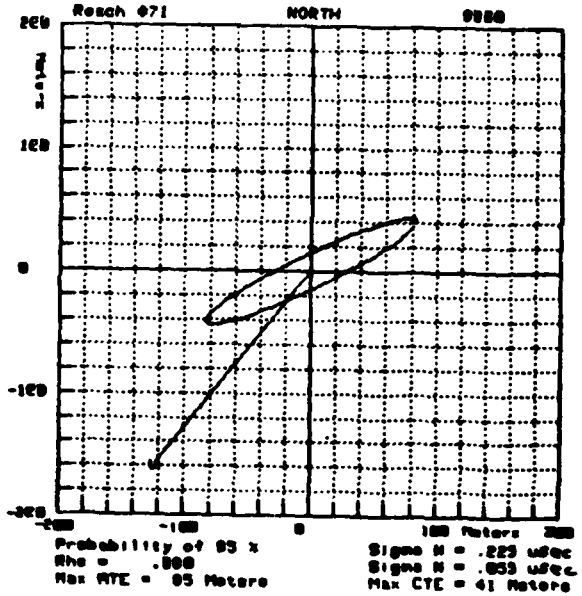
Reach 071
NORTH
9880
Meters
200
100
0
-100
-200
-200
-100
0
100
Meters
200
Probability of 95 %
Rho = .880
Max ATE = 85 Meters
Sigma N = .225 usec
Sigma N = .053 usec
Max CTE = 41 Meters

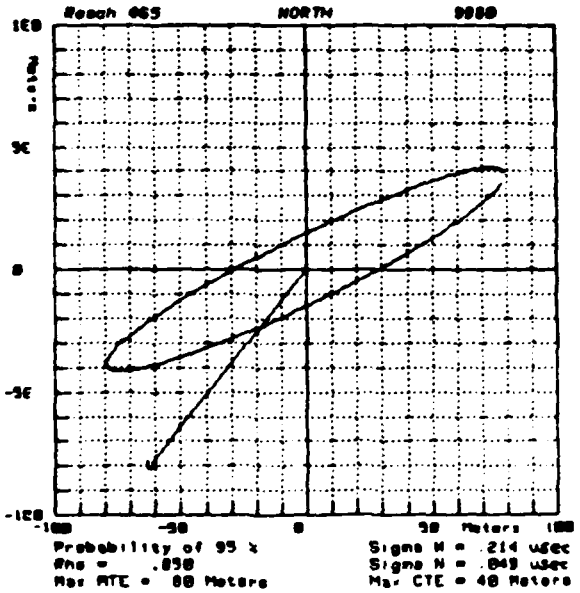
Reach 065
NORTH
9880
Meters
100
50
0
-50
-100
-100
-50
0
50
Meters
100
Probability of 95 %
Rho = .830
Max ATE = 88 Meters
Sigma N = .214 usec
Sigma N = .049 usec
Max CTE = 48 Meters

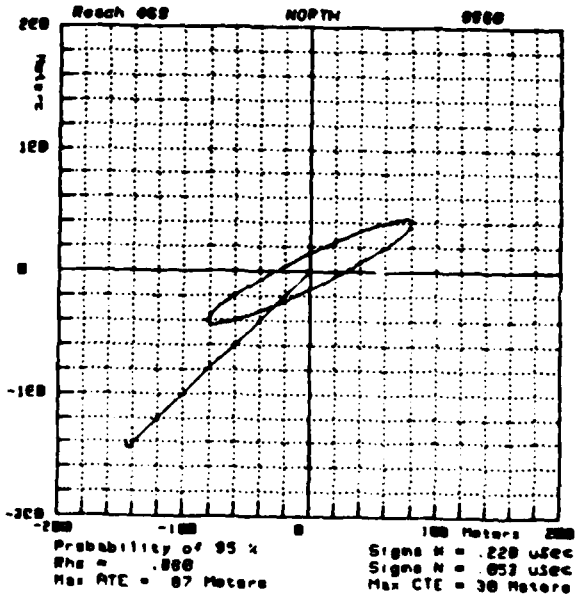
Reach 068
NORTH
9880
Meters
200
100
0
-100
-200
-200
-100
0
100
Meters
200
Probability of 95 %
Rho = .880
Max ATE = 87 Meters
Sigma N = .220 usec
Sigma N = .053 usec
Max CTE = 30 Meters

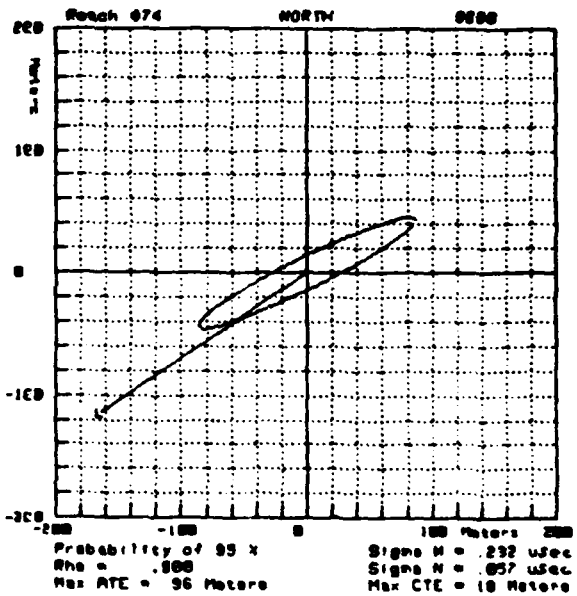
Reach 074
NORTH
9880
Meters
200
100
0
-100
-200
-200
-100
0
100
Meters
200
Probability of 95 %
Rho = .880
Max ATE = 96 Meters
Sigma N = .232 usec
Sigma N = .057 usec
Max CTE = 18 Meters

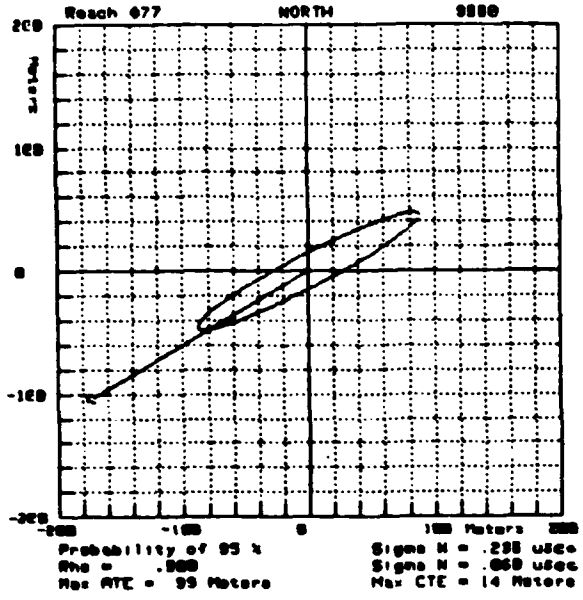
Reach 077
NORTH
9880
Meters
200
100
0
-100
-200
-200
-100
0
100 Meters
200
Probability of 95 %
Rho = .980
Max ATE = 99 Meters
Sigma N = .238 usec
Sigma N = .060 usec
Max CTE = 14 Meters

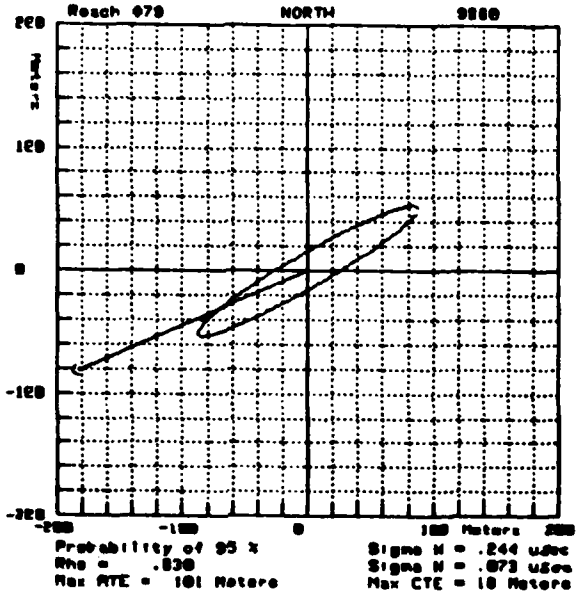
Reach 078
NORTH
9880
Meters
200
100
0
-100
-200
-200
-100
0
100 Meters
200
Probability of 95 %
Rho = .830
Max ATE = 101 Meters
Sigma N = .244 usec
Sigma N = .073 usec
Max CTE = 18 Meters

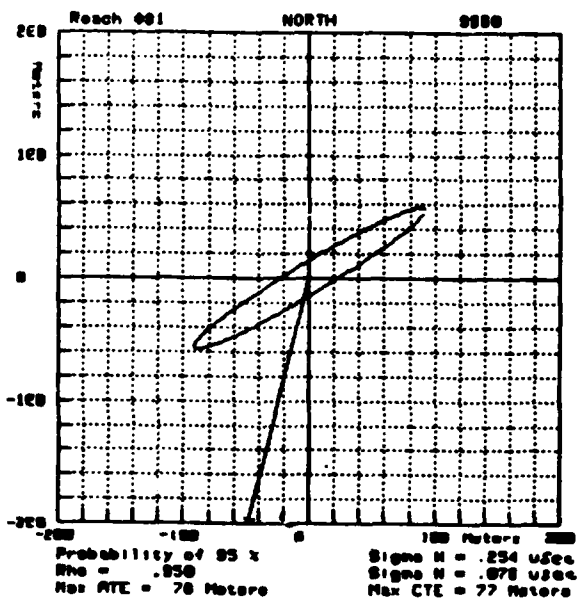
Reach 081
NORTH
9880
Meters
200
100
0
-100
-200
-200
-100
0
100 Meters
200
Probability of 95 %
Rho = .950
Max ATE = 78 Meters
Sigma N = .254 usec
Sigma N = .078 usec
Max CTE = 27 Meters

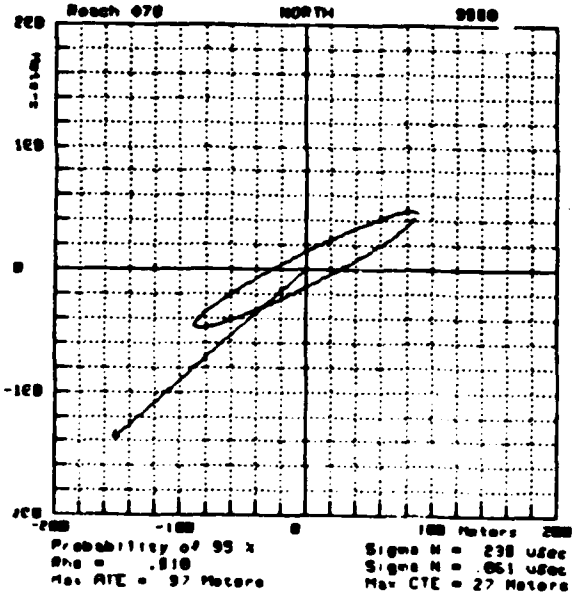
Reach 079
NORTH
9880
Meters
200
100
0
-100
-200
-200
-100
0
100 Meters
200
Probability of 95 %
Rho = .810
Max ATE = 97 Meters
Sigma N = .238 usec
Sigma N = .061 usec
Max CTE = 27 Meters

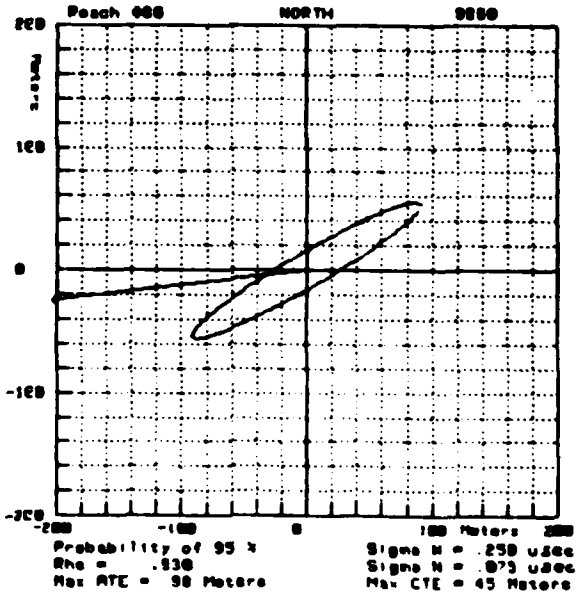
Reach 080
NORTH
9880
Meters
200
100
0
-100
-200
-200
-100
0
100 Meters
200
Probability of 95 %
Rho = .930
Max ATE = 98 Meters
Sigma N = .258 usec
Sigma N = .073 usec
Max CTE = 45 Meters

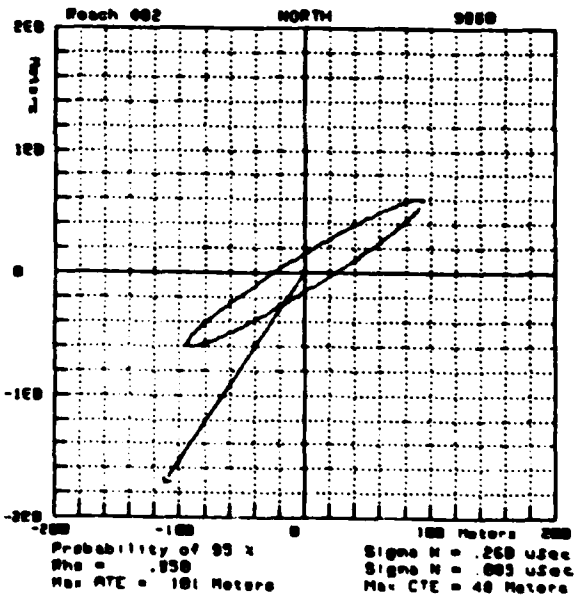
Reach 082
NORTH
9880
Meters
200
100
0
-100
-200
-200
-100
0
100 Meters
200
Probability of 95 %
Rho = .950
Max ATE = 101 Meters
Sigma N = .260 usec
Sigma N = .083 usec
Max CTE = 48 Meters

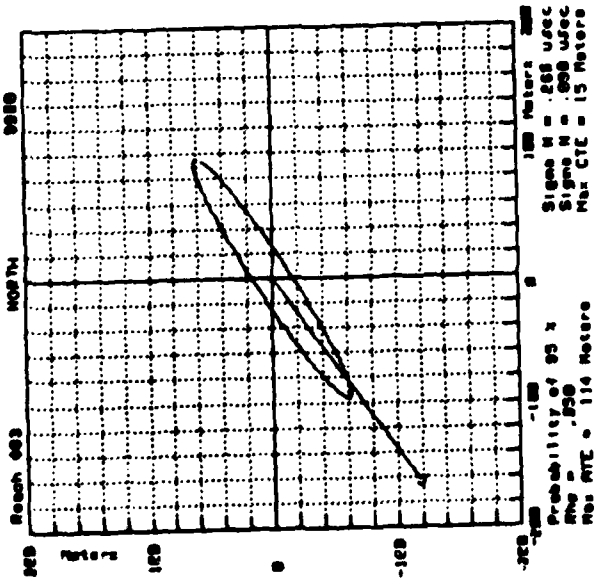
NORTH
Reach 003
Meters
Sigma N = .266 usec
Sigma N = .000 usec
Max CTE = 15 Meters
Probability of 95 %
Rho =
Max RTE = 114 Meters

PREDICTED ERROR ELLIPSE PLOTS

9960-N (NORTH BAY) - NON-DIFFERENTIAL

9960-W DIFFERENTIAL CORRECTIONS FROM MASSENA

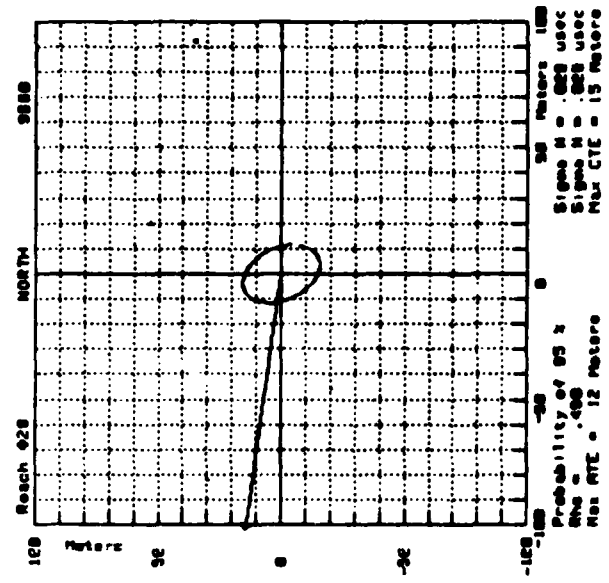
Reach 028
NORTH
Meters
Probability of 95 %
Rho = .460
Max ATE = 14 Meters
Sigma N = .008 usec
Sigma N = .028 usec
Max CTE = 16 Meters

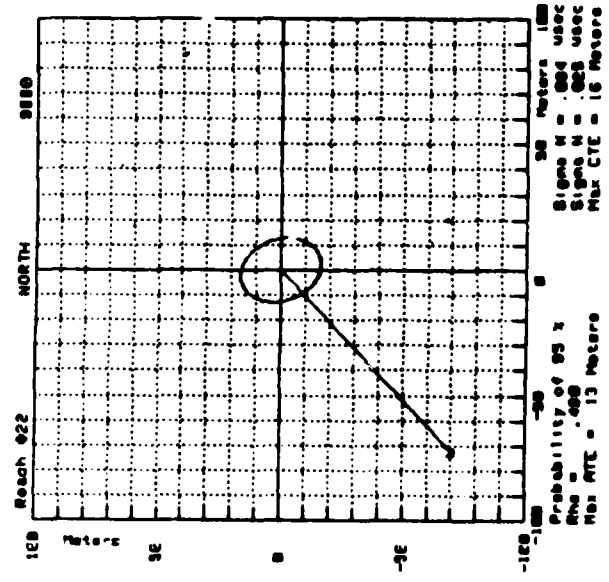
Reach 022
NORTH
Meters
Probability of 95 %
Rho = .488
Max ATE = 13 Meters
Sigma N = .004 usec
Sigma N = .028 usec
Max CTE = 16 Meters

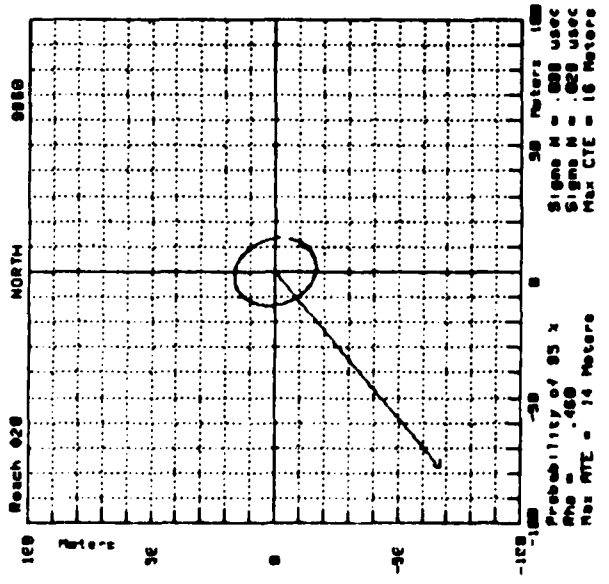
Reach 028
NORTH
Meters
Probability of 95 %
Rho = .460
Max ATE = 14 Meters
Sigma N = .008 usec
Sigma N = .028 usec
Max CTE = 16 Meters

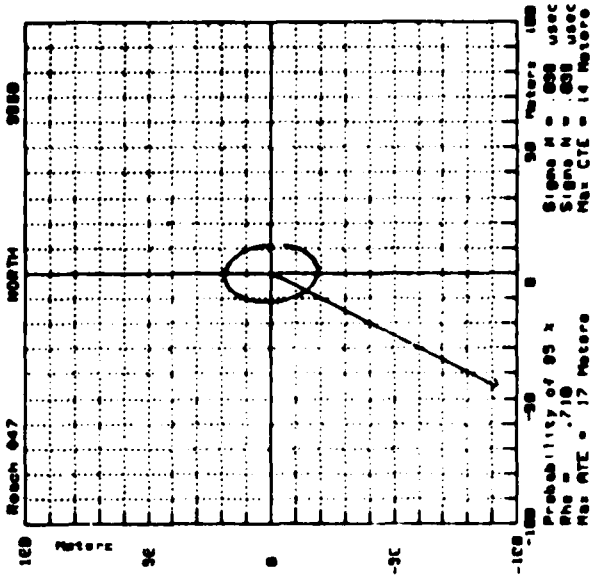
Reach 047
NORTH
Meters
Probability of 95 %
Rho = .710
Max ATE = 17 Meters
Sigma N = .000 usec
Sigma N = .028 usec
Max CTE = 14 Meters

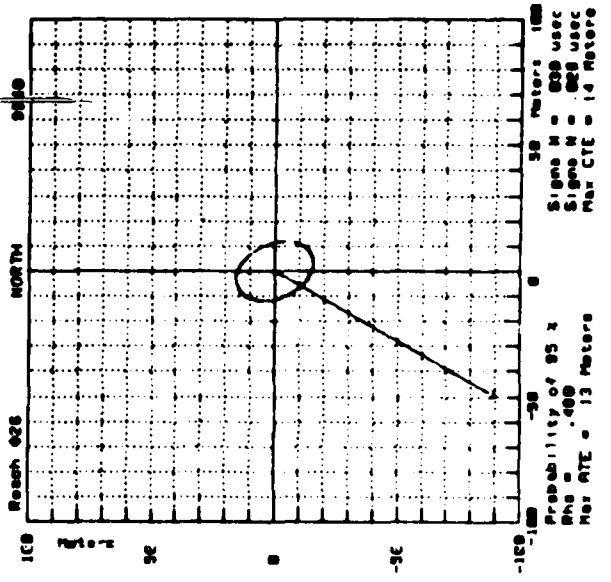
Reach 026
NORTH
Meters
Probability of 95 %
Rho = .488
Max ATE = 13 Meters
Sigma N = .000 usec
Sigma N = .028 usec
Max CTE = 14 Meters

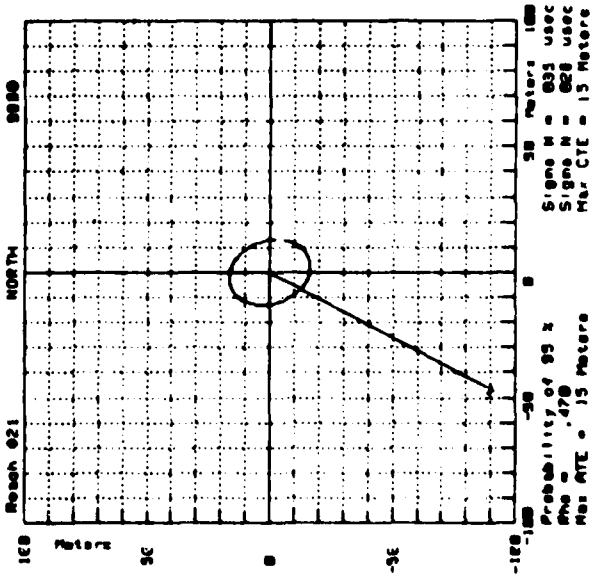
Reach 021
NORTH
Meters
Probability of 95 %
Rho = .470
Max ATE = 15 Meters
Sigma N = .031 usec
Sigma N = .028 usec
Max CTE = 15 Meters

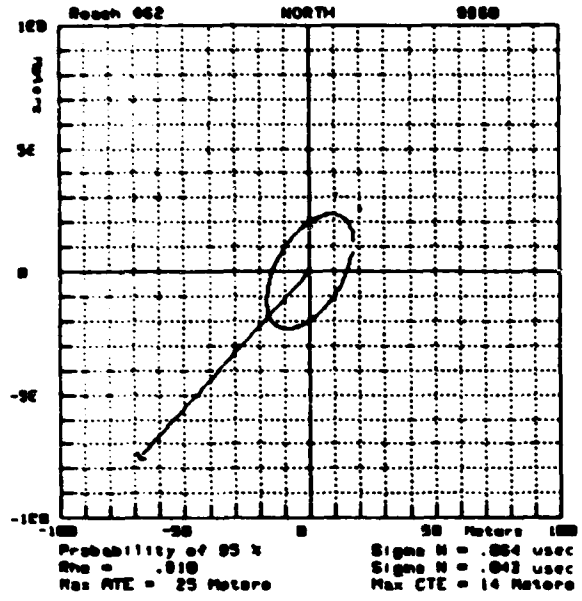
Reach 062
NORTH
9850
100
50
0
-50
-100
-100
-50
0
50
100
Meters
Probability of 95 %
Rho = .810
Max ATE = 25 Meters
Sigma N = .064 usec
Sigma N = .043 usec
Max CTE = 14 Meters

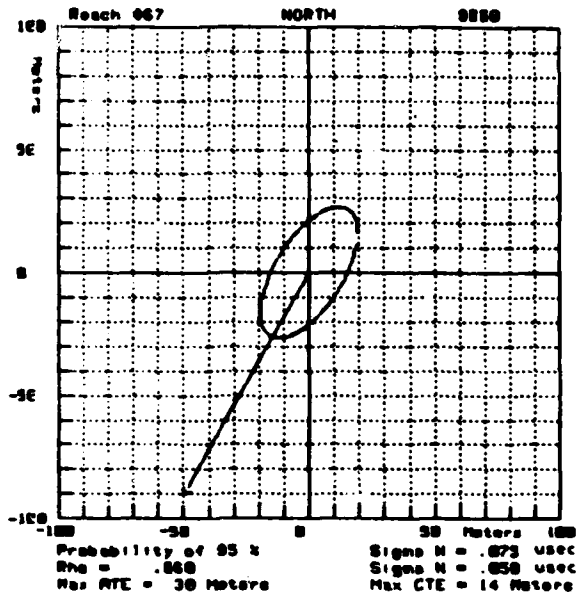
Reach 067
NORTH
9850
100
50
0
-50
-100
-100
-50
0
50
100
Meters
Probability of 95 %
Rho = .860
Max ATE = 30 Meters
Sigma N = .073 usec
Sigma N = .050 usec
Max CTE = 14 Meters

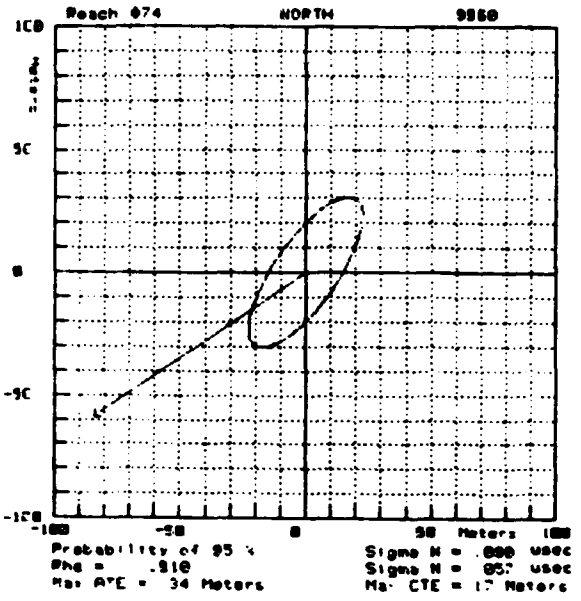
Reach 074
NORTH
9850
100
50
0
-50
-100
-100
-50
0
50
100
Meters
Probability of 95 %
Rho = .910
Max ATE = 34 Meters
Sigma N = .090 usec
Sigma N = .057 usec
Max CTE = 17 Meters

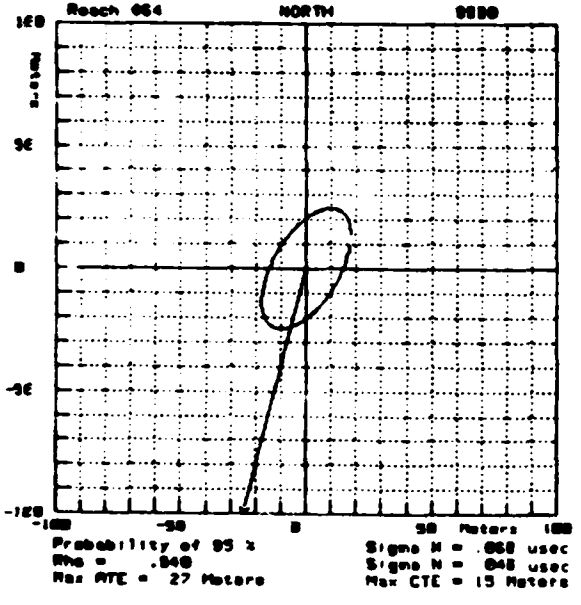
Reach 064
NORTH
9850
100
50
0
-50
-100
-100
-50
0
50
100
Meters
Probability of 95 %
Rho = .840
Max ATE = 27 Meters
Sigma N = .068 usec
Sigma N = .045 usec
Max CTE = 15 Meters

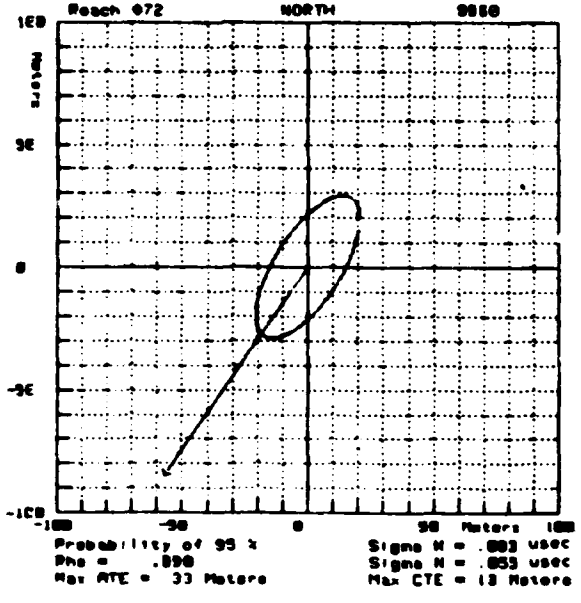
Reach 072
NORTH
9850
100
50
0
-50
-100
-100
-50
0
50
100
Meters
Probability of 95 %
Rho = .890
Max ATE = 33 Meters
Sigma N = .083 usec
Sigma N = .053 usec
Max CTE = 13 Meters

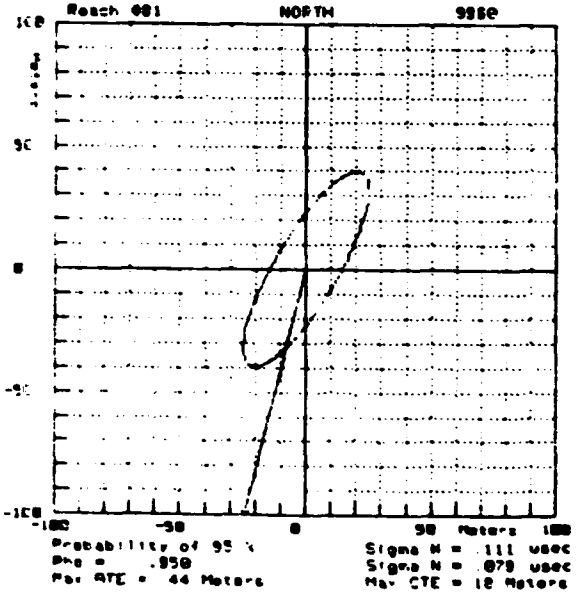
Reach 081
NORTH
9850
100
50
0
-50
-100
-100
-50
0
50
100
Meters
Probability of 95 %
Rho = .950
Max ATE = 44 Meters
Sigma N = .111 usec
Sigma N = .079 usec
Max CTE = 18 Meters

REFERENCES

1. Olsen, D.L., Ligon, J.L., Sedlock, A.J., and Isgett, C.E., "Precision Loran-C Navigation for the Harbor and Harbor Entrance Area," May 1980. U.S. Coast Guard Report No. CG-D-34-80. Available from the National Technical Information Service, Springfield, Virginia 22161 as AD-A086001.

2. "Quantification of the St. Marys River Loran-C Time Difference Grid Instability," The Analytic Sciences Corporation, August 1980. Published as U.S. Coast Guard Report No. CG-D-52-81. Available from the National Technical Information Service, Springfield, Virginia 22161 as AD-A108074.

3. Lewis, J.W. and Nelka, J.J., "Saint Lawrence Seaway Navigation Aid Study, Vol I" ARCTEC Inc., September 1978. Published as DOT report number DOT-SLS-63-78-1.I.

4. Olsen, D.L., "St. Marys River Loran-C Mini Chain Final Report," July 1981. U.S. Coast Guard Report No. CG-D-11-82. Available from the National Technical Information Service, Springfield, Virginia 22161 as PB82-255183.

5. "Minimum Performance Standards (MPS) Automatic Coordinate Conversion System," Report of RTCM Special Committee No. 75. November 1981. Appendix A.

6. Bowditch, N., American Practical Navigator, U.S. Government Printing Office, Washington, 1962.

7. Papoulis, A., Probability, Random Variables and Stochastic Processes, Mc-Graw-Hill Book Co., New York, 1965.

8. Van Trees, H.L., Detection, Estimation and Modulation Theory, Part I, John Wiley and Sons, Inc., New York, 1968.

9. Frank, R.L. and McGrew, D.L., "Real-Time Compensation of Loran-C/D Temporal Variations." Paper presented at the Third Annual Wild Goose Association Convention, Great Gorge, N.Y., October 1974.

10. DePalma, L.M. and Gupta, R.R., "Seasonal Sensitivity Analysis of the St Marys River Loran-C Time Difference Grid," The Analytic Sciences Corporation, June 1978. Published as U.S. Coast Guard Report No. CG-D-33-80. Available from the National Technical Information Service, Springfield, Virginia 22161 as AD-A085825.

11. Bertsche, W.R., Smith, M.W., Marion, K.L., and Cooper, R.B., "Draft SRA/RA Systems Design Manual for Restricted Waterways," Eclectech Associates, Inc., February 1982. Published as U.S. Coast Guard Report No. CG-D-77-81. Available from the National Technical Information Service, Springfield, Virginia 22161 as AD-A113236.